Title
TOTAL SPIN-EXCHANGE CROSS SECTIONS FOR ALKALI ATOMS FROM OPTICAL PUMPING EXPERIMENTS

Author
Gibbs, Hyatt McDonald.

Publication Date
1965-03-12

UCRL-16034

University of California

Ernest O. Lawrence Radiation Laboratory

TOTAL SPIN-EXCHANGE CROSS SECTIONS FOR ALKALI ATOMS FROM OPTICAL PUMPING EXPERIMENTS

Berkeley, California

DISCLAIMER

UNIVERSITY OF CALIFORNIA
Lawrence Radiation Laboratory
Berkeley, California

AEC Contract No. W-7405-eng-48

TOTAL SPIN-EXCHANGE CROSS SECTIONS FOR ALKALI ATOMS FROM OPTICAL PUMPING EXPERIMENTS

Hyatt McDonald Gibbs

(Ph. D. Thesis)

March 12, 1965

TOTAL SPIN-EXCHANGE CROSS SECTIONS FOR ALKALI ATOMS FROM OPTICAL PUMPING EXPERIMENTS

Contents

TOTAL SPIN-EXCHANGE CROSS SECTIONS FOR ALKALI ATOMS FROM OPTICAL PUMPING EXPERIMENTS

Hyatt McDonald Gibbs

Lawrence Radiation Laboratory and Department of Physics
University of California, Berkeley, California

March 12, 1965

ABSTRACT

The importance of the nuclear spins in the analysis of alkali spin-exchange experiments employing Zeeman optical pumping by circularly polarized light and performed in low magnetic fields is demonstrated. The signal for general nuclear spin is found for the Franzen-type transient experiment and for the Dehmelt-type steady-state experiment in the limit of low light intensity. The results are quite sensitive to the process assumed for the relaxation of the ground-state populations. The solutions are given for a general process in which randomly oriented disorientation fields interact with the spins of the alkali atom only through the electron spin. The steady-state signal expression includes the effects of self spin exchange and partial disorientation in the excited state. Only the diagonal elements of the density matrix are included.

A hyperfine optical pumping experiment employing the Franzen transient method is described in detail. It has been applied to the most precise determination to date of the total spin-exchange cross sections

$$\sigma_{Rb^{87}\text{-}Rb^{87}} = (2.03 \pm 0.20) \times 10^{-14}\ \text{cm}^2$$

and

$$\sigma_{Rb^{87}\text{-}Cs^{133}} = (2.18 \pm 0.31) \times 10^{-14}\ \text{cm}^2.$$

A scanning Fabry-Perot interferometer is used in estimating the densities of the alkali vapors. Problems introduced by the Fabry-Perot and overlooked in the past are discussed.

I. INTRODUCTION

In Part I a spin-exchange collision is defined and its importance outlined. The techniques for measuring spin-exchange cross sections are described briefly. A short history of the research of this thesis is given. The role of this research with respect to advances in the field by others is also discussed. Finally, the plan of this thesis is presented.

A. Definition and Origin of Spin-Exchange Collisions

In order to define a spin-exchange process, consider a collision between two hydrogen atoms. In such a collision the two atoms should interact in a manner described approximately by the molecular potentials for a molecule formed by the two atoms. The time for a collision is roughly the size of a molecule ($\approx$ interaction distance) divided by a typical kinetic velocity, for example, $T_c \approx 5\ \text{Å}/(5\times10^4\ \text{cm/sec}) = 10^{-12}$ sec. In contrast, the time for one Bohr orbit is about $T_e \approx 2\pi a_0/ac = 10^{-16}$ sec. Thus the interaction should be represented to a good approximation by the potentials found in the Born-Oppenheimer approximation. In the latter the nuclei are "clamped" in place, and the effective potential of the fast-moving electrons is calculated with the internuclear distance as a parameter. The motion of the nuclei is then calculated with the contribution to their motion from the electrons being given by the effective potential.

Each hydrogen atom participating in the collision has electronic spin of 1/2. The total electronic spin S for two such atoms is then 0 or 1. Because the two electrons are two identical fermions, the total electronic wave function must be antisymmetrical. The two possible electronic states, the singlet (S=0) and triplet (S=1) states, then correspond to symmetric and antisymmetric electronic space functions, respectively. In the symmetric space state the electrons have a high probability of being between the two protons. The two protons will then be attracted toward a common center, and a stable molecule might be possible. However, in a collision between two free atoms, a stable molecule will not result because conservation of kinetic energy and

linear momentum cannot be satisfied for recombination in a two-body collision. Nonetheless, the space-symmetric or spin singlet collision should lead to a pseudo-stable state, implying a large interaction cross section. In the spin triplet or space-antisymmetric state, the electrons avoid the region between the protons, and the interaction is repulsive. Thus the difference between the singlet and triplet potentials arises from the antisymmetry requirement on the total electronic wave function. The antisymmetry condition contains the Pauli principle, in terms of which one could say that the electrons with parallel spins (triplet) must avoid each other. See Fig. 1 for a rough idea of the form of the potentials for hydrogen.[1]

For the heavier alkalis the singlet binding energy is smaller and the equilibrium separation larger than for hydrogen.[2] The dissociation energies E are, for H_2, 4.48 eV; Li_2^7, 1.03; Na_2^{23}, 0.73; K_2^{39}, 0.51; Rb_2^{85}, 0.49; Cs_2^{133}, 0.45. The equilibrium separation R for H_2 is 1.07 Å and for Rb_2 and Cs_2 about 4 Å. This is not surprising, since the diameters of the Rb and Cs atoms are about five times the diameter of the hydrogen atom. The valence electrons which give rise to the binding are then farther from the nuclei.

The difference between the singlet and triplet interactions has been described and explained in terms of the antisymmetry requirement on the total electronic wave function. That this difference gives rise to observable results can be seen as follows. The total electronic wave function for the two atoms at large separations is a superposition of singlet and triplet wave functions. Since the singlet and triplet interactions are different, the total electronic wave function after the collision may be a different superposition of the singlet and triplet wave functions. There is thus a certain probability that two atoms (in a static external field of a few gauss) will undergo a collision with the change in quantum numbers

$$I_1 S_1 F_1 M_1 \; I_2 S_2 F_2 M_2 \rightarrow I_1 S_1 F_1' M_1' \; I_2 S_2 F_2' M_2',$$

where the primed numbers need not be the same as the unprimed numbers. Such collisions, which occur because of the difference in the

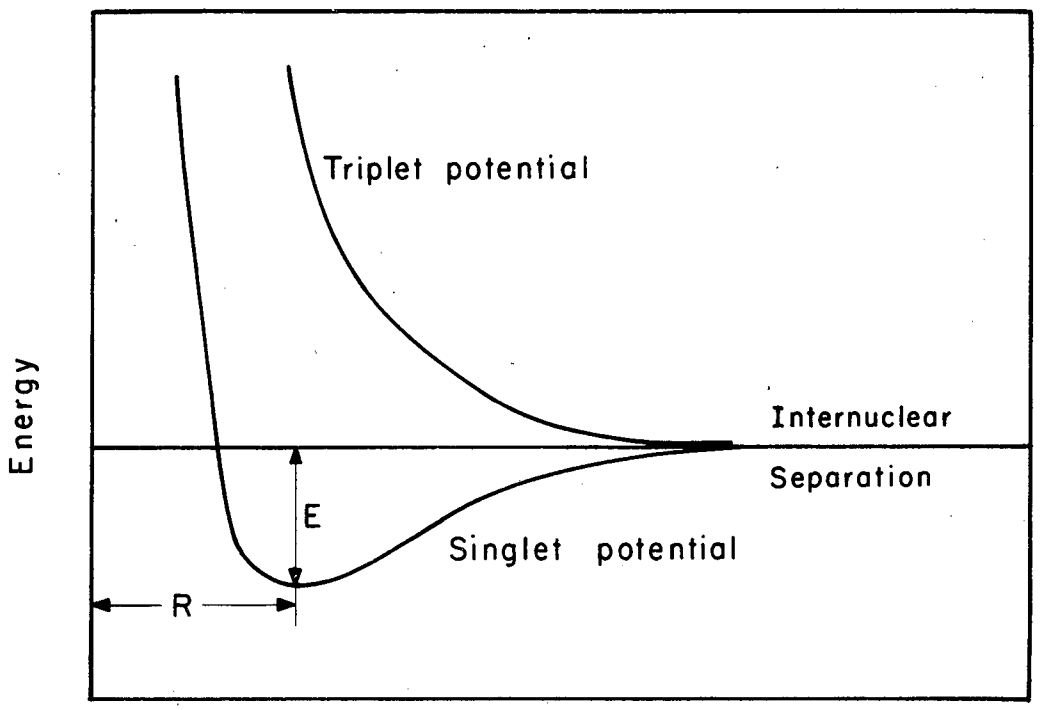

Fig. 1. The form of the interatomic potential between two hydrogen atoms.[1] R is the equilibrium separation and E is the dissociation energy.

singlet and triplet potentials, are called spin-exchange collisions. For zero nuclear spin, such a collision would be that of atoms with oppositely directed spins interchanging spin orientations during the collision.

In order to make a crude estimate for the cross section, consider the case of zero nuclear spin with the first atom in the spin-up state and the second with spin down, i. e. ,

$$\psi_i = \alpha(1)\beta(2) = \frac{1}{2}[\alpha(1)\beta(2)+\beta(1)\alpha(2)] + \frac{1}{2}[\alpha(1)\beta(2)-\beta(1)\alpha(2)] \equiv A + B,$$

where A is a triplet term and B is a singlet term. In the adiabatic time-dependent perturbation approximation, [3]

$$\psi_f = e^{-i\int\omega_t dt}\left[A+Be^{i\int(\omega_t-\omega_s)dt}\right].$$

Define $\phi \equiv \int(\omega_t-\omega_s)dt = \int(V_t-V_s)dt/\hbar$, then the probability for the first atom leaving the collision in the spin-down state is

$$P = \left|\beta(1)^*\alpha(2)^*\,\psi_f\right|^2 = \left|\frac{1}{2}(1-e^{i\phi})\right|^2 = \sin^2\phi/2.$$

But $\phi \approx (V_t-V_s)\,T_c/\hbar$, where the collision time $T_c \approx 10^{-12}$ sec and $V_t-V_s \approx 1$ eV; therefore $\phi \approx 10^3$ radians. Assuming this very large phase shift to be random, and averaging over many collisions, one finds that P becomes 1/2. Thus a spin-exchange collision is very likely to occur if the atoms are close enough for V_t-V_s to be appreciable. Thus $\sigma \approx 4\pi R^2 \approx 4\pi(4\times10^{-8}\text{cm})^2 \approx 2\times10^{-14}\text{cm}^2$. This value, which is several times a geometrical cross section, is typical for the spin-exchange cross section.

The first theoretical estimates of the cross section, by Purcell and Field[4] and by Wittke and Dicke, [5] are based on a semiclassical impact parameter method. Dalgarno has given a quantum mechanical description of the spin-exchange process in terms of the singlet and triplet scattering amplitudes. [6] Glassgold's work extends Dalgarno's treatment to several special cases using density matrix techniques. [7] In addition, he introduces the symmetrization necessary for the correct treatment of collisions between atoms with identical nuclei. The calculations of Part II of this thesis are based on the results of Dalgarno and Glassgold.

Glassgold and Lebedeff have obtained scattering amplitudes for one-electron atoms by solving the radial Schrödinger equation numerically, assuming various potentials as representations of the interaction.[8] They compare exact solutions with various approximations. They calculate differential cross sections, demonstrating the importance of proper symmetrization in the case of identical atoms. They also predict interesting resonances in the energy dependence of the cross sections. Their calculations apply primarily to spin-exchange collisions between hydrogen atoms.

Bender[9] and others[10] have calculated the line broadening and frequency shifts arising from spin-exchange collisions.

B. The Importance of Spin-Exchange Collisions

During the last 8 or 9 years there have been three or four dozen publications devoted to the study or application of the spin-exchange process. Some of the areas in which spin-exchange collisions are important will now be mentioned briefly.

In order to deduce correct densities of hydrogen atoms in interstellar space by observing the intensity of 21-cm radiation incident upon the earth, it is essential to understand all mechanisms affecting the relative populations of the ground-state hyperfine levels. The calculations by Purcell and Field[4] indicate that in many cases spin-exchange collisions are the predominant determinant of these populations.

The ground-state hyperfine separation of hydrogen is of considerable experimental interest because it can be calculated with great precision.[5] An accurate measurement yields information on the least known theoretical quantities: the proton recoil and structure factors. The first measurement of the separation was by the atomic beam method.[11] Wittke and Dicke made a paramagnetic resonance measurement,[5] the accuracy of which was limited by spin-exchange broadening. More precise determinations were made by transferring polarization from an optically pumped sodium or rubidium vapor to a hydrogen isotope by means of the spin-exchange process.[12] The most precise measurement to date is that by Crampton, Kleppner, and Ramsey,[13] employing the hydrogen maser. The maser oscillation frequency is

"pulled" by a mistuned cavity by an amount proportional to the atomic resonance width. By increasing the beam flux the resonance width can be increased by as much as a factor of four through the spin-exchange mechanism. The cavity is adjusted until the oscillation frequency is independent of the flux. The cavity frequency must then be centered on the atomic frequency unless the spin-exchange process itself introduces a shift. In fact it does, but it depends upon the atomic resonance width in the same manner as the cavity pulling but in the opposite sense. Thus any systematic frequency error which would ordinarily be introduced by the spin-exchange process is exactly canceled by compensating mistuning of the cavity. Verification of the accuracy of this method of tuning can be made by broadening the resonance by adding deuterium and noting that the frequency is not shifted. Thus a process which at one time limited the accuracy of a measurement was later understood sufficiently well to use it in improving the accuracy of the same measurement!

The technique of transferring polarization from an optically pumped species was first performed by Dehmelt between Na atoms and quasi-free electrons.[14] His measurement of the g value of the electron reduced the uncertainty of direct measurements of g_s from 5000 to 30 ppm, thus furnishing an important direct verification of the quantum electrodynamic corrections. Wilkinson and Crane have recently completed a direct measurement to 0.03 ppm by determining the difference between the orbital frequency and the spin precession frequency of free electrons in a magnetic field.[15]

Spin exchange has been utilized to polarize several atoms with S ground states in order to study the ground-state hyperfine structure: H, D, T, N^{14}, N^{15}, and P.[16] The hyperfine separations in nitrogen and phosphorus, which are large considering that there are no unpaired s-electrons, are believed to arise from exchange polarization of the closed shell core by the unpaired p electrons.[17]

Finally, but of primary importance for this thesis, spin-exchange collisions can be used to study the forces between atoms and thereby to optimize the interatomic potential parameters. Usually

considerable information exists concerning the singlet potential from molecular spectroscopy. However, the spin-exchange probe should yield useful information concerning the triplet potentials. As in the work of Glassgold and Lebedeff,[8] one can predict cross sections by assuming various forms for the potentials. Accurate measurements should help determine which potentials best describe the physical situation; for example, see the paper by Lebedeff on the determination of Lennard-Jones parameters from total scattering cross sections.[18]

The need for accurate measurements of spin-exchange cross sections to facilitate the study of interatomic potentials is the primary motivation behind the research of this thesis. Part II treats the question of how meaningful cross sections can be deduced from optical pumping experiments. Part III describes a precise measurement employing a transient optical pumping technique. The problem of deducing interatomic potential information from the cross sections is left to the theoreticians.

C. Techniques for Measuring Spin-Exchange Cross Sections

1. Optical Pumping Experiments

a. Steady-state optical pumping experiments

The technique of Dehmelt[14] was used in all the early spin-exchange measurements. This method, described in greater detail in II. D. 2, involves a determination of the change in the transmitted light of the pumped species when an rf resonance field is applied to the second species. In the limit of low light intensity, the signal depends upon the spin-exchange cross section, the densities of both species, and the relaxation times of both species. Crude measurements have been made by this technique of the cross sections for Na-Rb^{85},[19] Na-K,[20] and K-e^-.[20] A precise measurement of the Rb^{87}-Rb^{85} cross section has been performed by Jarrett,[21] who was the first to include an accurate density measurement with an optical pumping exchange cross-section measurement. A related experiment, in which the Zeeman resonances are resolved, is that of Anderson and Ramsey[22] on Na.

b. Transient optical pumping experiments

The Franzen technique for studying the relaxation of optically pumped species[23] has been applied to cross-section measurements of Rb^{87} by Bouchiat and Brossel,[24] of Rb-Cs by Grossetête,[25] and in the experiment of this thesis. The signal (see IIC) depends only on the cross section, the density of the second species, and the relaxation times of the first species. The deduction of the cross section from the signal is then somewhat less involved than the case of the Dehmelt experiment, since fewer auxiliary parameters must be determined.

2. Paramagnetic Resonance Experiments

The paramagnetic resonance experiments are often carried out at large fields (several thousand gauss) to decouple the electron from the nucleus. Optical pumping, optical pumping plus spin exchange, or the Maxwell-Boltzmann factor is used to give a population difference. Usually the line width of the $F = I + \frac{1}{2}$, $M = 0$ to $F = I - \frac{1}{2}$, $M = 0$ transition is determined. Under proper conditions the reciprocal of the line width or the spin-dephasing time T_2 is essentially equal to the spin-exchange time. The paramagnetic resonance experiments possess the great advantage that standards exist which permit precise density measurements by comparisons of absorption signals.

Hildebrandt, Booth, and Barth applied the technique to hydrogen;[26] Arditi and Carver, to Rb^{87};[27] Moos and Sands, to Rb^{85}, Rb^{87}, and Cs^{133};[28] Davidovits and Knable, to Rb^{87}.[29] Information on the scattering amplitudes and phase shifts has also been obtained in the Rb-e^- experiment of Balling, Hanson, and Pipkin[30] and that of Cs-e^- by Balling and Pipkin.[31] They find that the ratio of the line width to the line shift is independent of density but yields information about the phase shifts.

3. Atomic Beam Measurements

Crossed-beam experiments have the decided advantage of permitting the determination of differential cross sections and their kinetic energy dependence. Efficient single-atom detectors afford accurate

density-measuring capabilities as well. The other methods yield only total cross sections over a very limited energy range. If the additional complexities of the beam experiments can be overcome, they should produce a wealth of information. K-e^- measurements have been conducted at New York University by Rubin, Perel, and Bederson.[32]

D. The History and Significance of the Research of this Thesis Amidst the Rapid Advances in the Field

In light of the many spin-exchange measurements outlined in IC, it might seem that no further experiment is justified. But this research was undertaken in the summer of 1962 at the suggestion of Professor A. E. Glassgold that accurate spin-exchange cross sections would aid in the study of interatomic potentials. At that time there were no measurements with an asserted precision of better than a factor of two or three. At present there are six published measurements with a claimed precision of 20% or better.[21, 25, 28, 29] However, the quoted values of these precise cross sections for Rb are not in agreement: 1.9 ± 0.4, 0.85 ± 0.10, and 1.85 ± 0.23 in units of 10^{-14} cm^2. The less precise measurements vary over a much wider spectrum. Consequently, the research was carried to completion to offer another measurement by a different technique.

Dr. Joseph Winocur suggested that Franzen's method of studying spin relaxation be applied to a measurement of the Rb-Cs spin-exchange cross section. Suppose that, in the absence of the Cs, the Rb relaxation is represented by a characteristic time T_1. With the addition of the Cs the new relaxation time is $\tau = T_1 T_{E1}/(T_1+T_{E1})$, where T_{E1} is the Rb-Cs spin-exchange time. From the spin-exchange time, a cross section can be determined if the density is known. Recognizing the problem of procuring a shutter with the desired characteristics, the author made a study of the possibility of using the Dehmelt experiment[14] for a precise measurement. It was noted that all the previous papers neglected nuclear spin in the analysis except for that by Anderson and Ramsey,[22] whose experiment would be meaningless without its inclusion. In the winter of 1962 the author arrived at expressions for the Dehmelt signal for particular cases which clearly

showed the importance of the nuclear spins in deducing a cross section from the signal. Uniform relaxation was assumed; self exchange was neglected. Particular solutions of the Franzen-type signal[23] again demonstrated the importance of the nuclear spins. The signal is a single exponential, neglecting nuclear spin, but the sum of two exponentials for I = 3/2. The Franzen method was pursued because it had not been applied to spin-exchange measurements and because it involves the determination of fewer auxiliary parameters.

In the summer of 1963, Madame Grossetête vistied Berkeley and reported that she was performing a Franzen-type experiment and had arrived at a general solution for the signal for any value of the nuclear spin. Her calculations[33] and some experimental results[25] have since been published. Soon after her visit, the author extended his calculations to the case of arbitrary nuclear spin. The transient solution of IIC then stands as an independent confirmation of the density-matrix treatment by Grossetête.

In the winter of 1963 the calculations for the Dehmelt-type signal were repeated for arbitrary nuclear spin. In the fall of 1964 the calculations were again extended to allow for ground-state relaxation by electron randomization in addition to uniform relaxation.[34] The results bring into question Jarrett's precise measurement of the Rb^{87}-Rb^{85} cross section[21] (see IID), thereby increasing the need for further measurements of that cross section.

The cross-section measurements of Part III are the most precise determinations to date of the Rb^{87}-Rb^{87} and Rb^{87}-Cs^{133} total spin-exchange cross sections. It is true that these results may not be so significant as they would have been in the absence of other precise measurements. But for the Rb^{87}-Rb^{87} case they add weight to two previous measurements at the expense of three others. And for the Rb^{87}-Cs^{133} case they confirm the less precise measurement by Grossetête. Furthermore, these results represent a truly independent measurement, since the experimental details of the other transient experiments have not been published. In addition, some of the information gained in the study of the various problems which have arisen is of interest in its own right.

The primary experimental problem was that of obtaining a shutter with the desired characteristics (see IIIC. 4). Problems also arose in the interpretation of the density measurement data (IIIF. 1). The early work was done with Zeeman optical pumping, but difficulty was encountered with least-squares convergence of some of the data to the sum of two exponentials. The hyperfine pumping method, involving only a single exponential, gave no difficulty, and was used in measuring the cross sections reported in IIIG.

E. Plan of the Thesis

The thesis divides itself into two main parts. Part II is an analysis of the Franzen-type and Dehmelt-type experiments to determine the effects of including the nuclear spins. The various terms of the rate equations are discussed in detail. It is found that, in general, nuclear spin must be included if correct spin-exchange cross sections are to be deduced from Zeeman optical pumping experiments employing circularly polarized light and performed in weak magnetic fields. (Some confirmative data are presented in Part IV.) Part III contains a detailed description of a hyperfine optical pumping experiment used to measure the Rb^{87}-Rb^{87} and Rb^{87}-Cs^{133} spin-exchange cross sections. The spin-exchange time is determined by the Franzen technique; a scanning Fabry-Perot interferometer is utilized to estimate the density.

An outline of the topics to be treated is given in the introduction of each part, thereby eliminating any need for a more detailed discussion here. If the reader is primarily concerned with a summary of the experimental techniques and results see IIIA and IIIB (skim IIIB. 1) and IIIG.

II. THE IMPORTANCE OF NUCLEAR SPIN EFFECTS IN EXTRACTING ALKALI SPIN-EXCHANGE CROSS SECTIONS FROM ZEEMAN OPTICAL PUMPING EXPERIMENTS EMPLOYING CIRCULARLY POLARIZED LIGHT AND PERFORMED IN WEAK MAGNETIC FIELDS

A. Introduction

The motivation for and history of these calculations is given in ID.

One point of misunderstanding should be cleared up from the outset. There are two quantities referred to as spin-exchange cross sections: an example of the first is defined by Eq. (37); an example of the second is $1/T_{E1}\bar{v}d$, where T_{E1} is the spin-exchange time given by Eq (45), $\bar{v}$ is the average relative velocity between the colliding atoms, and d is the density of the species not being optically pumped. The cross sections of the two kinds will be represented by Q and σ, respectively. Since the collision time is much shorter than a period of the hyperfine precession, the hyperfine coupling has little effect during the collision. Therefore, since the spin-exchange process is an electronic interaction, the cross section for electron spin-exchange should be essentially independent of the nuclear spins. The cross section in this case is of the σ type and is the cross section reported by experimentalists. However, in a low magnetic field the electron spin is coupled to the nuclear spin by the hyperfine interaction, and the good quantum numbers are IJFM. For this case, the cross sections of interest are between different FM states and are of the Q type. They depend upon the nuclear spin I even though the interaction is diagonal in M_I. The Q cross sections are seen to be very nearly the product of a σ cross section (the cross section for $I = 0$) and a matrix element which is independent of I if M_S is a good quantum number. All the nuclear-spin effects referred to in this part arise from the nuclear-spin dependence of the matrix element, not of σ. The optical pumping signals can then depend upon the nuclear spin because of the hyperfine coupling. Failure to include these effects can lead to errors of several hundred per cent in the values of the spin-exchange cross sections deduced from optical pumping experiments.

The calculations apply to spin exchange between two alkali atoms in their ground states. The pumping radiation is assumed to be circularly

polarized D_1 light with equal-intensity hyperfine components. Restrictions are placed on the absorption in order to simplify the expressions for the signals. The rate equations used to describe the experiments are given in Section IIB; a diagonal density matrix is used. The following contributions to the rate equations are then discussed: 1, pumping radiation; 2, excited-state disorientation; 3, ground-state relaxation; 4, spin exchange between unlike atoms; and 5, self spin exchange. Solutions to the rate equations of Section IIB are obtained for the Franzen-type transient experiment[23] as applied to spin-exchange measurements in Section IIC; self-exchange effects are neglected. The expression for the signal in the usual Dehmelt-type steady-state spin-exchange experiment[14] is found in Section IID in the limit of low light intensity. Applications or comparisions are made to the results of Dehmelt,[14] Jarrett,[21] Balling et al.,[30] and Anderson and Ramsey.[22]

B. Rate Equations

Consider the description of the time variation of the populations of two different species of alkali atoms in a static magnetic field of weak intensity. The ISFM representation is then best. $\underset{\sim}{F}$ is the total angular momentum obtained by coupling the nuclear angular momentum $\underset{\sim}{I}$ to the electronic angular momentum $\underset{\sim}{S}$($\underset{\sim}{J} = \underset{\sim}{S}$, since $\underset{\sim}{L} = 0$). M is the projection of $\underset{\sim}{F}$ along the axis defined by the external magnetic field and the incident light beam. Species 1 is optically pumped and has a density in the ground state F_1M_1 of $p_{F_1M_1}$ and a total density of p. The second species is disoriented continuously during part or all of the experiment and has a density $d_{F_2M_2}$ in the ground state F_2M_2 and a total density d. The first species has a density $n_{J_1F_1M_1}$ in the excited state $J_1F_1M_1$. The time variation of $p_{F_1M_1}$ can be described as follows:

$$\dot{p}_{F_1M_1} = -p_{F_1M_1} \sum_{J_1'F_1'M_1'q} \int_0^\infty L_q(\nu) P'_{\nu q}(F_1M_1, J_1'F_1'M_1') \, d\nu$$

$$+ \sum_{J_1' F_1' M_1'} n_{J_1' F_1' M_1'} P'''(J_1' F_1' M_1', F_1 M_1)/\tau_{J_1'}$$

$$- p_{F_1 M_1} \sum_{F_1' M_1'} w(F_1 M_1, F_1' M_1') + \sum_{F_1' M_1'} p_{F_1' M_1'}, w(F_1' M_1', F_1 M_1)$$

$$- \sum_{\substack{F_1' M_1' \\ F_2 M_2 \\ F_2' M_2'}} \int \Big\{ p_{F_1 M_1} d_{F_2 M_2} Q_E(F_1 M_1 F_2 M_2, F_1' M_1' F_2' M_2') - p_{F_1' M_1'} d_{F_2' M_2'} Q_E(F_1' M_1' F_2' M_2', F_1 M_1 F_2 M_2) \Big\} f(v_E) v_E d^3 v_E$$

$$- \sum_{\substack{F_1' M'_1 \\ F_1'' M_1'' \\ F_1''' M_1'''}} \int \Big\{ p_{F_1 M_1} p_{F_1' M_1'} Q_{S1}(F_1 M_1 F_1' M_1', F_1'' M_1'' F_1''' M_1''') - p_{F_1'' M_1''} p_{F_1''' M_1'''} Q_{S1}(F_1'' M_1'' F_1''' M_1''', F_1 M_1 F_1' M_1') \Big\} f(v_{S1}) v_{S1} d^3 v_{S1}. \tag{1}$$

$\sum_q \int_0^\infty L_q(\nu) P'_{\nu q}(F_1 M_1, J_1' F_1' M_1') d\nu$ is the probability per unit time that an atom in the ground state $F_1 M_1$ will absorb a resonance photon and make a transition to the $F_1' M_1'$ substate of the $^2P_{J_1'}$ excited state; $L_q(\nu)d\nu$ is the light intenstiy with polarization q and with frequencies between ν and $\nu+d\nu$. $\frac{1}{\tau_{J_1'}} P'''(J_1' F_1' M_1', F_1 M_1)$ is the probability per unit time for the reverse process; $\tau_{J_1'}$ is the radiative lifetime of

an atom in one of the substates of the $^2P_{J_1'}$ excited state. The quantity $w(F_1M_1, F_1'M_1')$ is the probability per unit time for an atom in the substate F_1M_1 of the ground state to make a transition to the $F_1'M_1'$ substate of the ground state by relaxation processes excluding spin exchange. In the last two terms the subscript E refers to exchange between atoms of different species and S to exchange between atoms of the same species. $Q(F_1M_1F_2M_2, F_1'M_1'F_2'M_2')$ is the cross section for a spin-exchange collision between two atoms in which the first atom makes a transition from F_1M_1 to $F_1'M_1'$ and the second from F_2M_2 to $F_2'M_2'$. The function f(v) is the distribution of relative velocities v with the normalization $\int f(v)d^3v = 1$. The populations are then affected by 1, the pumping radiation, 2, excited-state disorientation, 3, ground-state relaxation, 4, spin exchange with the second species, and 5, self spin exchange between atoms of the same species.

The form of these equations corresponds to a diagonal density-matrix approach, which should be valid in the absence of coherence-producing interactions. The radio-frequency fields used in the experiments treated in this thesis are ordinarily applied in a manner producing very little coherence. Magnetic field inhomogeneities are usually sufficient to damp out any coherence effects in a time short compared with the other significant times of the problem. A solution of the rate equations, including the off-diagonal elements but neglecting nuclear spins, has been obtained by other workers; it is discussed in Section IID.4.

Each of the terms in Eq. (1) will now be discussed and the simplifying assumptions stated. The resulting rate equations are given in IIB. 6. For the experiments treated in this paper, the 2(2I+1) equations for each species (excluding excited-state equations) reduce to two equations with the variables being the longitudinal electronic polarizations of the various hyperfine levels as defined in (13). However, the particular assumptions made in Sections IIC and IID are necessary before this reduction is complete; therefore, the rate equations of IIB. 6 are not entirely in that form.

1. Pumping Radiation

a. Circularly polarized D_1 resonance radiation

It is assumed that the resonance radiation is filtered with only the D_1 line $(^2P_{1/2} \rightarrow {}^2S_{1/2})$ incident upon the resonance cell containing two alkali species. It is further assumed that it is circularly polarized so that M_1 must change by +1 for electric dipole transitions; i.e.,

$$L_q(\nu)P'_{\nu q}(F_1M_1,\ J_1'F_1'M_1') = L(\nu)P'_\nu(F_1M_1,\ \tfrac{1}{2}\ F_1'M_1{+}1)\ \delta_{J_1',\,1/2}\,\delta_{M_1',\,M_1+1}.$$

b. Equal-intensity hyperfine components throughout the cell

It should always be possible to write

$$P'_\nu(F_1M_1,\ \tfrac{1}{2}F_1'M_1{+}1) = P'(F_1M_1,\ \tfrac{1}{2}\ F_1'M_1{+}1)f(\nu-\nu^0{}_{F_1M_1,\,F_1'M_1'}),\ \text{where}$$

$f(\nu-\nu^0{}_{F_1M_1,\,F_1'M_1'})$ represents the broadening of the absorption line around the center frequency $\nu^0{}_{F_1M_1,\,F_1'M_1'}$ by, for example, Doppler or pressure effects; furthermore $\int_0^\infty f(\nu-\nu^0{}_{F_1M_1,\,F_1'M_1'})d\nu = 1$. Now assume that

$$\int_0^\infty L(\nu)f(\nu-\nu^0{}_{F_1M_1,\,F_1'M_1'})d\nu = L;$$

i.e., over the frequencies for which absorption occurs, the light at each point of the cell is independent of the frequency. Experimental care must be taken to achieve equal hyperfine components in the incident light; this can usually be done by regulating the amount of self-reversal in the lamp bulb, if one is able to monitor the components. Since the hyperfine components often have different absorption coefficients, the absorption must usually be kept low to approximate equal components throughout the cell (see IIB. 1. c).

The first term in (1) contains

$$\sum_{\substack{J_1'F_1'M_1' \\ q}} \int_0^\infty L_q(\nu) P'_{\nu q}(F_1 M_1, J_1' F_1' M_1') d\nu = L \sum_{F_1'} P'(F_1 M_1, \tfrac{1}{2} F_1' M_1 + 1)$$

$$\equiv LP'(F_1 M_1), \tag{2}$$

$$P'(F_1 M_1) \propto \sum_{F_1'} \left(\left| \left\langle I_1 J_1 F_1 M_1 \left| r(1,1) \right| I_1 J_1 F_1' M_1 + 1 \right\rangle \right|^2 \right)_{J_1 = 1/2}, \tag{3}$$

where $r(1, q)$ denotes the qth component of the valence electron position vector $\underset{\sim}{r}$, which is a tensor of rank 1; see Edmonds,[35] Chapter 5. Using Edmonds' (5.4.1) and (7.1.7), one finds

$$P'(F_1 M_1) \propto \sum_{F'_1} \begin{pmatrix} F_1 & 1 & F_1' \\ M_1 & 1 & -M_1 - 1 \end{pmatrix}^2 \Delta(F_1, F_1') . \tag{4}$$

The squared 3-j symbol in (4) is given in Table I (from Edmonds' Table 2). The quantities

$$\Delta(F_1, F_1') \equiv 6(2F_1+1)(2F_1'+1) \begin{Bmatrix} 1/2 & F_1' & I_1 \\ F_1 & 1/2 & 1 \end{Bmatrix}^2 = \Delta(F_1', F_1) \tag{5}$$

are given in Table II; they were obtained with the aid of Edmonds' Table 5. Then, for $F_1 = I_1 \pm 1/2$,

$$P'(\pm, M_1) = P'(F_1 M_1) = C\left[1 \mp M_1/(I_1 + 1/2)\right] = C\left[1 - 2(F_1 - I_1) M_1/(I_1 + 1/2)\right], \tag{6}$$

where $LP'(F_1 M_1)$ is the total probability per unit time that an atom in the substate $F_1 M_1$ will absorb a resonance photon; C is a constant independent of the quantum numbers of interest.

c. Low absorption

The experiments analyzed in this paper employ the transmission monitoring technique; the changes in the absorption constitute the signals.

Table I. Values of $\begin{pmatrix} F_1 & 1 & F'_1 \\ M_1 & 1 & -M_1-1 \end{pmatrix}^2$

F_1	F'_1: $I_1 + 1/2$	F'_1: $I_1 - 1/2$
$I_1 + 1/2$	$\frac{2[I_1^2 + 2I_1 + 3/4 - M_1 - M_1^2]}{(2I_1+1)(2I_1+2)(2I_1+3)}$	$\frac{2[I_1^2 - 1/4 - 2M_1I_1 + M_1^2]}{4I_1(2I_1+1)(2I_1+2)}$
$I_1 - 1/2$	$\frac{2[I_1^2+2I_1+3/4+(2I_1+2)M_1+M_1^2]}{4I_1(2I_1+1)(2I_1+2)}$	$\frac{2[I_1^2 - 1/4 - M_1 - M_1^2]}{(2I_1-1)2I_1(2I_1+1)}$

Table II. Values of $\Delta(F_1, F'_1) = 6(2F_1+1)(2F'_1+1)\begin{Bmatrix} 1/2 & F'_1 & I_1 \\ F_1 & 1/2 & 1 \end{Bmatrix}^2$

F_1	F'_1: $I_1 + 1/2$	F'_1: $I_1 - 1/2$
$I_1 + 1/2$	$\frac{(2I_1+2)(2I_1+3)}{2I_1+1}$	$\frac{4I_1(2I_1+2)}{2I_1+1}$
$I_1 - 1/2$	$\frac{4I_1(2I_1+2)}{2I_1+1}$	$\frac{2I_1(2I_1-1)}{2I_1+1}$

The absorption by the cell can be found as follows. The light intensity at frequency ν and time t at a penetration depth of x into the resonance cell of length ℓ decreases by

$$dL(\nu, x, t) = -L(\nu, x, t) \sum_{F_1 M_1 F_1'} p_{F_1 M_1}(x, t)\, P_\nu'(F_1 M_1, \tfrac{1}{2} F_1' M_1 + 1) h\nu \, dx \quad (7)$$

between x and $x+dx$; it is assumed that $L(\nu, x, t)$ is circularly polarized, so that $\Delta M_1 = +1$ in absorption. With the assumptions of IIB. 1. b (7) yields, for the absorption,

$$A(\ell, t) = L(0, t) - L(\ell, t) = \int_0^\ell L(x, t) \sum_{F_1 M_1} p_{F_1 M_1}(x, t) P'(F_1 M_1) h\nu \, dx. \quad (8)$$

The conditions necessary for maintaining the equality of the hyperfine components throughout the cell can be found by integrating (7):

$$L(\nu, x, t) = L(\nu, 0, t) \exp\left[-\int_0^x \sum_{F_1 M_1 F_1'} p_{F_1 M_1}(x', t) P_\nu'(F_1 M_1, \tfrac{1}{2} F_1' M_1 + 1) h\nu \, dx' \right]$$

$$= L(\nu, 0, t) \exp\left[-\int_0^x k_\nu(x', t) dx' \right], \quad (9)$$

where $L(\nu, 0, t)$ is constant over the frequencies for which the absorption is appreciable. $L(\nu, x, t) \approx L(\nu, 0, t)$ if the absorption is low, i. e., $k_0 \ell << 1$, where k_0 is the peak absorption coefficient. But for some cases slightly less stringent requirements are sufficient. For example, if the excited-state hyperfine separation and the Zeeman splittings are much less than the absorption width, the two resolved components are approximately equal to each other at each point of the cell if $k_0 \ell / (2I_1 + 1) << 1$. This requirement is satisfactory, since the difference in their absorption rates is only $1/(2I_1+1)$ times the total absorption rate. Experimentally, an extrapolation to zero absorption or a demonstration that the signals are independent of absorption should be made.

With the assumption that the absorbable light at each point in the cell is independent of frequency, the absorption (and the signals) can be expressed as a simple function of

$$\sum_{F_1M_1} p_{F_1M_1}(x,t)P'(F_1M_1) = Cp\left[1 - \sum_{F_1M_1} 2(F_1-I_1)M_1 p_{F_1M_1}/(I_1+\tfrac{1}{2})p\right], \tag{10}$$

which can be expressed as a function of the electronic polarization as follows. It can be shown that $\langle FM|S_z|FM\rangle = 2(F-I)M/(2I+1)$. Then the absorption is

$$A(\ell,t) \approx k\int_0^{\ell} L(x,t)\,(1 - P(x,t))dx, \tag{11}$$

with the absorption coefficient $k = Cph\nu$ and

$$P = 2\langle S_{1z}\rangle = 2\sum_{F_1M_1} p_{F_1M_1}\langle F_1M_1|S_{1z}|F_1M_1\rangle/p = \sum_{F_1} P_{F_1}, \tag{12}$$

$$P_{F_1=I_1\pm1/2} = P_{\pm} = \pm \sum_{M_1=-I_1\mp1/2}^{I_1\pm1/2} M_1 p_{I_1\pm1/2,\,M_1}/(I_1+1/2)p. \tag{13}$$

Here P is the longitudinal electronic polarization, and P_+ and P_- are the contributions to this polarization from the two hyperfine levels. Completely analogous polarizations D, D_+, D_- are defined for the second species. Although only P is needed to define the signal, P_+ and P_- usually appear in coupled equations and must be solved for separately in order to determine P. Or, since

$$\langle I_{1z}\rangle = \langle F_{1z}\rangle - \langle S_{1z}\rangle = I_1P_+ - (I_1+1)P_-, \tag{14}$$

the equations for $\langle \dot{S}_z\rangle$ and $\langle \dot{I}_z\rangle$ can be found and solved instead. In either case the $2(2I+1)$ equations for each species reduce to two equations in the cases treated in this paper. Consequently, the rate equations for P_+ and P_- rather than for $p_{F_1M_1}$ will be determined. Then

the absorption term of (1) gives

$$(\dot{P}_{\pm})_{Abs} = \mp L \sum_{M_1} M_1 p_{F_1 M_1} P'(F_1 M_1)/(I_1 + 1/2)p, \tag{15}$$

when (2), (6), and (13) are used.

2. Excited-State Disorientation

It is customary, in analyzing optical pumping signals in which a buffer gas at a pressure greater than 1 cm of Hg is used, to assume that complete mixing occurs in the excited state. In other words, the excited-state polarization relaxes nonradiatively in a time short compared with the radiative lifetime. Recently, excited-state disorientation cross sections have been reported which are considerably smaller than those found earlier for sodium. Yellin and Marrus[36] report for Rb^{87}-Ne collisions a cross section of 5×10^{-17} cm^2, which implies an excited-state relaxation time of $T \approx 0.4$ μsec for Jarrett's experiment (2.8 cm of Ne at 90° C).[21] The corresponding mixing parameter

$$q = \tau/(T + \tau) \tag{16}$$

(where $\tau = 2.85\times10^{-8}$ sec is the excited-state lifetime against spontaneous emission) is less than 10%, implying that Jarrett's conditions produced very little excited-state mixing. Since one of the primary objectives of this work is to determine the importance of the nuclear spins in Jarrett's experiment, it is of interest to investigate the necessity of the assumption of complete mixing. It will be shown that the signal for Jarrett's experiment (in the limit of low light intensity) is independent of the amount of excited-state disorientation, regardless of the mechanism producing the mixing.

By definition, the probabilities P'' must satisfy

$$\sum_{F_1 M_1} P''(J_1' F_1' M_1', F_1 M_1) = 1. \tag{17}$$

The time rate of change of the density of excited atoms in the $F_1' M_1'$ substate of the $^2P_{J_1'}$ excited state is

$$\dot{n}_{J_1'F_1'M_1'} = L \sum_{F_1M_1} p_{F_1M_1} P'(F_1M_1, J_1'F_1'M_1') \delta_{M_1', M_1+1} \delta_{J_1', 1/2}$$

$$-n_{J_1'F_1'M_1'}/\tau_{J_1'} - \sum_{J_1''F_1''M_1''} n_{J_1'F_1'M_1'} w_e(J_1'F_1'M_1', J_1''F_1''M_1'')$$

$$+ \sum_{J_1''F_1''M_1''} n_{J_1''F_1''M_1''} w_e(J_1''F_1''M_1'', J_1'F_1'M_1'), \tag{18}$$

where $w_e(J_1'F_1'M_1', J_1''F_1''M_1'')$ is the probability per unit time that an excited atom in state $J_1'F_1'M_1'$ will make a transition to the excited state $J_1''F_1''M_1''$ (without returning to the ground state by emission of a photon). Since the excited-state populations reach equilibrium very rapidly ($\leq \tau$), the equilibrium value of $n_{J_1'F_1'M_1'}$ can be used in (1). Notice that at equilibrium (18) is of the form

$$\underset{\sim}{R}\underset{\sim}{n} = L\underset{\sim}{m}, \tag{19}$$

where R is a matrix independent of the various populations, $\underset{\sim}{n}$ is a column vector with components $n_{J_1'F_1'M_1'}$, and $\underset{\sim}{m}$ has components

$$m_{J_1'F_1'M_1'} = \sum_{F_1M_1} p_{F_1M_1} P'(F_1M_1, J_1'F_1'M_1') \delta_{M_1', M_1+1} \delta_{J_1', 1/2}. \tag{20}$$

Therefore $\underset{\sim}{n}$ and $n_{J_1'F_1'M_1'}$ are proportional to L or higher-order terms in L. The reemission term of (1), which becomes, when (13) is used,

$$(\dot{P}_\pm)_{Re} = \pm \sum_{J_1'F_1'M_1'} n_{J_1'F_1'M_1'} \sum_{M_1} M_1 P''(J_1'F_1'M_1', F_1M_1)/(I_1+1/2)p\tau_{J_1'}, \tag{21}$$

is then proportional to L or higher-order terms in L. This term vanishes in the transient experiment of Section IIC for which $L = 0$; it will be found to be independent of P_+ and P_- for the Dehmelt-type steady-state experiment of Section IID.

3. Ground-State Relaxation

The most common assumption for the ground-state relaxation in optical pumping experiments is that it is uniform. It has been suggested that a better assumption is that the electron spin is randomized without affecting the nuclear spin.[37] Recently Bouchiat[38] has carried out a detailed analysis of relaxation in paraffin-coated cells. She assumes that the relaxation arises from the interaction of randomly oriented disorientation fields with the spin of the valence electron. This section contains a short derivation of the contributions to the rate equations from such an interaction which parallels the elegant density matrix treatment by Bouchiat. A discussion in terms of the assumptions of uniform relaxation and electron randomization is also given.

The general relaxation Hamiltonian satisfying the above restrictions can be written

$$\mathcal{H}' = \sum_{kq} a_k (-)^q S(1, q) H(k, -q), \tag{22}$$

where $H(k, q)$ is the qth component of a randomly oriented field of rank k [for example, a scalar contact field ($k = 0$) or a tensor dipole field ($k = 2$); see reference 38] and is independent of the alkali atom spin coordinates. $S(1, q)$ is the qth component of the spin of the valence electron of the alkali atom.[35]

Abragam[39] shows that, if $\mathcal{H}'(t) = AF(t)$, where A is an operator acting only on the variables of the alkali, and $F(t)$ is a random function independent of the alkali, the transition probability from state a to b of the alkali is

$$w_{ab} = |(a|A|b)|^2 J(\omega_{ab}), \tag{23}$$

and

$$J(\omega_{ab}) \equiv \int_{-\infty}^{\infty} g(\tau) e^{-i\omega_{ab}\tau} d\tau = 2\tau_c \left\langle F(t)F(t) \right\rangle / (1 + \omega_{ab}^2 \tau_c^2), \tag{24}$$

provided that

$$g(\tau) \equiv \left\langle F(t)F(t+\tau)\right\rangle = \left\langle F(t)F(t)\right\rangle \exp(-|\tau|/\tau_c), \qquad (25)$$

i.e., if the interaction can be characterized by a single correlation time τ_c.

It should be a good approximation to assume that the Hamiltonian (22) is the sum of several terms each of which satisfies the restrictions of Abragam's derivation. Then

$$w(F_1M_1, F_1'M_1') = \sum_q |(F_1M_1|S(1,q)|F_1'M_1')|^2 J_q(\omega_{F_1M_1, F_1'M_1'}), \qquad (26)$$

where $J_q(\omega_{F_1M_1, F_1'M_1'})$ is proportional to $\left\langle \sum_{k'k} a_{k'}^* a_k H^*(k', -q)H(k, -q)\right\rangle$, which is independent of q, since the fields are randomly oriented.

In a magnetic field of low intensity the hyperfine energy separation ΔW is much larger than the Zeeman separation ω_F. Furthermore, since the operator $S(1,q)$ is a tensor of rank one, M_1 can change by at most one unit in each relaxation event. Therefore, $J(\Delta W)$ and $J(\omega_F)$ are sufficient to characterize the ground-state relaxation. Then one has

$$w(F_1M_1, F_1'M_1')$$

$$= \sum_q |(F_1M_1|S(1,q)|F_1'M_1')|^2 (\delta_{F_1'F_1} J(\omega_F) + \delta_{F_1'F\pm1} J(\Delta W)) \qquad (27)$$

$$= \begin{pmatrix} F_1' & 1 & F_1 \\ -M_1' & M_1'-M_1 & M_1 \end{pmatrix}^2 \Delta(F_1, F_1') \left\{ \delta_{F_1, F_1'} \left[J(\omega_F) - J(\Delta W)\right] + J(\Delta W)\right\} /4. \qquad (28)$$

Equation (28) substituted into the third and fourth terms of (1) yields

$$\left(\sum_{M_1} M_1 \dot{p}_{F_1M_1}\right)_R = -\left[J(\omega_F) - J(\Delta W)\right] \sum_{M_1} M_1 p_{F_1M_1}/(2I_1+1)^2$$

$$-\left\{3 \sum_{M_1} M_1 p_{F_1M_1}/4 - \sum_{F_1'M_1'} \Delta(F_1, F_1')\Gamma(F_1, F_1', M_1') p_{F_1'M_1'}/4\right\} J(\Delta W). \qquad (29)$$

The quantities

$$\Gamma(F_1, F_1', M_1') \equiv \sum_{M_1} M_1 \begin{pmatrix} F_1 & 1 & F_1' \\ M_1 & M_1'-M_1 & -M_1' \end{pmatrix}^2 = M_1'\Gamma(F_1, F_1') \tag{30}$$

are given in Table III, which was found by using Table 2 of Edmonds.[35]

Table III. Values of $\Gamma(F_1, F_1', M_1') = \sum_{M_1} M_1 \begin{pmatrix} F_1 & 1 & F_1' \\ M_1 & M_1'-M_1 & -M_1' \end{pmatrix}^2 = M_1'\Gamma(F_1, F_1')$.

	F_1'	
F_1	$I_1 + 1/2$	$I_1 - 1/2$
$I_1+1/2$	$\dfrac{M_1'(4I_1^2 + 8I_1 - 1)}{(2I+1)(2I_1+2)(2I_1+3)}$	$\dfrac{M_1'(2I_1+3)}{2I_1(2I_1+1)}$
$I_1-1/2$	$\dfrac{M_1'(2I_1 - 1)}{(2I_1+1)(2I_1+2)}$	$\dfrac{M_1'(4I_1^2-5)}{(2I_1-1)2I_1(2I_1+1)}$

Now define two time constants

$$1/T_1 = [J(\omega_F) - J(\Delta W)]/(2I_1+1)^2, \tag{31}$$

$$1/T_1' = J(\Delta W). \tag{32}$$

Equations (13) and (29) give, for the contributions to the rate equations from ground-state relaxation,

$$(\dot{P}_+)_R = -P_+/T_1 - (2I_1^2+I_1+1)P_+/(2I_1+1)^2T_1' - (2I_1+2)(2I_1+3)P_-/2(2I_1+1)^2T_1', \tag{33}$$

$$(\dot{P}_-)_R = -P_-/T_1 - I_1(2I_1-1)P_+/(2I_1+1)^2T_1' - (2I_1^2+3I_1+2)P_-/(2I_1+1)^2T_1'. \tag{34}$$

To gain some insight into the time constants (31) and (32) consider the two limiting cases.

a. Zeeman relaxation

Let $J(\Delta W) << J(\omega_F)$, i.e., $T_1 << T_1'$; in this case the correlation time is much longer than the hyperfine period τ_{HF}. Relaxation then occurs within the Zeeman sublevels of each hyperfine level, but transitions between hyperfine levels are rare. The longitudinal electronic polarization of each hyperfine level relaxes as a single exponential of time constant T_1. T_1 is then the characteristic time for Zeeman relaxation in which the electron spin is randomized within each hyperfine level, but no transitions are made between hyperfine levels.

b. Relaxation by electron randomization

Let $J(\omega_F) \approx J(\Delta W)$, $T_1' << T_1$, $\tau_c << \tau_{HF}$; in this case both Zeeman and hyperfine transitions occur. The electron spin is completely randomized without affecting the nuclear spin. Such a model has been used by workers at Princeton.[37] The term electron randomization will be used to identify this limit, and T_1' is the electron randomization relaxation time.

Then in general if the relaxation occurs through random interactions of the alkali electron spin with randomly oriented disorientation fields not involving the alkali spins, the relaxation of the electronic polarization of each hyperfine level can be represented as the sum of two contributions: that from Zeeman relaxation [$J(\Delta W) << J(\omega_F)$, $\tau_c >> \tau_{HF}$, $T_1 << T_1'$] and that from electron randomization [$J(\Delta W) \approx J(\omega_F)$, $\tau_c << \tau_{HF}$, $T_1' << T_1$].

Equations (33) and (34) correspond to Eqs. (53) and (54) of Bouchiat[38] if (12) and (14) are recalled and her time constants T_e and T_n are related to T_1 and T_1' by

$$1/T_e = 1/T_1 + 1/T_1',$$

$$1/T_n = 1/T_1 + 2/(2I_1 + 1)^2 T_1'.$$

A Hamiltonian of the form of (22) was taken by Bouchiat to describe relaxation in wall-coated cells. It appears that (22) should hold for relaxation by collisions with buffer gas atoms. For example, Bernheim's model is of this type.[40] For buffer gas collisions the

correlation time is no longer than the collision time, $\approx 10^{-12}$ sec, which is much shorter than the hyperfine period. One would then expect disorientation by buffer gas collisions to satisfy the conditions for electron randomization.

There appear to be at least two reasons for retaining uniform relaxation as a decay channel in addition to the mechanism proposed by Bouchiat. First, in cells containing sidearms for controlling the densities of the various alkali vapors, effusion to and from the sidearms constitutes a uniform relaxation process; i. e., when an atom in a given F_1M_1 substate leaves the cell, it is replaced by an atom which has an equal probability of being in any of the $2(2I_1+1)$ possible substates. Second, if an atom sticks to the wall for a very long time, the relaxation will again be uniform. For example, if the atom undergoes many effective relaxation collisions of the Bouchiat type while on the wall, its initial polarization will be completely destroyed. Imperfections in the coating or small pools of alkali atoms could cause long dwell times.

Uniform relaxation can be included by adding to (28), $w(F_1M_1, F_1'M_1') = 1/2(2I_1+1)T_1''$, where T_1'' is the uniform relaxation time. Equations (33) and (34) readily become

$$(\dot{P}_+)_R = -P_+/T_1''' - (2I_1^2+I_1+1)P_+/(2I_1+1)^2T_1' - (2I_1+2)(2I_1+3)P_-/2(2I_1+1)^2T_1', \quad (35)$$

$$(\dot{P}_-)_R = -P_-/T_1''' - I_1(2I_1-1)P_+/(2I_1+1)^2T_1' - (2I_1^2+3I_1+2)P_-/(2I_1+1)^2T_1', \quad (36)$$

where $1/T_1''' \equiv 1/T_1 + 1/T_1''$ to simplify the subsequent equations. See Part IV for a discussion of experimentally determined relaxation times.

4. Spin Exchange Between Nonidentical Atoms

The results of Dalgarno's quantum-mechanical treatment of the spin-exchange process are used to describe the spin-exchange collisions between the two species.[6] Atoms 1 and 2 are assumed to be nonidentical and in doublet spin states. The stationary state of the molecule formed by atoms 1 and 2 is then either a singlet or triplet state. With each of the possible states there is associated a potential which describes the interaction of the two atoms. In the usual manner, the solution of the scattering problem leads to the scattering amplitudes, f_s and f_t, where the subscripts refer to singlet and triplet. Spin-orbit interactions are neglected in the collision. For spin-exchange collisions for which the initial states of atoms 1 and 2 are A and B and the final states A' and B', the cross section is[6]

$$Q(AB, A'B') = Q_1(A, B)\,\delta_{A,A'}\,\delta_{B,B'} + Q_2(AB, A'B'), \tag{37}$$

where

$$Q_1(A, B) = \int \left\{ \left| \frac{f_s+3f_t}{4} \right|^2 + \frac{1}{2}\mathrm{Re}\left[(f_s^*+3f_t^*)(f_t-f_s)\right] \left\langle AB \left| \underset{\sim}{S}_1 \cdot \underset{\sim}{S}_2 \right| AB \right\rangle \right\} d\Omega, \tag{38}$$

$$Q_2(AB, A'B') = \int |f_t - f_s|^2 \, d\Omega \left| \left\langle A'B' \left| \underset{\sim}{S}_1 \cdot \underset{\sim}{S}_2 \right| AB \right\rangle \right|^2, \tag{39}$$

and $\underset{\sim}{S}_1$ and $\underset{\sim}{S}_2$ are the electronic angular momenta of atoms 1 and 2. In the experiments discussed in this paper, contributions from the direct cross section, Q_1, cancel out because only net changes in state populations are detected. From (39) it is seen that the spin-exchange experiments considered here yield information about the interatomic potentials only through the quantity $\int |f_t - f_s|^2 \, d\Omega$.

The matrix element of $\underset{\sim}{S}_1 \cdot \underset{\sim}{S}_2$ between FM states is found as follows. By Edmonds,[35] (5.2.4),

$$\left\langle F_1' M_1' F_2' M_2' \left| \underset{\sim}{S}_1 \cdot \underset{\sim}{S}_2 \right| F_1 M_1 F_2 M_2 \right\rangle =$$

$$\sum_q (-)^q \left\langle F_1' M_1' \left| S_1(1, q) \right| F_1 M_1 \right\rangle \left\langle F_2' M_2' \left| S_2(1, -q) \right| F_2 M_2 \right\rangle . \tag{40}$$

Then by the Wigner-Eckart theorem, Edmonds' (5.4.1),

$$\left\langle F_1' M_1' F_2' M_2' \left| \underset{\sim}{S}_1 \cdot \underset{\sim}{S}_2 \right| F_1 M_1 F_2 M_2 \right\rangle =$$

$$\sum_q (-)^{q+F_1'+F_2'} (-)^{(M_1'+M_2')} \begin{pmatrix} F_1' & 1 & F_1 \\ -M_1' & q & M_1 \end{pmatrix} \begin{pmatrix} F_2' & 1 & F_2 \\ -M_2' & -q & M_2 \end{pmatrix} (F_1' \| S_1(1) \| F_1)(F_2' \| S_2(1) \| F_2). \tag{41}$$

Application of (7.1.7) and (5.4.4) of Edmonds leads to

$$Q_2(F_1 M_1 F_2 M_2,\ F_1' M_1' F_2' M_2') / \int |f_t - f_s|^2 \, d\Omega$$

$$= \left| \left\langle F_1' M_1' F_2' M_2' \left| \underset{\sim}{S}_1 \cdot \underset{\sim}{S}_2 \right| F_1 M_1 F_2 M_2 \right\rangle \right|^2$$

$$= \frac{9}{4}(2F_1+1)(2F_1'+1)(2F_2+1)(2F_2'+1)$$

$$\times \sum_q \begin{pmatrix} F_1' & 1 & F_1 \\ -M_1' & q & M_1 \end{pmatrix}^2 \begin{pmatrix} F_2' & 1 & F_2 \\ -M_2' & -q & M_2 \end{pmatrix}^2 \begin{Bmatrix} 1/2 & F_1' & I_1 \\ F_1 & 1/2 & 1 \end{Bmatrix}^2 \begin{Bmatrix} 1/2 & F_2' & I_2 \\ F_2 & 1/2 & 1 \end{Bmatrix}^2 . \tag{42}$$

The following selection rules are immediately apparent:

$M_1 + M_2 = M_1' + M_2'$, $|\Delta M_1| \leq 1$, $|\Delta M_2| \leq 1$. Using (5), one has

$$Q_2(F_1 M_1 F_2 M_2,\ F_1' M_1' F_2' M_2') =$$

$$\frac{\int |f_t - f_s|^2 \, d\Omega}{16} \Delta(F_1, F_1') \Delta(F_2, F_2') \sum_q \begin{pmatrix} F_1' & 1 & F_1 \\ -M_1' & q & M_1 \end{pmatrix}^2 \begin{pmatrix} F_2' & 1 & F_2 \\ -M_2' & -q & M_2 \end{pmatrix}^2 . \tag{43}$$

Then the exchange term in (1) becomes, with (13),

$$(\dot{P}_{\pm})_E = \frac{\mp 1}{4T_{E1}d} \sum_{\substack{F_1'M_1' \\ F_2M_2 \\ F_2'M_2'}} \frac{\Delta(F_1, F_1')\Delta(F_2, F_2')}{(I_1 + 1/2)p}$$

$$\times \sum_{M_1 q} M_1 \begin{pmatrix} F_1' & 1 & F_1 \\ -M_1' & q & M_1 \end{pmatrix}^2 \begin{pmatrix} F_2' & 1 & F_2 \\ -M_2' & -q & M_2 \end{pmatrix}^2$$

$$\times (p_{F_1M_1}\, d_{F_2M_2}\, {}^{-p}_{F_1'M_1'}\, d_{F_2'M_2'}), \tag{44}$$

where

$$\frac{1}{T_{E1}} = \frac{d}{4} \iint |f_t - f_s|_E^2 \, d\Omega \, v_E f(v_E) d^3 v_E = \frac{d}{T_{E2}p} \cdot \tag{45}$$

Here T_{E1} is the time which characterizes the influence of the second species upon the first species through the spin-exchange interaction. Similarly, T_{E2} indicates the effect upon the second species arising from spin-exchange collisions with atoms of the first species. The normalization is in agreement with accepted convention. Equations (44) are not yet in a useful form because they depend upon the populations and not just upon the polarizations. The further assumptions made for the particular experiments in Sections IIC and IID will correct this situation.

A short digression will show that the cross sections derived here agree with the results of Glassgold.[7] From (43) one has, for the case in which the second species is unpolarized,

$$\sum_{\substack{F_2M_2 \\ F_2'M_2'}} Q_2(F_1M_1F_2M_2,\ F_1'M_1'F_2'M_2')$$

$$= 2(2I_2+1) \frac{\int |f_t - f_s|^2}{16} d\Omega \Delta(F_1, F_1') \begin{pmatrix} F_1' & 1 & F_1 \\ -M_1' & M_1' - M_1 & M_1 \end{pmatrix}^2 \tag{46}$$

$$= 2(2I_2 + 1) \int \sigma\,(fm, f'm'; \theta) d\Omega \qquad (47)$$

in the notation of Glassgold with $f = F_1$ and $m = M_1$. The $\Delta(F_1, F_1')$ defined by (5) and given in Table II are identical to the $\Delta(f, f')$ of Glassgold, which are listed in his Table I. Therefore, by Edmonds' (3.7.3),

$$\sigma(fm, f'm'; \theta) = \frac{1}{3} \left| \frac{f_1 - f_0}{4} \right|^2 \Delta(f, f')(fmf'-m' \,|\, 1\ m-m')^2, \qquad (48)$$

where $f_1 = f_t$ and $f_0 = f_s$. Equation (48) agrees with Eq. (4.6) of Glassgold's paper.

If one defines

$$Q_2(F_1 M_1 F_2 M_2,\ F_1' M_1' F_2' M_2') = \pi S_0^2 \left| \left\langle F_1' M_1' F_2' M_2' \left| P_1 + e^{i\phi} P_0 \right| F_1 M_1 F_2 M_2 \right\rangle \right|^2_{\substack{\text{Average} \\ \text{over } \phi}} \qquad (49)$$

then (44) are still valid if $1/T_{E1}d$ is replaced by $\pi S_0^2 \bar{v}/2$. This substitution places the rate equation in the form used, for example, by Anderson and Ramsey.[22] This approach is similar to the semiclassical description used by Wittke and Dicke[5] and by Purcell and Field.[4] P_1 and P_0 are the projection operators for a total electronic angular momentum of 1 or 0. The relative phase shift, ϕ, between the singlet and triplet parts of the wave function, arises from the difference between the singlet and triplet potentials, which describe the molecule formed by an alkali atom of each kind. For a "strong" collision, ϕ is assumed to be large and random ($\langle \cos\phi \rangle = 0$); collisions not classified as strong are neglected. The maximum impact parameter for which a strong collision occurs, S_0, is usually taken as the one for which the particle will have zero velocity at the top of the centrifugal barrier for the singlet potential. Glassgold and Lebedeff have discussed the validity of this approximation.[8]

5. Self Spin Exchange

Glassgold[7] has shown that the cross section for identical atoms, corresponding to (37), is

$$Q(AA', A''A''') = \int \left| \left\langle A''A''' \left| \mathcal{J} \right| AA' \right\rangle \right|^2 d\Omega/2, \tag{50}$$

where the first atom in the collision has electronic spin $\underset{\sim}{\sigma}_1/2$ and undergoes a transition from state A (representing $F_1 M_1$) to A'' in an exchange collision with the second atom of spin $\underset{\sim}{\sigma}'_1/2$, which makes a transition from A' to A''':

$$\mathcal{J} = F_d(\theta) + F_x(\theta)\, \underset{\sim}{\sigma}_1 \cdot \underset{\sim}{\sigma}'_1 + (-)^{2i+1} Q [F_d(\pi - \theta) + F_x(\pi - \theta) \underset{\sim}{\sigma}_1 \cdot \underset{\sim}{\sigma}'_1], \tag{51}$$

$$F_d = (f_s + 3f_t)/4, \tag{52}$$

$$F_x = (f_t - f_s)/4, \tag{53}$$

$$\underset{\sim}{I} = \underset{\sim}{I}_1 + \underset{\sim}{I}'_1; \; I_1 = I'_1 = i, \tag{54}$$

$$\underset{\sim}{S} = \underset{\sim}{S}_1 + \underset{\sim}{S}'_1 = \underset{\sim}{\sigma}/2; \; S_1 = S'_1 = 1/2. \tag{55}$$

Here Q is the operator which interchanges both the electronic and nuclear spins; $Q = Q_n Q_e$, where

$$Q_e \left| IM_I SM_S \right\rangle = (-)^{S+1} \left| IM_I SM_S \right\rangle, \tag{56}$$

$$Q_n \left| IM_I SM_S \right\rangle = (-)^{I+2i} \left| IM_I SM_S \right\rangle. \tag{57}$$

For a general operator O,

$$\left\langle A''A''' \left| QO \right| AA' \right\rangle = \left\langle A'''A'' \left| O \right| AA' \right\rangle; \tag{58}$$

the first quantum numbers of each bra or ket always refer to the first atom.

The factor of 2 in (50) is necessary in order to avoid counting final states twice. The cross section is then

$$
\begin{aligned}
Q(AA', A''A''') = \int \Big[& |F_d(\theta)|^2 \delta_{A, A''} \delta_{A', A'''} + |F_d(\pi-\theta)|^2 \delta_{A, A'''} \delta_{A', A''} \\
& + (-)^{2i+1} 2 \operatorname{Re} \Big\{ F_d^*(\theta) F_d(\pi-\theta) \, \delta_{A, A', A'', A'''} \\
& + F_d^*(\theta) F_x(\pi-\theta) \left\langle AA' \left| \underset{\sim}{\sigma}_1 \cdot \underset{\sim}{\sigma}'_1 \right| AA' \right\rangle \delta_{A, A''} \delta_{A', A'''} \\
& + F_d^*(\pi-\theta) F_x(\theta) \left\langle A'A \left| \underset{\sim}{\sigma}_1 \cdot \underset{\sim}{\sigma}'_1 \right| AA' \right\rangle \delta_{A, A'''} \delta_{A', A''} \\
& + F_x^*(\theta) F_x(\pi-\theta) \left\langle A''A''' \left| \underset{\sim}{\sigma}_1 \cdot \underset{\sim}{\sigma}'_1 \right| AA' \right\rangle \left\langle A'''A'' \left| \underset{\sim}{\sigma}_1 \cdot \underset{\sim}{\sigma}'_1 \right| AA' \right\rangle \Big\} \\
& + 2 \operatorname{Re} F_d^*(\theta) F_x(\theta) \left\langle AA' \left| \underset{\sim}{\sigma}_1 \cdot \underset{\sim}{\sigma}'_1 \right| AA' \right\rangle \delta_{A, A''} \delta_{A', A'''} \\
& + 2 \operatorname{Re} F_d^*(\pi-\theta) F_x(\pi-\theta) \left\langle A'A \left| \underset{\sim}{\sigma}_1 \cdot \underset{\sim}{\sigma}'_1 \right| AA' \right\rangle \delta_{A, A'''} \delta_{A', A''} \\
& + |F_x(\theta)|^2 \left| \left\langle A''A''' \left| \underset{\sim}{\sigma}_1 \cdot \underset{\sim}{\sigma}'_1 \right| AA' \right\rangle \right|^2 \\
& + |F_x(\pi-\theta)|^2 \left| \left\langle A'''A'' \left| \underset{\sim}{\sigma}_1 \cdot \underset{\sim}{\sigma}'_1 \right| AA' \right\rangle \right|^2 \Big] d\Omega/2 \, .
\end{aligned}
\tag{59}
$$

Fortunately, none of the terms involving deltas contributes to the rate equations, as can be seen by substituting (59) into (1). The $|F_x(\theta)|^2$ term in (59) is the cross section one would expect between two nonidentical atoms. The $|F_x(\pi-\theta)|^2$ term arises because no distinction can be made between the incident and target atoms. The $2 \operatorname{Re} F_x^*(\theta) F_x(\pi-\theta)$ term arises from the quantum-mechanical identity of the two colliding atoms. An estimate of the interference term using the model of Purcell and Field is given in Appendix I and indicates that it is small compared with the other two terms, at least for Rb^{87}; it will be neglected entirely in the subsequent calculations. Equation (59) in (1) produces, with the aid of (13) and the fact that $\int |F_x(\theta)|^2 d\Omega = \int |F_x(\pi-\theta)|^2 d\Omega$,

$$(\dot{P}_{\pm})_{S1} = \frac{\mp 1}{4\,T_{S1}P} \sum_{\substack{F_1'M_1' \\ F_1''M_1'' \\ F_1'''M_1'''}} \frac{\Delta(F_1, F_1'')\Delta(F_1', F_1''')}{(I_1+1/2)p} \sum_{M_1} M_1$$

$$\times \begin{pmatrix} F_1'' & 1 & F_1 \\ -M_1'' & q & M_1 \end{pmatrix}^2 \begin{pmatrix} F_1''' & 1 & F_1' \\ -M_1''' & -q & -M_1' \end{pmatrix}^2 (p_{F_1M_1}\,p_{F_1'M_1'} - p_{F_1''M_1''}\,p_{F_1'''M_1'''}). \tag{60}$$

Here T_{S1}, defined by

$$\frac{1}{T_{S1}} = \frac{p}{4} \iint |f_t - f_s|^2_{S1}\, d\Omega\, v_{S1}\, f(v_{S1}) d^3 v_{S1}, \tag{61}$$

is the self-spin-exchange time for the first species; for the second species,

$$\frac{1}{T_{S2}} = \frac{d}{4} \iint |f_t - f_s|^2_{S2}\, d\Omega\, v_{S2}\, f(v_{S2}) d^3 v_{S2}\,. \tag{62}$$

6. Simplified Rate Equations

Combining the results of this section, one has

$$\dot{P}_{F_1 = I_1 \pm 1/2} = \mp L \sum_{M_1} \frac{M_1 p_{F_1M_1}\, P'(F_1M_1)}{(I_1+1/2)p}$$

$$\pm L \sum_{J_1'F_1'M_1'} \frac{n_{J_1'F_1'M_1'}}{L} \sum_{M_1} \frac{M_1 P''(J_1'F_1'M_1', F_1M_1)}{(I_1+1/2)p\,\tau_{J_1'}}$$

$$- \frac{P_{\pm}}{T_1'''} - \delta_{F_1, I_1+1/2}\,[(2I_1^2+I_1+1)P_+ - (I_1+1)(2I_1+3)P_-]/(2I_1+1)^2 T_1'$$

$$-\delta_{F_1,I_1-1/2}\,[I_1(2I_1-1)P_+ + (2I_1^2+3I_1+2)P_-]/(2I_1+1)^2T_1'$$

$$\mp \frac{1}{4T_{E1}^d} \sum_{\substack{F_1'M_1' \\ F_2M_2 \\ F_2'M_2'}} \frac{\Delta(F_1,F_1')\Delta(F_2,F_2')}{(I_1+1/2)p} \sum_{M_1 q} \begin{pmatrix} F_1' & 1 & F_1 \\ -M_1' & q & M_1 \end{pmatrix}^2 \begin{pmatrix} F_2' & 1 & F_2 \\ -M_2' & -q & M_2 \end{pmatrix}^2$$

$$\times M_1 (p_{F_1M_1}{}^d{}_{F_2M_2} - p_{F_1'M_1'}{}^d{}_{F_2'M_2'})$$

$$\mp \frac{1}{4T_{S1}^p} \sum_{\substack{F_1'M_1' \\ F_1''M_1'' \\ F_1'''M_1'''}} \frac{\Delta(F_1,F_1'')\Delta(F_1',F_1''')}{(I_1+1/2)p} \sum_{M_1 q} \begin{pmatrix} F_1'' & 1 & F_1 \\ -M_1'' & q & M_1 \end{pmatrix}^2 \begin{pmatrix} F_1''' & 1 & F_1' \\ -M_1''' & -q & M_1' \end{pmatrix}^2$$

$$\times M_1 (p_{F_1M_1}\, p_{F_1'M_1'} - p_{F_1''M_1''}\, p_{F_1'''M_1'''}) \,. \qquad (63)$$

Clearly additional assumptions are necessary before these equations involve only $P_\pm$ and $D_\pm$ and none of the individual populations.

C. Transient Experiment

In this section the rate equations are solved for the case of a Franzen[23] transient experiment applied to the measurement of the spin-exchange cross section in a resonance cell containing the vapors of two alkalis. The first species is optically pumped and the envelope of the decay in the dark of its electronic polarization is traced out, yielding a single relaxation time τ if the nuclear spin is neglected. In the presence of the second species, which is continuously disoriented by an rf field, the relaxation time is shortened to

$$1/T = 1/\tau + 1/T_{E1}, \qquad (64)$$

neglecting the nuclear spins. A measurement of the density of the

second species then permits a determination of the spin-exchange cross section. This transient experiment has the advantage that the density and relaxation times of only one of the two species must be measured, whereas in the steady-state experiments they must be determined for both species.

The transient signal is conveniently defined as

$$S(I_1, t) = \frac{A(\infty) - A(t)}{A(\infty) - A(0)} \ , \tag{65}$$

where the absorption at time t is given by (11). Equation (11) becomes, on the assumption that P is independent of x and that L is approximately independent of x and t,

$$A(\ell, t) \approx k\ell\,[1-P(t)]\ L. \tag{66}$$

In that case,

$$S(I_1, t) \approx P(t)/P(0) = \left\langle S_{1z}(t) \right\rangle / \left\langle S_{1z}(0) \right\rangle \ . \tag{67}$$

If the resonance cell contains no buffer gas, P should be independent of x because of the rapid motion of the atoms; L is approximately independent of x and t if the absorption is kept small. At any rate, (67) is valid only if experimental care is taken to satisfy (66); otherwise the signal becomes a much more complicated function of the polarization, as indicated by (11) and (65).

The continuous application of the rf field at the resonance frequency of the second species,

$$\approx 2.8\ H_0/(2I_2+1)\ \text{Mc/sec}, \tag{68}$$

where H_0 is the static magnetic field strength in gauss, results in equal populations among the substates of each hyperfine state throughout the experiment. Consequently, one has in (63)

$$d_{F_2M_2} = d_{F_2}/(2F_2+1) \tag{69}$$

and

$$d_{F_2'M_2'} = d_{F_2'}/(2F_2'+1). \tag{70}$$

(It may take a time "T_2" in paramagnetic resonance nomenclature for

the spins to dephase after the application of the rf field; but since the field is applied continuously and is sufficiently strong to overpower the pumping effect of the light, the coherence will not reappear.)

It is necessary to exclude the self-exchange term in (63) from the following solution because of its nonlinear character. Experimentally this is a good approximation whenever T_{S1} is much longer than the shortest time constants affecting the relaxation; for example, for two alkalis, cross exchange dominates over self exchange when $d >> p$. The importance of self exchange is also reduced because there is no change in the absorption if the two atoms undergoing a collision have both initial and final states in the same hyperfine state,

$$\Delta A \propto \Delta \sum_M Mp_{FM} \propto M_1(-1) + M_1'(-1) + M_1''(+1) + M_1'''(+1) = 0, \qquad (71)$$

since $M_1 + M_1' = M_1'' + M_1'''$ always.[23]

With (69), (70), $T_{S1} = \infty$, and $L = 0$ the $1/T_{E1}$ term in (63) becomes identical in form to the T_1' term in (29) or (33) and (34). Then

$$\dot{P}_+ = -P_+/T_1''' - (1/T_{E1} + 1/T_1')[(2I_1^2+I_1+1)P_+ + (I_1+1)(2I_1+3)P_-]/(2I_1+1)^2, \qquad (72)$$

$$\dot{P}_- = -P_-/T_1''' - (1/T_{E1}+1/T_1')[I_1(2I_1-1)P_+ + (2I_1^2+3I_1+2)P_-]/(2I_1+1)^2. \qquad (73)$$

Alternatively, with the aid of (12) and (14),

$$\langle \dot{S}_{1z} \rangle = -(1/T_1''' + 1/T_1' + 1/T_{E1}) \langle S_{1z} \rangle + 2(1/T_1' + 1/T_{E1}) \langle I_{1z} \rangle /(2I_1+1)^2, \qquad (74)$$

$$\langle \dot{I}_{1z} \rangle = -[1/T_1''' + (1/T_1' + 1/T_{E1})2/(2I_1+1)^2] \langle I_{1z} \rangle. \qquad (75)$$

The solution of the above equations yields, for the signal for a Franzen-type spin-exchange experiment,

$$S(I_1, t) = (1-a)\exp(-t/\tau_1) + a\exp(-t/\tau_2), \qquad (76)$$

where

$$1/\tau_1 = 1/T_1 + 1/T_1' + 1/T_1'' + 1/T_{E1}, \qquad (77)$$

$$1/\tau_2 = 1/T_1 + 1/T_1'' + 2(1/T_1' + 1/T_{E1})/(2I_1 + 1)^2, \tag{78}$$

$$a = 2\langle I_{1z}(0)\rangle /(4I_1^2 + 4I_1 - 1)\ \langle S_{1z}(0)\rangle \tag{79}$$

$$= 4[I_1 P_+(0) - (I_1+1)P_-(0)]/(4I_1^2 + 4I_1 - 1)P(0), \tag{80}$$

where I_1 is the nuclear spin of the first species, T_{E1} is defined by (45), and T_1, T_1', T_1'' are the times for Zeeman relaxation, electron randomization, and uniform relaxation, respectively. $\langle S_{1z}\rangle$ and $\langle I_{1z}\rangle$ are defined by (12) and (14). Note that for $I_1 = 0$ or $I_1 = 1/2$, $P_- = 0$, implying $\langle I_{1z}\rangle = 2I_1 \langle S_{1z}\rangle$. For $T_1'' = T_{E1} = \infty$ these results agree with Bouchiat;[38] for $T_1 = T_1' = T_1'' = \infty$, with Grossetête.[33]

For a single species, the relaxation of the electronic polarization is a single exponential if the relaxation is by Zeeman or uniform transitions only and is the sum of two exponentials [with characteristic times in the ratio $(2I_1 + 1)^2/2$] if it is by electron randomization only. The experimental results of Bouchiat and Brossel[41] for Rb^{87} in paraffin-coated cells indicate that, at least in some cases, the relaxation is a single exponential; i. e., Zeeman or uniform relaxation is dominant. On the other hand, one would expect buffer gas collisons to produce relaxation by electron randomization, since the correlation time is short compared with the hyperfine period if the collision is elastic.

In summary, the signal for the Franzen-type transient experiment, neglecting self spin exchange, is given by (76). In general, the signal is the sum of two exponentials. For Zeeman or uniform relaxation the ratio of the time constants ranges from 1 to $(2I + 1)^2/2$, depending upon the relative sizes of T_1, T_1'', and T_{E1}. For the electron randomization case, the ratio is always $(2I_1+1)^2/2$. In either case, the nuclear spin effects must be included in the analysis if correct spin-exchange cross sections are to be deduced. See Part IV for experimental support of (76).

D. Steady-State Experiments in the Limit of Low Light Intensity

1. Rate Equations

In this section some experiments are analyzed in the limit of low light intensity, for which

$$p_{F_1M_1} = p/2(2I_1+1) + \pi_{F_1M_1}, \tag{81}$$

$$d_{F_2M_2} = d/2(2I_2+1) + \delta_{F_2M_2}, \tag{82}$$

where the deviations $\pi_{F_1M_1}$ and $\delta_{F_2M_2}$ of the populations from the depolarized values are small and proportional to L in first order. Substitution of (81) and (82) into (63), dropping terms proportional to L^2 (e.g., $\pi_{F_1M_1} L$, $\pi_{F_1M_1}\delta_{F_2M_2}$, etc.) immediately, leads to the following rate equations in the limit of low light intensity (see Appendix II for the details);

$$\dot{P}_+ \approx \frac{(2I_1+2)(2I_1+3)}{6(2I_1+1)^2}\left(L_+C+\frac{D_++D_-}{T_{E1}}\right)-\left[\frac{1}{T_1'''}+\left(\frac{1}{T_1'}+\frac{1}{T_{E1}}\right)\frac{2I_1^2+I_1+1}{(2I_1+1)^2}+\frac{2I_1(2I_1-1)}{3(2I_1+1)^2T_{S1}}\right]P_+ \tag{83}$$

$$-\frac{(2I_1+2)(2I_1+3)}{2(2I_1+1)^2}\left(\frac{1}{T_1'}+\frac{1}{T_{E1}}+\frac{2}{3T_{S1}}\right)P_- ,$$

$$\dot{P}_- \approx \frac{2I_1(2I_1-1)}{6(2I_1+1)^2}\left(L_-C+\frac{D_++D_-}{T_{E1}}\right)-\frac{I_1(2I_1-1)}{(2I_1+1)^2}\left(\frac{1}{T_1'}+\frac{1}{T_{E1}}+\frac{2}{3T_{S1}}\right)P_+$$

$$-\left[\frac{1}{T_1'''}+\left(\frac{1}{T_1'}+\frac{1}{T_{E1}}\right)\frac{2I_1^2+3I_1+2}{(2I_1+1)^2}+\frac{(2I_1+2)(2I_1+3)}{3(2I_1+1)^2T_{S1}}\right]P_- . \tag{84}$$

The corresponding equations for the second species are found by setting $L_+ = L_- = 0$, interchanging $P_\pm$ and $D_\pm$, and replacing the subscript 1 by 2 in (83) and (84). L_+ and L_-, defined by (A-16), are independent

of the polarizations and are linearly proportional to the light intensity L; $L_+ = L_- = L$ for complete mixing. Recall that the hyperfine components in the incident light are equal; i.e., L_+ and L_- do not refer to unequal pumping components.

Transforming to the $\langle S_{1z} \rangle$ and $\langle I_{1z} \rangle$ representation by using (12) and (14), one finds

$$\langle \dot{S}_{1z} \rangle = [(I_1+1)(2I_1+3)L_+C/2 + I_1(2I_1-1)L_-C/2 + (4I_1^2+4I_1+3)\langle S_{2z} \rangle / T_{E1}] / 3(2I_1+1)^2$$

$$- \left[\frac{1}{T_1'''} + \frac{1}{T_1'} + \frac{1}{T_{E1}} + \frac{4I_1(2I_1+2)}{3(2I_1+1)^2 T_{S1}} \right] \langle S_{1z} \rangle + 2 \left(\frac{1}{T_1'} + \frac{1}{T_{E1}} + \frac{1}{T_{S1}} \right) \langle I_{1z} \rangle / (2I_1+1)^2, \tag{85}$$

$$\langle \dot{I}_{1z} \rangle = I_1(2I_1+2)[(2I_1+3)L_+C/2 - (2I_1-1)L_-C/2 + 4\langle S_{2z} \rangle / T_{E1}] / 3(2I_1+1)^2$$

$$+ \frac{4I_1(2I_1+2)\langle S_{1z} \rangle}{3(2I_1+1)^2 T_{S1}} - \left[\frac{1}{T_1'''} + 2 \left(\frac{1}{T_1'} + \frac{1}{T_{E1}} + \frac{1}{T_{S1}} \right) / (2I_1+1)^2 \right] \langle I_{1z} \rangle . \tag{86}$$

The corresponding equations for the second species are again found by setting $L_+ = L_- = 0$ and interchanging the subscripts 1 and 2 in (85) and (86). Thus in the limit of low light intensity the rate equations reduce to four linear equations.

2. Dehmelt Experiment

The experiment analyzed in this section was first used by Dehmelt to estimate the sodium-electron spin-exchange cross section.[14] A resonance cell contains two atomic species or one atomic species and quasi-free electrons. The first species is optically pumped, and the transmitted resonance radiation is monitored. The signal can be defined as

$$S(I_1, I_2) = [A(0, H_2') - A(0, 0)] / [A(H_1', 0) - A(0, 0)], \tag{87}$$

where $A(H_1', H_2')$ is the absorption in the presence of two rf fields (H_1' disorients species 1, etc.). The absorption is given by (11), provided that the incident light is constant over the frequencies for which

the absorption is appreciable. It will be assumed that $L(x, t)$ or $L(x, H_1', H_2')$ is the same at each point in the cell for arbitrary values of the rf fields; i.e., $L(x, H_1', H_2') = L(x, 0, 0) = L(x)$. This should be a good approximation in the limit of low light intensity, for which—because the polarization is always small—the absorption changes very little with polarization changes. One has $P(x, H_1', H_2') = f(x)P(H_1', H_2')$, where $P(H_1', H_2')$ is independent of x and $f(x)$ is approximately independent of H_1' and H_2' since the polarization is small [see (90) below]. Then

$$S(I_1, I_2) \approx 1 - P(0, H_2')/P(0, 0), \tag{88}$$

since $P(H_1', 0) = 0$. For $I_1 = 0$, (88) is valid for any absorption if the polarization is low.

Applying H_2' is equivalent to reducing the relaxation time of the second species to zero; therefore, $P(0, H_2') = P(T_2 = 0)$ and

$$S(I_1, I_2) \approx 1 - P(T_2=0)/P(T_2) = 1 - \left\langle S_{1z}(T_2 = 0)\right\rangle / \left\langle S_{1z}(T_2)\right\rangle . \tag{89}$$

By solving the four simultaneous equations (85) and (86) and the corresponding equations for the second species, one finds, at equilibrium ($\left\langle \dot{S}_{1z}\right\rangle = 0$, etc.),

$$\left\langle S_{1z}\right\rangle \approx \Big[(I_1+1)(2I_1+3)\Big(\frac{1}{T_1'} + \frac{1}{T_{E1}} + \frac{1}{T_{S1}} + \frac{2I_1+1}{2T_1'''}\Big) L_+C - I_1(2I_1-1)$$

$$\times \Big(\frac{1}{T_1'} + \frac{1}{T_{E1}} + \frac{1}{T_{S1}} - \frac{2I_1+1}{2T_1'''}\Big)L_-C\Big] \Big/ 6(2I_1+1)[\beta(1) - \alpha(1)\alpha(2)/\beta(2)] \tag{90}$$

where

$$\alpha(1) = \frac{1}{T_{E1}}\left(\frac{1}{T_1'} + \frac{1}{T_{E1}} + \frac{1}{T_{S1}} + \frac{4I_1^2 + 4I_1 + 3}{6T_1'''}\right) , \tag{91}$$

$$\beta(1) = \left(\frac{1}{T_1'} + \frac{1}{T_{E1}}\right)\left(\frac{1}{T_1'} + \frac{1}{T_{E1}} + \frac{1}{T_{S1}}\right) + \frac{4I_1^2+4I_1+3}{2T_1'''}\left(\frac{1}{T_1'} + \frac{1}{T_{E1}} + \frac{2}{3T_{S1}}\right) + \frac{(2I_1+1)^2}{2T_1'''^2} . \tag{92}$$

Then

$$S(I_1, I_2) \approx a(1)a(2)/\beta(1)\beta(2) \tag{93}$$

is the signal for the Dehmelt-type[14] steady-state experiment in the limit of low light intensity. I_1 is the nuclear spin, $1/T'''_1 = 1/T_1 + 1/T''_1$, T_1 the Zeeman relaxation time, T''_1 the uniform relaxation time, T'_1 the electron randomization relaxation time, and T_{S1} and T_{E1} the self- and cross-exchange times of the pumped species; I_2, T_2, T''_2, T'_2, T_{S2}, and T_{E2} are the corresponding quantities for the other species.

The signal is independent of L_+ and L_-, i.e., of any assumptions about excited-state disorientation. But (90) indicates that the electron polarization depends upon the excited-state disorientation. However, the signal is defined as the ratio of two signals, and the disorientation effects cancel out. S=0 for $T'''_2 = 0$ or $T'_2 = 0$ because the second species is not affected by the rf field, since it is never oriented. Similarly, S=0 for $T'''_1 = 0$ or $T'_1 = 0$ because the first species is not pumped. For $T_{E1} = \infty$, S=0, since disorienting the second species has no effect upon the first species in the absence of spin exchange. Equation (93) is not valid for both $T'''_1 = \infty$ and $T'_1 = \infty$.

If $T'''_1 = T'''_2 = \infty$, i.e., the relaxation is by electron randomization only,

$$S(I_1, I_2)\Big|_{T'''_1 = T'''_2 = \infty} = \frac{1}{T_{E1}T_{E2}} \left(\frac{1}{T'_1} + \frac{1}{T_{E1}}\right)^{-1} \left(\frac{1}{T'_2} + \frac{1}{T_{E2}}\right)^{-1}. \tag{94}$$

Also

$$S(0, 0) = \frac{1}{T_{E1}T_{E2}} \left(\frac{1}{T'''_1} + \frac{1}{T'_1} + \frac{1}{T_{E1}}\right)^{-1} \left(\frac{1}{T'''_2} + \frac{1}{T'_2} + \frac{1}{T_{E2}}\right)^{-1}, \tag{95}$$

which is identical to (94) in the limit $T'''_1 = T'''_2 = \infty$. Therefore, nuclear spin effects are unimportant if the ground-state relaxation is predominantly by electron randomization.

In order to compare the results above with earlier analyses by other authors, it is useful to compare the rate equations for the case $I_1 = I_2 = 0$; Eqs. (1) become, with $n_{F'_1 M'_1} = n/2(2I_1+1)$ for complete mixing, $C = 1/2$, $T_{S1} = T_{S2} = T'_1 = T'_2 = \infty$, $M_S = \pm 1/2$:

$$\dot{p}_{1/2} = Lp_{-1/2}/2 - (p_{1/2} - p/2)/T_1''' - (p_{1/2}d_{-1/2} - p_{-1/2}d_{1/2})/T_{E1}d,$$

$$\dot{p}_{-1/2} = -Lp_{-1/2}/2 - (p_{-1/2} - p/2)/T_1''' - (p_{-1/2}d_{1/2} - p_{1/2}d_{-1/2})/T_{E1}d,$$

$$\dot{d}_{1/2} = -(d_{1/2} - d/2)/T_2''' - (d_{1/2}p_{-1/2} - d_{-1/2}p_{1/2})/T_{E1}d, \tag{96}$$

$$\dot{d}_{-1/2} = -(d_{-1/2} - d/2)/T_2''' - (d_{-1/2}p_{1/2} - d_{1/2}p_{-1/2})/T_{E1}d.$$

Using $p_{\pm 1/2} = [p \pm (p_{1/2} - p_{-1/2})]/2$, one has

$$\dot{p}_{1/2} - \dot{p}_{-1/2} = Lp/2 - \left(\frac{L}{2} + \frac{1}{T_1'''} + \frac{1}{T_{E1}}\right)(p_{1/2} - p_{-1/2}) + (d_{1/2} - d_{-1/2})/T_{E2}, \tag{97}$$

$$\dot{d}_{1/2} - \dot{d}_{-1/2} = -\left(\frac{1}{T_2'''} + \frac{1}{T_{E2}}\right)(d_{1/2} - d_{-1/2}) + (p_{1/2} - p_{-1/2})/T_{E1}.$$

By comparing (97) with the rate equations used by Dehmelt[14] to describe his sodium-electron experiment, one finds that the following identifications must be made: $p = N$, $d = n$, $1/T_{E1} = nvQ$, $T_1''' = \tau(I_0 = 0)$, $T_2''' = T_e$. Then with $Qnv << 1/\tau$ or $1/T_e$, (95) becomes, with $T_1' = T_2' = \infty$,

$$S_D(0, 0) = nNT_e\tau v^2 Q^2. \tag{98}$$

Of course, I_1 was actually 3/2, for which (93) becomes, with $T_1' = T_2' = T_{S1} = T_{S2} = \infty$,

$$S_D(3/2, 0) = 3nNT_e\tau v^2 Q^2/8 = 3S_D(0, 0)/8. \tag{99}$$

Therefore, if the experiment is performed in the limit of low light intensity, the cross section deduced from a given signal becomes $(8/3)^{1/2} = 1.63$ times as large if nuclear spin is included in the analysis, if the ground-state relaxation of the alkali is by Zeeman or uniform transitions only, and if self exchange is negligible. But if the ground-state relaxation is by electron randomization, (98) is valid (with $T_e = T_2'$ and $\tau = T_1'$) for arbitrary I_1.

3. Jarrett Experiment

Comparison of (96) with Eqs. (12) and (13) of the paper by Jarrett[21] indicates $1/T_{E1}d = v_r Q_x$, $1/T_1''' = 1/T_2''' = 2R$, $p = N$, and $d = aN$; therefore, with $T_1' = T_2' = \infty$, (95) becomes

$$S_J(0, 0) = aN^2 v_r^2 Q_x^2 (2R + Nv_r Q_x)^{-1} (2R + aNv_r Q_x)^{-1}, \qquad (100)$$

which is Jarrett's S_x/S, as can be verified by solving for the latter from (18) of Jarrett's paper. But from (94) it is seen that if the relaxation is by electron randomization only, (100) is valid for general nuclear spin and includes self exchange (with $T_1''' = T_2''' = \infty$ and $1/T_1' = 1/T_2' = 2R$). However, if Zeeman or uniform relaxation is dominant, (93) implies a large correction to the deduced cross section for the actual nuclear spins ($I_1 = 3/2$, $I_2 = 5/2$). These effects may be demonstrated by assuming Jarrett's experimental values of the parameters and signal and then deducing the spin-exchange cross section. This author estimates $k_0\ell/4 \approx 1/3$ for Jarrett's experiment; the fact that $k_0\ell/4$ is not much less than 1 [which is the condition that (11) hold in his experiment] is ignored in the following discussion.

For spin exchange between Rb^{85} and Rb^{87} one has

$$1/T_{S1} \approx p/T_{E1}d \quad \text{and} \quad 1/T_{S2} \approx 1/T_{E1}, \qquad (101)$$

because $\int |f_t - f_s|^2 d\Omega$ is only weakly dependent upon nuclear properties. With $T_{E2} = T_{E1}d/p$, $T_2''' = T_1'''$, $T_2' = T_1'$, in (93), the cross sections Q are deduced with $R = 413\ \text{sec}^{-1}$, $N = 3.33\times10^{11}\ \text{cm}^{-3}$, $a = d/p = 2.59$, $v_r = 4.59\times10^4$ cm/sec, and $S_x/S = S_J = 0.107$. Values of Q are found for Zeeman or uniform relaxation ($T_1' = \infty$, $T_1''' = 1/2R$) and for relaxation by electron randomization ($T_1' = 1/2R$, $T_1''' = \infty$). By the nature of the measurement, the self-exchange contributions to R were presumably eliminated. $Q_J = 1.7\times10^{-14}\ \text{cm}^2$ is the cross section deduced by Jarrett, neglecting the nuclear spins. A comparison of the deduced cross sections for different assumptions is given in Table IV. The nuclear spins are important in the analysis of Jarrett's experiment unless the ground-state relaxation is by electron randomization only.

Table IV. Rb^{87} -Rb^{85} spin-exchange cross sections deduced from the data of Jarrett (reference 21). $Q_J = 1.7\times10^{-14}$ cm^2.

I_1	I_2	Relaxation: Zeeman, uniform, or electron randomization	Self exchange included?	Q/Q_J
0	0	Z or U	Yes or No	1
3/2	5/2	Z or U	No	4.6
3/2	5/2	Z or U	Yes	6.8
0	0	ER	Yes or No	1
3/2	5/2	ER	Yes or No	1

This author has not determined which relaxation mechanism predominated in Jarrett's experiment. However, the following discussion is pertinent. The relaxation time of the electronic polarization in a cylindrical cell containing a buffer gas can be approximated by[23]

$$\frac{1}{\tau} = \frac{1}{\tau_{wall}} + \frac{1}{\tau_{buffer}} , \tag{102}$$

$$\tau_{wall} = \frac{p}{D_0 p_0}\left[\left(\frac{2.405}{a}\right)^2+\left(\frac{\pi}{L}\right)^2\right]^{-1} , \tag{103}$$

$$\tau_{buffer} = p_0/N_0\,\sigma\bar{v}p, \tag{104}$$

where p is the pressure of the buffer gas, D_0 is the diffusion coefficient at atmospheric pressure p_0, a and L are the radius and length of the cell, N_0 is the density of inert gas atoms at p_0 and at the temperature of the vapor cell, σ is the disorientation cross section, and $\bar{v}$ is the mean relative velocity between inert gas atom and alkali. For Rb in Ne, $D_0 = 0.31$ cm^2/sec, $\sigma = 5.2\times10^{-23}$ cm^2, and $N_0 = 2.29\times10^{19}$ cm^{-3} at 47° C.[23] For Jarrett's case $p = 2.8$ cm of Ne, $a = 2.5$ cm, $L = 1.43$ cm, $T = 90°$ C, implying $\tau_{wall} \approx 21$ msec and $\tau_{buffer} \approx 0.38$ sec. Wall collisions should dominate for Jarrett's experiment, giving $\tau \approx 21$ msec, but Jarrett found ≈ 1 msec. In deriving

τ_{wall} it was assumed that every wall collision produces complete disorientation, implying that $\tau_{wall} \geq 21$ msec. If, however, the cell contained some impurity in the vapor phase, the relaxation might be greatly accelerated and be dominated by electron randomization. The cross section deduced by Jarrett would then be unchanged by the addition of the nuclear spins into the analysis, and would be in agreement with the paramagnetic resonance measurement by Moos and Sands[28] and that of IIIG.

4. Off-Diagonal Density Matrix Elements

In the derivation of the general expression (93), the off-diagonal elements of the density matrix were neglected. Balling, Hanson, and Pipkin[30] have carried out an analysis for zero nuclear spin for a general density matrix. It is of interest to compare their result with this work. The polarization for $I_1 = I_2 = 0$ can be found from (97) or (90) with $T_{S1} = T_{S2} = T_1' = T_2' = \infty$ and $L_+ = L_-$:

$$P = P_+ = LC/\left[\frac{1}{T_1'''} + \frac{1}{T_{E1}} - \frac{1}{T_{E1}T_{E2}}\left(\frac{1}{T_2'''} + \frac{1}{T_{E2}}\right)^{-1}\right]. \qquad (105)$$

Equation (76) of Balling et al. is to be compared with the above, with P, T_1''', T_{E1}, T_{E2}, and T_2''' substituted for $\langle P(R)\rangle$, T_{1R}, T_{eR}, T_{ee}, and T_{1e} respectively:

$$P_{BHP} \propto 1/\left[\frac{1}{T_1'''} + \frac{1}{T_{E1}} - \frac{1}{T_{E1}T_{E2}}\left(\frac{1}{T_2'''} + \frac{1}{T_{E2}} + \frac{\omega_1^2\tau_2}{1+\tau_2^2(\omega_0-\delta\omega_0-\omega)^2}\right)^{-1}\right], \qquad (106)$$

where $\omega_1 = -g_J\frac{\mu_0 H_2'}{\hbar}$, $\omega_0 = -g_J\frac{\mu_0 H_0}{\hbar}$, $\delta\omega_0$ is the spin-exchange frequency shift, and

$$1/\tau_2 = 1/T_{2e} + 1/T_{E2}. \qquad (107)$$

Here T_{2e} is essentially the time required for coherence effects to damp out, i.e., the usual "T_2" in magnetic resonance nomenclature; T_{2e} should not be confused with T_2 of this work, which is a "T_1"

time for the second species. For $H_2' = 0$ there are no coherence effects, and (105) and (106) agree. For

$$(H_2')^2 >> \left[\frac{1}{T_1'''}\left(\frac{1}{T_2'''}+\frac{1}{T_{E2}}\right)+\frac{1}{T_2''' T_{E1}}\right]\left(\frac{1}{T_{E2}}+\frac{1}{T_{2e}}\right)\Bigg/\left(\frac{1}{T_1'''}+\frac{1}{T_{E1}}\right)(g_J\mu_0/\hbar)^2 \tag{108}$$

(106) agrees with (105) in the limit $T_2''' \to 0$, implying that the second species is completely disoriented. On the assumption that all the time constants are equal to 1 msec, (108) requires $H_2' >> 0.4$ milligauss. Thus when the resonance is saturated the polarization, obtained from an arbitrary density matrix, reduces to the diagonal-treatment value at equilibrium. The time required to reach equilibrium is related to T_{2e} for the off-diagonal contributions. If T_{2e} is made short—for example, by increasing the inhomogeneity of the static field—the coherence effects are damped out more rapidly, but a larger rf field must be applied to saturate the resonance. In general, T_{2e} should be made small compared with the period of switching the rf fields; H_2' is then chosen large enough to saturate the resonance, i.e., satisfy (108).

Although the frequency shifts and line shapes resulting from spin-exchange collisions can be seen and studied, nonetheless, the calculations of this section apply to realizable experiments in which these effects are unimportant. For a much more thorough demonstration of the unimportance of the off-diagonal matrix elements, see references 33 and 38. This problem is difficult to treat in general, but it should be clear that if a state possesses no coherence initially it cannot acquire any by relaxation processes, which are random.

Even though it is unrelated to the discussion of this section, one other aspect of the paper by Balling et al.[30] may be worth mentioning. They state that they demonstrate in an appendix that their results are valid for general nuclear spin. However, using their Table IV and their Eq. (24) and making the simplifying assumptions that the second species is disoriented [i.e., $P(e) = 0$)] and that $\rho(e, R)$ is diagonal, this author finds that $dP_e(Rb^{87})/dt$ is not proportional to $P_e(Rb^{87})$ as in their (A14), but rather arrives at the Eqs. (72) and (73) of Section IIC of this paper with $I_1 = 3/2$, $I_2 = 0$. They have recently pointed out that their (A14) is in error.[30]

5. Anderson and Ramsey

Anderson and Ramsey[22] (AR) have performed an experiment to measure the self-spin-exchange cross section in sodium. The steady-state populations are needed to analyze their experiment, not just the electronic polarization. They define $p_{1,\pm1}/p = 1/8 \pm \delta_{AR}$, $p_{2,\pm1}/p = 1/8 \pm \beta_{AR}$, and $p_{2,\pm2}/p = 1/8 \pm \alpha_{AR}$.

It is shown in Appendix III that, if complete reorientation occurs in the excited state ($q \approx 0.8$ for Na in 3 cm of He at 154°C (AR conditions) and with $\sigma = 23 \times 10^{-16}$ cm^2 (reference 42)),

$$\pi_{F_1 M_1} = M_1 \pi_{F_1}, \tag{109}$$

where $\pi_{F_1 M_1}$ is defined in (81), and that

$$\pi_{\pm} = \pm(I_1 + 1/2) p P_{\pm} \Bigg/ \sum_{M_1 = -I_1 \mp 1/2}^{I_1 \pm 1/2} M_1^2 . \tag{110}$$

From (83) and (84) with $T_{E1} = \infty$ (single species) and $L_+ = L_- = L$ (complete mixing in the excited state), and using (110), one finds that at equilibrium

$$\pi_{\pm} = \frac{\dfrac{LCp}{2I_1+1}\left(\dfrac{1}{T_1'} + \dfrac{1}{T_{S1}} \pm \dfrac{2I_1+1}{2T_1'''}\right)}{\dfrac{1}{T_1'}\left(\dfrac{1}{T_1'} + \dfrac{1}{T_{S1}}\right) + \dfrac{4I_1^2+4I_1+3}{2T_1'''}\left(\dfrac{1}{T_1'} + \dfrac{2}{3T_{S1}}\right) + \dfrac{(2I_1+1)^2}{2T_1'''^2}} . \tag{111}$$

Equation (111) as applied to the experiment of Anderson and Ramsey is given in Table V. Notice that if the ground-state relaxation were by electron randomization only, the signals would be independent of the exchange time. Since they used 3 cm of He buffer gas, one might at first expect electron randomization to dominate. However, for a spherical cell,[40]

$$\tau_{wall} = R^2 p / \pi^2 D_0 p_0 \approx 100 \text{ msec}, \tag{112}$$

Table V. Comparison of population differences for the Anderson and Ramsey (AR) experiment (reference 22)
($T_{S1} \equiv 2T_2$, $T_1''' \equiv T_1$, $LC/2 \equiv A$, $I_1 = 3/2$; see IID5).

Anderson and Ramsey (uniform relaxation)	This work	
	Zeeman or uniform relaxation ($T_1' = \infty$)	Electron randomization ($T_1 = \infty$)
$\delta_{AR} = \dfrac{-A\left(\frac{32}{T_1^2} + \frac{5.4}{T_1T_2} - \frac{3.8}{T_2^2}\right)}{\left(\frac{8}{T_1} + \frac{2.78}{T_2}\right)\left(\frac{32}{T_1^2} + \frac{16.5}{T_1T_2}\right)}$	$\dfrac{\pi_-}{p} = \dfrac{-AT_1}{8}\left(\dfrac{1}{T_1} - \dfrac{1}{4T_2}\right)\left(\dfrac{1}{T_1} + \dfrac{3}{8T_2}\right)^{-1}$	$\dfrac{\pi_-}{p} = \dfrac{AT_1'}{2}$
$(p_{1,\pm1}/p = 1/8 \pm \delta_{AR})$	$= \dfrac{-A\left(\frac{32}{T_1^2} + \frac{8}{T_1T_2} - \frac{4}{T_2^2}\right)}{\left(\frac{8}{T_1} + \frac{3}{T_2}\right)\left(\frac{32}{T_1^2} + \frac{16}{T_1T_2}\right)}$	
$\beta_{AR} = \dfrac{A\left(\frac{32}{T_1^2} + \frac{27.6}{T_1T_2} + \frac{3.8}{T_2^2}\right)}{\left(\frac{8}{T_1} + \frac{2.78}{T_2}\right)\left(\frac{32}{T_1^2} + \frac{16.5}{T_1T_2}\right)}$	$\dfrac{\pi_+}{p} = \dfrac{AT_1}{8}\left(\dfrac{1}{T_1} + \dfrac{1}{4T_2}\right)\left(\dfrac{1}{T_1} + \dfrac{3}{8T_2}\right)^{-1}$	$\dfrac{\pi_+}{p} = \dfrac{\pi_-}{p}$
$(p_{2,\pm1}/p = 1/8 \pm \beta_{AR})$	$= \dfrac{A\left(\frac{32}{T_1^2} + \frac{24}{T_1T_2} + \frac{4}{T_2^2}\right)}{\left(\frac{8}{T_1} + \frac{3}{T_2}\right)\left(\frac{32}{T_1^2} + \frac{16}{T_1T_2}\right)}$	
$\alpha_{AR} = \dfrac{A\left(\frac{64}{T_1^2} + \frac{44}{T_1T_2} + \frac{7.6}{T_2^2}\right)}{\left(\frac{8}{T_1} + \frac{2.78}{T_2}\right)\left(\frac{32}{T_1^2} + \frac{16.5}{T_1T_2}\right)}$	$\dfrac{2\pi_+}{p}$	$\dfrac{2\pi_+}{p}$
$(p_{2,\pm2}/p = 1/8 \pm \alpha_{AR})$		

$$\tau_{buffer} = p_0/N_0 \sigma \bar{v}p \approx 310 \text{ sec} \qquad (113)$$

for Na in 3 cm of He at 154° C (D_0=1 cm^2/sec, $\sigma \approx 3\times10^{-26}$ cm^2, R = 5 cm, $\bar{v} = 1.6\times10^5$ cm/sec, $N_0 = 1.7\times10^{19}$ cm^{-3}).[22] The measured relaxation time was 87 msec, in excellent agreement with the wall relaxation time. Consequently, Zeeman or uniform relaxation may dominate; such would seem to be the case in light of the reasonable cross section deduced by Anderson and Ramsey assuming uniform relaxation.

III. SPIN-EXCHANGE CROSS-SECTION MEASUREMENTS BY HYPERFINE PUMPING

A. Introduction

The calculations in Part II were executed to ascertain the importance of nuclear spin effects in deducing spin-exchange cross sections from optical pumping signals in order to determine the experiment best adapted to precise measurements of the cross sections. It was found that the nuclear spins are important and that they complicate the analysis considerably. However, Part II is concerned only with Zeeman pumping, in which the hyperfine components of the pumping radiation are assumed to be equal. In Part III an experiment is described in which the hyperfine components of the pumping light are made as different as possible. A large difference in populations of the two hyperfine levels results, and the Franzen technique is used to determine the relaxation time in the dark.[23] In the absence of Zeeman pumping within each hyperfine level, the situation is that of a two-level system, and the relaxation is described by a single exponential. The complexities of analysis caused by the nuclear spins and discussed in Part II are then absent. Since the principal objective of this research was to make accurate measurements of spin-exchange cross sections, the hyperfine method was used for most of the measurements.

This hyperfine experiment is similar to that of Bouchiat and Brossel,[24] except that circularly polarized light is employed instead of unpolarized light. This variation is made because the light is polarized by passing through the Kerr cell shutter, and it is difficult to destroy the polarization without sacrificing intensity. In addition, rf fields are applied to both species to prevent Zeeman pumping and hence to simplify the rate equations. Experimentally, identical signals are found if the rf fields are removed and the component of the earth's field along the direction of the light beam is bucked out. Both the D_1 and D_2 lines are used in the pumping radiation.

The plan of Part III is as follows. In Section IIIB the theory of the hyperfine experiment is presented, a brief summary of the techniques employed is given, and representative data are displayed.

Detailed descriptions of the components of the relaxation time equipment are given in Section IIIC. The analysis of the relaxation time data is described in Section IIID. The density measurement apparatus and data analysis are presented in Sections IIIE and IIIF, respectively. Finally, Section IIIG is a summary of the spin-exchange cross-section measurements by the hyperfine method.

B. Description of the Hyperfine Experiment

1. Theory of the Hyperfine Experiment

The significant differences between the assumptions of Part II and Part III are as follows: (a) the hyperfine components in the incident light are assumed to be unequal here, although transitions from different hyperfine levels of the same excited fine-structure state to a given ground-state hyperfine level are assumed to be unresolved in absorption; (b) D_2 light is included as well as D_1 light in the pumping radiation; (c) an rf field is continuously applied to the first species as well as to the second in order to nullify any Zeeman pumping; (d) the requirement of low absorption of IIB. 1 is replaced by the less stringent restriction that the fractional deviation of the population of each hyperfine level from its unpolarized value be much less than the reciprocal of the absorption factor $k_{F_1}\ell$, where ℓ is the absorption length. As in Part IIC it is assumed that no buffer gas is used, so that the populations are essentially independent of position in the cell.

Eq. (7) can be extended to include the D_2 radiation:

$$dL(\nu, x, t) = -L(\nu, x, t) \sum_{\substack{F_1 M_1 \\ F_1' J_1'}} p_{F_1 M_1}(x, t)\, P_\nu'(F_1 M_1, J_1' F_1' M_1 + 1)\, h\nu\, dx. \tag{114}$$

In analogy with IIB. 1, we have

$$P_\nu'(F_1 M_1, J_1' F_1' M_1 + 1) = P'(F_1 M_1, J_1' F_1' M_1 + 1)\, f(\nu - \nu^0_{F_1 M_1, J_1' F_1' M_1'}). \tag{115}$$

With the rf fields applied and in the absence of a buffer gas,

$$p_{F_1 M_1}(x, t) = p_{F_1}(t)/(2F_1+1), \tag{116}$$

$$d_{F_2 M_2}(x, t) = d_{F_2}(t)/(2F_2+1). \tag{117}$$

Integrating (114) over the appropriate frequencies and assuming that the upper hyperfine states are unresolved in absorption, one finds that the total light of the F_1 to J_1' transition at a distance x into the cell decreases by

$$dL^{J_1'}_{F_1}(x, t) = -L^{J_1'}_{F_1}(x, t)\, p_{F_1}(t)$$

$$\times \sum_{M_1 F_1'} P'(F_1 M_1, J_1' F_1' M_1+1)\, h\nu\, dx/(2F_1+1) \tag{118}$$

between x and $x+dx$. Define an absorption coefficient for the transition from F_1 to J_1':

$$k^{J_1'}_{F_1} = \sum_{M_1 F_1'} P'(F_1 M_1, J_1' F_1' M_1+1)\, h\nu\, p_{F_1}(\infty)/(2F_1+1). \tag{119}$$

Then

$$\sum_{F_1 J_1'} L^{J_1'}_{F_1}(x, t) = \sum_{F_1 J_1'} L^{J_1'}_{F_1}(0)\, \exp(-k^{J_1'}_{F_1} x)$$

$$\times \exp\left[-(p_{F_1}(t) - p_{F_1}(\infty))\, k^{J_1'}_{F_1} x/p_{F_1}(\infty)\right]. \tag{120}$$

The absorption is

$$A(\ell, t) \equiv \sum_{F_1 J_1'} \left[L^{J_1'}_{F_1}(0) - L^{J_1'}_{F_1}(\ell) \right]$$

$$= -\sum_{F_1 J_1'} L^{J_1'}_{F_1}(0) \left\{ \exp(-k^{J_1'}_{F_1} \ell) \right.$$

$$\left. \times \exp\left[-(p_{F_1}(t) - p_{F_1}(\infty)) k^{J_1'}_{F_1} \ell / p_{F_1}(\infty) \right] - 1 \right\} . \qquad (121)$$

Since the Franzen technique[23] is employed, the signal is defined as

$$S(I_1, t) = [A(\infty) - A(t)]/[A(\infty) - A(0)] \qquad (122)$$

as in (65), where A(t) is given by (121).

The low absorption criterion for the hyperfine experiment is

$$\left| k^{J_1'}_{F_1} \ell \; [p_{F_1}(0) - p_{F_1}(\infty)]/p_{F_1}(\infty) \right| << 1, \qquad (123)$$

in order that the signal reduce to the simple expression (noting that $p_- = p - p_+$ with + and - referring to $F_1 = I_1 \pm 1/2$)

$$S = [p_+(t) - p_+(\infty)]/[p_+(0) - p_+(\infty)] . \qquad (124)$$

To investigate the implications of (123), consider absorption of D_2 light by the $F_1 = I_1 - 1/2$ level:

$$L_-^{3/2}(\ell, t) = L_-^{3/2}(0) \exp(-k_-^{3/2} \ell) \exp[-(p_-(t) - p_-(\infty)) k_-^{3/2} \ell / p_-(\infty)], \qquad (125)$$

$$L_-^{3/2}(\ell, 0)/L_-^{3/2}(\ell, \infty) = \exp[-(p_-(0) - p_-(\infty)) k_-^{3/2} \ell / p_-(\infty)]. \qquad (126)$$

Equation (123) requires then

$$[L_-^{3/2}(\ell, 0) - L_-^{3/2}(\ell, \infty)]/L_-^{3/2}(\ell, \infty) << 1, \qquad (127)$$

i.e., as the population of a hyperfine level changes from its thermal equilibrium value to its pumped value, the change in peak absorption should be small compared with the light intensity of that transition. If $p_{F_1}(0) = 0$, (123) reduces to $k^{J'}_{F_1} \ell << 1$, which is the restriction of Part II.

For the hyperfine pumping experiment using the Franzen method of detection, Eq. (1) becomes, by summing over M_1 and using (28), (31), (43), (45), (59), (61), (116), and (117),

$$\dot{p}_{F_1} = - \sum_{F_1' M_1' M_1} \Delta(F_1, F_1') \left[(2I_1+1)^2 \delta_{F_1, F_1'} / T_1 + 1/T_1' \right] \begin{pmatrix} F_1' & 1 & F_1 \\ -M_1' & M_1'-M_1 & M_1 \end{pmatrix}^2$$

$$\times \left[p_{F_1}/(2F_1+1) - p_{F_1'}/(2F_1'+1) \right]/4 \quad - p_{F_1}/T_1'' + (2F_1+1)p/2(2I_1+1)T_1''$$

$$- \sum_{\substack{M_1 F_2 M_2 \\ F_1' M_1' F_2' M_2'}} \Delta(F_1, F_1') \Delta(F_2, F_2') \sum_q \begin{pmatrix} F_1' & 1 & F_1 \\ -M_1' & q & M_1 \end{pmatrix}^2 \begin{pmatrix} F_2' & 1 & F_2 \\ -M_2' & -q & M_2 \end{pmatrix}^2$$

$$\times \left[p_{F_1} d_{F_2}/(2F_1+1)(2F_2+1) - p_{F_1'} d_{F_2'}/(2F_1'+1)(2F_2'+1) \right]/4T_{E1}^d$$

$$- \sum_{\substack{M_1 F_1' M_1' \\ F_1'' M_1'' F_1''' M_1'''}} \Delta(F_1, F_1'') \Delta(F_1', F_1''') \sum_q \begin{pmatrix} F_1''' & 1 & F_1 \\ -M_1'' & q & M_1 \end{pmatrix}^2 \begin{pmatrix} F_1''' & 1 & F_1' \\ -M_1'' & -q & -M_1' \end{pmatrix}^2$$

$$\times \left[p_{F_1} p_{F_1'}/(2F_1+1)(2F_1'+1) - p_{F_1''} p_{F_1'''}/(2F_1''+1)(2F_1'''+1) \right]/4T_{S1}^p. \tag{128}$$

By Edmonds'[35] (3.7.8) and (6.2.9),

$$\dot{p}_{F_1} = -p_{F_1}/T_1'' + (2F_1+1)p/2(2I_1+1)T_1''$$
$$+ (1/T_1' + 1/T_{E1} + 1/T_{S1}) \left[-3p_{F_1} + \sum_{F_1'} p_{F_1'} \Delta(F_1, F_1')/(2F_1'+1)\right]/4. \tag{129}$$

With $p_- = p - p_+$ and with Table II,

$$\dot{p}_+ = -(1/T_1' + 1/T_1'' + 1/T_{E1} + 1/T_{S1})p_+$$
$$+ (2I_1+2)(1/T_1' + 1/T_1'' + 1/T_{E1} + 1/T_{S1})p/2(2I_1+1). \tag{130}$$

Then

$$p_+(t) = (p_+(0) - p_+(\infty)) \exp\left[-(1/T_1' + 1/T_1'' + 1/T_{E1} + 1/T_{S1})t\right] + p_+(\infty) \tag{131}$$

with

$$p_+(\infty) \approx (2I_1+2)p/2(2I_1+1). \tag{132}$$

Then (124) becomes

$$S(I_1, t) = \exp\left[-(1/T_1' + 1/T_1'' + 1/T_{E1} + 1/T_{S1})t\right], \tag{133}$$

where T_1' and T_1'' are the electron randomization and uniform ground-state relaxation times(see IIB. 3), T_{E1} is the characteristic time for spin-exchange collisions between nonidentical atoms (see IIB. 4), and T_{S1} is the characteristic time for self spin exchange (see IIB. 5).

Clearly the hyperfine experiment has distinct advantages over the Zeeman experiment of IIC, as is readily seen by comparing (133) with (76). The hyperfine experiment involves fewer parameters, and the functional form of the signal is simpler. Self exchange is included in the analysis of the hyperfine experiment. Finally, the restriction upon the permissible absorption is slightly less stringent.

Consider the case of hyperfine pumping of a single species; then (133) is simply

$$S = \exp(-t/\tau), \tag{134}$$

where

$$1/\tau = 1/T_1' + 1/T_1'' + 1/T_{S1}. \tag{135}$$

If several corresponding values of $1/\tau$ and the density n can be determined, then a plot of $1/\tau$ versus n is a straight line (assuming T_1' and T_1'' are constant throughout the experiment) with intercept $1/T_1'+1/T_1''$ and slope

$$d(1/\tau)/dn = \int\int |f_t - f_s|^2_{S1} \, d\Omega v_{S1} \, f(v_{S1}) d^3 v_{S1}/4 \equiv B_{S1} \qquad (136)$$

from (61). Assuming that the relative velocities follow a Maxwell-Boltzmann distribution and that $\int |f_t - f_s|^2_{S1} \, d\Omega$ is approximately independent of energy over the range of normal relative velocities, one can write (136) as

$$d(1/\tau)/dn = \sigma \bar{v} \, , \qquad (137)$$

where σ is the spin-exchange cross section and $\bar{v}$ is the average relative velocity

$$\bar{v} = [8kT(1/M_1 + 1/M_2)/\pi]^{1/2} = \left[2.118 \; T(1/M_1+1/M_2)\right]^{1/2} \qquad (138)$$

for the general case of nonidentical atoms (T in °K, M_1 and M_2 in atomic mass units, and $\bar{v}$ in 10^4 cm/sec).

Clearly, then, if τ and n can be determined, so can σ. The techniques for measuring τ and n are briefly outlined in Section III B.2; the involved experimental details are given in Sections III. C through III. F.

2. Outline of Experimental Techniques

A block diagram of the apparatus is given in Fig. 2, and a photograph of some of the equipment is shown in Fig. 3. A deviation from the thermal equilibrium hyperfine populations is achieved by hyperfine optical pumping.[24, 43-46] To accomplish this a hyperfine filter removes most of the light absorbable by atoms in one of the two hyperfine levels. The absorption cells used in most of the experiments were Pyrexcubes approximately 2 inches on each edge, coated with Paraflint, and containing no buffer gas. Sidearms with hammers and breakoffskies containing the alkali metals are attached to the cell. The densities of the alkali vapors are regulated by varying the temperature of

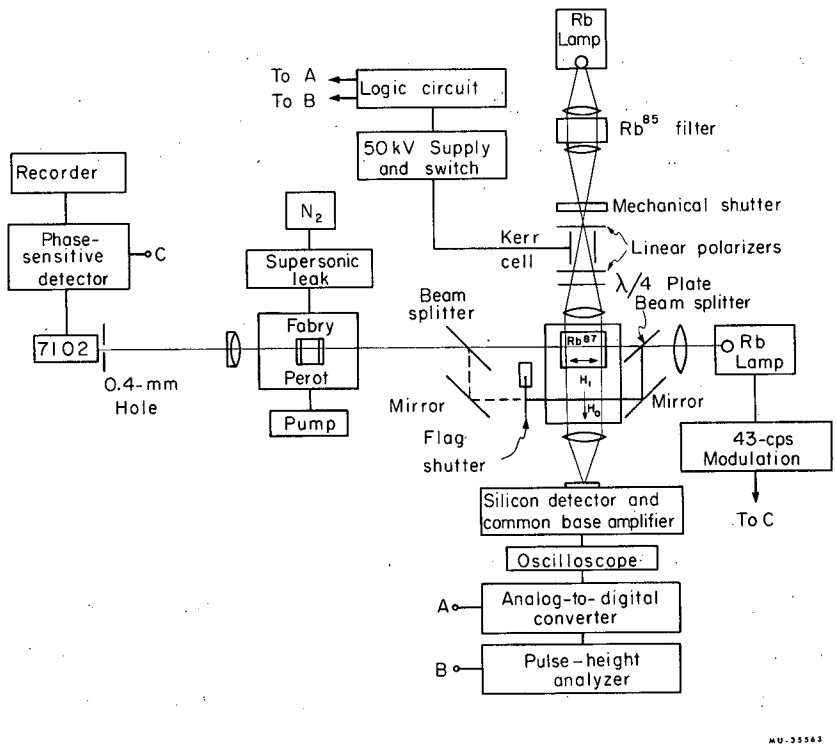

Fig. 2. Block diagram of the experimental apparatus for spin-exchange cross-section experiment by hyperfine optical pumping.

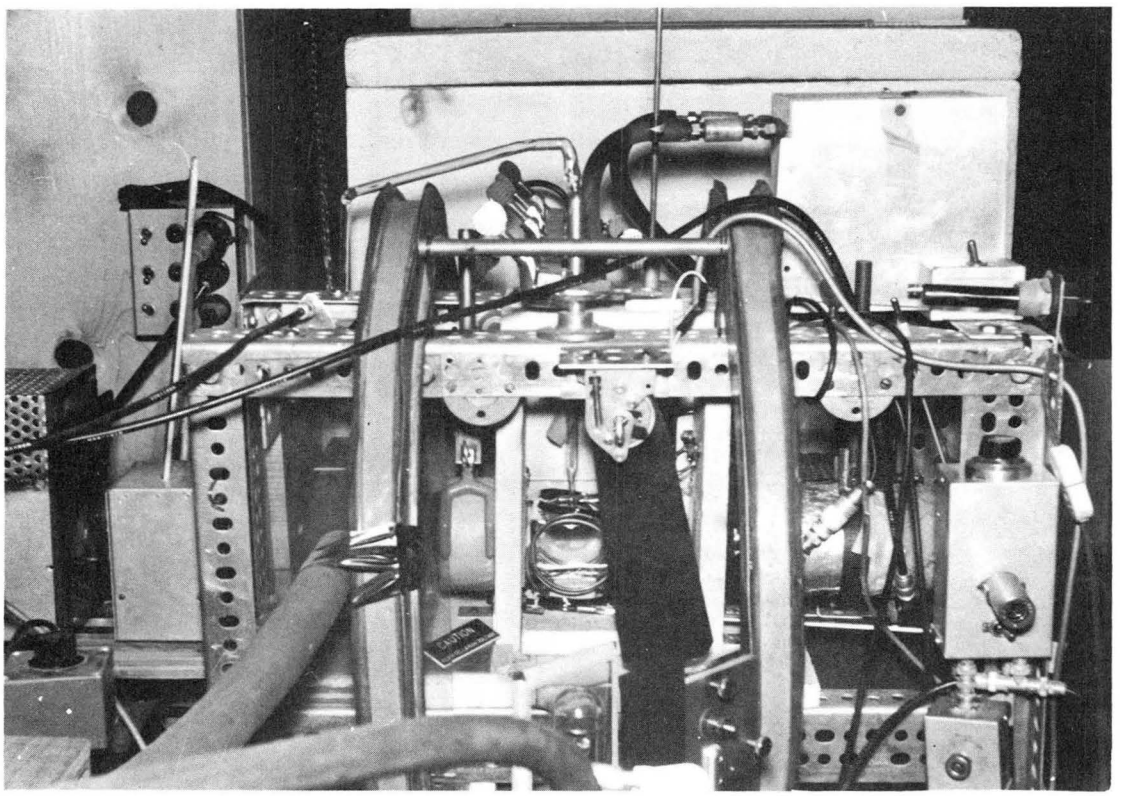

ZN-4878

Fig. 3. Part of the experimental apparatus. The resonance cell, the heart of the experiment, is shown in the rf coils near the center of the photograph. The pumping lamp, hyperfine filter, Kerr cell enclosure, and lens are to the left of the shutter. The detector and its lens are contained in the cylinder to the right. The density-measurement lamp is hidden behind the oven. The flag shutter, a beam splitter, and a mirror used in the density measurement are in the foreground.

the respective sidearms, which are always well below the temperature of the cell ($\approx 78\,^{\circ}C$). The cell and attached sidearms are situated inside their respective ovens. Coils for producing a small steady magnetic field along the direction of the pumping light and perpendicular rf fields surround the cell. The polarization is monitored by observing the transmitted light with a silicon photocell. The signal is amplified by a common base amplifier and a Tektronix 502 oscilloscope.

The relaxation time is determined by the method of Franzen.[23] A Kerr cell shutter is used to provide fast rise and fall times. Imperfections in the Kerr cell make it necessary to use a mechanical shutter as well for long off intervals (> 70 msec). A logic circuit was designed to decrease the off interval by a fixed increment each cycle for 16 cycles and then repeat. For example, the light might be cut off for 75 msec, on for 425 msec, off for 70, on for 430, etc., down to off for 0 and on for 500. Figure 4 is a photograph of the total light for such a situation. A signal of about 5% can be seen at the top; generally, the signals are smaller. When the top portion of Fig. 4 is amplified 25 times, one obtains Fig. 5. The light level at the upper left-hand corner is proportional to the initial polarization. The light is cut off for an interval of time, during which the polarization relaxes in the dark. The light is then turned on rapidly; the bright spot indicates the new level of polarization. The pumping transient is the trace from the bright spot back to the initial level. The envelope of the pumping transients, defined by the bright spots, locates the curve $\exp(-t/\tau)$. A pulse-height analyzer is used as a data accumulator to improve the precision of the measurements. Figure 6 displays three sets of data points from the analyzer and the corresponding least-squares best-fit curves.

The density measurement is performed by determining $\int k(\nu)d\nu \propto n$ with the aid of a Fabry-Perot interferometer.[47] The resonance radiation of the alkali species whose density is to be determined is divided into two beams, one of which traverses the cell and the other by-passes it. With suitably placed mirrors and beam splitters the beams are carefully brought back together and made to pass through

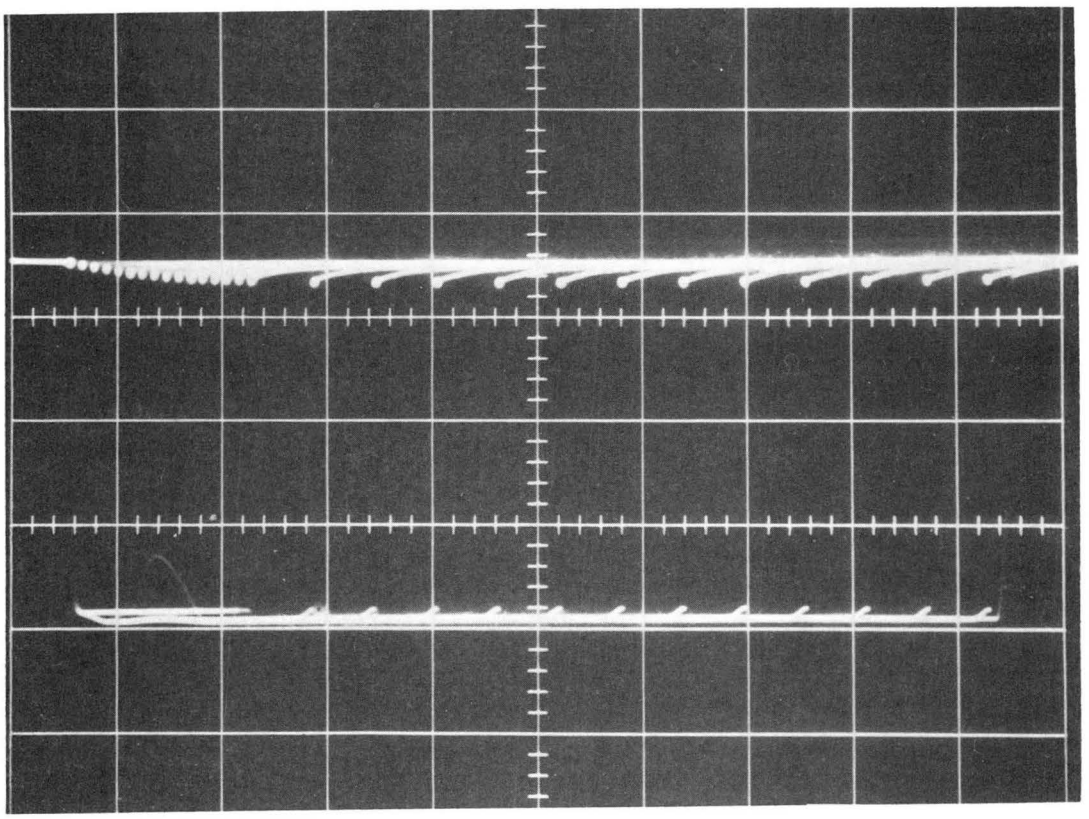

ZN-4831

Fig. 4. Total light signal with hyperfine pumping; 5 mV/cm, 25 msec between long off intervals, 5 msec between short off intervals.

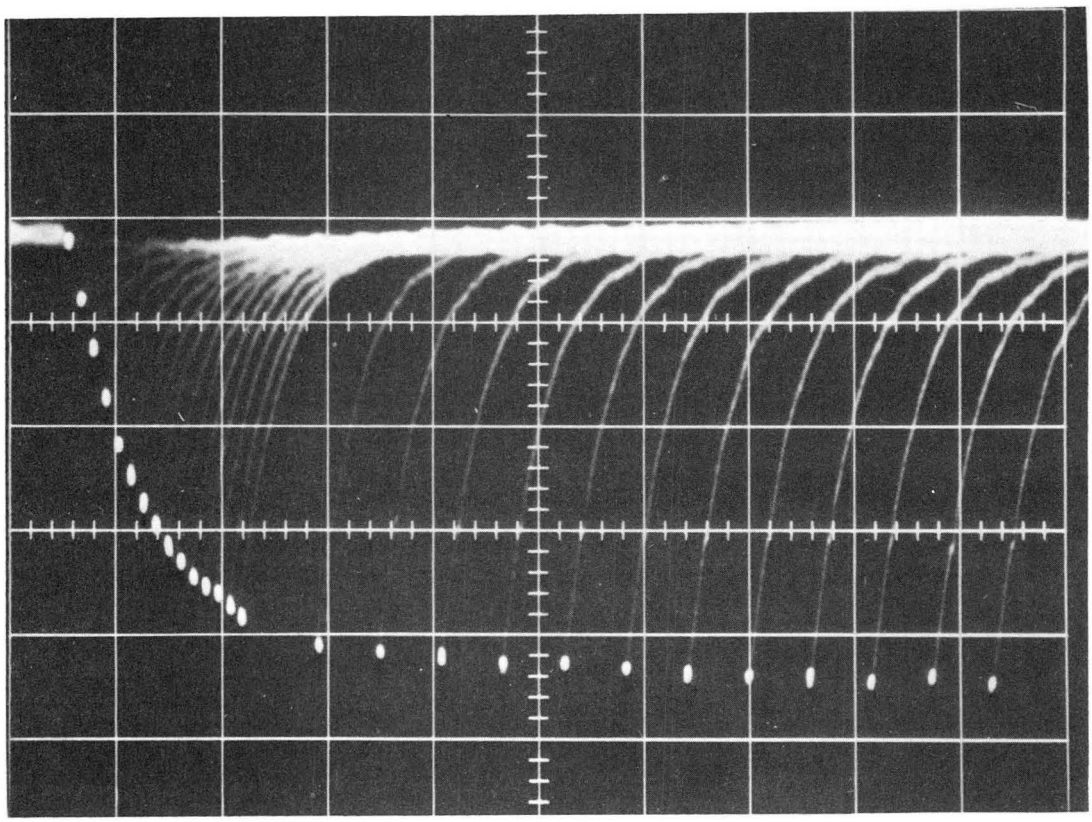

ZN-4832

Fig. 5. The top of Fig. 4 amplified 25 times; 0.2 mV/cm.

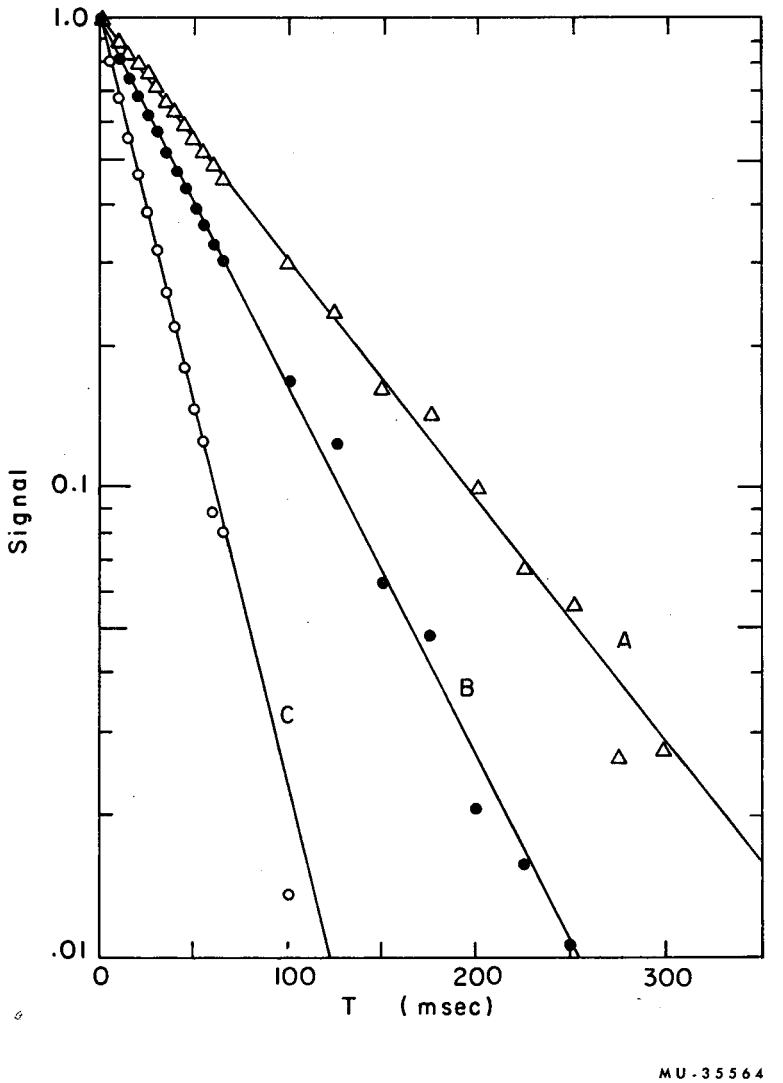

Fig. 6. Relaxation-time data chosen at random from run 7; straight lines are the least-squares best fits. Curve A: $T_{Rb^{87}} = 24°$ C, 20 accumulation cycles, tape number 519, $1/\tau = 11.89 \pm 0.18$ sec^{-1}; B: 30°, 20, 533, 18.12 ± 0.28; C: 38°, 20, 551, 38.12 ± 0.37.

the Fabry-Perot parallel to each other. The center spot of the ring system of each is focused on a 0.4-mm pinhole placed in front of a liquid-nitrogen-cooled 7102 photomultiplier. The light is electronically chopped at 86 cps in order that phase-sensitive detection can be employed. The spectral profile of the radiation is traced out by scanning through several orders of the ring system. This is accomplished by evacuating the chamber containing the Fabry-Perot etalon and then allowing dry nitrogen to enter the chamber linearly through a supersonic leak.

A two-position flag shutter operating at ≈ 0.15 cps switches back and forth between the two beams. In the absence of absorbing atoms the two beams are equalized so that no appreciable difference between them can be detected over a complete order; see Fig. 7. This requires that the two beams pass through the same part of the Fabry-Perot because the finesse may change from one region of the plates to another (see Section IIIE.5). In the presence of absorbing atoms, the beam passing through the cell is, of course, diminished; see Fig. 8. With a natural Rb source and only Rb^{87} atoms in the cell, the Rb^{85} peaks can be used to verify that the normalization is maintained; little difficulty is experienced on this point, giving credence to the normalization when such a check is not possible. The observed absorption coefficient at the frequency ν is then calculated as

$$k(\nu) = [\ln I(\nu)/I'(\nu)]/\ell \ , \qquad (139)$$

where $I(\nu)$ is the intensity at ν of the beam around the cell and is equal to the intensity of the beam incident upon the absorbing atoms; $I'(\nu)$ is the intensity transmitted through the cell of absorption length ℓ. The numerical integration of $k(\nu)$ over all frequencies is then proportional to the density. Because the slit function of the Fabry-Perot is not a delta function, the observed absorption coefficient at any frequency is not equal to the true absorption coefficient (the integral of which is proportional to the density). This leads to problems discussed in Section IIIF.

The results of the relaxation time and density measurements are combined to determine the cross section; a summary of the spin-

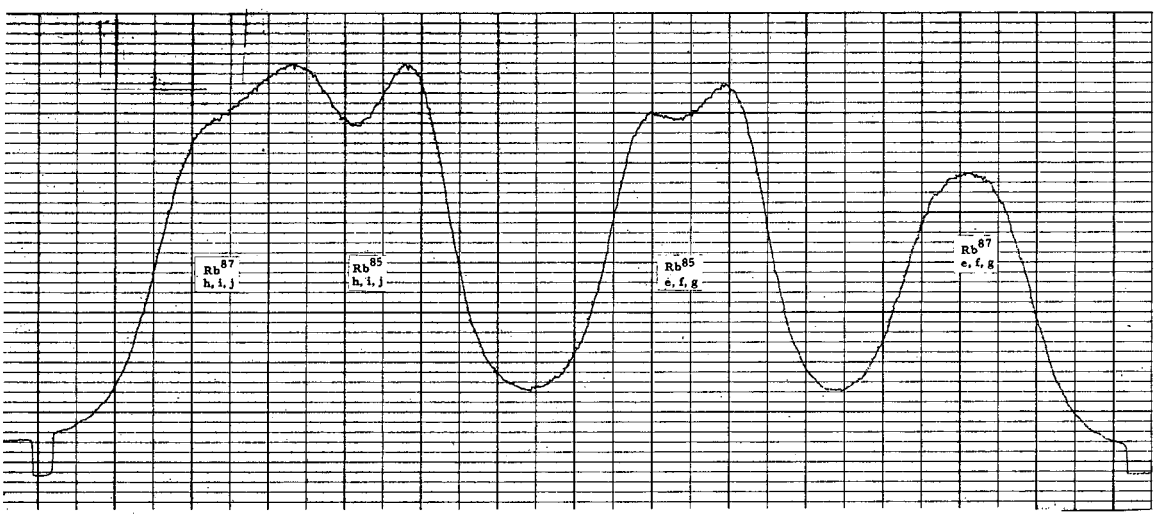

MU-35443

Fig. 7. Density measurement normalization of 7800-Å line with a natural Rb lamp heated to help equalize the hyperfine components and broaden the lines. There was no Rb in the cell. The flag shutter changes position every 3 sec. (chart speed 2 in./min), although it is difficult to detect it from the scan; 0.3 sec integration time in the phase-sensitive detector; 12 mm spacer.

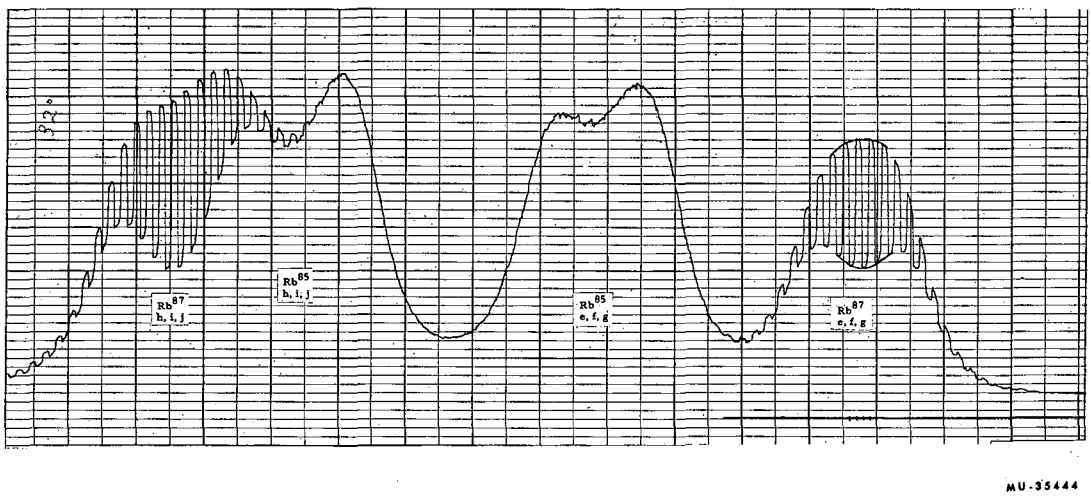

Fig. 8. Density scan showing absorption of natural Rb 7800-Å radiation by Rb^{87}.

exchange cross sections determined by the hyperfine method is given in Section IIIG.

C. Detailed Description of the Relaxation-Time Equipment

A block diagram of the experimental equipment has been given in Fig. 2. Each piece of apparatus utilized in the relaxation time measurements is now described.

1. Source of Resonance Radiation

In order to study relaxation times as short as 10 to 20 msec without sacrificing signal strength, a pumping time in the same range is highly desirable. In this connection, "pumping time" refers to the pumping time in the absence of relaxation processes; the apparent pumping time with relaxation may be somewhat shorter. To achieve such pumping times a relatively intense source of resonance radiation is required, particularly since a large portion of the light is lost by the limiting apertures of the two shutters and by reflection losses at the surfaces of the many glass plates through which the light must pass.

The Hartley oscillator circuit of Brewer[48] was used throughout these experiments. A 1-kilohm 5-watt variable resistor was added between the 300-volt supply and the lamp. This resistor appeared to reduce the tendencies of the lamp to drift. It also served as a power input regulator; the amount of self-reversal can be adjusted in this manner and the relative intensities of the hyperfine components altered. This feature is of greater interest for the Zeeman experiments in which equal hyperfine components are assumed in the analysis.

The lamp bulbs are spherical with a diameter of 1 to 1.25-in. They are prepared as follows. Several Pyrex bulbs are blown and attached to a tube by the glassblowers, as shown in Fig. 9. This assembly is connected to the vacuum system (see Fig. 10), inside the oven. The vial containing the Rb metal and a hammer are placed in a tube connected to the assembly but situated outside the oven. The assembly is baked at 350 to 400° C for 24 or more hours, until a vacuum of 10^{-6} mm Hg or better is achieved. The Rb vial is then broken and the

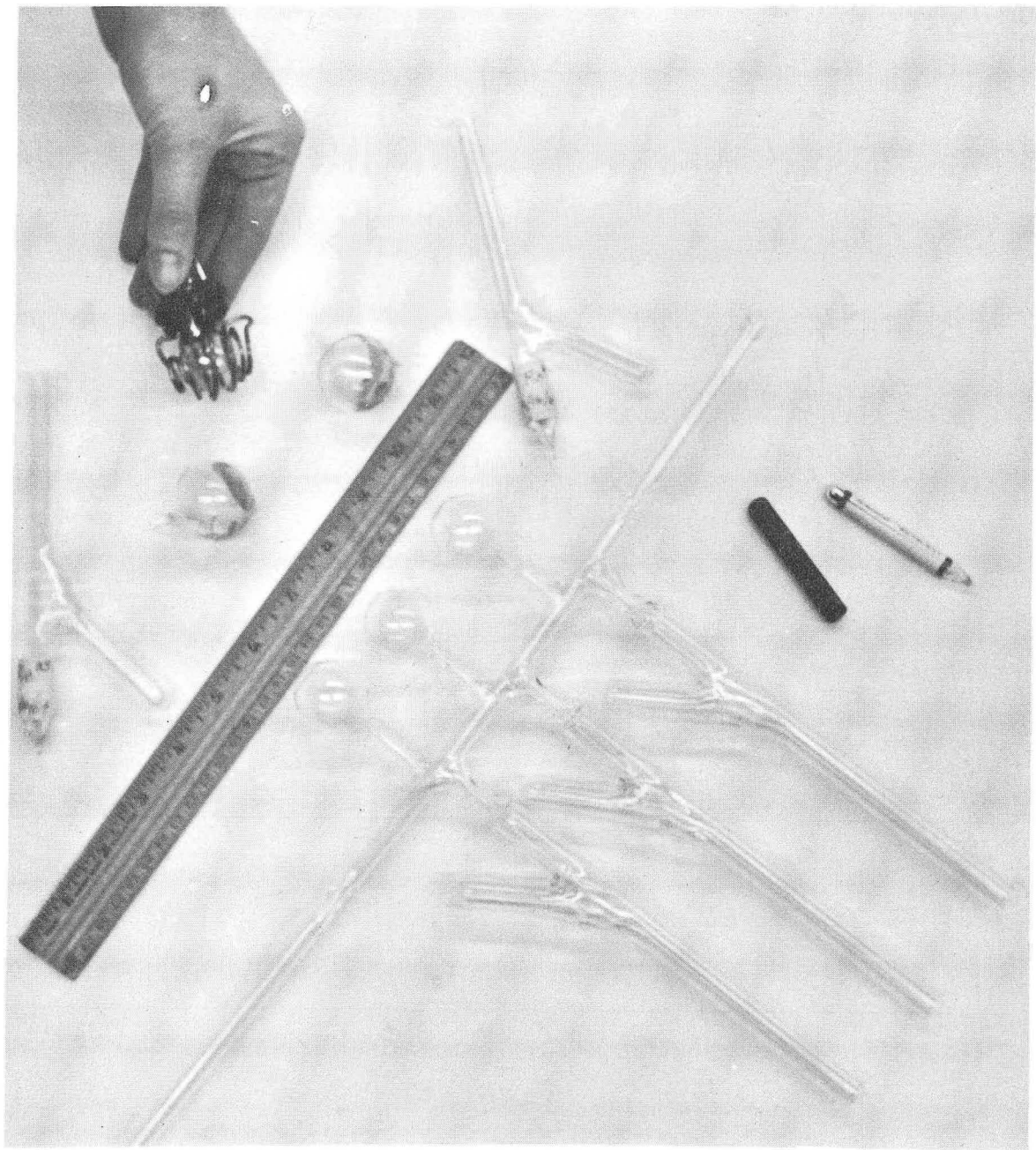

ZN-4879

Fig. 9. Lethia lending a hand with the experiment. She is holding an oscillator coil (used in the density measurement lamp) containing a lamp bulb. The assembly of bulbs and sidearms is connected to the vacuum system for distillation of the alkali. The naturally occurring elements are delivered in large vials (as on the right) which are broken by large glass-enclosed ferromagnetic hammers (the slug is next to the vial). The elements are obtained from A. D. MacKay, Inc., 198 Broadway, New York 38, New York, in 1-g ampules.

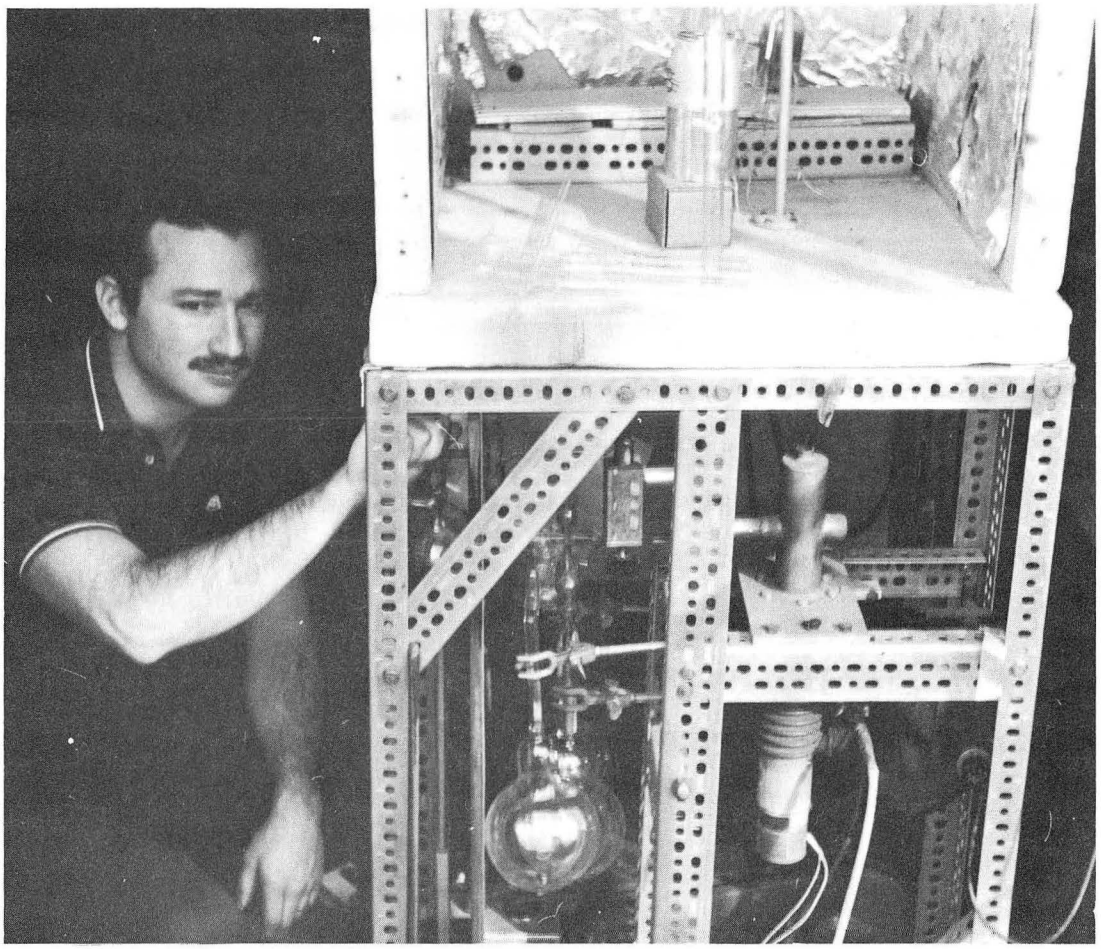

ZN-4880

Fig. 10. Gerry Wick closing off one arm of the oil manometer; the various components of the vacuum system should be easily recognized.

metal laboriously distilled into the bulbs. When a pressure of 10^{-6} mm Hg is again reached, 1 mm Hg of argon is added. An oil manometer is used to determine the carrier gas pressure. A bulb is then sealed off and removed from the vacuum system. As described by Brewer, a short stem on the bulb serves as a reservoir; large amounts of metal have been used without migration problems. The bulb life is long— at least several months of almost continuous use. However, a breaking-in period of several hours seems to be necessary for new bulbs before stability is attained.

The lamp is shown in Fig. 11. In operation the side plate is attached, to insulate the bulb from temperature fluctuations in the room. The output of the lamp depends strongly on the temperature of the bulb through the mechanism of self-reversal. As mentioned previously, the temperature can be altered by varying the input power to the oscillator or by using a heater or blower.

After a warm-up of a few hours and with only small temperature fluctuations in the room, the drift of the light is usually no more than a few tenths % of the total light in 10 minutes. The lamp noise is about 0.1% of the total light. The signals are typically 1 to 5% of the total light. The time required to accumulate 32 points defining a relaxation curve is normally about 0.25 minute. Thus the lamp drift is usually slow compared with the cycle time of the measurement. Excellent signal-to-noise ratios are usually obtained by accumulating data for 10 minutes.

Placing one of the lamp bulbs in the coil of a more powerful oscillator does not appear to increase either the light output or the power absorbed by the bulb. Thus the characteristics of the bulb itself — temperature, size, and carrier gas — are the primary determinants of the output features of the lamp.

A Varian lamp was also tried but found to be less intense, perhaps only because of the smaller surface area of the lamp bulb.

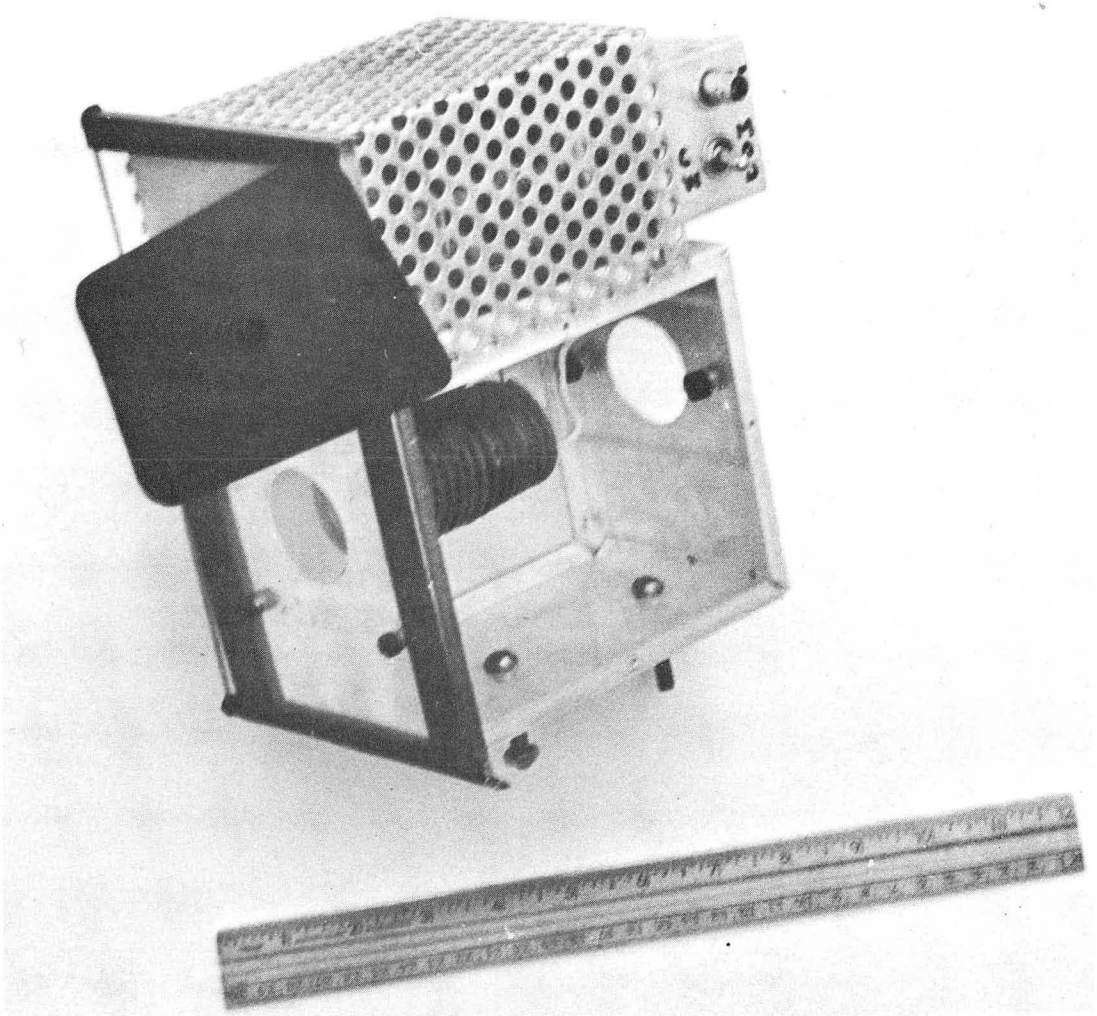

ZN-4881

Fig. 11. The pumping lamp (Brewer circuit). The starter wire, permitting starting without opening the lamp box, is seen at the back of the coil that contains the lamp bulb. The oscillator is contained in the two boxes attached to the lamp box.

Fig. 12(a). Relative intensities and separations of the hyperfine-structure components of the Rb^{87} and Rb^{85} $5^2P_{1/2} \rightarrow 5^2S_{1/2}$ transitions at 7947 Å. W is the energy relative to the fine-structure energy.[49]

Transition	Rb^{87}			Rb^{85}		
	$\tilde{\nu}-\tilde{\nu}_0$ (mK)	I	f value	$\tilde{\nu}-\tilde{\nu}_0$ (mK)	I	f value
a	125.5	7.43	1/48	52.1	28.6	10/324
b	152.7	37.2	5/48	64.2	100.0	35/324
c	-102.5	37.2	5/48	-49.3	100.0	35/324
d	-75.3	37.2	5/48	-37.2	80.0	28/324

The relative intensities I are normalized so that the largest is 100 (a natural abundance ratio of 2.59 is assumed for the ratio of Rb^{85} to Rb^{87} densities). The f values are normalized so that their sum is 1/3 for each isotope. The theoretical f values (and I) can be calculated as in Appendix IV.

Fig. 12(b). Relative intensities and separations of the hyperfine-structure components of the Rb^{87} and Rb^{85} $5^2P_{3/2} \rightarrow 5^2S_{1/2}$ transitions at 7800 Å. W is the energy relative to the fine structure energy.[49]

Transition	Rb^{87}			Rb^{85}		
	$\tilde{\nu}-\tilde{\nu}_0$(mK)	I	f value	$\tilde{\nu}-\tilde{\nu}_0$(mK)	I	f value
e	132.3	6.4	2/48	55.3	33.4	27/324
f	134.7	16.1	5/48	56.3	43.2	35/324
g	140.1	16.1	5/48	58.5	34.6	28/324
h	-93.3	3.2	1/48	-45.1	12.3	10/324
i	-87.9	16.1	5/48	-43.0	43.2	35/324
j	-79.0	45.0	14/48	-38.9	100.0	81/324

The relative intensities I are normalized so that the largest is 100 (a natural abundance ratio of 2.59 is assumed for the ratio of Rb^{85} to Rb^{87} densities). The f values are normalized so that their sum is 2/3 for each isotope. The f values (and I) can be calculated as in Appendix IV.

(a)

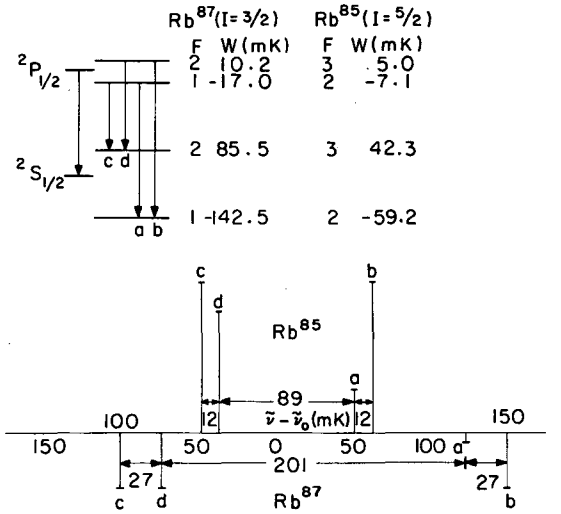
Rb87(I=3/2) Rb85(I=5/2)
F W(mK) F W(mK)
2 10.2 3 5.0
1 -17.0 2 -7.1
2 85.5 3 42.3
1 -142.5 2 -59.2
2P1/2
2S1/2
c d
a b
Rb85
89
12
12
100
150
150
50
0
50
100
201
27
27
Rb87

(b)

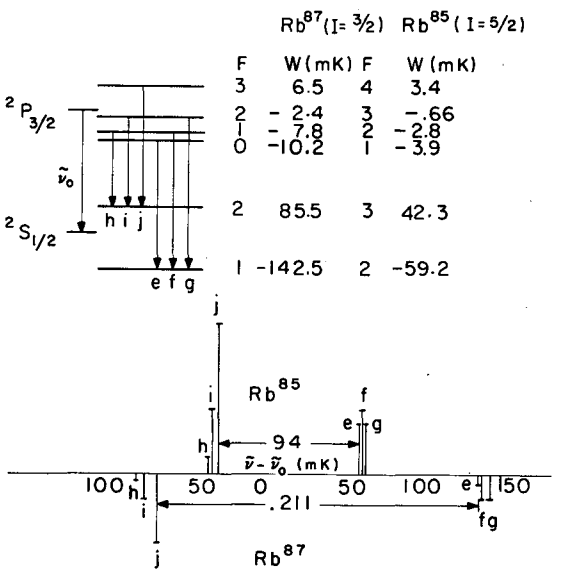
Rb87(I=3/2) Rb85(I=5/2)
F W(mK) F W(mK)
3 6.5 4 3.4
2 -2.4 3 -.66
1 -7.8 2 -2.8
0 -10.2 1 -3.9
2 85.5 3 42.3
1 -142.5 2 -59.2
2P3/2
2S1/2
Rb85
94
100
50
0
50
100
150
211
Rb87

MU-35565

2. Hyperfine Filter

In order to achieve a large deviation from the thermal equilibrium ratio of the hyperfine populations, it is desirable to eliminate one of the hyperfine components from the pumping radiation. This can be done easily in Rb because of the near coincidence of the wavelengths of Rb^{87} and Rb^{85}, the abundance of both isotopes, and the fact that inert gases can be used to shift the frequency of peak absorption. As suggested by other experimenters,[24, 43-46] a filter cell of Rb^{85} with 6 cm of argon was constructed to absorb light emitted in transitions to the F = 2 level of Rb^{87}; see Fig. 12. The efficiency of the filter is illustrated in Figs. 13 and 14 for a natural Rb lamp. The filter is seen to greatly reduce the ratio of the two hyperfine components for both the D_1 and D_2 lines.

The cell is cylindrical and is constructed by sealing (with a torch) flat circular windows about 3/16 in. thick into the ends of a 2-in.-diameter tube 2.5 in. long. The Rb^{85} was obtained from Oak Ridge National Laboratory as RbCl. Their isotopic analysis indicates 99.0±0.05 % Rb^{85} and 1.0±0.05 % Rb^{87}. Calcium is used to reduce the RbCl under vacuum, as described by Alley.[50] A distillation distance of only a few inches is used because of the tendency of the Rb to interact with the glass. The outside of the cell is silvered to decrease the light losses.

Insertion of the hyperfine filter and its two lenses into the system reduced the apparent light signal from 200 mV to 75 mV (the expression "light signal" refers to the output of the common-base amplifier which follows the silicon detector). However, with the Rb^{87} sidearm at 25°C, the hyperfine signal was ≈2.4 mV or about the same as the Zeeman signal with 200 mV of pumping light. This is probably because the filter eliminates most of the unused Rb^{85} light. The cell is housed in a 3×4×5-in. chassis box with a heater in the bottom and a mercury thermometer at the top center; see Fig. 15. The temperature is usually between 55 and 60°C.

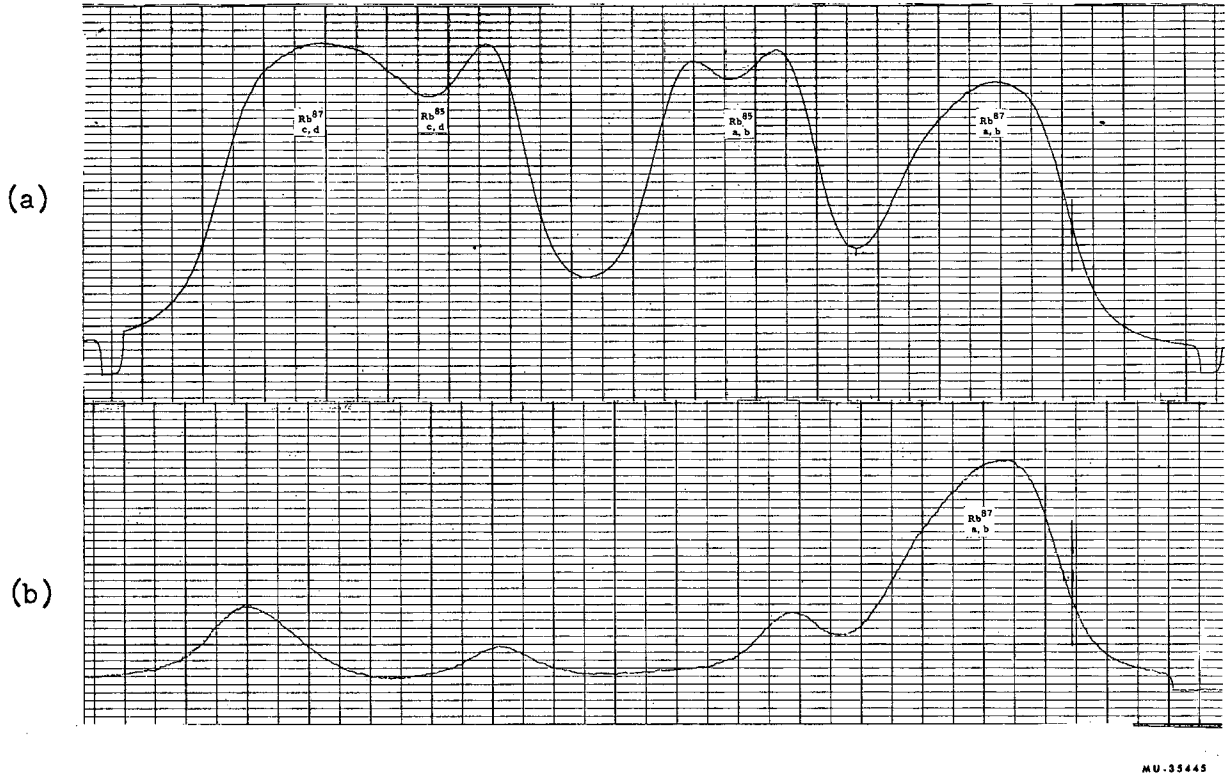

Fig. 13. Effect of Rb^{85} filter cell on the 7947-Å line from a natural Rb lamp. The traces are in approximately the correct frequency relationship to one another (estimated by adding filter while still scanning). The intensities are not normalized. (a) Without filter. (b) With filter.

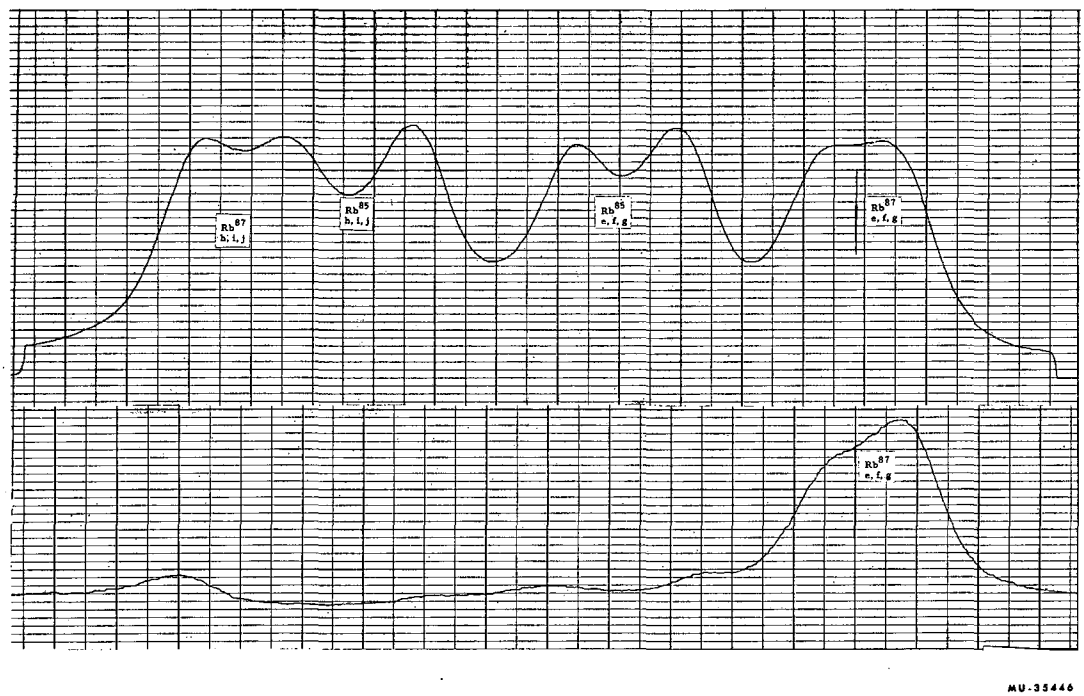

Fig. 14. Effect of Rb^{85} filter cell on the 7800-Å line from a natural Rb lamp. The traces are in approximately the correct frequency relationship to one another. The intensities are not normalized. (a) Without filter. (b) With filter.

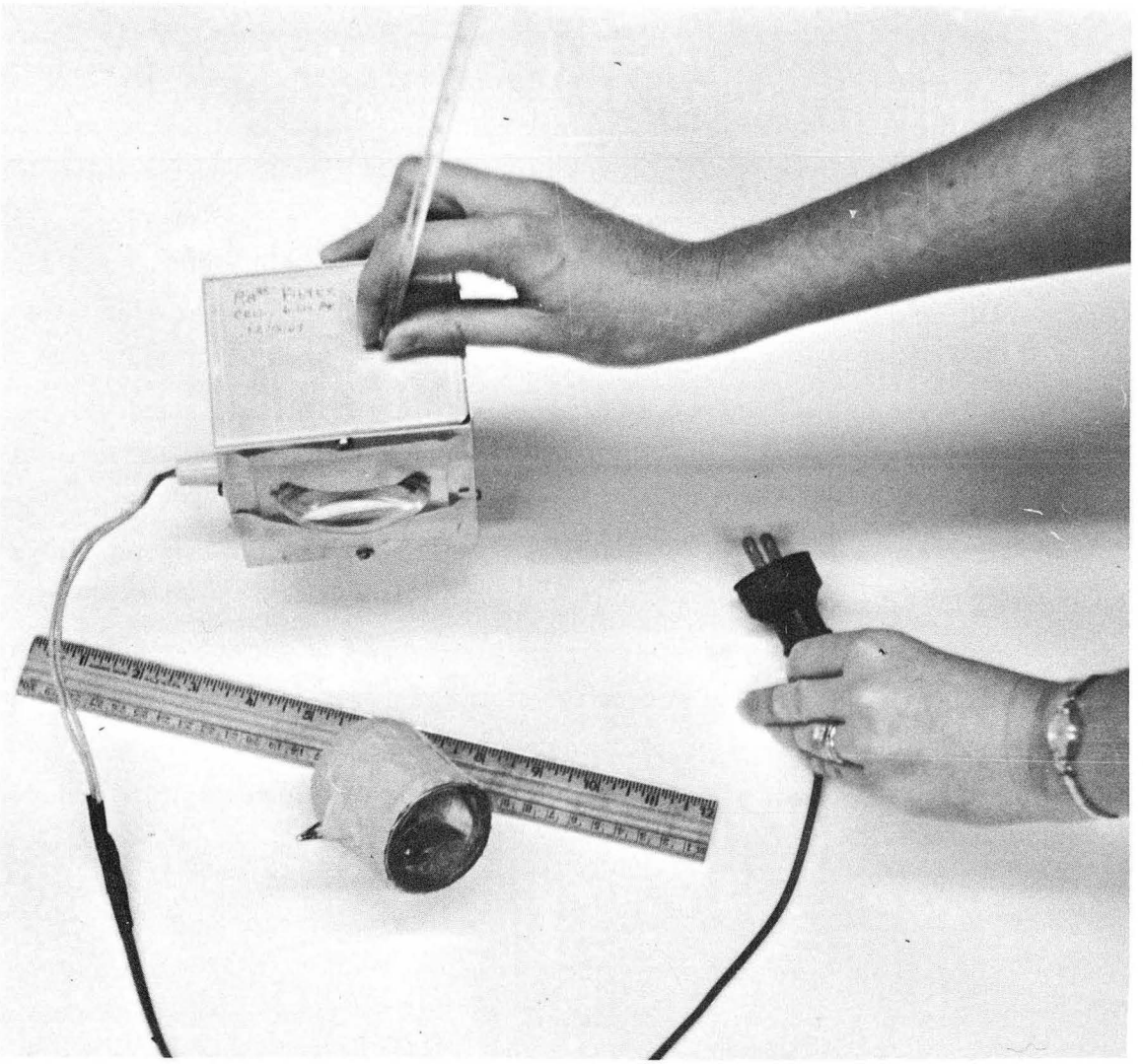

ZN-4882

Fig. 15. The Rb^{85} filter cell and enclosure. The cell is wrapped in masking tape to protect the silver coating.

3. Interference Filters, Polarizers, and Quarter-Wave Plates

No D_1 or D_2 filter is used in the hyperfine relaxation time measurements. But for Zeeman pumping and for studying the spectral profiles of the D lines emitted by the lamp, narrow-band ($\approx$ 80 Å) interference filters are used which were obtained from Spectrolab. These filters have a peak transmisssion of $\approx$ 90%, with 0% transmission for several hundred angstroms on either side.

In order to eliminate as much background light as possible, a trimmer filter immediately precedes the detector. It also was obtained from Spectrolab; its transmission is $\approx$ 85% at 8000 Å and $\approx$ 0% above 12000 Å and below 7000 Å throughout the visible spectrum.

In order for the Kerr cell to operate as a shutter it must be preceded by and followed by a linear polarizer; two HN32 polarizers were purchased with the Kerr cell. For Zeeman pumping, the second polarizer is followed by a quarter-wave plate designed for 8000 Å and purchased from Spectrolab. Free samples of circular polarizers from Polaroid produced essentially identical results. For convenience, the quarter-wave plate is not removed during the hyperfine runs. Consequently, Zeeman pumping also occurs, and the rf resonances can be located easily.

4. Shutters

The requirements imposed upon the shutter by the experiment are discussed in subsection IIIC. 4a. In IIIC. 4b comments are made on the various shutters considered. The Kerr cell shutter is discussed in IIIC. 4c and its problems and the supplementary mechanical shutter in IIIC. 4d.

a. Requirements.

In order to study relaxation times as short as 10 msec and not introduce shutter effects, rise and fall times of 1 msec or less are needed. Because the signal may be only 1% of the total light, the rise and fall times should refer to the time required to reach 99.9% of the final value rather than 63%. The shutter should also be capable of rapid cycling for thousands of cycles, in order that data can be accumulated efficiently. The "off" interval should be easily variable from

1 msec to seconds, and the "on" interval should be 100 msec or longer to ensure that the saturated polarization is attained each cycle. Finally an aperture at least 1/2 in. in diameter is needed to achieve reasonable pumping times.

b. Shutters considered

The undesirable characteristics of various rejected shutters will now be given. Camera shutters usually have rise and fall times of a few milliseconds, must be reset to change the off interval, and are not readily adaptable to electronic cycling. If a fan-type rotor blade is driven fast enough to produce short on and off times with a reasonable aperture, the on interval is much less than 100 msec. In addition, either the blade or the speed must be changed to alter the off interval.

An effort was made to cut a lamp on and off by screen-modulating an rf amplifier. It was found that the shape of the leading edge of the light pulse is strongly dependent upon the temperature of the lamp. For a given off interval the temperature could be adjusted to give a fairly square leading corner, but then for other off intervals the corner would be spiked or rounded. For example, if the temperature was adjusted to give a square corner for a 1-msec off interval, for a 10-msec off interval the rounding effect was more than 10% of the total light. Such an effect would completely obscure a 1% signal. Thus the idea of electronic switching of the lamp was discarded.

Stepper motors were not considered until after the purchase of the Kerr cell. The mechanical shutter used in conjunction with the Kerr cell was driven by a two-position stepper relay; its on and off times are 5 to 10 msec.

Solid-state Kerr cells were considered only briefly but not seriously because of the quoted acceptance angles of 1 to 2% compared with 30% for the liquid Kerr cells. However, it is possible that the problem of increased "off" transmission (to be discussed in IIIC. 4d) of the liquid Kerr cells would not be present.

In view of the desire to cycle rapidly with variable off intervals, and in light of the difficulties and limitations of the alternatives mentioned above, the "perfect" shutter, a Kerr cell, was purchased from

Electro-Optical Instruments. The Kerr cell is their Model K93/150P filled with specially purified nitrobenzene. The first major disappointment of this experiment was the failure of the Kerr cell to perform as a perfect shutter (see IIIC. 4d).

c. Kerr cell shutter

The Kerr cell and its enclosure, constructed of Plexiglas, brass, and nylon screws, are shown in Figs. 16 and 17. RG-8/U cable, with its shield removed to reduce its capacitance, connects the high-voltage terminal of the enclosure to the high-voltage switch. The cable is placed inside a thick rubber hose for further insulation. Because of the large aperture (0.93×1.5 in.) and moderate length (4.1 cm) of the Kerr cell, the full-open voltage is in excess of 50 kilovolts. The Kerr cell was later modified to a separation of 0.8-in. to reduce the required voltage to about 45 kV.

For a discussion of the operation of a Kerr cell shutter see reference 51. A Kerr cell can be operated normally open or normally closed, depending upon whether the linear polarizers before and after the Kerr cell have their transmission axes parallel or perpendicular to each other (both must be at 45 deg with respect to the electric field). The percentage optical transmission when the polarizer and analyzer angles are ϕ and a respectively is[51]

$$_{\phi}T_{a} = 50 \{\cos^2(\phi - a) - \sin(2\phi)\sin(2a)\sin^2[\pi(V/V_0)^2/2]\} \qquad (140)$$

where V is the applied voltage and $V_0 = 300\,d/(2lK)^{1/2}$ volts; d(cm) is the plate separation, l(in cm) is the light path under the influence of the electric field, and K is the Kerr constant ($\approx 4 \times 10^{-5}$ for nitrobenzene). This transmission is plotted for the normally open ($\phi = a = 45$ deg) and normally colsed ($\phi = -a = 45$ deg) cases in Fig. 18. The peculiar requirements of this experiment make the normally open case more desirable. A fast "light on" or rise time is more important than a fast "off" or fall time. The fall time produces only an uncertainty in the zero of time. A slow rise time may distort the signal by rounding the leading corners of the light. From Fig. 18 it is apparent that for a given displacement from V_0 or 0, the corresponding change

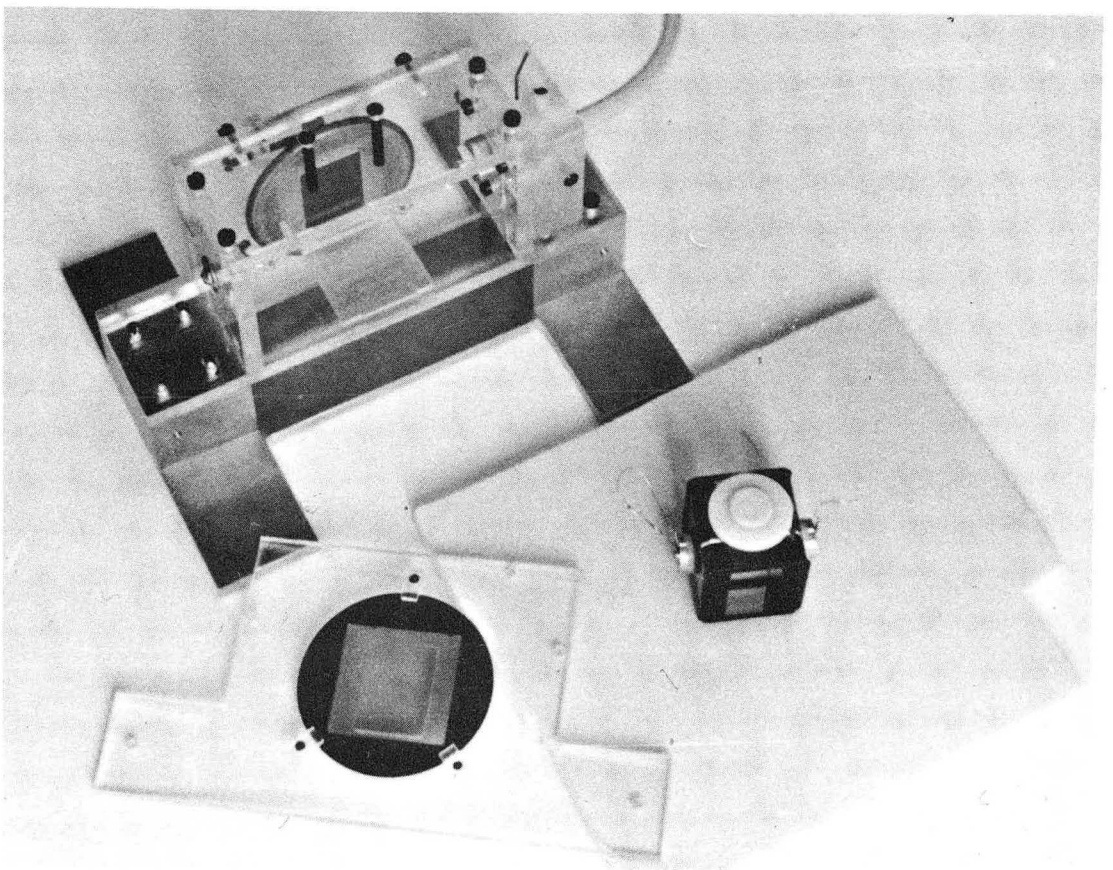

ZN-4883

Fig. 16. Kerr cell with mounted polarizer and enclosure.

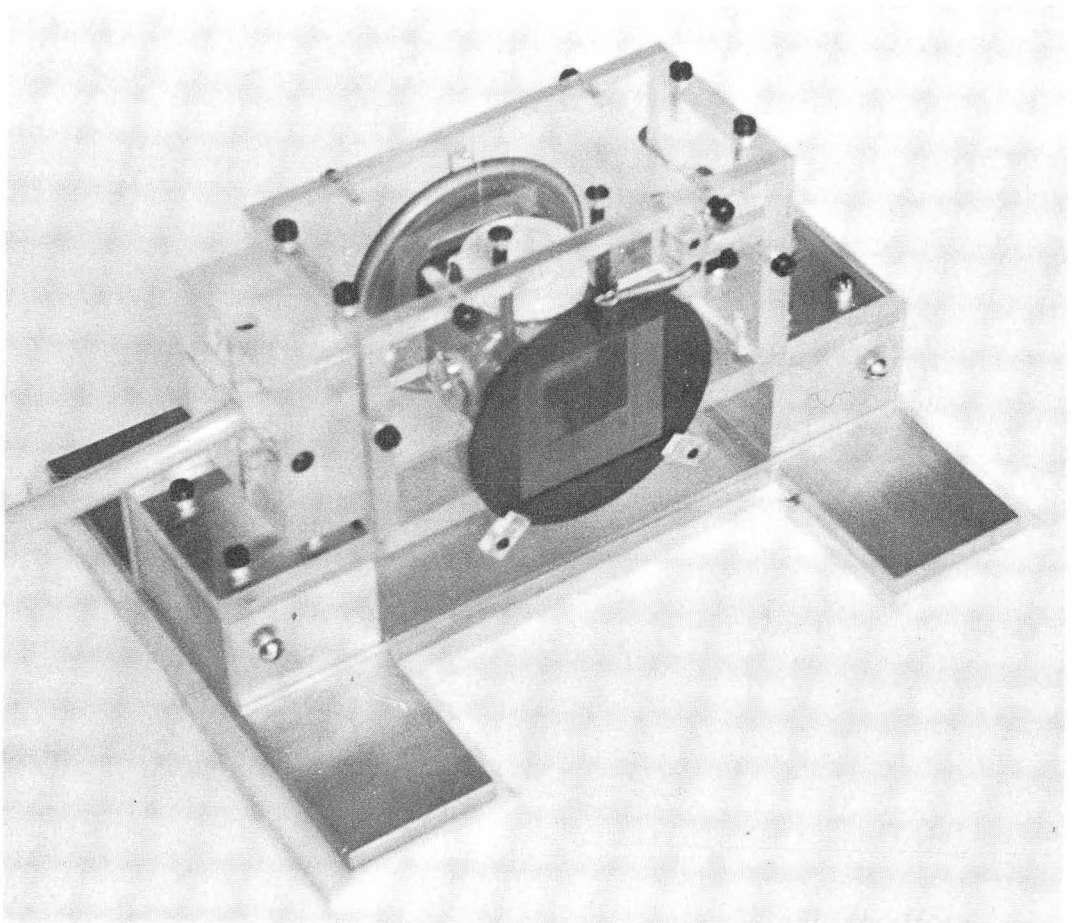

ZN-4884

Fig. 17. Kerr cell in enclosure. In operation the cable is further insulated by a thick rubber hose.

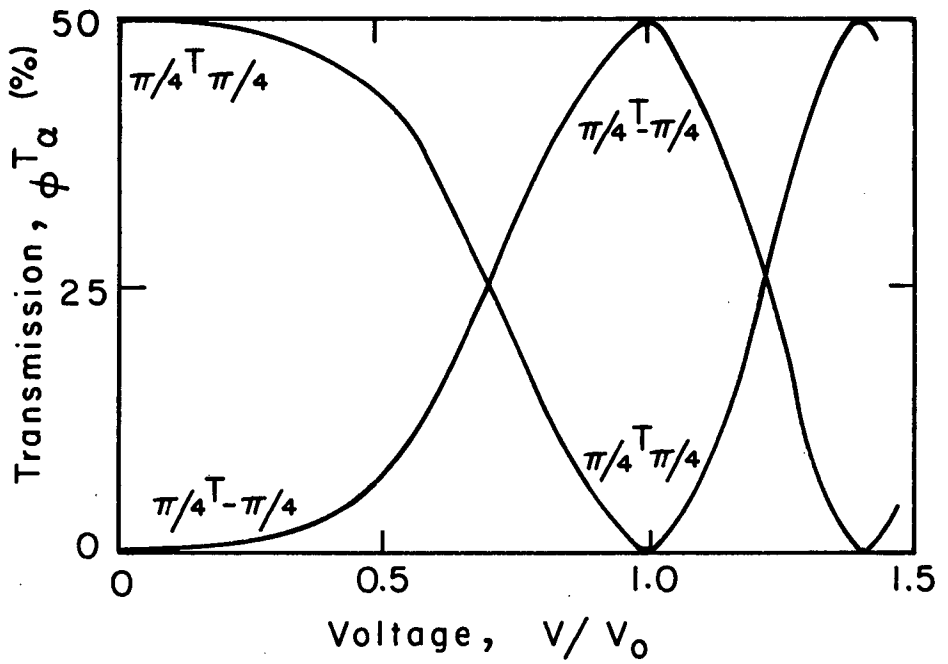

MU-35566

Fig. 18. The transmission versus applied voltage characteristic curve of a Kerr cell shutter with the first linear polarizer at angle ϕ with respect to the electric field and the second at angle α: $_{\phi}T_{\alpha} = 50\{\cos^2(\phi-\alpha)-\sin 2\phi \sin 2\alpha \sin^2[\frac{\pi}{2}(V/V_0)^2]\}$.

in the transmission is smaller near 0 than V_0. In the actual switching circuit the voltage swings between $\approx 0.05\ V_0$ and V_0 rather than 0 and V_0, but the above statement still holds for displacements from V_0 and $0.05\ V_0$. Furthermore, if the normally closed position were used the voltage would have to be extremely well-regulated to keep the light constant to 0.01%. The normally open mode was consequently chosen.

The relaxation time for the Kerr effect is a molecular time constant and is usually about a nanosecond. The switching times of the Kerr cell shutter are then determined by the rise and fall times of the applied voltage. It is well known that Kerr cells are widely used for photographic work in the submicrosecond region. A short high-voltage pulse is used to open the shutter and pass a short light pulse, the shape of which is usually unimportant. For the transient experiments, rectangular pulses up to several seconds in duration are needed. It appeared impossible to extend the usual Kerr cell pulse techniques to the many-millisecond region. After experimentation with various circuits, that given in Fig. 19 was finally adopted. The 6BK4 is a sharp-cutoff beam triode rated at 27 kV. These remarkable tubes have been operated successfully at voltages in excess of 50 kV. Their lifetime in the circuit of Fig. 19 is many months in most cases. Normally the grids of the four switch tubes are driven 5 to 10 V positive to reduce their plate resistance as much as possible. This reduces the plate voltage to 2 or 3 kV, for which case the shutter is open. When the grids are driven 40 V negative, the switch tubes are cut off and the Kerr cell is charged through the 10-MΩ resistor and by means of the cathode-follower action of the charge tubes; the shutter closes. Without the charge tubes the RC charging time would be the product of the 10-MΩ resistance and the capacitance (100 pF) of the Kerr cell (25 pF) and its associated circuitry, or about 1 msec. The charge tubes reduce this charging time by effectively adding resistance in parallel with the 10-MΩ resistor. The value of the latter is chosen as the minimum possible in order not to exceed the current rating of the high-voltage supply (5 mA in this case). Faster charge times could be obtained with heftier supplies.

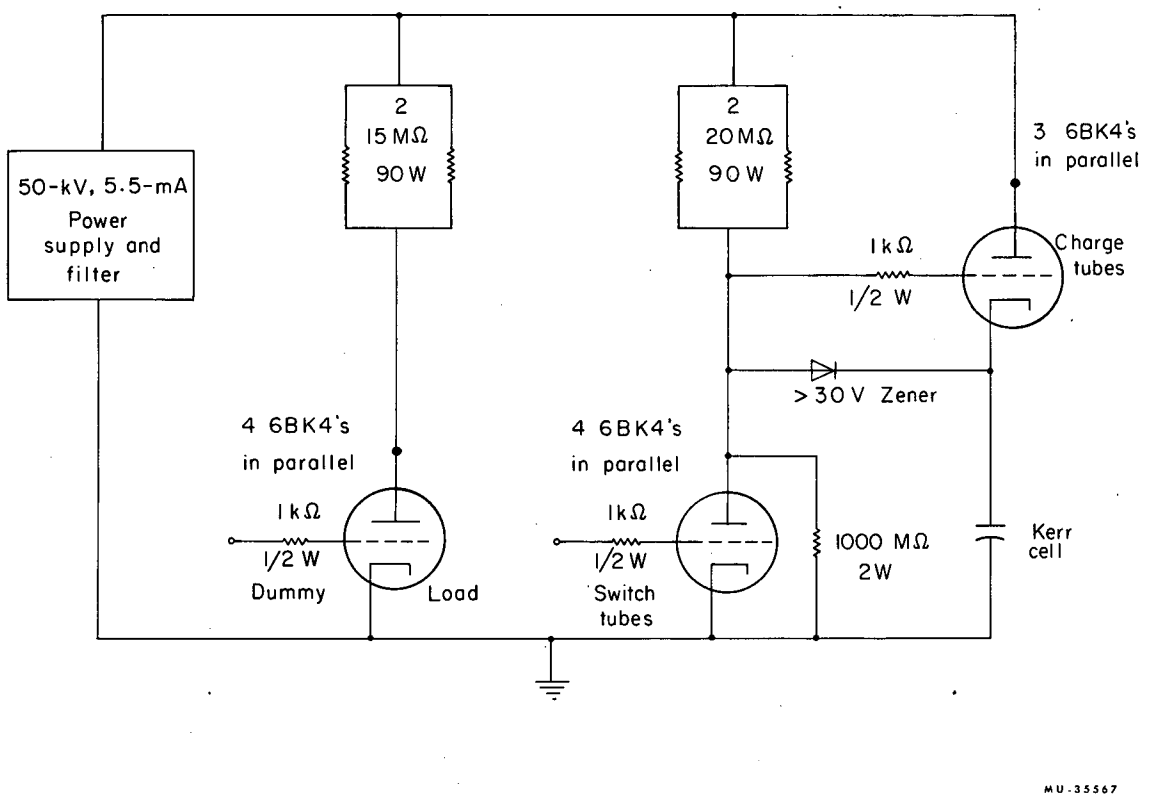

Fig. 19. The Kerr cell switch circuit diagram.

Even though the high-voltage supply is regulated against line voltage changes and is well filtered, the output still varies with load. A constant voltage is desirable in order that once the fully closed voltage is reached no further adjustments be necessary to compensate for a change in power-supply output voltage. This problem is eliminated by the dummy load tubes, which are pulsed by a signal which is the inverse of that applied to the switch tubes except that it is never positive. The power supply then sees a constant load, and its output voltage is constant.

The Zener diode cuts off the charge tubes during the discharge of the Kerr cell; when this diode fails excessive current flows from the supply through the charge and switch tubes.

Note that the charge tubes are floating up to 50 kV above ground. Their filaments must be powered by a floating supply or a very-high-voltage isolation transformer. The brute force method of 5 4FH 1.5-V batteries is used in this case. The life of these batteries is no more than a couple of days if used continuously to supply three tubes. In preliminary observations in which a fast off time is unimportant, the filaments are often cut off and the Zener diode shorted by a short clip lead. The circuit then operates as before except that the Kerr cell is charged through the 10-MΩ resistor only. A switch with a 4-in. insulator shaft is used to switch the charge tube filaments on and off. A meter, also removed 4 in. from the panel, monitors the filament voltage and can be observed through a protective Plexiglas window. The other details of the construction of the circuit can be seen in Fig. 20. Large air gaps and Plexiglas are used for insulation. Dux Seal is used to reduce corona from sharp points. To protect against the high voltage and against x rays the circuitry is completely enclosed in a steel rack cabinet with a safety switch on the door. A ventilating blower is used to circulate air around the resistors.

For completeness, a further specification of componets will now be given: Universal Voltronics BAL 50-kV 5.5-mA high-voltage power supply with a 0.01% filter; model 500S Sorensen line voltage regulator; two 15-MΩ and two 20-MΩ IRC, type MVR 90-watt high-voltage resistors; a 1N2993 IRC Zener diode, 11 RCA 6BK4 electron tubes.

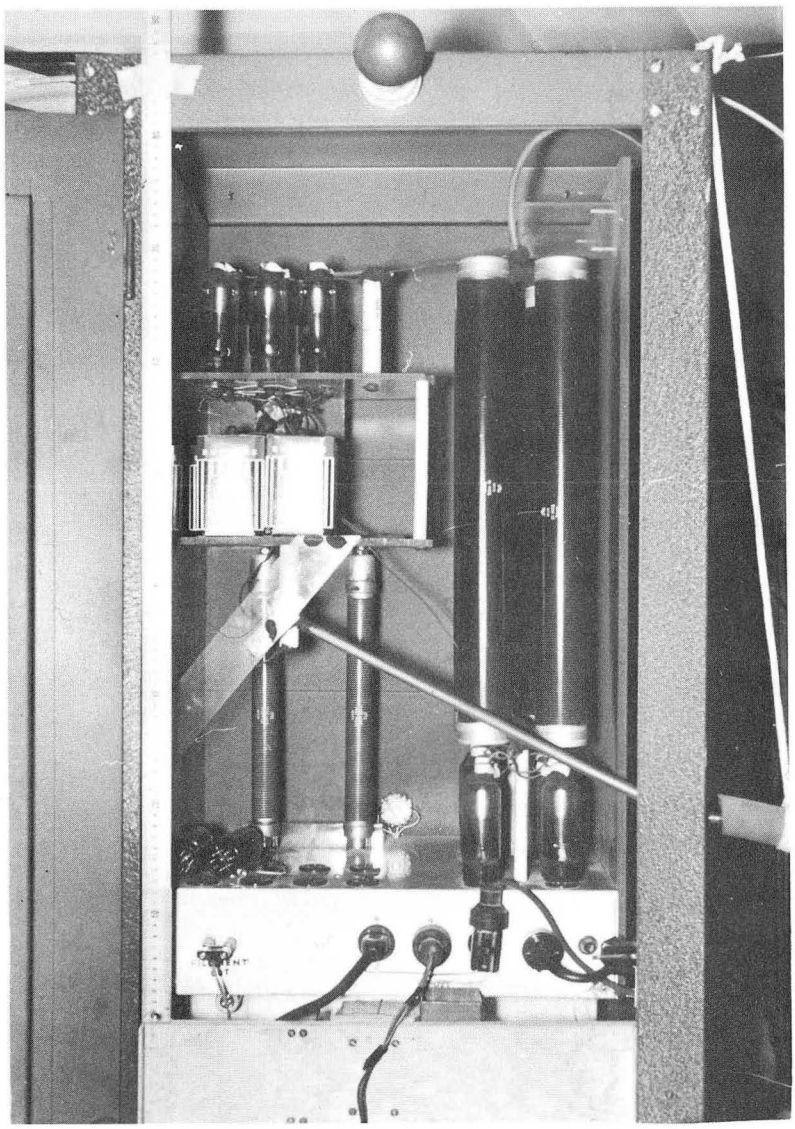

ZN-4885

Fig. 20. Construction of the high-voltage switching circuit for the Kerr cell. Notice the use of large air gaps and Plexiglas for insulation. The dummy load resistors and tubes can be seen behind the switch resistors and tubes.

The performance of the Kerr cell switching circuit combined with the Kerr cell can be judged from Figs. 21 through 23. Figure 21 demonstrates the decrease in fall time when the three charge tubes are used as explained previously. The time to fall to 10% of the initial value is about 0.5 msec. Figure 22 illustrates the amount by which a 6-V positive bias on the switch tube grids speeds up the rise time. Figure 23 indicates a rise time to the 90% level of less than 0.1 msec. That this is reasonable can be seen as follows. The Kerr cell and associated circuitry has a capacitance of about 100 pF. The plate resistance of each switch tube is approximately 5 MΩ. Then with four tubes, RC = 0.125 msec. The Kerr cell transmission-versus-voltage relation decreases the switching time further, but this is partially offset by the increase in plate resistance with a decrease in voltage.

Since the signal may be only 1% of the total light, a 90% criterion is insufficient. The lower trace of Fig. 23 is a 40-times magnification of the top part of the upper trace. Notice that the bright spot (caused by z-axis pulse to oscilloscope), which appears to be well to the right of the saturation point in the upper trace, is seen in the lower trace to be almost 0.2% from the top. Consequently, the actual data point is taken 0.4 to 0.5 msec after the light starts on to allow for the light to reach its maximum value. The data are taken at the beginning of the bright spot, which can be adjusted for the optimum value. If the spot is moved too far to the left it is elongated by the fast rise time and drops below the pumping transient. Clearly, if the initial polarization is represented by the maximum (initial) value of the light intensity, a false apparent signal is observed if the data are taken too early on the rise curve. In summary, so far as the optical pumping process is concerned, the Kerr cell cuts the light on in less than 0.1 msec, but the observation of the initial point used to monitor the polarization must be delayed 0.4 to 0.5 msec to allow the deviation of the light from its maximum value to be a small percentage of the pumping signal.

The Kerr cell shutter admirably fulfills all the requirements given in IIIC. 4a with one subtle exception: in the "off" mode the light is not completely off. Notice in Fig. 4 that there is a "zero" line

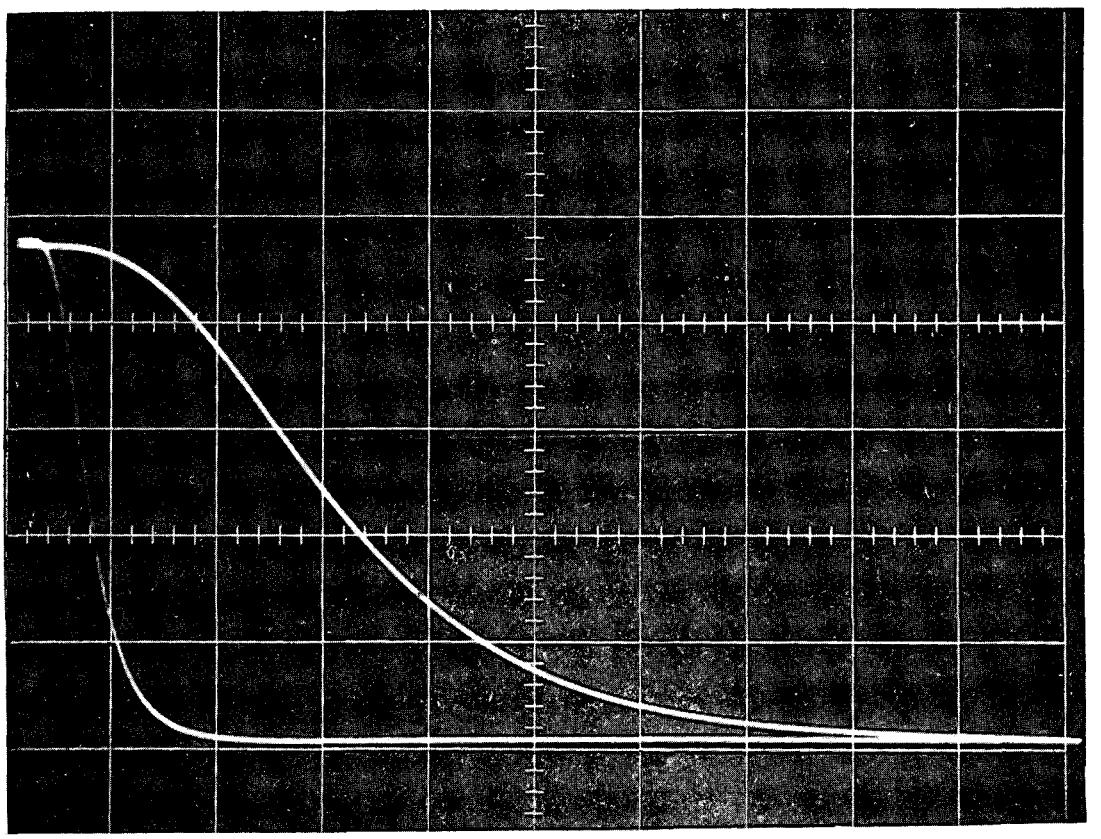

ZN-4833

Fig. 21. Improvement in the off transient of the light when three charge tubes are added to the Kerr cell switch circuit; 10 mV/cm, 0.5 msec/cm.

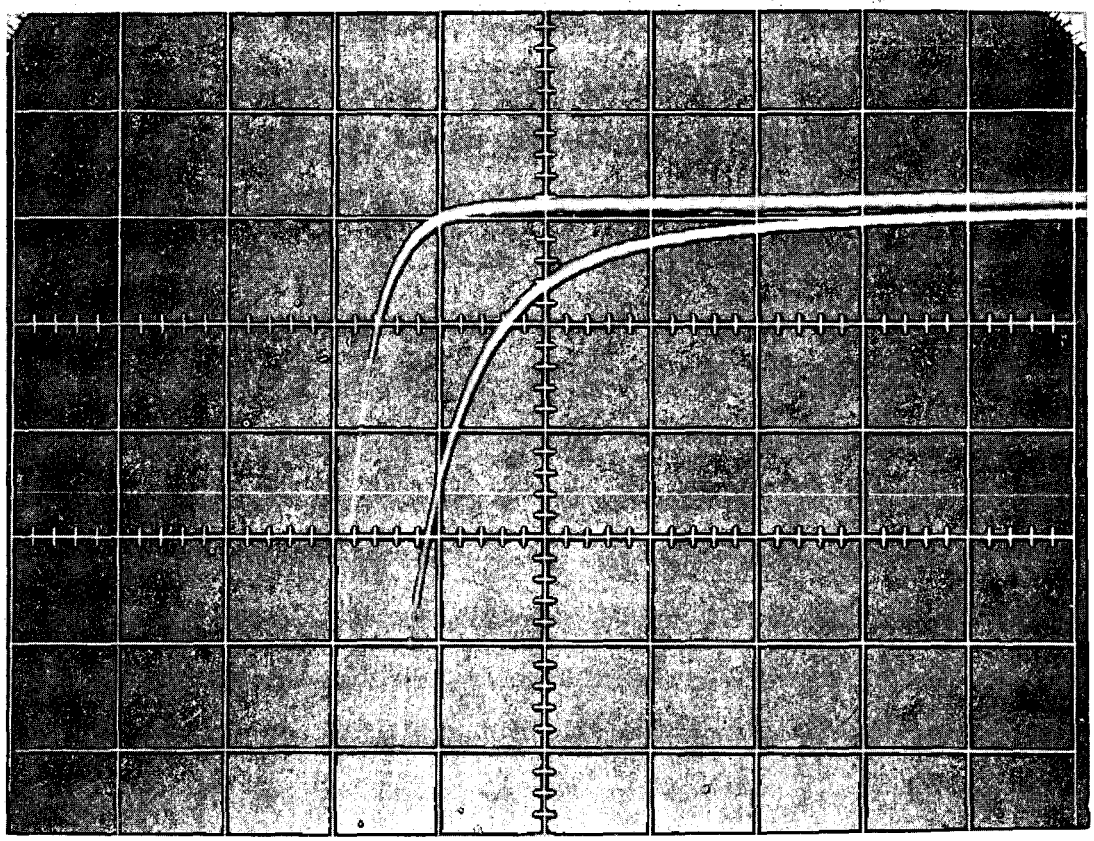

ZN-4834

Fig. 22. Decrease in rise time of the light by driving the grids of the switch tubes 6 V positive; 0.5 mV/cm, 0.1 msec/cm.

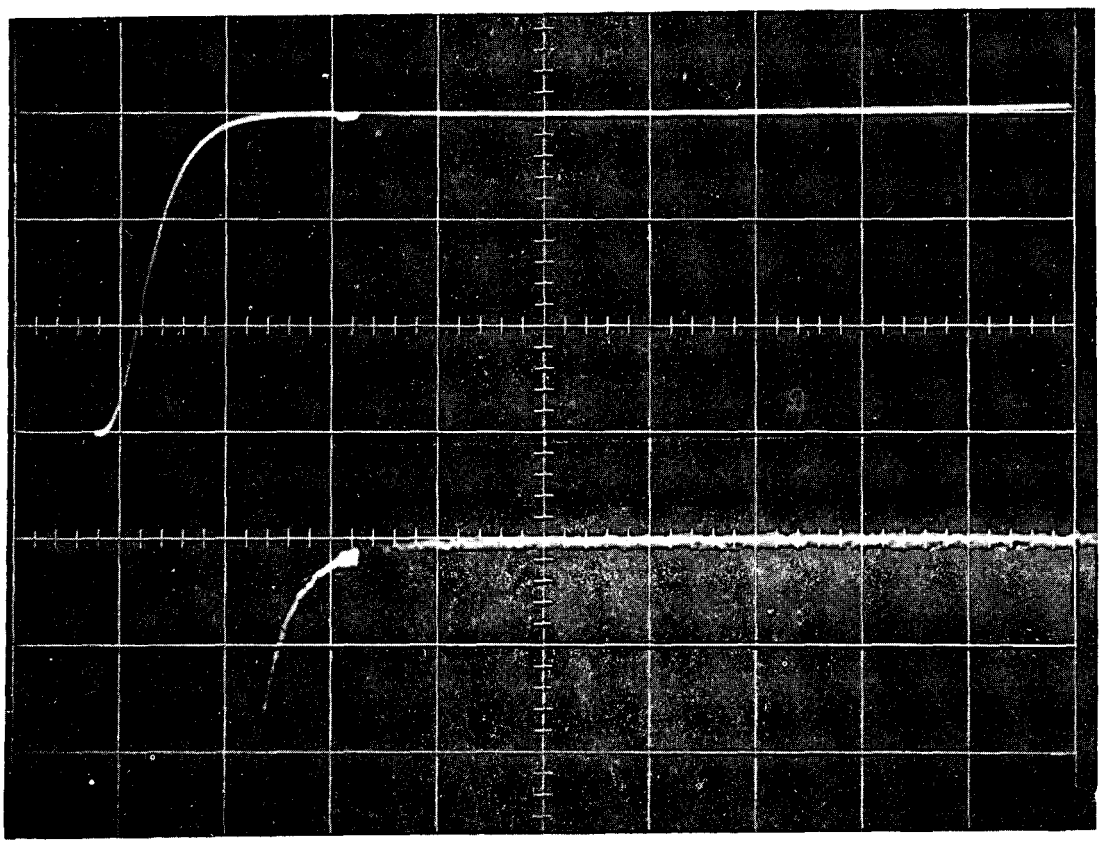

ZN-4835

Fig. 23. Rise transient of the light, 0.1 msec/cm. Upper trace is of the total light; 20 mV/cm. Lower trace is 40-times enlargement of the top of the upper trace; 0.5 mV/cm.

underneath the closely spaced points (taken with the Kerr cell alone) which lies above the "zero" line defined by the mechanical shutter. This problem is treated in the next paragraph.

d. Kerr cell shutter problem and mechanical shutter

The failure of the Kerr cell shutter to completely extinguish the light evidently stems from two contributions. First, the HN32 polarizers transmit about 1% of the 7947-Å light when crossed. Several other polarizers have been tried but with no better success. The second contribution is a function of the purity of the nitrobenzene. If the voltage is adjusted to minimize the off transmission for short times (< 50 msec) the transmission increases at later times. This is shown in Fig. 24. The upper trace is a representation of the voltage applied to the Kerr cell; the voltage is seen to be constant during the off interval. The lower trace shows the corresponding light signal. The off transmission is as large as 10% in some regions. One might at first expect this to be a fair approximation to zero light intensity. But if the pumping time with 10% transmission is comparable to or shorter than the relaxation time, the system will be maintained in a pumped state by the smaller intensity. Thus it is necessary to eliminate such large off transmissions. It is believed that the effect may be the result of a reduction of the electric field by ionic impurities attracted to the electrodes. The Kerr cell was refilled twice by Electro-Optical Instruments and once by Kappa Scientific. For several months after a refilling the effect was usually less than 3%; such was the case during the runs reported here.

In order to eliminate the 3% off transmission, an electrically operated mechanical shutter is synchronized with the Kerr cell for long off intervals. The Kerr cell is still used to provide short rise and fall times; the mechanical shutter transients are of the order of 5 to 10 msec, as shown in Fig. 25. The peak in the center of the figure arises from a bounce of the mechanical shutter. It could be eliminated by reducing its aperture, but it is largely removed by the Kerr cell (see Fig. 4). The shutter was made by Photographic Instrumentation Development Co., now out of business. It consists of a light-weight

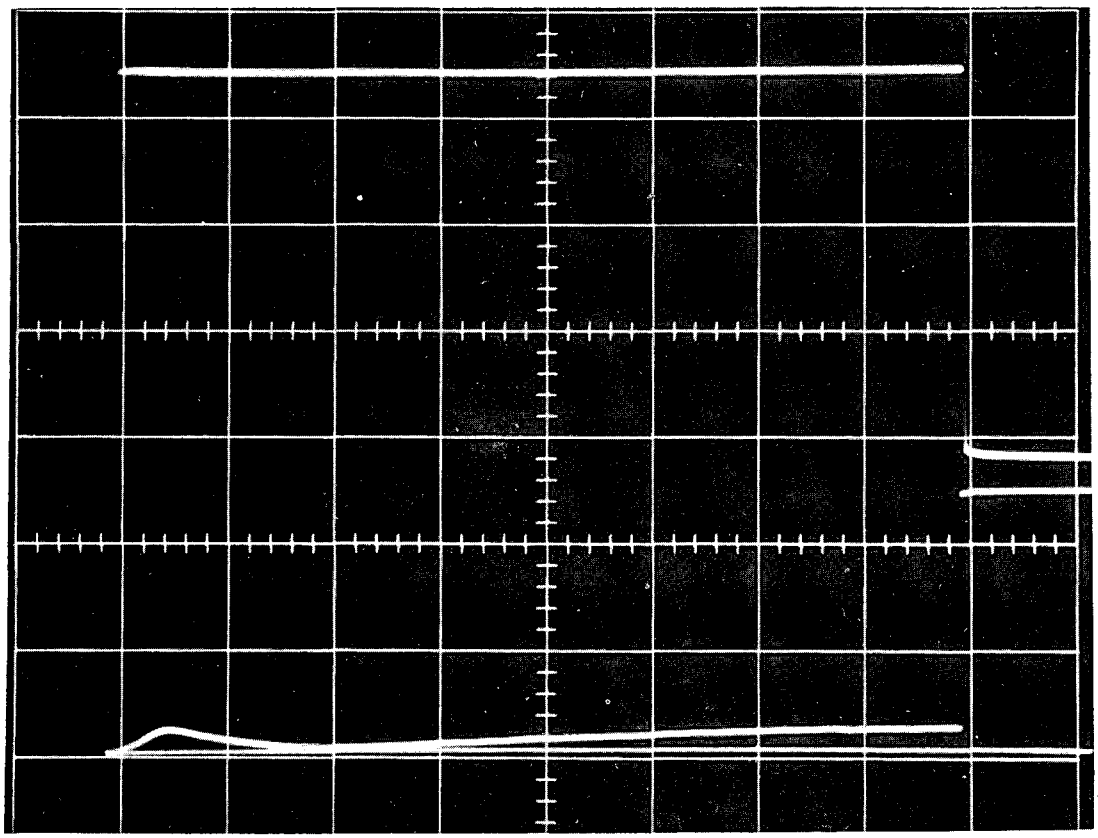

ZN-4836

Fig. 24. "Off" transmission of the Kerr cell shutter; 0.5 sec/cm. The upper trace represents the Kerr cell voltage; 1 V/cm (voltage divider). The lower trace shows the total transmitted light; 0.2 V/cm.

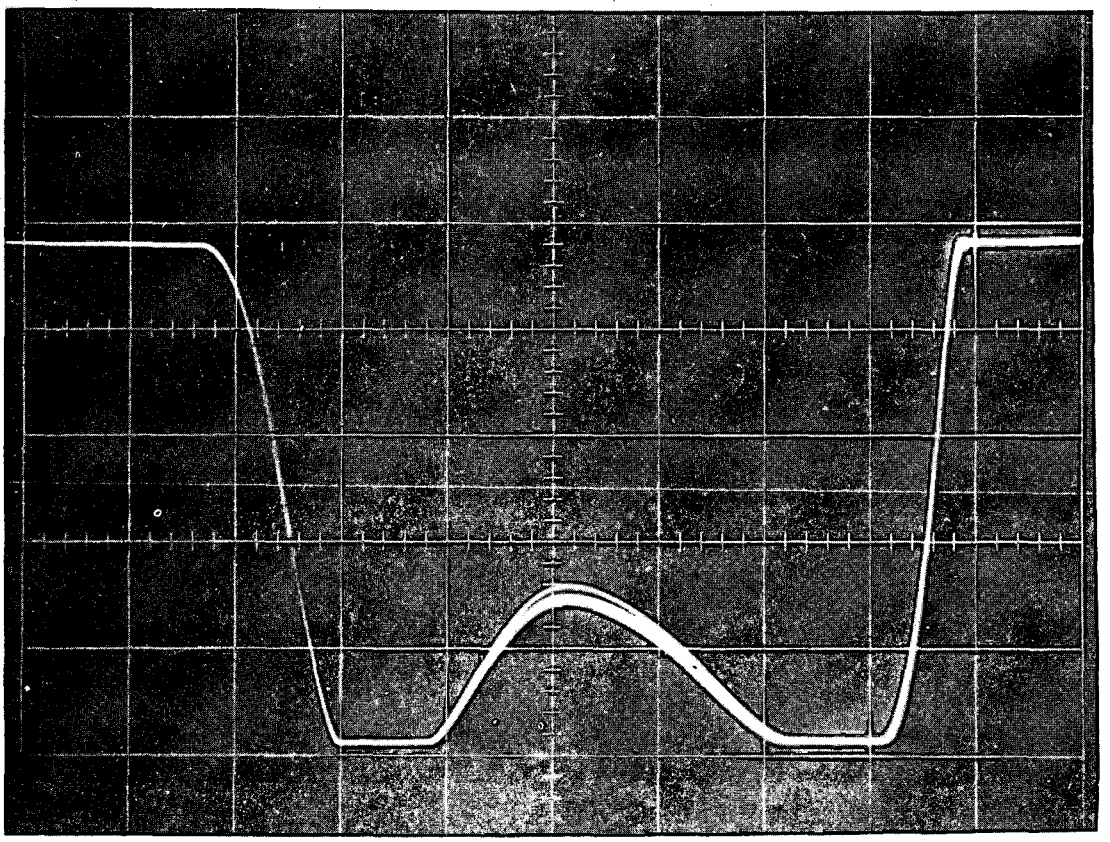

ZN-4839

Fig. 25. Total transmitted light, showing the transient characteristics of the electrically operated mechanical shutter; 10 mV/cm, 10 msec/cm.

metallic blade operated by a Ledex rotary solenoid. The blade is confined between two narrowly spaced surfaces containing a 9/8-in. - diameter aperture. The latter must be further reduced to eliminate bounce transients. Approximately 100 volts is required to actuate the shutter rapidly and 15 volts to hold it open. A circuit was designed to provide such a sequence of voltages to avoid overheating the solenoid.

During most of the runs the Kerr cell and mechanical shutter were used simultaneously to obtain data at 16 different off intervals from 0 to 375 msec spaced 25 msec apart. Then data at 16 shorter intervals $0, 5, \cdots, 75$ msec were taken with the Kerr cell alone; over this region the off transmission is 1 or 2% at most.

The effect of each of the shutters upon the signals is demonstrated in Figs. 26 and 27. In both photographs the lower series of bright spots defines the relaxation curve as determined using both shutters. The upper series in Fig. 26 is for the Kerr cell only; the errors are even larger for longer relaxation times. The upper series in Fig. 27 is with the mechanical shutter only; the magnitude of the signal is reduced by 25% because of pumping during the rise time of the shutter. Under the conditions of a long relaxation time and short pumping time, a reduction in the signal of 75% has been observed upon removing the Kerr cell. The signal as observed on the oscilloscope certainly depends upon which shutter is used. Consequently every effort was made to optimize the shutter in order to minimize the uncertainty in the measurements. However, it is interesting to compare deduced relaxation times for the various shutters with the resonance cell conditions held fixed. For conditions as in Figs. 26 and 27, with both shutters $1/\tau = 11.81 \pm 0.11$ sec^{-1}, with the Kerr cell only, $1/\tau = 12.67 \pm 0.10$; with the mechanical shutter only, $1/\tau = 8.40 \pm 0.73$. Perhaps the last value could be improved considerably by a more careful consideration of the long rise and fall times. For longer pumping times the effects would be less important.

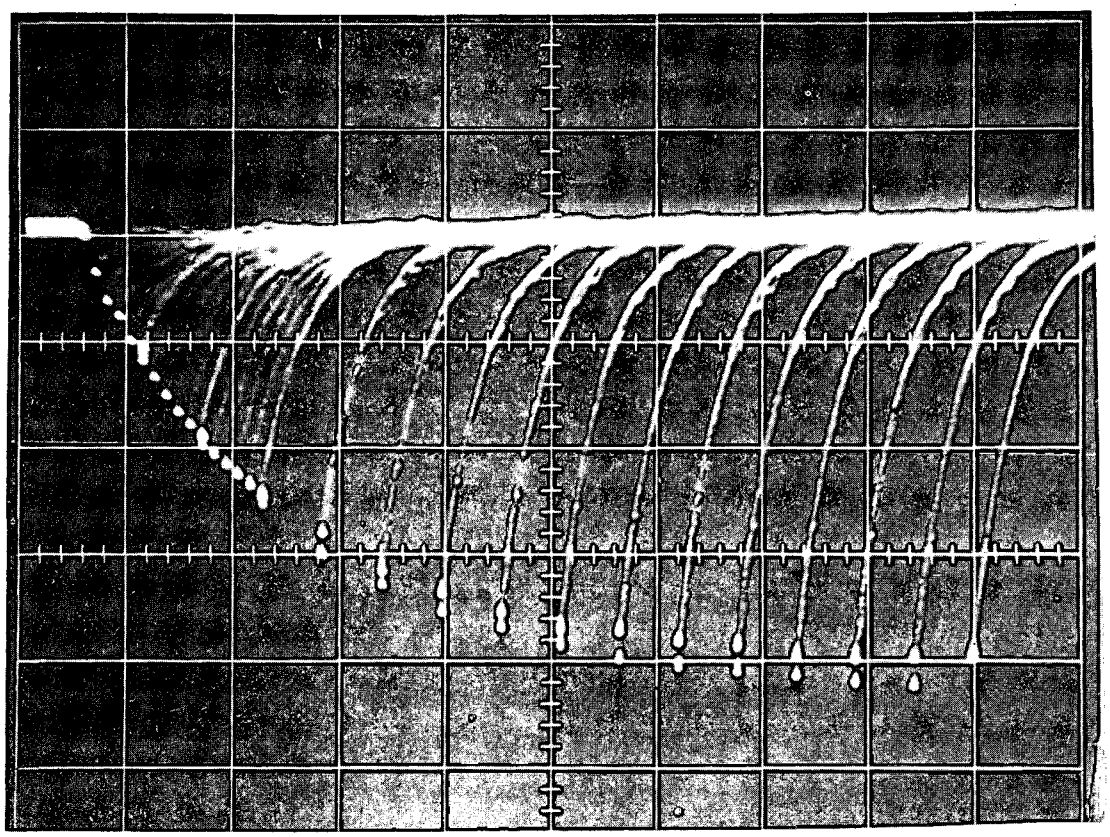

ZN-4837

Fig. 26. Hyperfine pumping signal; 0.2 mV/cm, 25 msec between long off intervals, 5 msec between short. Lower bright spots: Kerr cell and mechanical shutter. Upper bright spots: Kerr cell only.

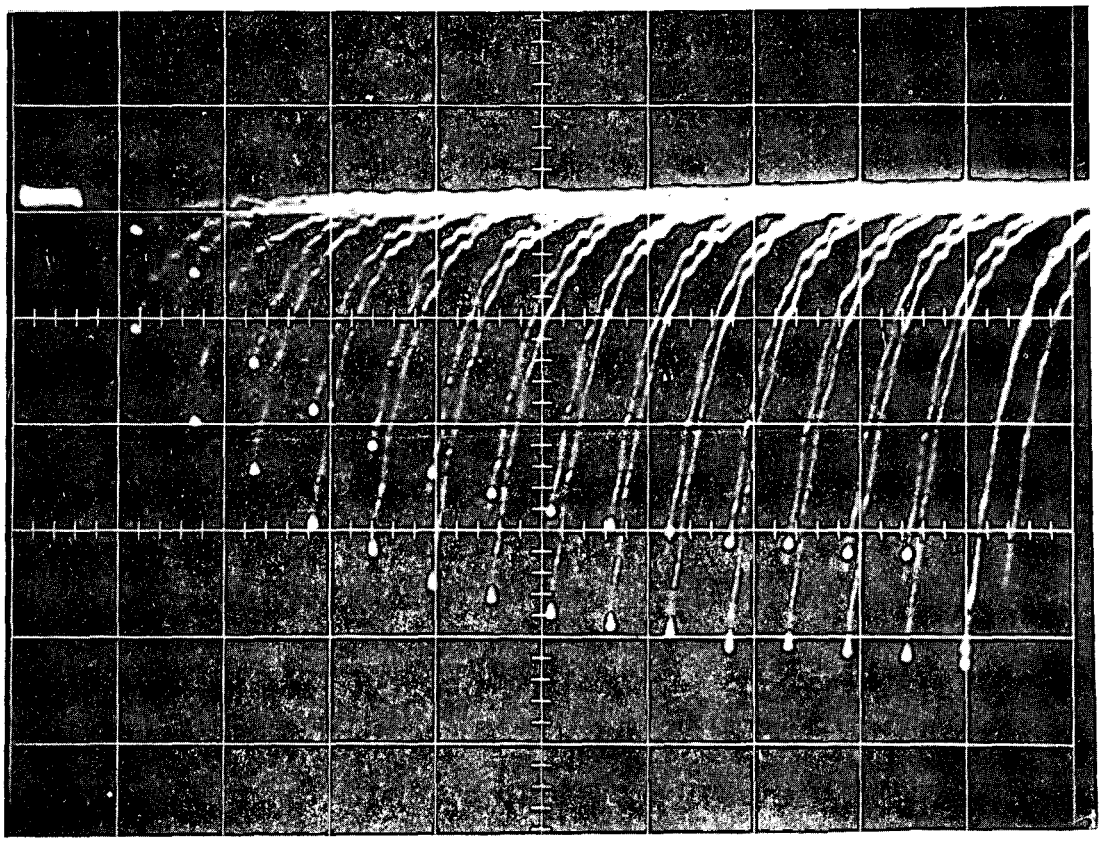

ZN-4838

Fig. 27. Same conditions as Fig. 26 except the upper bright spots are for the mechanical shutter only.

5. Resonance Cell

The resonance cell used in runs 4 through 8 is shown in Fig. 28. The cell is prepared as follows. The cubical cell is blown by the glass-blowers from square tubing; the lower sidearms initially consist of 2 or 3 in. of 10-mm tubing. After being cleaned with chromic acid, the resonance cell is attached to the vacuum through a removable liquid nitrogen U trap. The end of a 3- or 4-in. 10-mm tube is sealed off. Paraflint[52] is poured into the tube and gently melted over a Bunsen burner until the Pariflint is about 1 in. deep. After the Paraflint has solidified, one end of the tube is connected to the stem of the resonance cell through a seal-off. The other end containing the Paraflint is situated outside of the oven. The tube is slanted so that, when heated, the Paraflint runs into the stem. Poor coatings have resulted from excessive heating of the Paraflint during distillations in which gravity had to be overcome. The cell is baked at 350° to 400° C for 24 hours or more, until the pressure is below 10^{-6} mm Hg. After the oven has cooled and the trap immersed in liquid N_2, the Paraflint is melted and coaxed into the resonance cell or its stem. The Paraflint tube is then removed. When the vacuum is sufficiently good, the cell is removed from the system. By rotating the cell over a Bunsen burner, the walls are evenly covered with a thick coating of Paraflint. The cell is baked overnight at 150° to 160° C to remove the excess coating from the walls. Sometimes the Bunsen burner must be used again to clear seal-offs or streaks; the bulb is then rebaked. The water drop test is then applied: the stem is opened and a drop of water inserted. In a successfully coated cell the water gathers into a bead and rolls freely around the cell, not adhering to any point.

Each sidearm consists of a vial (with break-offsky) of the desired metal and a subsidearm containing a glass-enclosed ferromagnetic hammer. The vial is filled in the same manner as the lamp bulbs (see IIIC.1) and often at the same time. The Rb^{87} used contains less than 1% Rb^{85}. The vials are constructed as a part of the sidearm tube (as in Linde gas liters) rather than as small unattached vials in order that the break-offsky cannot avoid the hammer. Short sidearms were

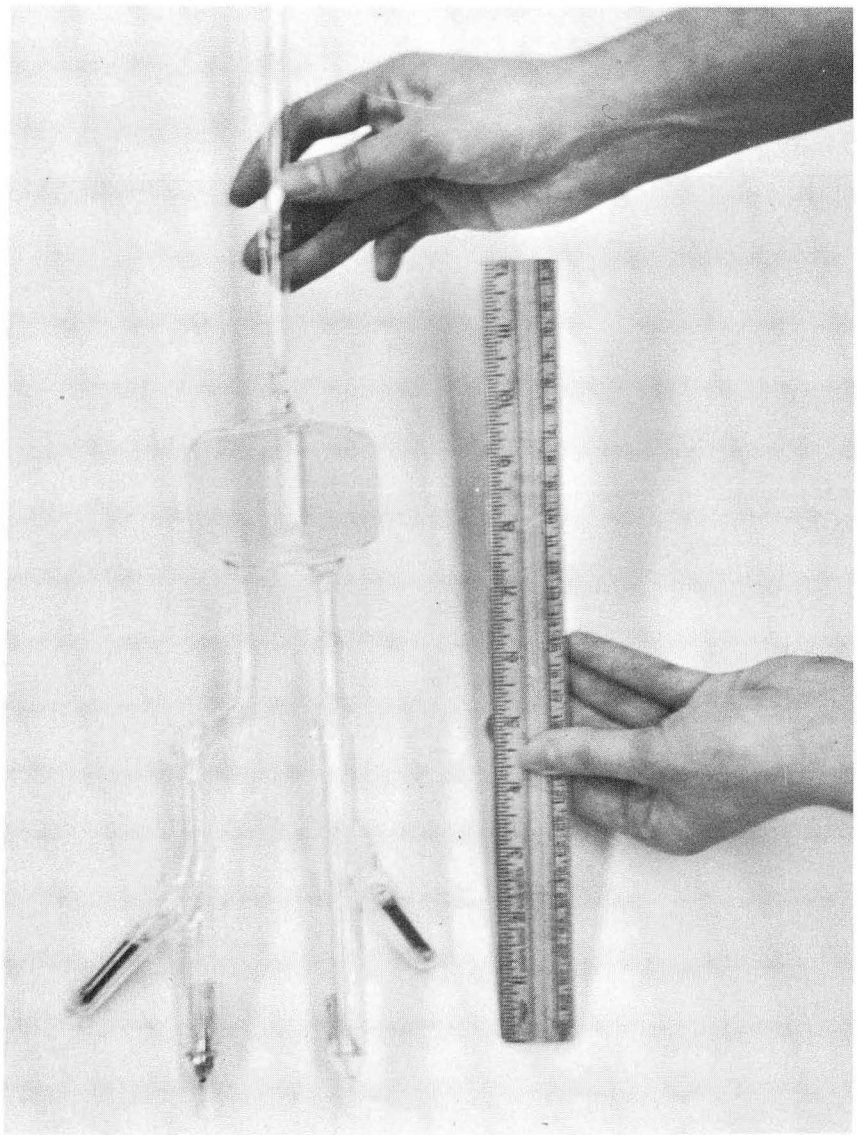

ZN-4886

Fig. 28. Resonance cell with Rb^{87} and Cs sidearms used in runs 4 through 8.

used because of space limitations; sometimes difficulty was encountered in trying to break the vials, but persistence always brought success. The sidearms are attached to the cell. The whole assembly is attached to the vacuum system with the cell in its oven and the sidearms in their respective ovens.

The cell used in runs 4-8 was sealed from the system after a good vacuum was attained but before either vial was opened. The Rb^{87} vial was opened at 4 p.m., 12/2/64. The Rb^{87} sidearm was maintained at 25°C, the resonance cell at 73°C, and the Cs (unopened) sidearm at 44°C. At 8:30 a.m., 12/3, a 0.1% signal was observed; by 6 p.m., 12/4, it had increased to 0.4%. But a week after opening the vial, the relaxation time was still only 30 to 40 msec. In this discussion, relaxation time refers to a single exponential approximation to the Zeeman optical pumping relaxation curve. The cell was then baked for several hours at 110°C (the melting point of Paraflint is $\approx$ 100°C); the relaxation time lengthened to $\approx$ 140 msec.

Whenever the Rb^{87} sidearm was heated to 40° or 45°C for several hours, the relaxation time at 25°C would be less than 140 msec (as short as 50 or 60 msec has been observed) and would remain so until the cell was reheated to 110°C for a few hours. The relaxation time then always returned to the 140 to 150-msec range. This change of relaxation time resulting from a long exposure to a high Rb density must arise from Rb atoms either adhering to the coating or interacting with impurity atoms of the coating. When the coating is melted these disorientation centers are presumably mixed in with the vastly greater number of coating atoms. Upon solidification, there is little chance that one of these centers will be on the surface. This relaxation-time change was discovered in analyzing run 4; it partially destroyed the usefulness of that run. In runs 5 through 8 the data at the higher densities were taken rapidly, and then data were taken at low densities to verify that the relaxation time had not changed appreciably. But in run 4 the cell was subjected to high densities for many hours.

In an earlier cell (containing only one sidearm) the Rb^{87} vial was opened with the cell connected to the vacuum system. No signal or absorption was observed, even after 1 week. After the sidearm

was gently flamed, absorption was seen; a signal was also seen but only with a buffer gas. Presumably an aging process occurs in a new cell, and Rb is absorbed by the walls. With the cell open to the pumps this process is probably very slow because the density is always low. After the sidearm is flamed the walls are contaminated with Rb atoms, allowing a signal to be seen only with a buffer gas. With the cell pumped out and maintained at 70°C, the relaxation time gradually lengthened to 500 msec, decreasing approximately linearly down to 300 msec at 30°C. The contamination on the walls accelerated the aging process; after the Rb was driven from the walls a large signal could be seen without a buffer gas and with the cell open to the pumps.

In the next cell (two sidearms) a similar procedure was followed, except that when the relaxation time reached 20 msec the forepump was accidentally shut off for about 45 minutes, allowing the impurity background to become high. The signal was destroyed, but returned after heating the cell to ≈ 110°C for a day. Relaxation times of 275 and 375 msec were measured at 110°C and 71°C, respectively. The relaxation time was approximately the same from 30° to 70°C.

6. Detector and Amplfiers

a. Detector requirements

The detector should possess the following properties: high efficiency at 8000 Å, flat frequency response from 0 to 100 kc, and linearity. The frequency response criterion is arrived at by demanding that, for a step-function light signal, the detector output reach 99.99% of its maximum value in 0.1 msec. Assuming an exponential rise, this implies that the characteristic time be about 10 μsec. To avoid distortion of the signal, dc coupling is used throughout.

Among phototubes only the few with an S1 or S20 response are efficient at 8000 Å. The former were avoided because of the slow transient response observed by Brewer,[53] which produces an effect similar to and larger than the optical pumping signal. A careful study of this effect was not made here, but a few per cent initial overshoot was observed for a 6570 phototube and a few per cent sag for a 7102

photomultiplier. A silicon photovoltaic cell[54] was chosen as the detector for the following reasons. It is an efficient detector with its peak response at 8000 Å. It is relatively insensitive to small magnetic fields; consequently, it can be used close to the cell without ferromagnetic shielding to monitor the light intensity even when the magnetic field is varied or modulated. Its dynamic response is a few μsec, depending upon the size of the cell and its load.[54] It is known to possess a linear response when connected to low resistance loads. The performance of the silicon detector and its amplifier are discussed next.

b. Silicon detector and amplifiers

An amplifier with a low input impedance (of the order of ohms if possible) is desirable in order to increase the frequency response and linearity of the silicon cell. This suggests a transistor amplifier. A common-emitter circuit resulted in an inadequate frequency response. The common-base configuration, which possesses the lowest input impedance of the three common circuits, was then selected.[55] The circuit is given in Fig. 29. To test the frequency response, a lamp was chopped at 20 kc/sec and checked to be approximately square with a 6291 photomultiplier. When viewed by the silicon detector and common-base amplifier, the signal was rounded corresponding to a 5-μsec characteristic time. A 10-kΩ terminal resistor was used in the above test and throughout the experiments. Assuming the 2N35 to be a typical transistor, one expects the corresponding input resistance to be less than 50 Ω, compared with more than 1 kΩ for the common-emitter circuit or more than 100 kΩ for the common collector circuit.[55] It is then not surprising that the frequency response of the common-base configuration should be adequate.

The linearities of the detector and amplifier were checked using the inverse square law. A masked-down dial light was used as a source and checked to be a point source with a 1P21 photomultiplier. Figure 30 demonstrates the extreme linearity of the system over a wide range of input intensities; the terminal resistances listed in the figure neglect the 1 MΩ of the oscilloscope used to measure the output voltages. The data were taken with a 2N1308 transistor (which was used prior to the

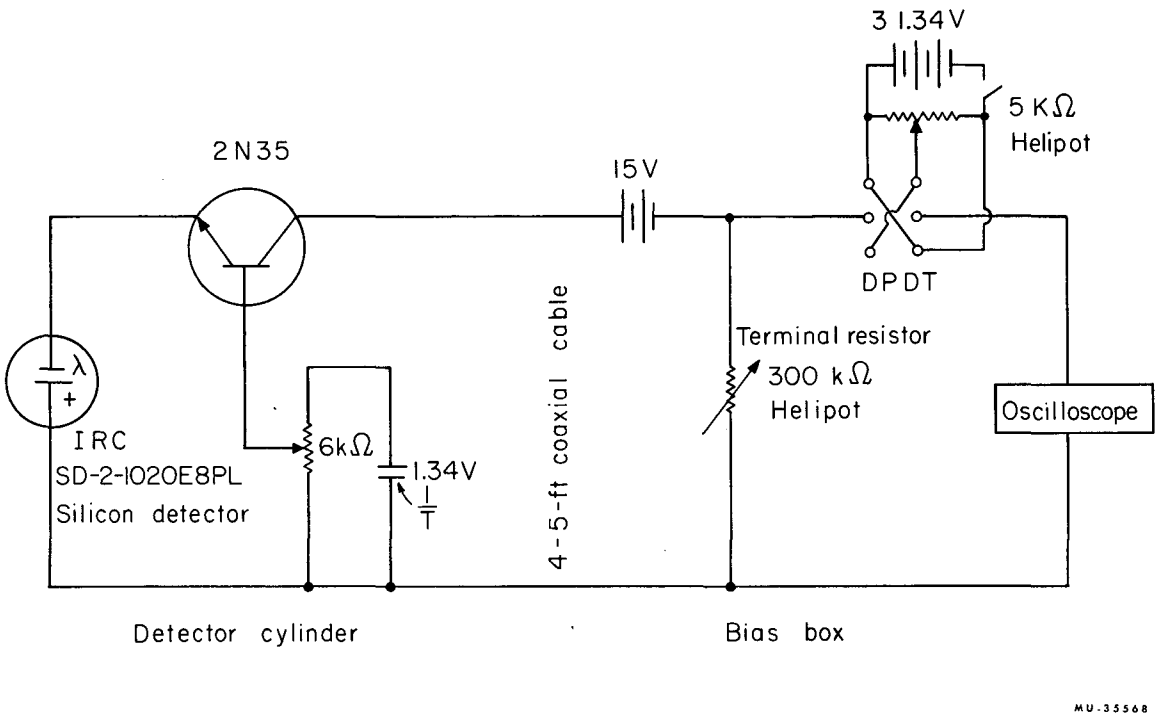

Fig. 29. Circuit diagram of the common-base amplifier and bias box.

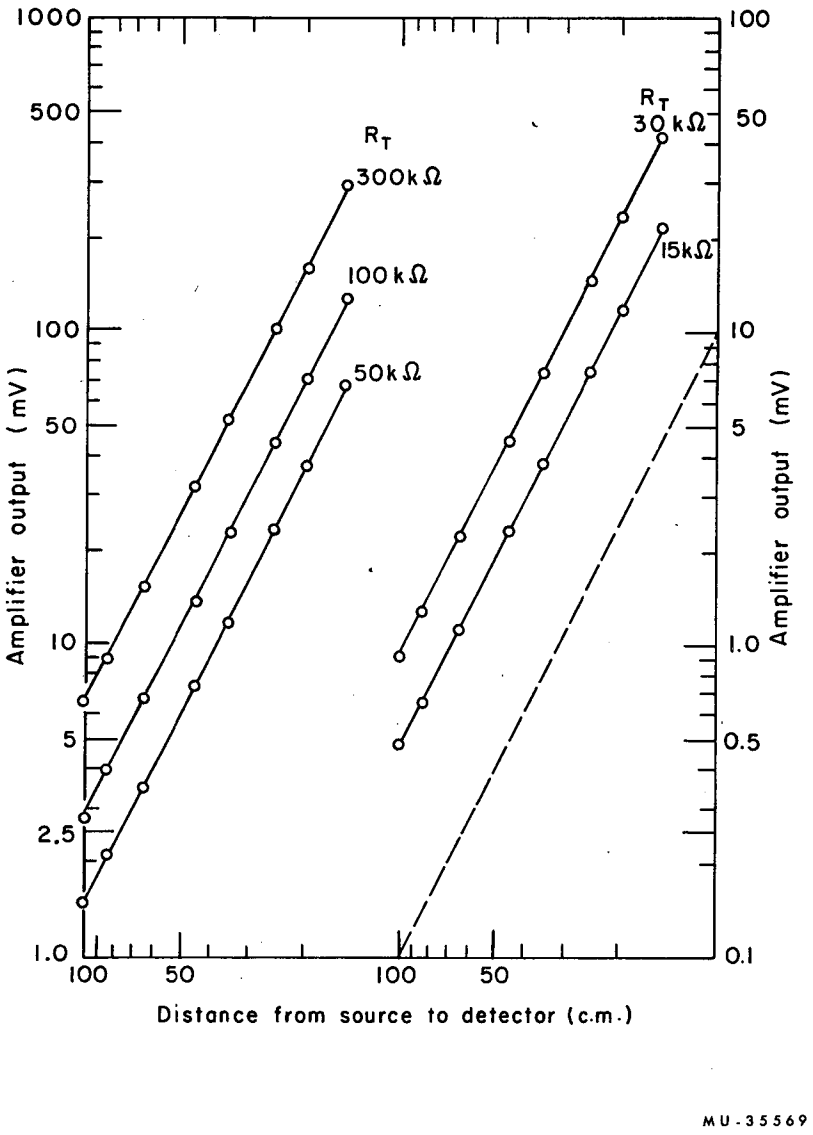

Fig. 30. Linearity of the detector-amplifier system. Common-base amplifier output as a function of distance from point source to detector with the terminal resistor R_T as a parameter. The dashed curve has slope -2; the other curves are parallel to it if they obey the inverse-square law.

study of the sag effect), although similar but less extensive data were taken with a 2N35.

The output of the common-base amplifier is fed into a Tektronix 502 oscilloscope. Since the desired signal rides on a modulated background 20 to 100 times as large, the bias box portion of Fig. 29 is necessary. The signals are usually observed on the 0.5- or 1-mV/cm scales, and are usually about 2 cm in size. For further amplification the voltage to the oscilloscope plates (6 V/cm of deflection) is shifted down by 225 V and applied to a cathode follower. The output of the latter travels through 30 feet of coaxial cable to another room where the analog-to-digital converter is located.

c. Sag effect

The silicon detector and common-base amplifier then fulfill beautifully the requirements of IIIC. 6a. But, as in the case of the Kerr cell, obvious requirements have been omitted: that the system not be sensitive to small temperature changes, and, clearly, that without a resonance cell no signal be observed. These problems are treated together because the cure for the second involves maintaining the detector at 0°C; with the temperature fixed, the first problem is nonexistent. However, before the detector was cooled the signal would drift badly as the room temperature changed.

That an apparent signal can be observed without a resonance cell is shown in Fig. 31, in which a spurious signal of 0.4% is seen. Recalling that the true signal may be only 1% of the total light, this so-called sag effect is clearly undesirable. In Zeeman optical pumping experiments the polarization can be destroyed by applying an rf field of the proper frequency or by bucking out the earth's field along the propagation vector of the pumping radiation; the latter was done for Fig. 32. The bright spots of the lower trace fail to lie on the horizontal line passing through the first one, as they should. Likewise, the upper bright spots are not a true representation of the signal. An excellent approximation to the true signal is obtained by subtracting point by point the lower bright spots from the upper. This is so because both

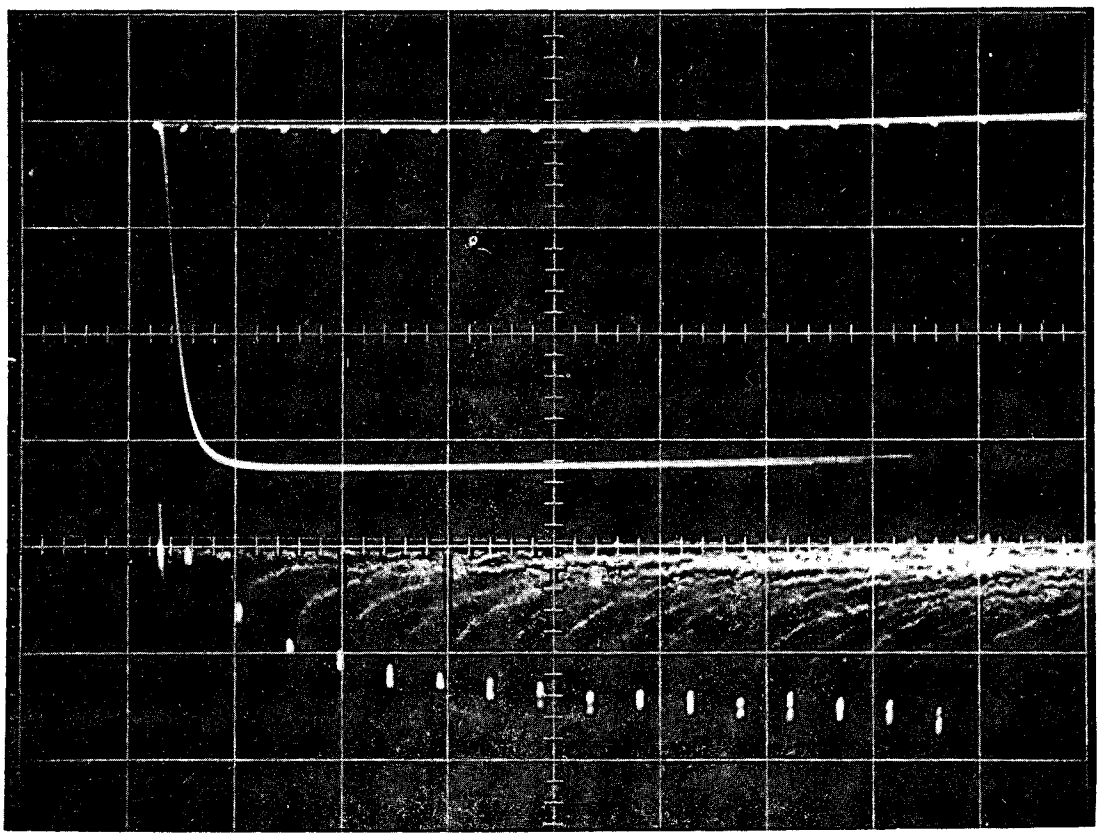

ZN-4840

Fig. 31. Sag effect with no resonance cell; 2 msec/cm. Upper trace is of the total light; 100 mV/cm. Lower trace is a 100-times enlargement of the top of the upper trace; 1 mV/cm.

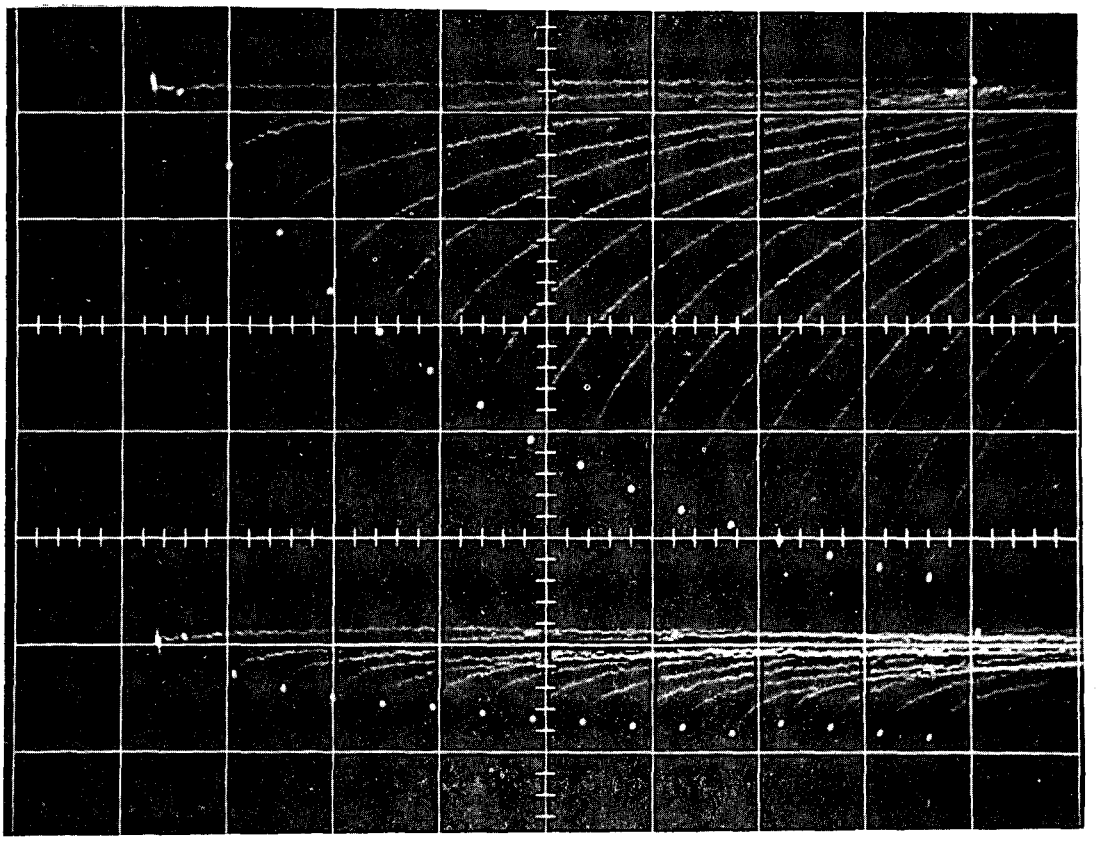

ZN-4841

Fig. 32. Zeeman optical pumping signal; upper curves are with the field parallel to the light direction, the lower with it perpendicular. In the latter case the bright spots would lie on a horizontal line were it not for the sag effect; 2 mV/cm, 2 msec/cm.

traces "ride" on a huge background which is approximately the same for both. But besides being aesthetically displeasing, the subtraction method is not possible in the hyperfine experiment unless the polarization is destroyed by microwaves.

It was not obvious at first that the sag effect arises in the detector-amplifier system, but systematic checks eliminated the Kerr cell and oscilloscope.

The sag effect is quantitatively defined here as the difference, in per cent of the total modulated light, between the amplifier output with constant illumination and the output after an off interval several times as long as the characteristic time of the effect (about 5 msec, see Fig. 31). Becuase of the short time constant of the sag effect, an occasional failure to eliminate it in the hyperfine runs (data points were taken no closer than 5 msec apart) resulted only in a small displacement of the first one or two points from the straight line defined by the other points (semilog plot).

The sag effect as observed with various transistors in three different detector-amplifier systems ranges from 0.1 to 0.4%. It is independent of any background of unmodulated light. It appears to be independent of the terminal resistance. It does not appear to vary from one detector to another. It does vary from one transistor to another, even from one to another of the same type. The effect is highly temperature-dependent, as shown in Fig. 33. The figure may not be completely accurate, but it is given to indicate the trends. It should be remarked that, because of the construction of the detector-amplifier systems, the temperatures of both were usually altered simultaneously. However, the effect was observed to change when an ice pack was placed against the transistor only. In addition, the strong dependence upon which transistor is used indicates that the effect should be attributed to the transistor and not to the silicon detector.

Figure 33 clearly gives the clue to the empirical cure: the effect is seen to pass through zero at about 21 °C for a particular 2N35 transistor. But 21°C is an inconvenient temperature. It was observed that a forward bias in the base-emitter loop increases the effect. The

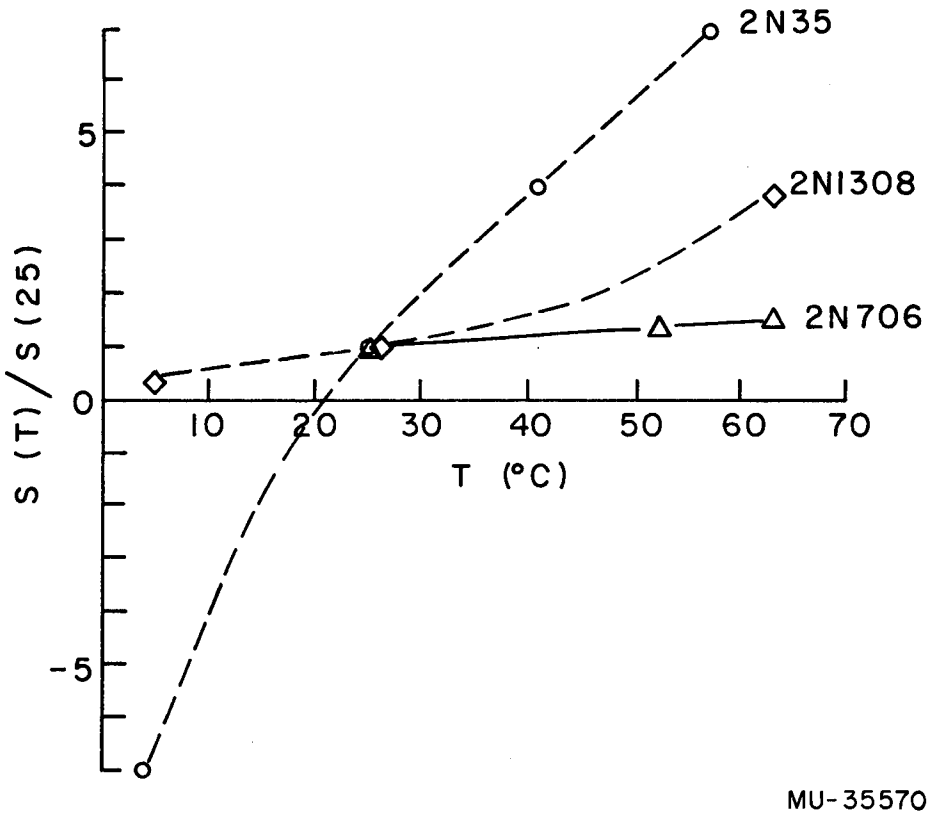

Fig. 33. Sag effect S(T) versus temperature T normalized to 25° C. The curves indicate the trends, but they may be in error.

cure is then to cool the transistor to 0° C, resulting in a rise or negative sag effect; the forward bias is then increased until the rise effect is eliminated. No assertion is made that the response is then completely free from sag or rise effects, but they are less than 0.02%. For the final detector-amplifier system, Fig. 34 shows the sag effect at room temperature in the presence of a 1% signal. Figure 35 is of the same signal at 0° C. The gain and noise are reduced by cooling the system and adjusting the bias to eliminate the sagging.

The cooling is accomplished by circulating ice water from a Vachel ice chest through a brass cylinder ≈ 3 in. in diameter and 4 in. long containing the transistor, mercury cell, and potentiometer in a 1.25-in. hole extending about 3/4 of the length of the cylinder (an Eastern Industries, Model A1, Type 100 pump is used). The silicon cell is mounted in a machined slot on one end of the cylinder. The 15-V battery and terminal resistor are in a separate box removed from the detector by about 5 ft of RG-71/A low-capacitance coaxial cable.

Every observed phenomenon deserves at least a conjecture for an explanation! The collector current of a transistor is known to vary with temperature because of changes in reverse-bias saturation current and in the emitter-base junction resistance.[56] Below 10° C the saturation current is ≈ 0; above 10° C it doubles about every 8° to 10° C. The emitter-base junction resistance has a negative temperature coefficient of resistance. With these facts the sag effect can be qualitatively understood as follows. At temperatures above 25° C the collector current is dominated by the reverse-bias saturation current. When the illumination is suddenly applied to the detector the collector current increases, the transistor heats slightly, and the collector current consequently is increased further. Then as the heating occurs the output voltage increases, appearing as a rounded corner, i.e., the sag effect. At 0° C, on the other hand, the reverse-bias current is negligible. When the illumination is suddenly applied the transistor is again heated; this time the temperature increase causes a decrease in the emitter-base voltage which in turn reduces the collector current and output, i.e., an overshoot or rise effect occurs (see Fig. 73 of reference 55).

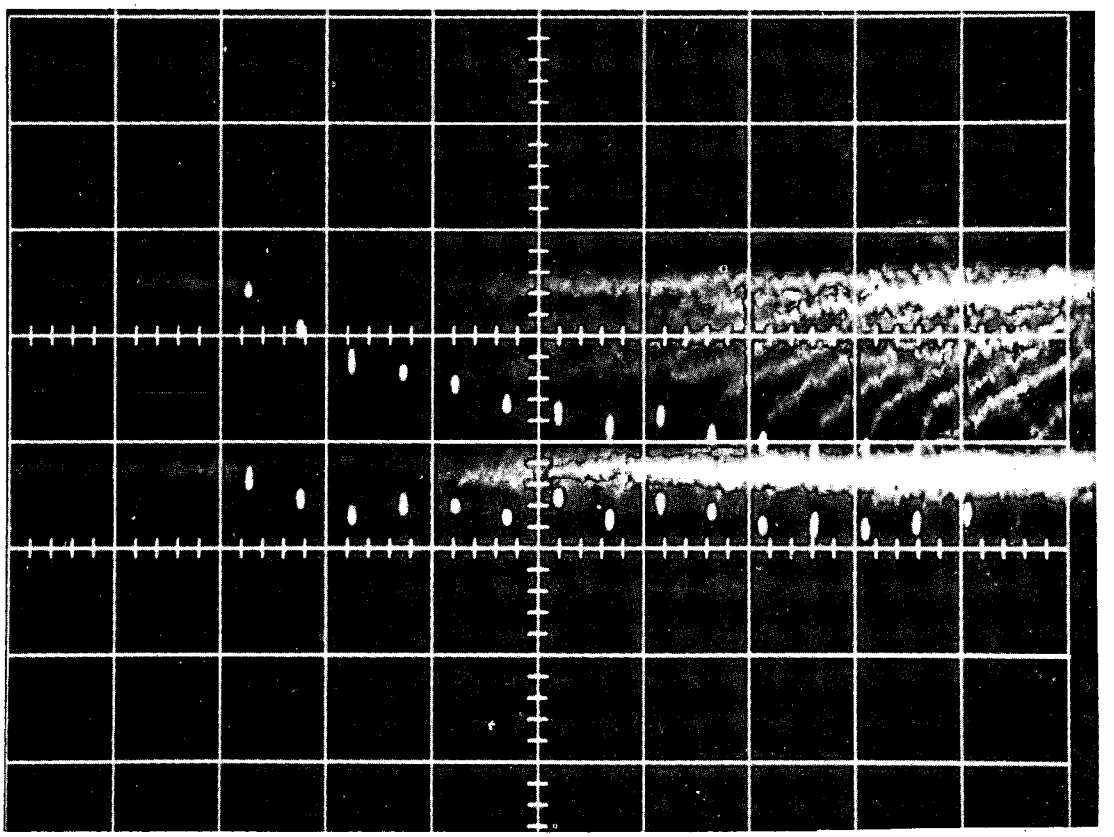

ZN-4842

Fig. 34. Zeeman optical pumping signal and sag effect at room temperature with final detector-amplifier system; 0.5 mV/cm, 5 msec between bright spots.

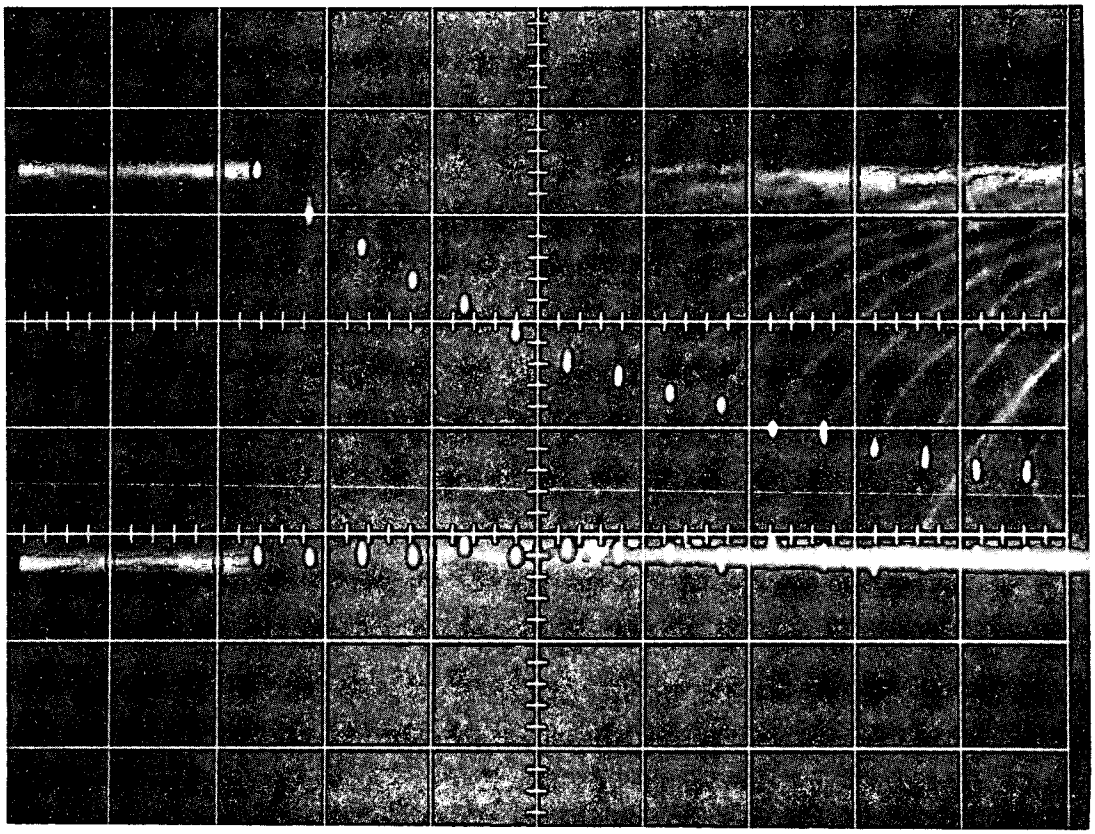

ZN-4843

Fig. 35. Zeeman optical pumping signal and sag effect (≈ 0) with the final detector-amplifier system iced; 0.2 mV/cm, 5 msec between bright spots.

Hunter states that the thermal time constant of switching transistors is generally of the order of milliseconds.[57] For a 2N1301 transistor, the RCA Handbook gives 10 msec. Thus the time required for the transistor to change temperatures after a change in power dissipation is in the same range as the characteristic time of the sag effect.

Quantitatively, Hunter gives 0.7μA/°C at 30°C as a typical increase in collector current for an increase in ambient temperature.[58] The temperature of a typical transistor increases by about 0.15°C per mW increase in dissipated power.[59] With a 50-kΩ terminal resistor, 22.5-V battery, and a typical modulated light signal, a modulated output of 0.5 V is observed. The power change between the two levels is than 0.2 mW. The change in output voltage arising from the temperature change caused by the light intensity change is then (0.2 mW) (0.15°C/mW)(0.7 μA/°C)(50 kΩ) = 1 mV. This is 0.2% of the output signal, in excellent agreement with typical sag effects observed at room temperature.

Since the reverse-bias saturation current increases with temperature, so should the sag effect (as in Fig. 33). The behavior of the sag effect at room temperature and above is then explained in terms of the saturation current. The behavior at low temperatures has been explained in terms of changes in the emitter-base junction resistance; quantitatively these changes produce changes in the collector current comparable to those caused by the saturation current at higher temperatures (see Fig. 73 of reference 55 again). In addition the same figure shows that an increase in emitter-base forward bias effectively shifts the curves for saturation current versus temperature to lower temperatures, i.e., saturation current effects become important at lower and lower temperatures. The empirical cure described earlier merely equalizes the two thermal effects of opposite signs

7. Logic Circuit

The term logic circuit refers here to all the circuitry required to obtain the desired sequence of events in time. Forgetting about the complications of the mechanical shutter, pulse-height analyzer, etc., what circuitry will cut off the light every T seconds for N decreasing

intervals of time from $(N-1)\tau$ down to 0 in units of τ and then repeat the cycle? The author is grateful to Professor Howard Shugart for outlining the logic of the scheme diagrammed in Fig. 36. A square-wave generator operating at $1/\tau$ cps triggers another generator with period $T \gg \tau$; the second generator ignores all trigger pulses that occur before it has completed its cycle (for example, a Tektronix 162). A flip-flop is driven by a "light-off" pulse occurring at the beginning of the T pulse and by a pulse delayed from the light-off pulse by $(N+1/2)\tau$ (for example, a Tektronix 161 can be delayed by triggering off of the Tektronix 162 sawtooth). The output of this flip-flop allows only N + 1 cycles of the square wave to pass each time the T generator is triggered. After suitable differentiation and shaping, the output of the AND gate triggers an N-count ring counter. The latter is a counter which puts out a pulse for every N input pulses. Finally the light-off and light-on pulses trigger a flip-flop which, when suitably amplified, controls the Kerr cell switch.

In the actual experiment, several complications were added. As mentioned earlier, for long off intervals a mechanical shutter is synchronized to fall within the Kerr cell off interval. Provision is made for taking one cycle with long off intervals (Kerr cell plus mechanical shutter), the next with short intervals (Kerr cell only), etc. Command pulses for the pulse-height analyzer are formed. Finally, a switch for starting and stopping is included which always starts the run with the longest long off interval and stops it with the shortest short off interval. Figure 37 is an "analytic continuation" of Fig. 36 into the "complex plane." The circled letters in Fig. 37 refer to traces in Figs. 36 through 38. The quantities in parentheses refer to values of parameters or to equipment used in the experiment. Square wave #1 is generated by a General Radio 1210-C signal generator; square wave #2, by an Exact Electronics 250. AND #1 and Delay #1 are formed by a mercury relay, as are AND's #2 and #5. AND's #3 and #4 are formed by applying the input signals to the control and screen grids of a pentode. The N ring counter consists of a Hewlett-Packard AC-4G decade counter with feedback removed, giving N = 16.

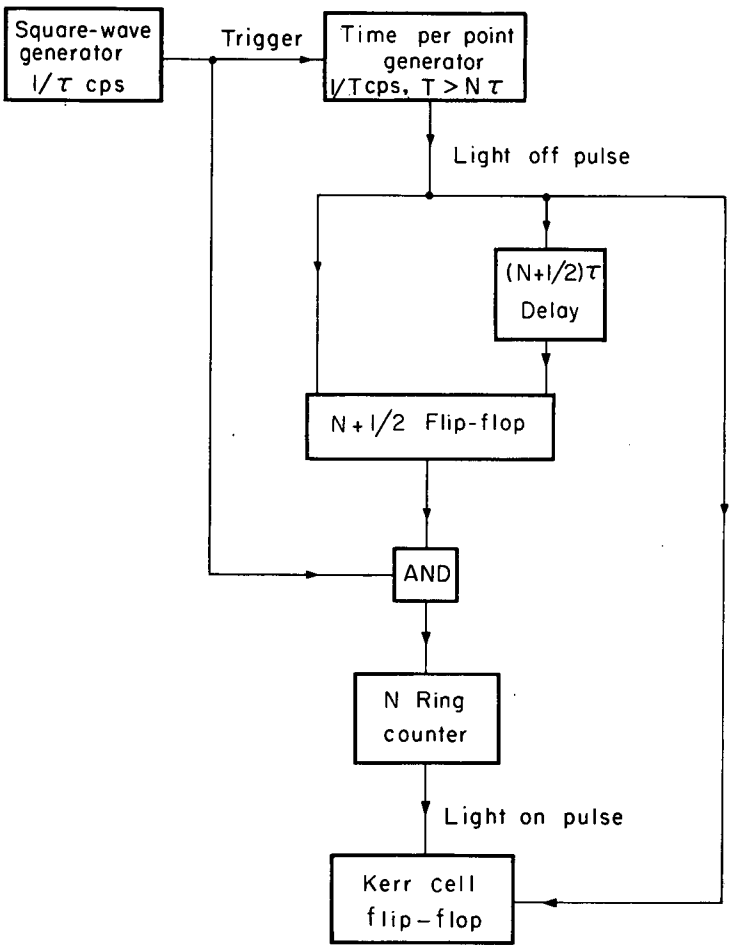

Fig. 36. Logic block diagram for decreasing the light-off interval from (N-1)τ down to 0 in steps of τ. The light is cut off every T seconds.

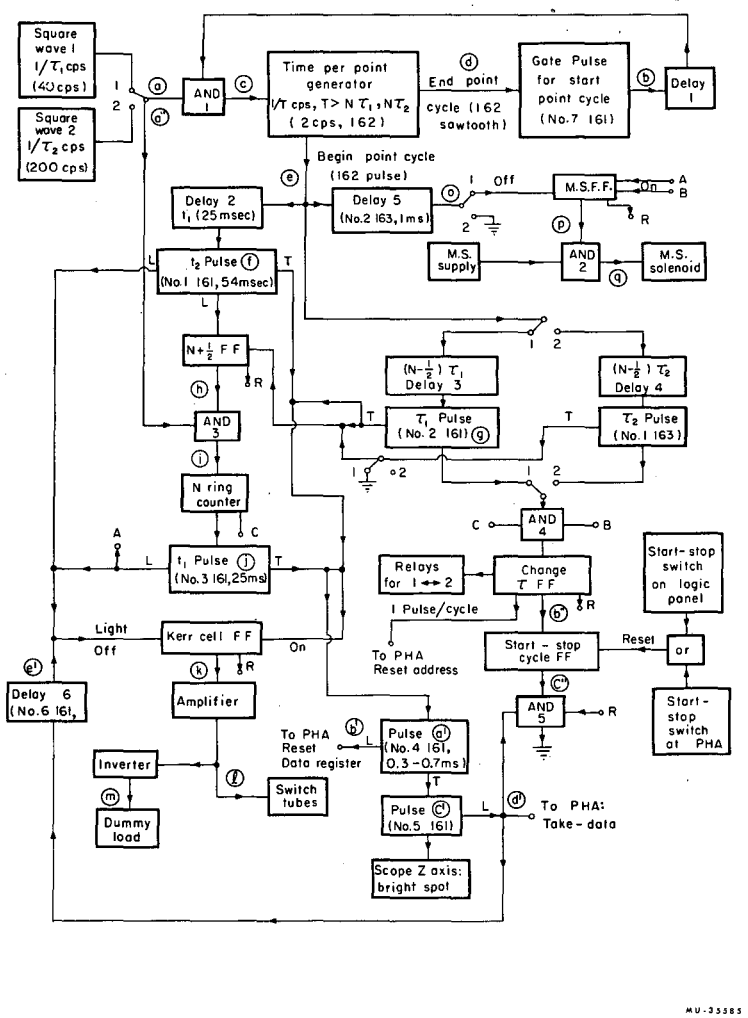

Fig. 37. Final logic circuit block diagram. Legend: 161, 162, 163, standard Tektronix pulsers; FF, flip-flop; L, leading edge of pulse; T, trailing edge of pulse; PHA, pulse-height analyzer; M. S., mechanical shutter.

Delay #1 is necessary because a few milliseconds are required for the 162 sawtooth voltage to return to its initial value at the end of a point cycle. If the sawtooth does not start from the same level every cycle, the pulses triggered by the sawtooth will not possess the proper time relationship to those initiated by the begin-point-cycle pulse. The delay effected by the t_1 pulse following the ring counter is necessary to prevent the Kerr cell from passing the light before the mechanical shutter is open. Delay #2 is then necessary in order that the shortest off interval of the Kerr cell be zero. Delays 2 through 4 are produced by triggering off of the 162 sawtooth. Delay #5 may be necessary to prevent the mechanical shutter from closing before the Kerr cell. Not every tube of the logic circuit is represented by a square in Fig. 37. For example, each flip-flop is followed by a cathode follower. In certain cases pulses must be amplified, inverted, or differentiated; simple triode circuits are then used. Wherever two pulses are joined together in Fig. 37, it is assumed that they are mixed in such a way to eliminate feedback from one into the circuitry of the other (usually by diodes). The logic circuit can probably be understood best by comparing each step in Fig. 37 with the photographs of Figs. 38 through 40.

8. Pulse Height Analyzer as a Data Accumulator

The pulse-height analyzer is applied to this experiment as follows. Pulses from the logic circuit select an address: 0 for time 375 msec, 1 for time 350, etc. The voltage representing the signal for that off interval is converted to a train of 500-kc/sec pulses proportional to the voltage. These pulses are counted and then stored in the memory for that address. The address is then advanced and the process repeated. This process can be seen with the aid of Fig. 41.

The input from the oscilloscope is applied to the analog-to-digital converter at all times; see (a) in Fig. 41. A few tenths of a millisecond before data are to be taken, the reset pulse (g) resets the data register to zero and reads the number of counts stored in the memory of that address. At the point at which data are to be taken, the take-data pulse (b) closes the linear gate (c), the stretcher holds the value of the input

Fig. 38. All traces have the same uncalibrated horizontal sweep rate and are triggered by the begin-point-cycle pulse.

(a) Signal generator 40-cps square wave; 20 V/cm.
(b) Gate pulse for starting point cycle; 20 V/cm.
(c) AND of (a) and (b) differentiated and inverted; 20 V/cm.
(d) Tektronix 162 sawtooth; 100 V/cm.
(e) Tektronix 162 positive pulse (begin-point-cycle pulse); 100 V/cm.
(f) t_2 pulse; 100 V/cm.
(g) τ_1 pulse; 100 V/cm.
(h) N + 1/2 flip-flop; 50 V/cm.
(i) AND of (a) and (h) differentiated; 100 V/cm.
(j) t_1 pulse; 50 V/cm.
(k) Kerr cell flip-flop; 100 V/cm.
(l) Signal to switch tubes of Kerr cell switch; zero level is also shown; 50 V/cm.
(m) Signal to dummy load of Kerr cell switch; 50 V/cm.
(n) Light modulated by Kerr cell only; 50 mV/cm.
(o) Delay #5; 50 V/cm.
(p) Mechanical shutter flip-flop; 100 V/cm.
(q) Mechanical shutter solenoid voltage; 100 V/cm.
(r) Light modulated by mechanical shutter only; 100 mV/cm.
(s) Light modulated by mechanical shutter and Kerr cell; 50 mV/cm.

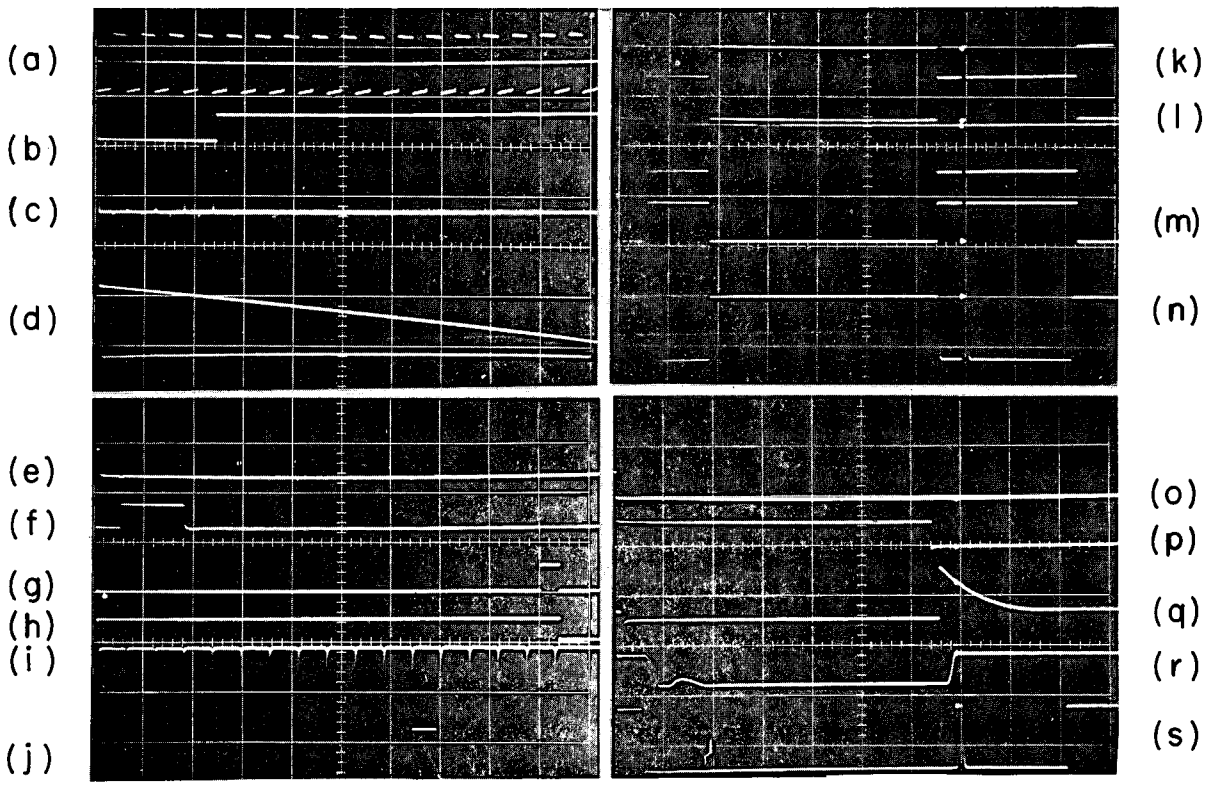

ZN-4864

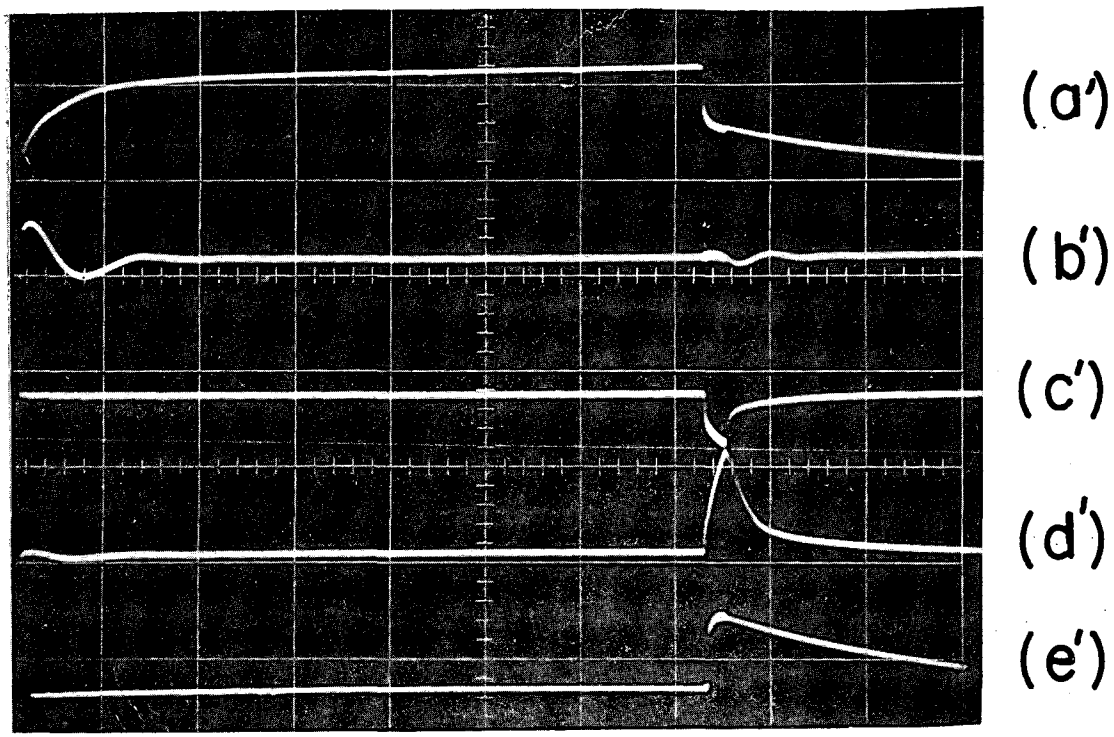

ZN-4865

Fig. 39. All traces are triggered by the #4 161; the horizontal sweep rate is 50 μsec/cm.
(a') #4 161; 50 V/cm.
(b') Pulse to PHA to reset data register; 20 V/cm.
(c') #5 161; 50 V/cm.
(d') Pulse to PHA to take data; 20 V/cm.
(e') #6 161; 50 V/cm.

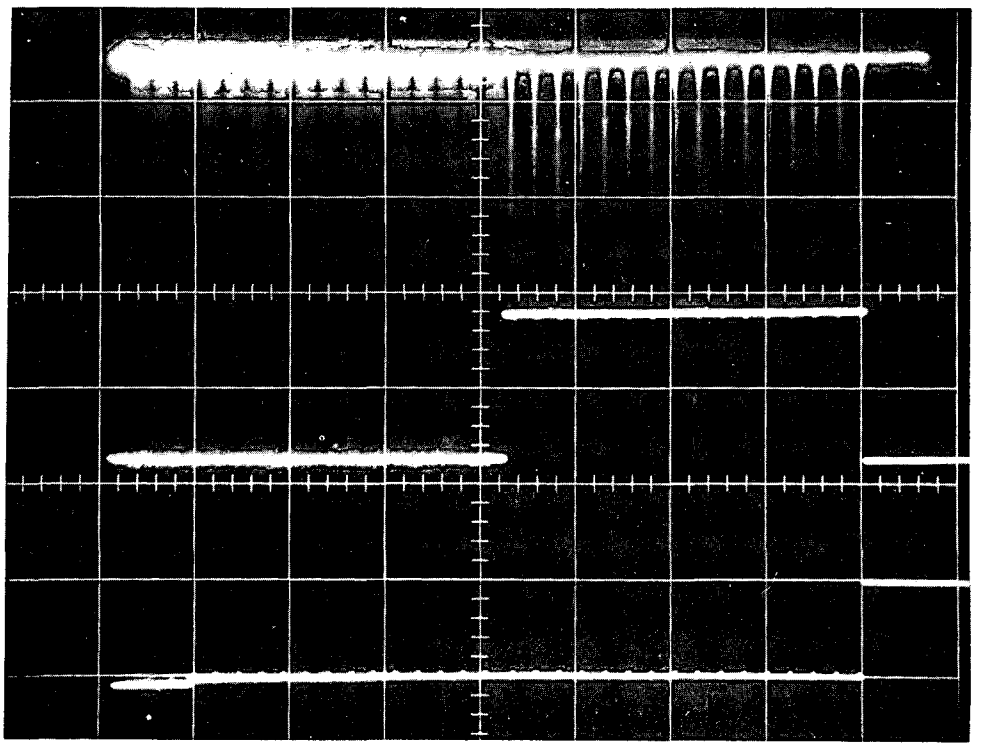

ZN-4866

Fig. 40. All traces are triggered at the same point in the cycle; 2 sec/cm. These traces are taken for a run of a single complete cycle, i.e., the start-stop switch is flipped on and back off immediately.
(a") Input to ring counter; 100 V/cm.
(b") Change τ flip-flop; 50 V/cm.
(c") Start and stop cycle flip-flop; 50 V/cm.

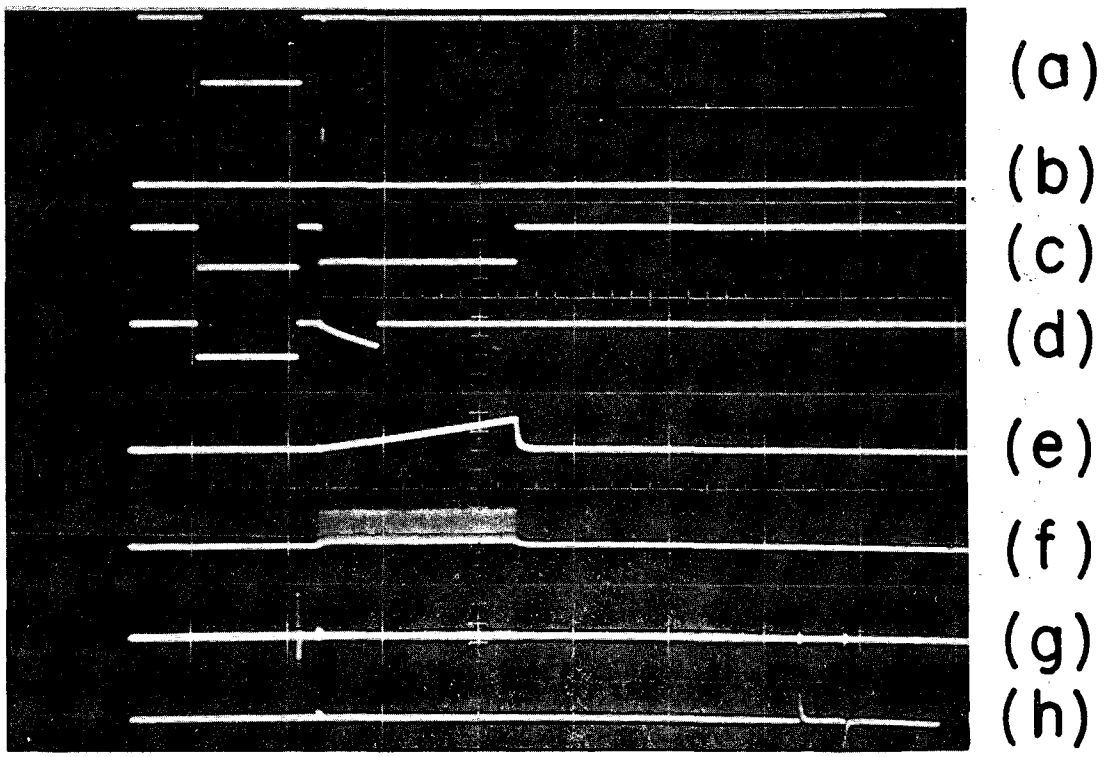

ZN-4867

Fig. 41. Analog-to-digital converter operation; 2 msec/cm, various vertical amplifications.
(a) Input of same form as light signal; (b) take-data pulse; (c) linear gate; (d) stretcher (loading by scope causes it to sag and end conversion too soon); (e) ramp; (f) 500 kc/sec; (g) reset data register and read from the memory; (h) write into the memory and advance address.

just before the gate was closed (d), and the ramp (e) and 500-kc/sec oscillator (f) are started. When the ramp reaches the value of the stretcher voltage, the discriminator cuts off the oscillator (f) and ramp (e) and opens the linear gate (c). The 500-kc/sec counts are accumulated in the data register; 10 or 12 msec after the take-data pulse, a pulse writes the number of counts in the data register into the memory. A second pulse then advances the address, and the cycle is repeated. The reset-address-scaler pulse resets the address to zero whenever desired, so that not all of the available 256 channels need be used. Upon completion of the data accumulation the data are printed out, punched on cards, and analyzed by the computer.

The number of counts from the ADC per input volt was increased by adding 1800 pF in parallel with the 600-pF ramp capacitor and operating with a 0.4% channel width. It was decreased by reducing the oscillator frequency from 2 to 0.5 Mc/sec, as required by the data register add-1 scaler. Typically one obtains 15 counts/V, implying 75 to 300 counts for the usual 5- to 20-V input signal. The signal is then easily seen with good resolution after a single cycle of accumulation. The analyzer is still of great importance in increasing the precision of the measurements by averaging out random noise and slow drifts and by eliminating the necessity of relying on photographs (and oscilloscope precision). Periodic linearity tests of the entire system from the oscilloscope input to the printed output of the analyzer indicate that the linearity is better than 1%. The pulse height analyzer and other relaxation time equipment can be seen in Figs. 42 and 43.

9. Miscellaneous

a. Ovens

The ovens for the resonance cell and the two sidearms were constructed of 3/4-in. maronite and brass screws. The sidearm ovens are a single oven divided by a 1/4-in. Transite partition. The top of the sidearm oven is also the bottom of the resonance cell oven. The oven contains two perpendicular rf coils both perpendicular to the pumping radiation axis. A mirror, situated in the half of the oven not containing the cell, can be lowered and used to reflect the pumping light into the Fabry-Perot by means of the density-measurement optics.

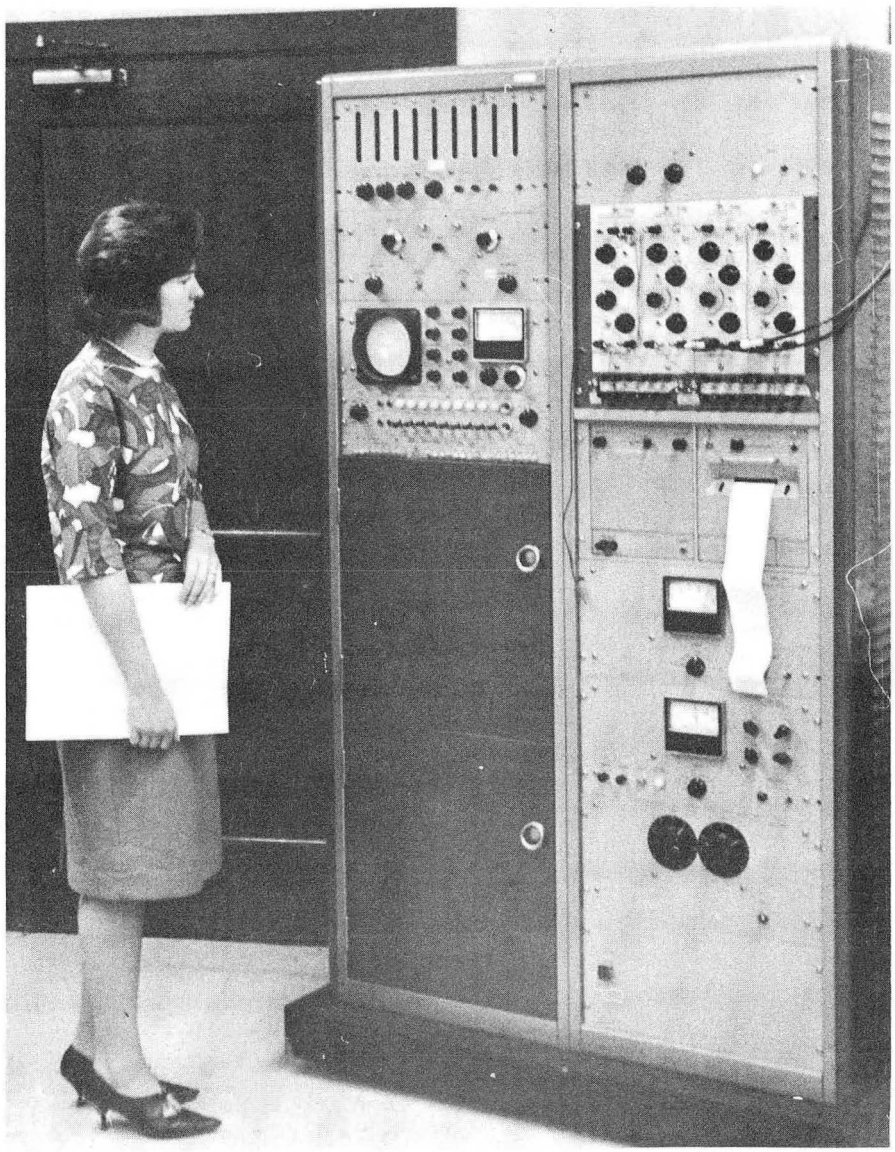

ZN-4887

Fig. 42. Lethia Gibbs examining the RCL 256-channel pulse-height analyzer with Tektronix pulsers used to modify it.

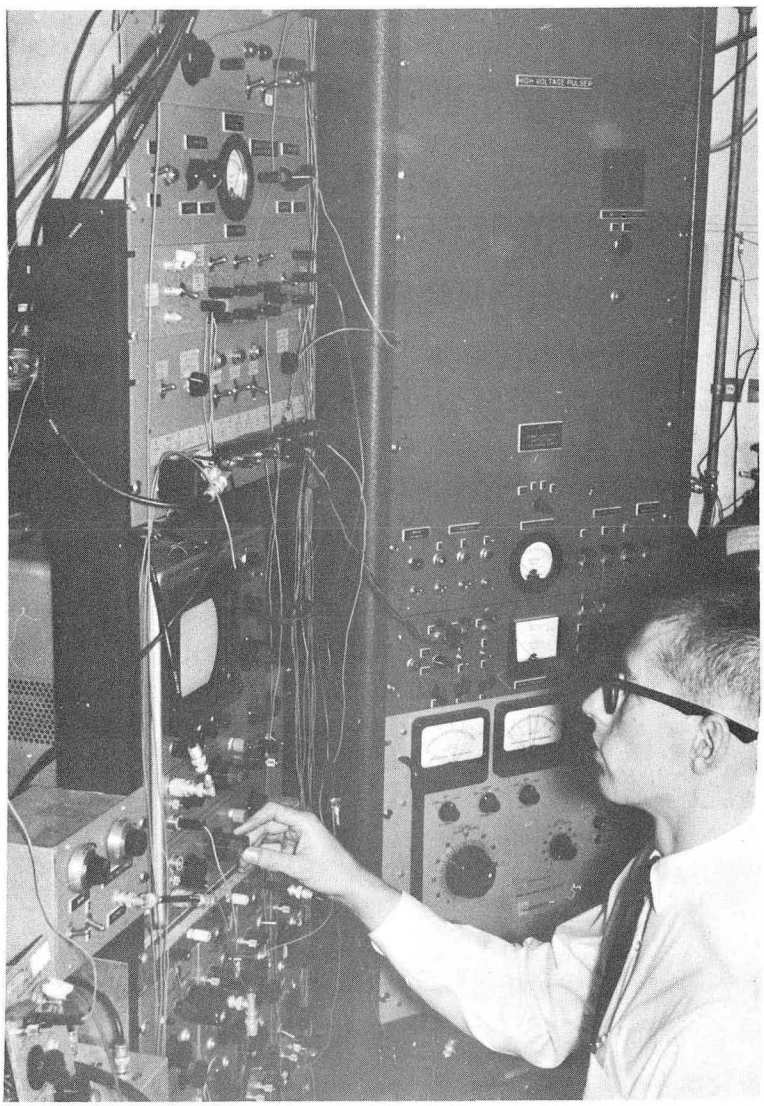

ZN-4888

Fig. 43. The relaxation-time measurement electronic equipment. The Kerr cell switch and high-voltage supply are on the right, the Tektronix pulsers are below the scope, the logic circuitry is in the rack above the scope.

The oven is heated by blowing compressed air through several turns of copper tubing enclosed in a Maronite oven (heated by a glow coil) into the oven. The system results in a maximum temperature gradient across the cell of 10°C, as measured by four mercury thermometers situated around the cell. The many necessary windows and openings in the oven greatly reduce the effectiveness of the insulation. However, since the density is determined by the temperature of the sidearm, the oven temperature is important only for determining the relative velocity. The sidearms are heated electrically; a Fenwal 17110-0 thermostat is used.

b. Room thermostat

Another Fenwal thermostat switches an electric fan between two levels of operation: line voltage and a variable lower voltage. The fan blows outside air into the room. Although it is not always cool enough outside for the system to work ideally, runs were made only on cool days in order that the room be maintained at a fixed temperature. Otherwise, lamp and electronic drifts greatly complicate the experiment.

c. Static magnetic field

A magnetic field of a few gauss is supplied by Helmholtz coils of roughly 50-cm diameter. The coils produce a field of 9 G/A. The current, supplied by a 6-V storage battery usually in parallel with a 6-V regulated supply, is controlled by means of series resistors. The rf field of the second species (when present) is usually 2.8 Mc/sec, so the resonant magnetic field is about $2I_2 + 1$ gauss. The static field is then an order of magnitude larger than the earth's field, but small enough that the nuclear and electronic angular momenta are tightly coupled.

For the Zeeman experiments, a simple circuit was designed to switch the magnetic field, at the command of the logic circuit, between the above value and a value adjusted to buck out the component of the earth's field along the pumping-radiation axis.

d. Radio-frequency fields

The oven contains two perpendicular sets of rf coils. The permanent coil consists of two coils of 2.5 turns of 1/8-in. copper tubing, 2.5 in. in diameter, and 2.25 in. apart. The temporary coil, inserted when necessary with the cell, is of similar dimensions and constructed of 6 to 8 turns of #12 insulated copper.

In the single isotope runs a Tektronix 190B signal generator was used at 2.8 Mc/sec. For the Rb^{87}-Cs^{133} runs, a Laboratory-made rf oscillator was used because it possessed a "bad" second harmonic. If the first harmonic at 2.8 Mc/sec is resonant for Cs^{133} the second is resonant for Rb^{87} (the rf output is quite broad). Rb^{87} was pumped; its resonance at the second harmonic could be found easily, and the Cs^{133} was then disoriented as well.

That the resonances are saturated is tested by two methods. First, an increase in power produces no reduction in the signal. Second, for Zeeman pumping the transmitted light intensities for static field parallel (with rf) and static field perpendicular (with no rf) are equal.

e. Vacuum system

The vacuum system (see Fig. 10) consists of a Duo-Seal forepump, a Consolidated Vacuum Corp. PMC 115 oil diffusion pump, a NRC Equipment Corp. 501 thermocouple gauge between the forepump and diffusion pump, two Veeco valves, a 22-in. oil manometer, a Westinghouse 5966 ion gauge, and a liquid nitrogen trap. The last two items are situated within a large oven constructed of 2-in. Maronite. The oven can be easily dismantled; the walls contain numerous plugged holes through which various nonbakeable materials have been distilled.

D. Relaxation-Time Data Analysis

The unnormalized signals, UNS(t), from the pulse-height analyzer are punched onto cards and least-squares fitted [after being normalized to S(t) = UNS(t)/UNS(0)] by the Berkeley campus 7090 computer to the theoretical curve

$$F(t) = A \exp(-t/\tau) + CT, \tag{141}$$

where

$$1/\tau = 1/T_1' + 1/T_1'' + 1/T_{S1} + 1/T_{E1}. \tag{142}$$

Figure 6 contains data at three different temperatures chosen at random from run #7. The points plotted are the data points less the best-fit background, i.e., $[S(t) - CT]/(1-CT)$. The straight lines are the best-fit curves $[F(t) - CT]/(1 - CT)$. Only 20 cycles of accumulation were used, because the data were taken during the time taken to scan the Fabry-Perot from the end of one of the peaks to its reappearance in the next order. In some earlier runs 50 cycles were used, with a corresponding improvement in signal-to-noise ratio.

In order to be completely explicit in the area of data handling, a brief summary of the formulae will now be given. The quantity

$$Q = \sum_{i=1}^{n} W_i [S(t_i) - F(t_i, b_k)]^2 \tag{143}$$

is minimized. The W_i, the weights of the n data points, are taken to be equal. The b_k are the parameters A, CT, and τ in (141), $k = 1, 2, \cdots, p$. The minimization leads to the set of equations

$$\sum_{k=1}^{p} DEL(k)\, P(k, j) = Q(j), \tag{144}$$

where

$$P(k, j) = \sum_{i=1}^{n} W_i [\partial F(t_i)/\partial b_k][\partial F(t_i)/\partial b_j], \tag{145}$$

$$Q(j) = \sum_{i=1}^{n} W_i [\partial F(t_i)/\partial b_j][S(t_i) - F(t_i)], \tag{146}$$

and DEL(k) is the calculated estimate of the correction to be applied to b_k to minimize Q:

$$b_k \rightarrow b_k + \mathrm{DEL}(k). \tag{147}$$

The quantities involving $F(t_i)$ in (145) and (146) are evaluated at the trial values. The DEL(k) are found by inverting P; the new trial values are placed in (145) and (146) and new corrections calculated. This process is continued until the correction for each parameter is less than 10^{-4} of the value of the parameter. In the program used, only 25% of the correction is applied each cycle; approximately 20 to 25 iterations are normally required to satisfy the convergence criterion.

Since the weights are assigned arbitrarily, the only meaningful standard deviation is that of external consistency, i. e., of how well the points fit the assumed form of the curve. These standard deviations are calculated by

$$\sigma(k) = [\mathrm{WVAR}\ \ P^{-1}(k,k)]^{1/2}, \tag{148}$$

where the weighted variance is

$$\mathrm{WVAR} = \sum_{i=1}^{n} W_i [S(t_i) - F(t_i)]^2 / \mathrm{DEGF}; \tag{149}$$

the number of degrees of freedom, DEGF, is equal to the number of data points n minus the number of parameters. The standard deviations of $1/\tau$ rarely ranged outside of 0.5 to 2% of $1/\tau$; $\sigma(A) \approx 0.005$ A, $\sigma(CT) \approx 0.001$ CT.

The values of $1/\tau$ and $\sigma(1/\tau)$ are matched with the corresponding density values and the cross section determined as described in IIIG.

E. Detailed Description of the Density-Measurement Apparatus and Techniques

See Fig. 2 for a block diagram of the apparatus and Section IIIB for a description of the density-measurement technique. Most of the apparatus and all the computer routines used in the analysis are the work of Dr. Robert J. Hull. It should be made clear that this is not the first density measurement by the scanning Fabry-Perot method.[60]

1. Lamp

The circuit diagram of the density-measurement lamp, shown in Fig. 44, is patterned after Diagram 2 of Alley's report.[37] It is a multivibrator oscillating at 25 Mc/sec; the screen grid is modulated, usually at 86 cps. The rf choke and coil containing the lamp bulb are removed from the remainder of the circuit by about 18 in. of coaxial cable for convenience, and are contained in a $3\times4\times5$-in. aluminum box. The latter is equipped with a small heater for regulating the self-reversal and relative intensities. The lamp bulbs are the same as those described in IIIC. 1.

2. Optics

The use of mirrors and beam splitters to obtain the two desired beams is shown in Fig. 2. The alignment of the components is described in subsection IIIE. 5. The transmission of the beam splitters is approximately 50%; the mirrors are front-surface silver coated. The detector lens (36 cm focal length) is an achromat, making it possible to focus the ring system for the infrared with the use of visible light. It is a high-quality lens which, it is hoped, minimizes spherical aberrations and coma. Interference filters are necessary in order to eliminate undesired lines. The filters are described in IIIC. 3. A trimmer filter is always used. When the 7947-Å line of Rb is being observed, two Spectrolab filters are necessary to eliminate unwanted lines. A single filter is used for the 7800-Å line. A Kodak Wratten filter 87C is found to eliminate stray lines that pass through the 8944-Å filter for Cs.

The flag shutter is driven by a Leland two-position stepper or solenoid powered by about 10 volts dc at 1 A, switched by a ≈ 0.15-cps multivibrator and Hg switch.

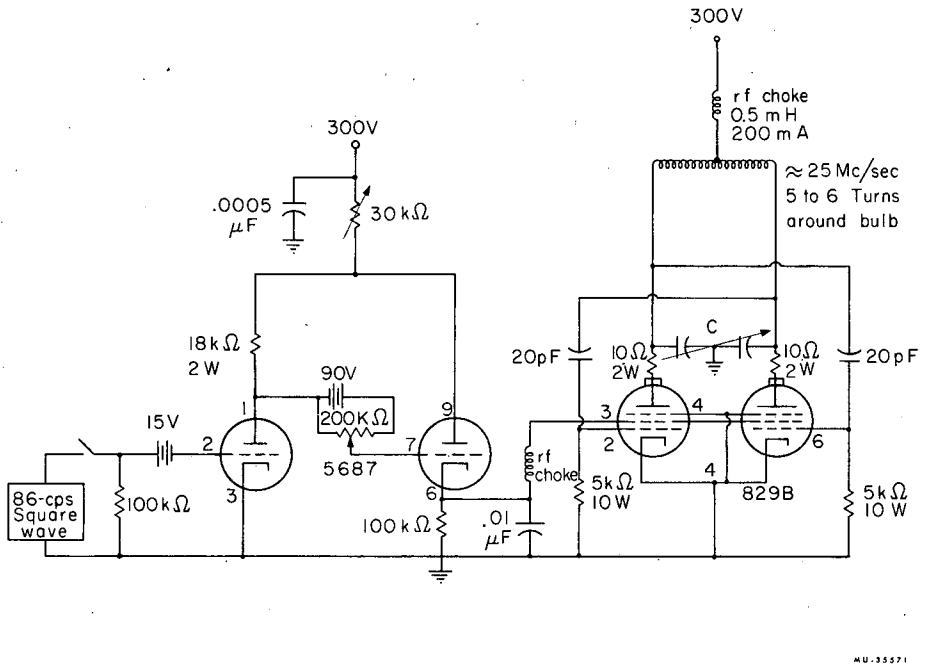

Fig. 44. Density-measurement lamp circuit diagram. C is a Hammarlund HFBD-65-E capacitor, variable from 12.5 to 63 pF.

3. The Fabry-Perot Etalon and Chamber

The Fabry-Perot plates, obtained from Aurora Precision Optics, are quoted to be flat to $\lambda/200$ in the green. They were silver-coated by Mr. Dan O'Connell of the Lawrence Radiation Laboratory to have a transmission of 5% at 8000 Å. The spacers were made by the department machinists; they consist of Invar pins housed in aluminum rings and accurate to $\lambda/4$. A 12-mm spacer was used for the Rb scans and 10 mm for the Cs scans. The etalon can be seen in Fig. 45.

The etalon is enclosed by a brass cylindrical vacuum chamber about 6 in. in diameter and 10 in. long. Dr. Robert Hull is seen removing the etalon from the chamber in Fig. 46. The end plate at the exit of the chamber is flat to $\lambda/4$ to minimize distortion of the ring system. The screws for adjusting the parallelism of the plates are controlled by extensions which reach the outside of the chamber through 0-ring seals. The chamber rests on a mount which can be rotated about a vertical or horizontal axis. This enables one to focus the center spot on the pinhole along the optical axis.

The Fabry-Perot is scanned by changing the index of refraction of the medium between the plates. The equation for constructive interference in a Fabry-Perot is[61]

$$2\mu t \cos\theta = m\lambda, \tag{150}$$

where μ is the index of refraction, t is the plate separation, θ is the angle of observation with respect to the perpendicular to the plates, m is the order number, and λ is the wavelength. At $\theta = 0$ deg a change in index of refraction corresponds to a change

$$\Delta m = 2t\,\Delta\mu/\lambda \tag{151}$$

in the order number. Dry nitrogen ($\mu \approx 1.0003$ at 1 atm) is leaked into the evacuated ($\mu = 1.0000$) chamber; the pop-off valve opens at 1 atm after approximately 7.5 orders with a 10-mm spacer at 8000 Å. The gas is leaked into the chamber so that the pressure increases linearly with time by means of a supersonic leak.[62] The scanning rate has been checked and found to be linear to within 1% per order. A backing gauge

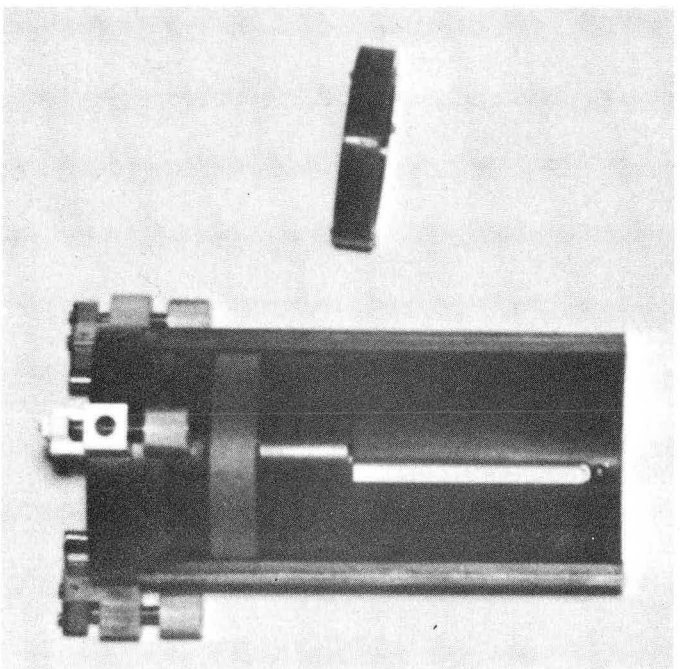

ZN-4889

Fig. 45. Top view of Fabry-Perot etalon and spacer.

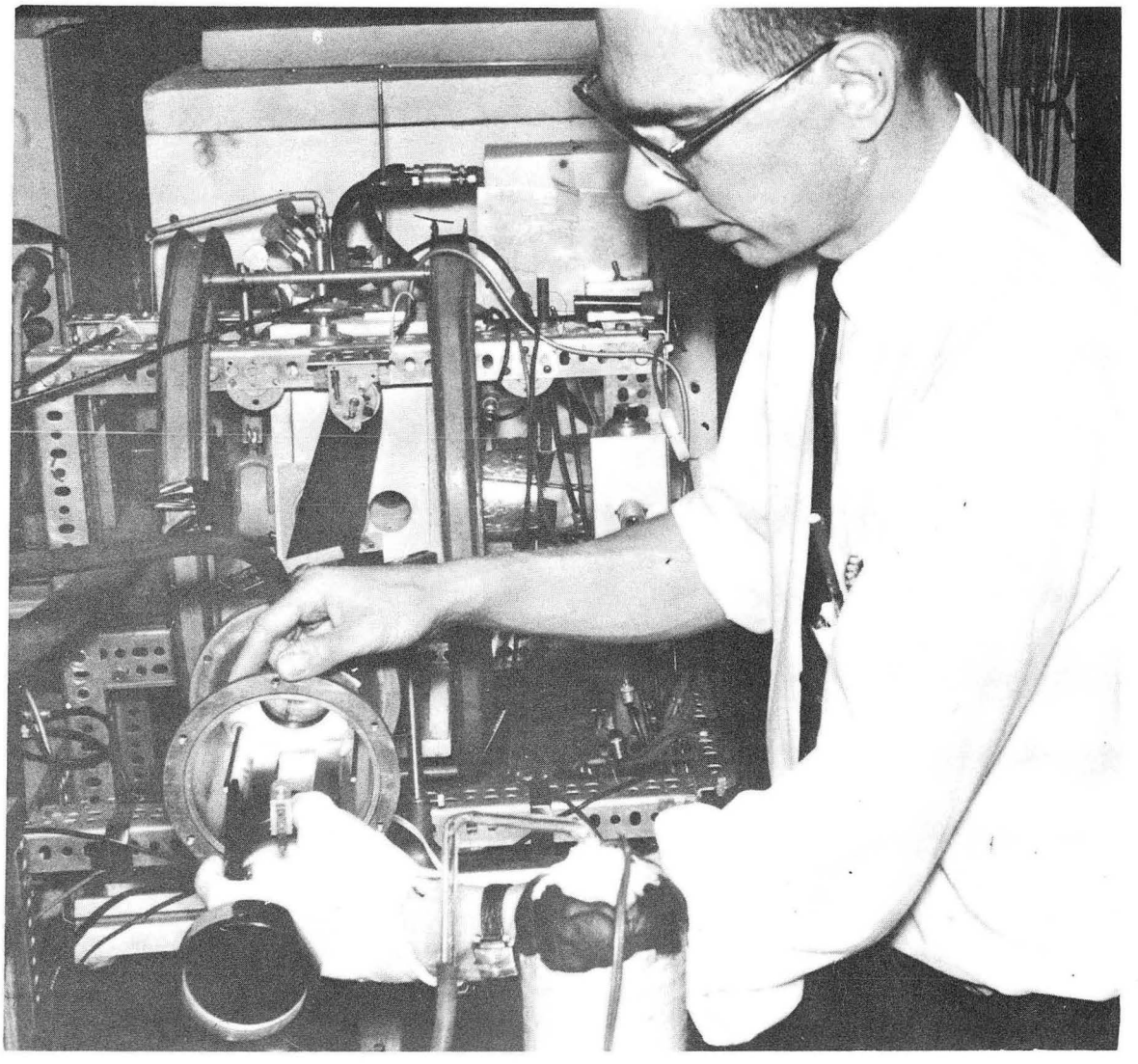

ZN-4890

Fig. 46. Dr. Robert Hull operating on the Fabry-Perot etalon.

pressure of 18 to 20 lb/in.^{2} is usually used. The supersonic leak consists of a fine capillary 5 to 10 mm long formed in a small tube by the glassblower; several sizes were made and a suitable size was chosen by trial and error. An empty gas tank is used in parallel with the chamber to reduce the scanning rate. A Duo-Seal forepump is used for evacuating the chamber.

The intensity of the ring system when the density measurement lamp is used is too weak to be seen. A Cd Osram lamp with a red filter is used for aligning the plates and focusing the center spot on the pinhole. For aligning the plates a diffusing screen is placed in front of the lamp in order to approximate a broad source. The setup for adjusting the parallelism of the plates is shown in Fig. 47. The fringes are observed in the mirror at the far left, and the pressure on the plates adjusted so that the rings do not change in size when one moves his head from side to side or up and down. The center spot of the ring system is then focused on the photomultiplier pinhole.

4. Detector and Associated Electronics

An RCA 7102 photomultiplier operated at 1200 V is placed just behind the 0.4-mm pinhole. A stream of cool nitrogen flows around the tube, greatly reducing the noise. The nitrogen vapor boils from a 5-liter Dewar of liquid nitrogen containing a 600-Ω resistor operated at 140 V. The photomultiplier output drives a phase-sensitive detector (PSD) designed and constructed by A. George and the Electronics Shop. Similar curves are obtained by using a Princeton Applied Research PSD, but the latter has less sensitivity. The PSD time constant is usually set at 0.3 sec, which is a factor of 10 less than the 3 sec that the flag shutter is in each of its positions. Some of the density measurement apparatus is shown in Fig. 48.

5. Normalization

There are two problems in normalizing the density measurement in the absence of the absorbing atoms: (a) the two beams must pass through the same part of the Fabry-Perot and have their ring systems concentric, and (b) the intensities of the two ring systems

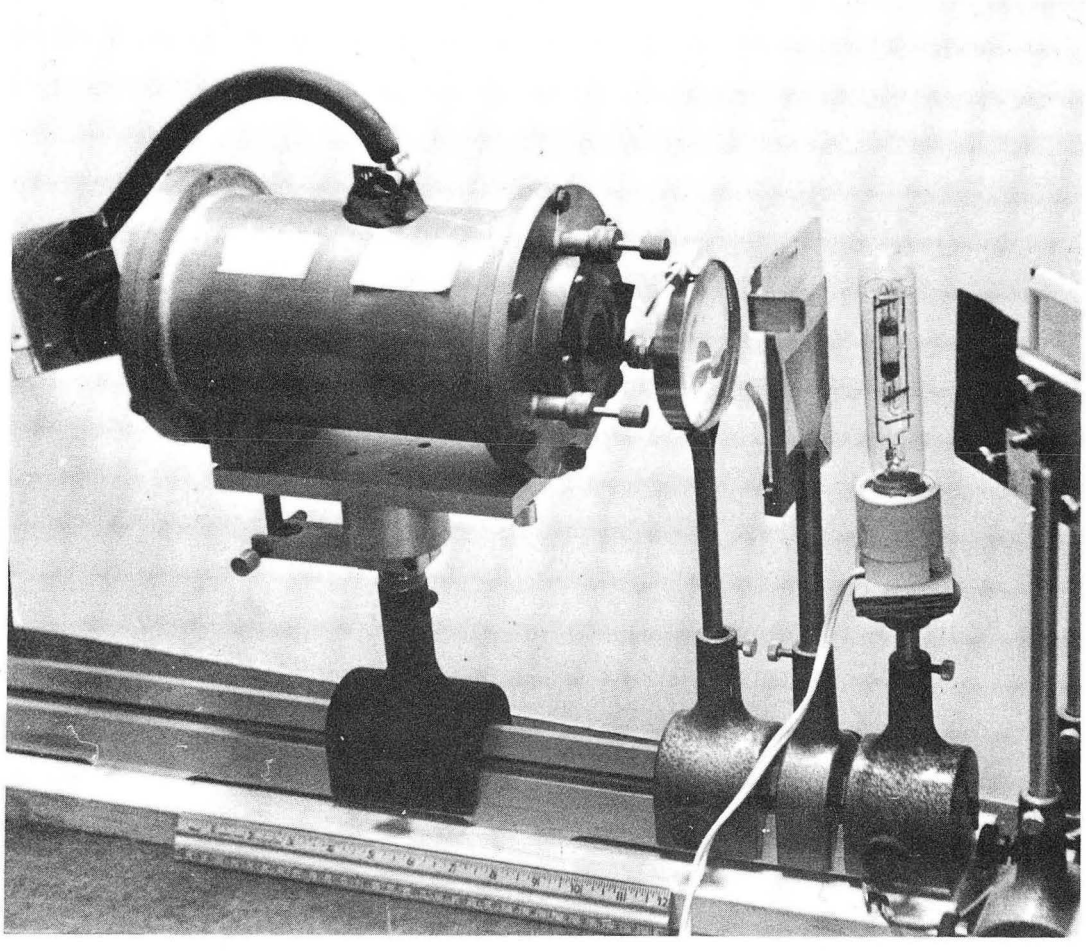

ZN-4891

Fig. 47. Optical arrangement for alignment of the Fabry-Perot. The light from the Cd Osram lamp passes through a red filter, diffusing screen, lens, and Fabry-Perot, and the rings are observed in the mirror at the far left.

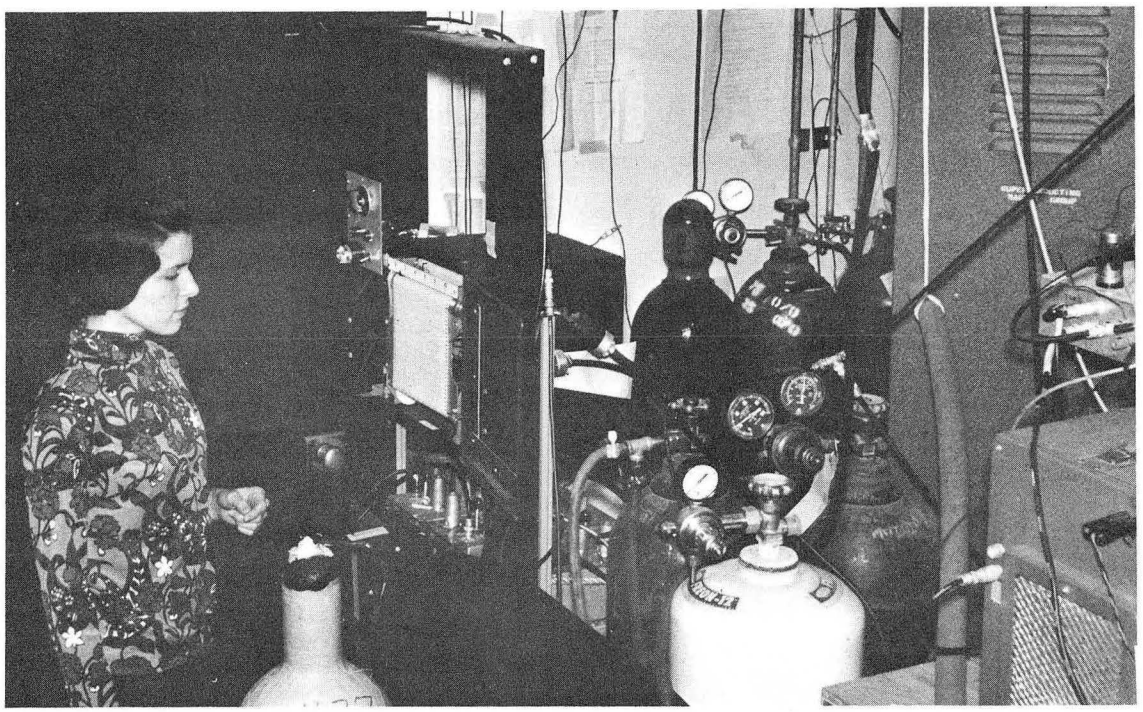

ZN-4892

Fig. 48. Mrs. Rachel King inspecting a scan of Rb^{87} absorption of natural Rb radiation. The auxiliary volume for decreasing the scanning rate and the Freon and nitrogen tanks can be seen. The phase-sensitive detector is under the recorder. The photomultiplier and detector lens are covered with a black cloth supported by a cardboard frame to permit operation with the room lights on.

Fig. 49. Cs^{133} 8944-Å spectral profiles with flag shutter in operation; 12-mm spacer (10-mm spacer was used in the density scans).

(a) Normalized; 0.3 sec integration time.

(b) Unnormalized because the ring systems of the two beams are not concentric at the pinhole. L and R refer respectively to left (through cell) and right beams. Note that it would be impossible to normalize the beams by equalizing their intensities; the intensities are already equal just to the right of the peaks and near the valleys. Curves have been drawn to indicate that the patterns are shifted with respect to each other. 1.0 sec.

(c) An effect similar to (b) is obtained when the Fabry-Perot is badly out of adjustment. 0.3 sec.

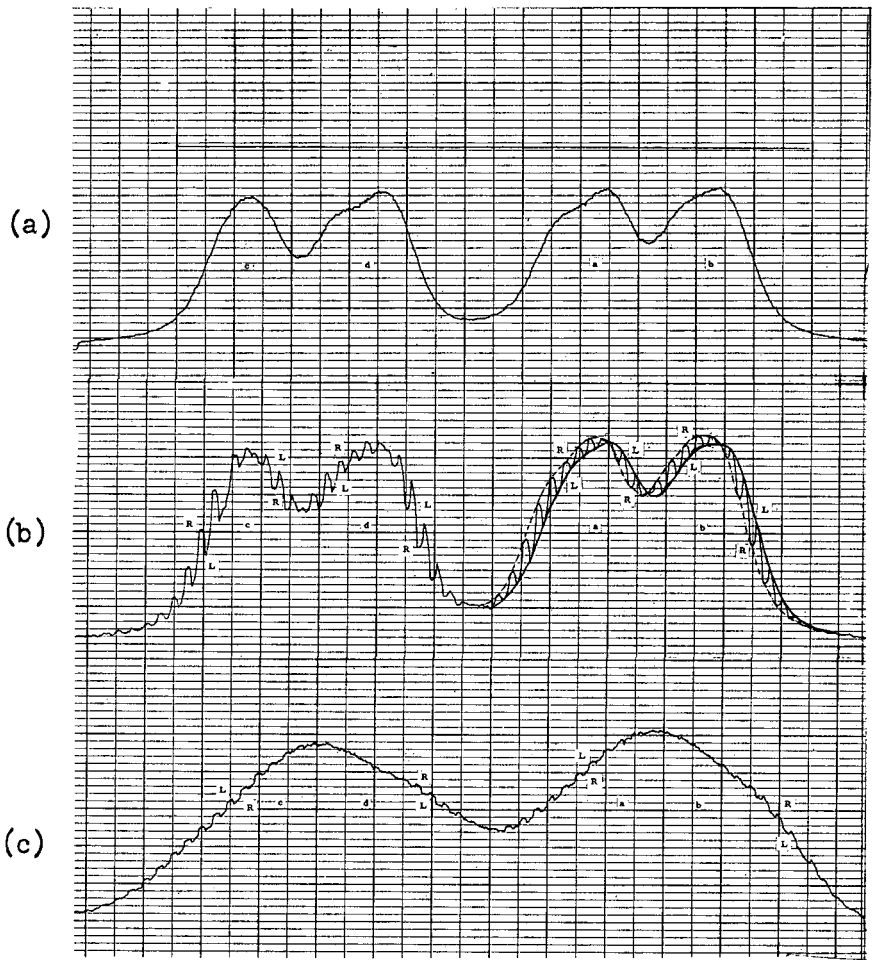
(a)
(b)
(c)
MU-35447

must be equal. Condition (b) follows easily once (a) is achieved. The finesse of the plates almost surely varies from one portion of the plates to another. Since the observed spectral profiles depend upon the finesse, normalization cannot be realized unless (a) is satisfied. Figure 7 shows a properly normalized scan for Rb; a similar curve for Cs is seen in Fig. 49(a). Figure 49(b) demonstrates the case in which (a) is not satisfied.

The following procedure has been found effective in normalizing the density measurement:

(a) Form a cross hair with two fine wires across a hole punched in black paper. Place the hole against the front of the lamp bulb. Enclose and heat the lamp and run it on CW for greater light intensity.

(b) Remove the filters, normalizing polarizer (used in one beam for normalizing the peaks), Fabry-Perot, and detector lens.

(c) It is assumed that the detector and its lens and the Fabry-Perot are situated on an optical bench. Adjust two pointers (rods ground to a sharp point) to the height of the center of the oven windows. Make sure that they are centered over the optical bench, with a level for example. Adjust the bench so that the two pointers and the center of the left (as seen from the detector) oven windows are collinear.

(d) Sighting along the pointers, center the pinhole on the now-defined optical axis.

(e) Adjust the lamp until it is also centered on the axis.

(f) Adjust the lenses to give an image of the bulb and cross hairs on the pinhole, using the beam passing through the cell (left side). Make sure that the lenses are centered on the optical axis.

(g) Adjust the beam splitters to be vertical and at about 45 deg with respect to the optical axis, using a level and 45-deg right triangle.

(h) Adjust beam splitter #2 so that it is as far to the left as if can be and still pass all the light through the left side.

(i) Adjust mirror #2 to be at approximately 45 deg and vertical. The distance between beam splitter #2 and mirror #2 (measured on a perpendicular to the optical axis) should be set equal to the separation between centers of the left and right oven windows.

(j) Using two pointers on the optical axis, adjust mirror #2 until the images of the 4 oven holes are concentric. This ensures that parallel light coming through the oven is parallel and concentric through the Fabry-Perot.

(k) Adjust mirror #1, and if necessary beam splitter #1, to give concentric images of the bulb and cross hairs at all points along the optical axis.

(l) Replace and retune the Fabry-Perot and refocus the ring system.

(m) Replace the filters and normalizing polarizer and remove the hole at the lamp.

(n) Scan until a peak is reached. Equalize the beams using the normalizing polarizer.

Sometimes the beam by-passing the cell is perturbed by accidentally hitting one of the mirrors. On several occasions the normalization has been restored as follows. Scan to a peak and stop. Place a punched hole outside the lamp in a position that maximizes the transmitted light through the cell. Then adjust the mirrors to maximize the light by-passing the cell. Remove the hole and equalize the beams; if the normalization is not restored, repeat the detailed normalization procedure.

Since the center spot is the image of a small part of the lamp bulb, a defining aperture could be used at the lamp at all times. However, the system would than be sensitive to small changes in the lamp position. With a large-area source, the bulb position is not critical.

Although there is labor involved in normalizing the measurements in this fashion, it does have great advantages in situations in which the absorbing atoms cannot be quickly removed. If there are lamp drifts which are slow compared with 0.15 cps, they are unimportant in finding $k(\nu)$ by this method. Furthermore, one is freed of the problems of matching up wings, etc., which arise when the two scans are taken separately.

6. Finesse Measurement

The finesse, N, is

$$N = F_\sigma / \Delta\sigma , \tag{152}$$

where the free spectral range is related to the plate separation by

$$F_\sigma = 1/2t \tag{153}$$

and $\Delta\sigma$ is the instrument width at half maximum.[63] N is then the ratio of the order width to the observed width of an infinitely narrow input line. Experimentally in this experiment, a narrow line of Cs is used which passes through the 7947-Å Rb filters.[64] A 1.5-mm spacer is used to make the instrument width greater than the width of the input line; the observed width is then approximately the instrument width. The auxiliary volume is closed and Freon gas is used in order to increase the scanning rate (μ-1 is about 4 times as large for Freon as for air). A 1-in. aperture at the entrance of the Fabry-Perot was used throughout the finesse and density measurements. Larger apertures yield lower finesses. Figure 50 is a finesse scan yielding $N \geq 29$; the usual value throughout these experiments was 22 to 30.

F. Density-Measurement Data Analysis

One would expect from the discussion of IIIB. 2 that the calculation of the density from scans such as Fig. 8 would be a straightforward process. In subsection IIIF.1 the complications introduced by the non-delta-function character of the instrument function are discussed. Subsection IIIF. 2 describes the procedures actually used to estimate the densities from the scans.

1. Complications Introduced by the Instrument Function

The calculations of Kostkowski and Bass,[65] indicating that $\int k(\nu)\, d\nu$ is preserved to an excellent approximation even when the width and peak of the absorption profile are greatly altered by a large instrument width, were made on the assumption of a Gaussian instrument function. However, the instrument function of a Fabry-Perot is an Airy function,[63]

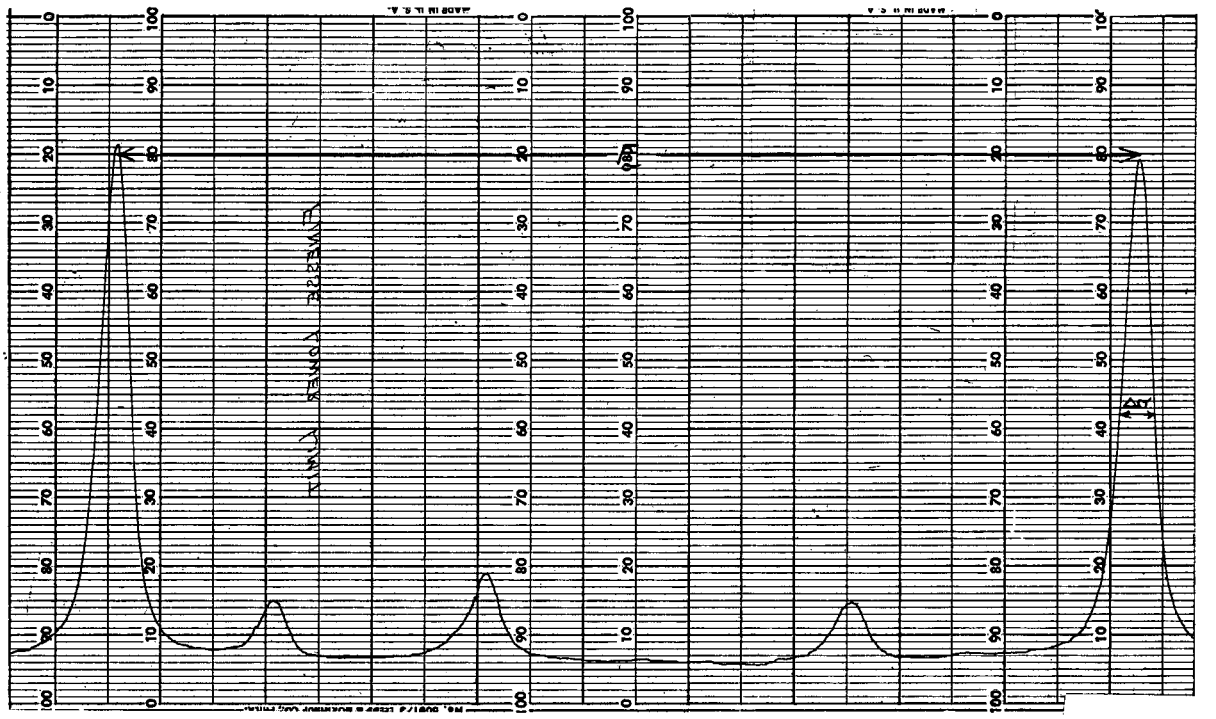

MU-35448

Fig. 50. Finesse scan using narrow Cs line passed by the 7947-Å filter (≈ 80-Å band-pass). Freon scanning gas, 1.5-mm spacer, N ≈ 29 to 30.

$$g(\nu) = [1 + (4R \sin^2(\pi \nu/F_\sigma))/(1 - R)^2]^{-1}, \tag{154}$$

where R is the reflectivity, ν is the frequency, and F_σ is the free spectral range. An effective R is determined in practice as follows. The finesse for perfectly flat plates is determined by the reflectivity,

$$N_R = \pi (R)^{1/2}/(1 - R). \tag{155}$$

In general, the finesse N is reduced by the nonflatness of the reflecting surfaces. An effective reflectivity is found by using (155) with N_R replaced by N,

$$R_e = 1 + \pi^2/2N^2 - \pi[1 + (\pi/2N)^2]^{1/2}/N \approx 1 - \pi/N, \tag{156}$$

for high finesse. The effective reflectivity is then used in (154) to give a fair representation of the instrument. Once $g(\nu)$ is known the observed function $I_0(\nu)$ can be found if the input $f(\nu)$ to the instrument is known:

$$I_0(\nu) = \int f(\nu') g(\nu - \nu')\, d\nu'. \tag{157}$$

Suppose the beam of light by-passing the cell is represented by $f(\nu)$; then that passing through the cell is given by

$$f(\nu) \exp[-k_T(\nu) \ell], \tag{158}$$

where $k_T(\nu)$ is the <u>true</u> absorption coefficient and ℓ is the absorption path length. The observed intensity through the cell is then

$$I_0'(\nu) = \int f(\nu') \exp[-k_T(\nu')\ell]\, g(\nu - \nu')\, d\nu'. \tag{159}$$

The <u>observed</u> absorption coefficient is defined as

$$k_0(\nu) = \ell^{-1} \ln [I_0(\nu)/I_0'(\nu)]. \tag{160}$$

Clearly, if g is proportional to a delta function, then

$$k_0(\nu) \to k_T(\nu). \tag{161}$$

But for an actual instrument, there seems to be no simple relationship between the observed and true absorption coefficients.

The effect of the instrument has manifested itself clearly in two experimental ways. First, absorption is observed between orders for a low finesse or high density. Recall that for Doppler broadening[66]

one has

$$k_T(\nu) = k_T(\nu_0) \exp\{-[2(\nu - \nu_0)\ (\ln 2)^{1/2}/\Delta\nu_a]^2\}, \qquad (162)$$

where

$$\Delta\nu_a = 2(2RT \ln 2/M)^{1/2}\ \nu_0/c \qquad (163)$$

is 13 mK (1mK = 10^{-3} cm^{-1}) for the Cs^{133} 8944-Å line and 18.4 mK for the 7800-Å line of Rb^{87} at T ≈ 78° C, the temperature of the oven in all of the runs. The width of each absorption line is then known, since there is no buffer gas and the lines are Doppler-broadened. The ratio of the true absorption peaks is also known by calculating transition probabilities (see Fig. 12 and Appendix IV). The information about $k_T(\nu)$ offers a critical test to be applied in estimating the credibility of the $k(\nu)$ deduced from $k_0(\nu)$. In particular, $k_T(\nu)$ is less than $0.01k_T(\nu_0)$ for $|\nu - \nu_0| \geq 1.3\ \Delta\nu_a$. That this is not always true of $k_0(\nu)$ is shown clearly in Fig. 51 of the 8944-Å line of Cs taken with a finesse of about 12. Since the peaks are roughly 300 mK apart, the absorption coefficient is seen to be about 0.4, or more than 50% of $k_0(\nu_0)$, more than 100 mK from the center of the line! This effect has been checked and does not arise from a lack of normalization. In fact, it was also observed by Winocur and Pyle[67] in the absorption of the 4215-Å line of Rb by Sr ions; in that experiment normalization was no problem, since the ions could be modulated on and off by means of the discharge. Computer calculations by Dr. Hull confirm that this effect is introduced by the interferometer. This can be understood as follows. Approximate the instrument function by

$$g(\nu - \nu') = 1 = g_1 \qquad |\nu' - \nu| < \Delta\sigma$$

$$= 0.04 = g_2 \qquad |\nu' - \nu| > \Delta\sigma\ . \qquad (164)$$

Approximate the emission line by a rectangle of unit height and width $\Delta\nu_e$. Assume that the absorption appears as a rectangular dip of 0.25 in the center of the emission line with a width $\Delta\nu_a = \Delta\nu_e/3$. Assume for simplicity that $\Delta\sigma = \Delta\nu_a$. With the instrument function centered on the emission line, the true peak is observed. With g_1 just inside f, the absorption coefficient is quite small, since where g is large the

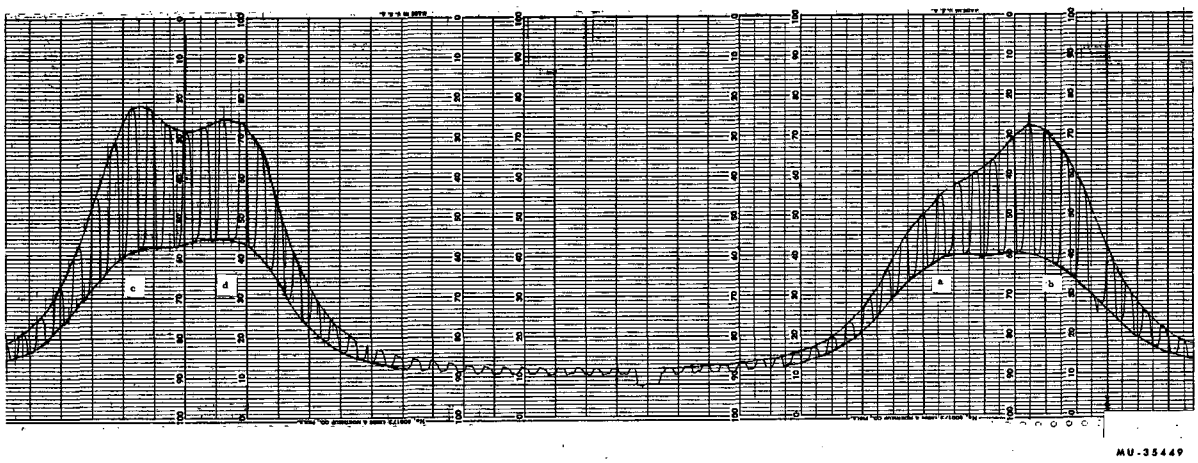

Fig. 51. Cs 8944-Å scan, demonstrating "absorption" between orders; 8-mm spacer, finesse of 12.

absorption is zero. But when g_1 is outside f, f = 0 for $g_1 \neq 0$, so all the contribution to $k_0(\nu)\ell$ comes from the wings of g. But the wings are essentially constant over an absorption width, i.e., they treat the profile as would an instrument of zero finesse or no resolution. In other words, for g_1 outside f the observed absorption coefficient is the same as would be deduced by observing the two integrated intensities with any detector. This simplified argument explains the general characteristics of Fig. 52. The size of the between-order absorption relative to the peak absorption depends upon (a) g_2/g_1, i.e., the finesse, and (b) the total absorption $\int f(\nu)\ \{1 - \exp[-k(\nu)\ell]\}\, d\nu / \int f(\nu)\, d\nu$. It is found that the area under $k_0(\nu)$ out to the minimum is much closer to the true area than the area under $k_0(\nu)$ for all frequencies. In practice, for low absorption, one can usually distinguish between $I_0(\nu)$ and $I_0'(\nu)$ only out to the minimum. Because of this between-order $k_0(\nu)$, areas of $k_0(\nu)$ are considered for density measurement purposes only for low absorption.

The second instrument effect arises when there are two lines very close together, as for the $^2P_{1/2} \rightarrow {}^2S_{1/2}$, F = 2, 7947-Å line of Rb^{87} and the $^2P_{1/2} \rightarrow {}^2S_{1/2}$, F = 3, 7947-Å component of Rb^{85}. Consider a cell containing Rb^{87} only, irradiated with light from a natural Rb lamp. Three of the 7947-Å peak absorption coefficients of Rb^{87} should be equal. For an unheated lamp in which the Rb^{85} components were 3 to 4 times as intense as the Rb^{87} components and the observed widths were $\Delta\tilde{\nu}_e^{87} \approx 30$ mK and $\Delta\tilde{\nu}_e^{85} \approx 40$ mK, the ratios were close to 0.5:0.25:1.0. For a heated lamp with almost equal components and $\Delta\tilde{\nu}_e^{87} \approx 40$ mK and $\Delta\tilde{\nu}_e^{85} \approx 80$ mK, the ratios were about 1.0:0.95:1.0. Only the conditions in the lamp were changed between the two situations. In the first case the instrument adds to the intensities of the c and especially of the d components of Rb^{87} a large background light from the much more intense Rb^{85} lines nearby; consequently, the observed peak absorption coefficients are grossly depressed in value. As the lamp was heated the $k_0(\nu_0)$ of the b component did not change appreciably. But the $k_0(\nu_0)$'s of the c and d components increased, approaching that of the b component. This occurs because the Rb^{87}

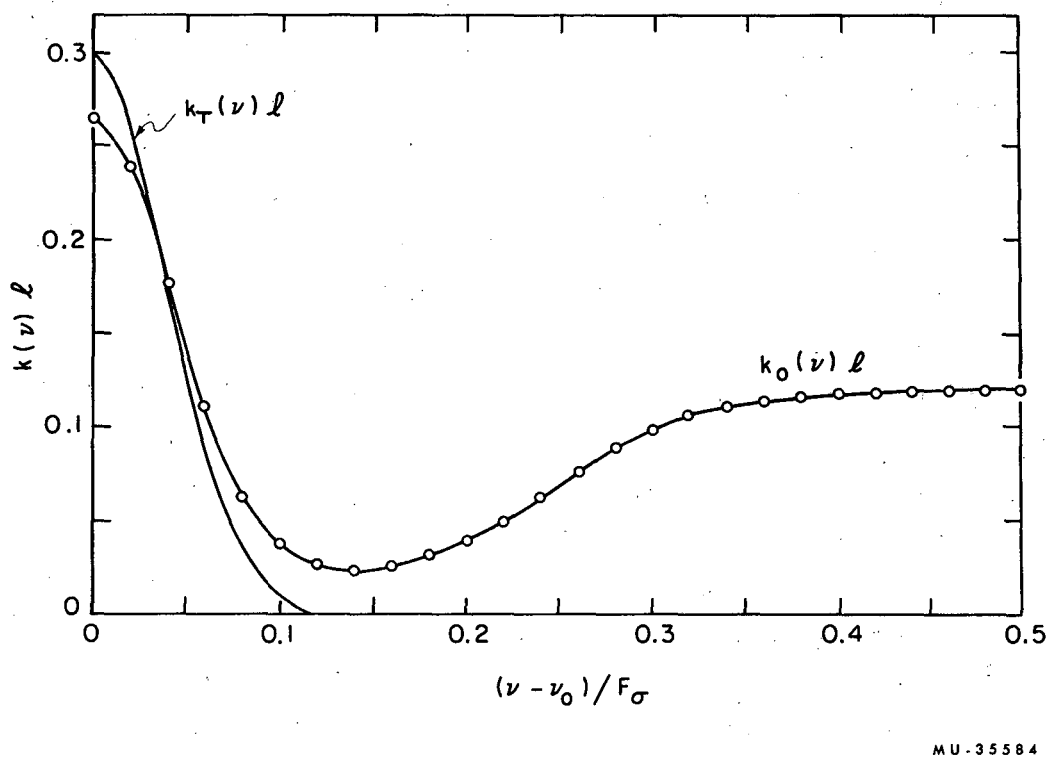

Fig. 52 Computer calculations showing the "observed" absorption coefficient $k_0(\nu)$, which results from the distortion of the input profiles by the Fabry-Perot; ℓ is the absorption path length. The author is indebted to Dr. Hull for this curve; this and other results will probably be published in greater detail in the near future. N=50, $\Delta\sigma/\Delta\nu_a$=0.219, $\Delta\nu_a$=20mK, $\Delta\nu_e/\Delta\nu_a$=2.0.

light gained intensity relative to the Rb^{85} light, thus reducing the effectiveness of the background from the latter. Again Dr. Hull has made computer calculations verifying, at least qualitatively, the validity of the above explanation for the unequal $k_0(\nu_0)$'s.

Presumably sufficient arguments have been given to convince anyone that there are problems in applying a Fabry-Perot interferometer to the measurement of a density. The task now becomes that of convincing the reader that meaningful density measurements can be made with this instrument. The argument is based on the agreement between the following estimates of the density. First, on the basis of the success in explaining the complications just described, there is reason to believe that Eqs. (154) and (157) accurately describe the effects of the instrument upon the true profile. Then calculations can be made to determine the $k_0(\nu_0)$ for a given $k_T(\nu_0)$ and, consequently, the inverse. Obtaining $k_T(\nu_0)$ from $k_0(\nu_0)$ and knowing that the absorption line is Doppler-broadened, one can compute $\int k_T(\nu)\,d\nu$. Second, at low densities the $\int k_0(\nu)\,d\nu$ is believed to be close to $\int k_T(\nu)\,d\nu$, as discussed above; this assumes a high finesse (≈ 25). These methods as applied to the Rb^{87} and Cs^{133} density measurements are discussed in the next subsection.

2. Methods for Estimating Densities

a. $k(\nu_0)$ Method

The density measurement scans are analyzed as follows. Smooth curves defined by the shutter positions are penciled in. The zero is drawn in, using the zeros obtained with a flag during the scan. Five to 10 points, usually 0.1 in. apart are marked along the zero line in the region of the peak absorption. The values of the zero, $I_0'(\nu)$, and $I_0(\nu)$ are measured at each of the marks. An ingenious machine belonging to Professor John Reynolds' group is used; one sets a cross-hair on the point, presses a button, and waits a second for the coordinates to be punched onto an IBM card. The cards are analyzed by another of Dr. Hull's computer programs, which computes $k_0(\nu)\ell$. The peak $k_0(\nu_0)\ell$ is then chosen from the 5 to 10 values.

The finesse N and spacer thickness t are assumed known. The effective reflectivity is found by using (156), and the effective instrument width $\Delta\sigma$ is obtained by setting (152) equal to (155) with the effective reflectivity used in the latter. The observed width $\Delta\nu_e^0$ is measured in a few places and assumed to be constant throughout a run, the lamp conditions being fixed. The true emission width $\Delta\nu_e^T$ is found by using the correction $\Delta\nu_e^T = (\Delta\nu_e^0 - 0.64\Delta\sigma)/0.98$ for $1 < \Delta\nu_e^T/\Delta\sigma < 3$ from Minkowski and Bruck.[68] Computer solutions by Dr. Hull are then used to find $k_T(\nu_0)\ell$ from $k_0(\nu_0)\ell$ when N, t, $\Delta\nu_a$, and $\Delta\nu_e^T/\Delta\nu_a$ are known.

From Appendix IV one has

$$\int k_T(\nu)\,d\nu\Big|_{J'\to 1/2\ F} = \lambda_0^2(2J'+1)\,n_F/16\pi\tau_{J',1/2} = \lambda_0^2(2J'+1)(2F+1)n/32(2I+1)\pi\tau_{J',1/2}. \quad (165).$$

For the $^2P_{3/2} \to {}^2S_{1/2}$, F = 1 transition in Rb^{87}, λ_0 = 7800 Å, I=3/2, $\tau = (2.78 \pm .09)\times 10^{-8}$ sec,[69] and ℓ = 1.96" (the absorption length for runs 4 through 8):

$$n_{Rb^{87}} = 0.92\times 10^{12}\left[\int k_T(\tilde{\nu})\,\ell\,d\tilde{\nu}\right]\Big|_{\substack{7800\ \text{Å}\\ \text{e, f, g}\\ \ell=1.96"}} \text{cm}^{-3} \quad (166)$$

where the integral is in cm^{-1}. For a single Doppler absorption line $\int k(\tilde{\nu})\,\ell\,d\tilde{\nu}$ is given by[66]

$$(\pi)^{1/2}\,k_T(\tilde{\nu}_0)\,\ell\,\Delta\tilde{\nu}_a/2(\ln 2)^{1/2}. \quad (167)$$

Computer solutions indicate that for the purposes of obtaining the area under $k(\nu)$, the e, f, g components of Rb^{87} are represented well by a single Gaussian of width 1.1 $\Delta\nu_a$. The composite height is found as described above. Then one has

$$\int k_T(\tilde{\nu})\ell\,d\tilde{\nu} \approx (\pi)^{1/2}\left[k_T(\tilde{\nu}_0)\ell\right]\Big|_{\substack{7800\ \text{Å}\\ \text{e, f, g}}} (1.1\,\Delta\tilde{\nu}_a)\,/2(\ln 2)^{1/2}. \quad (168)$$

For the runs on Rb^{87}, $\Delta\tilde{\nu}_a$ = 18.4 mK and

$$n_{Rb^{87}} = [k_T(\tilde{\nu}_0)\ell]\Big|_{\substack{7800 \\ e, f, g \\ \ell = 1.96''}} \quad (1.98\times10^{10})\ \text{cm}^{-3}. \quad (169)$$

Now consider the absolute value calibration of the Rb^{87} density in run 5. Figure 53 is the density measurement scan used; Fig. 54 gives the machine-read, computer-calculated values of $k_0(\nu)$. Table VI contains the numerical values of the various quantities necessary for estimating the density by the $k(\nu_0)$ method. The correction curve used to find $k_T(\nu_0)$, given $k_0(\nu_0)$, is shown in Fig. 55.

For the Cs measurements, from Appendix IV, one has

$$\int k_T(\nu)\, d\nu\Big|_{1/2\ F' \to 1/2\ F} = \lambda_0^2 \Delta(F, F')\, n_F / 24\pi(2F+1)\tau_{1/2,1/2}$$
$$\approx \lambda_0^2 \Delta(F, F')\, n/48\pi(2I+1)\ \tau_{1/2,1/2}, \quad (170)$$

where the $\Delta(F, F')$ are given in Table II. For the $^2P_{1/2} \to {}^2S_{1/2}$, F transition in Cs, $\lambda_0 = 8944$ Å, $I = 7/2$, $\tau = (3.8\pm0.4)\times10^{-8}$ sec,[70] and $\ell = 1.96$ in., one has

$$n_{Cs^{133}} = 3.46\times10^{13}\left[\int k_T(\tilde{\nu})\ell\, d\tilde{\nu}\right]\Big|_{\substack{F' \to F \\ 8944\ \text{Å} \\ \ell = 1.96\ \text{in.}}} \Big/ \Delta(F, F')\ \text{cm}^{-3}, \quad (171)$$

with the integral in cm^{-1}. Again for a single Doppler absorption line, (167) yields, with $\Delta\tilde{\nu}_a \approx 13$ mK,

$$n_{Cs^{133}} = 47.9\times10^{10}[k_T(\tilde{\nu}_0)\ell]\Big|_{\substack{F' \to F \\ 8944\ \text{Å} \\ \ell = 1.96\ \text{in.}}} \Big/ \Delta(F, F')\ \text{cm}^{-3}. \quad (172)$$

See Fig. 56 for the labeling and intensities of the Cs transitions. Figures 57 and 58 are the scan and values of $k_0(\nu)$ for one temperature of run 8. Again Table VI summarizes the $k(\nu_0)$ estimate of the density. The $k_0(\nu_0) \to k_T(\nu_0)$ correction curve is given in Fig. 55. Because the four components are fairly well resolved, the Cs density is estimated by using each. Table VI indicates an extreme disagreement of only 13% between the various estimates.

Table VI. Absolute density measurements by $k(\nu_0)$ method.

Run	5			8		
Date	1/24/65			2/13/65		
Time	1250			1722		
Sidearm temperature (°C)	24			22		
Element	Rb^{87}			Cs^{133}		
Component	7800:e, f, g	8944: a		b	c	d
N	≈ 25			≈ 25		
R_e	0.88			0.88		
t(mm)	12			10		
$\Delta\sigma$(mK)	16.7			20		
T_{oven} (°C)	78			78		
$\Delta\nu_a$ (mK)	18.4			13		
$\Delta\nu_e^0$ (mK)	47-49			≈ 33		
$\Delta\nu_e^T$ (mK)	37-39			20-21		
$(\Delta\nu_e^T/\Delta\nu_a)_{calc.}$	2.0-2.1			1.5-1.6		
$(\Delta\nu_e^T/\Delta\nu_a)_{used}$	2.0			1.5		
$k_0(\nu_0)\ell$	0.285	0.0635	0.183		0.166	0.122
$k_T(\nu_0)\ell$	0.42	0.096	0.28		0.25	0.185
Eq. for n	(169)			(172)		
$\Delta(F, F')$		21/4	63/4		63/4	45/4
n (10^{10} cm^{-3})	0.82	0.87	0.85		0.77	0.79

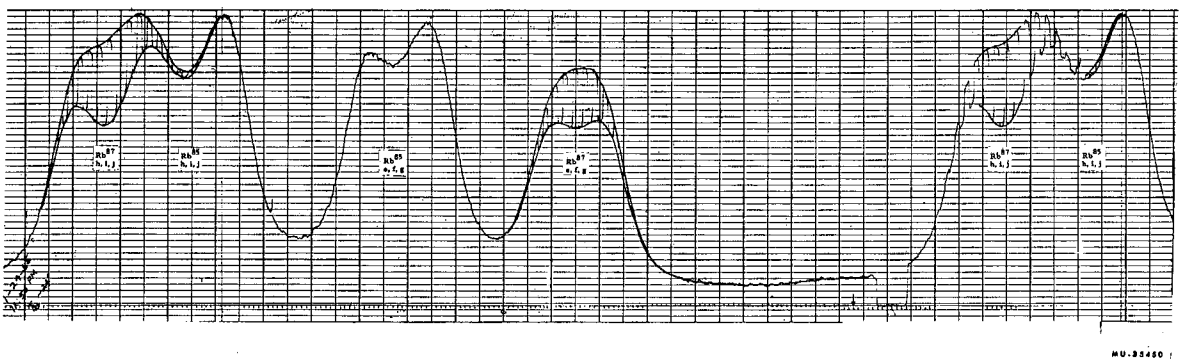

Fig. 53. Density measurement scan; Rb^{87} absorption of 7800-Å line of natural Rb lamp. Run 5, 1/24/65, 12:50 p.m., $T_{Rb^{87}} = 24°$ C.

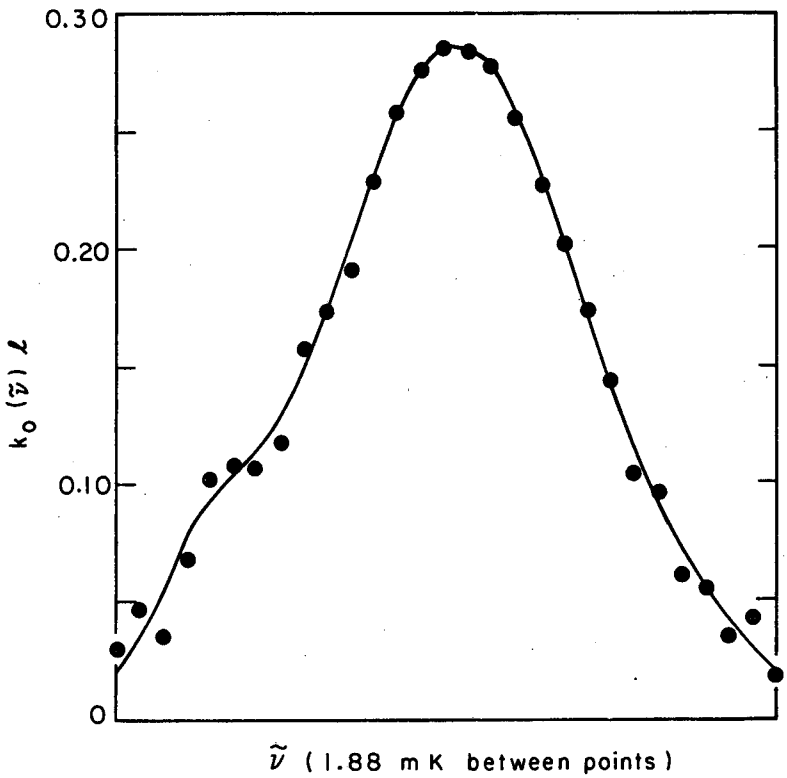

Fig. 54. Observed absorption coefficient for the e, f, and g components of the 7800-Å line of Rb^{87} as read from the density scan shown in Fig. 53; t=12 mm, $\Delta\nu_a$=18.4 mK, $\Delta\nu_e/\Delta\nu_a$= 2.0.

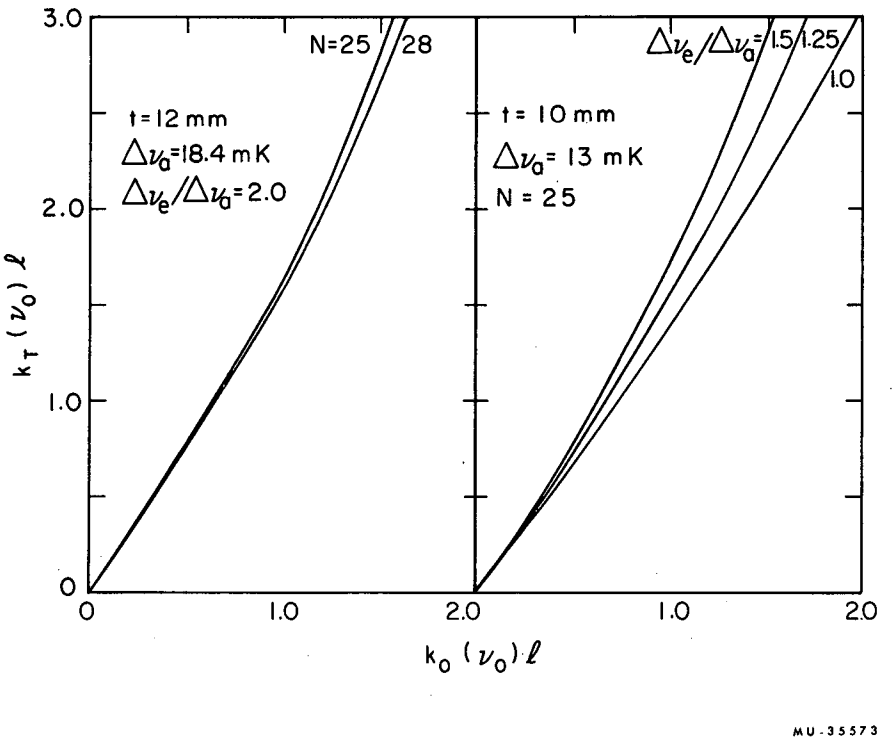

Fig. 55. Corrections for obtaining the true peak absorption coefficient $k_T(\nu_0)$ from the observed value $k_0(\nu_0)$. The corrections apply to single Gaussian emission and absorption lines. The corrections were found by computer calculations by Dr. Hull, which are to be published.

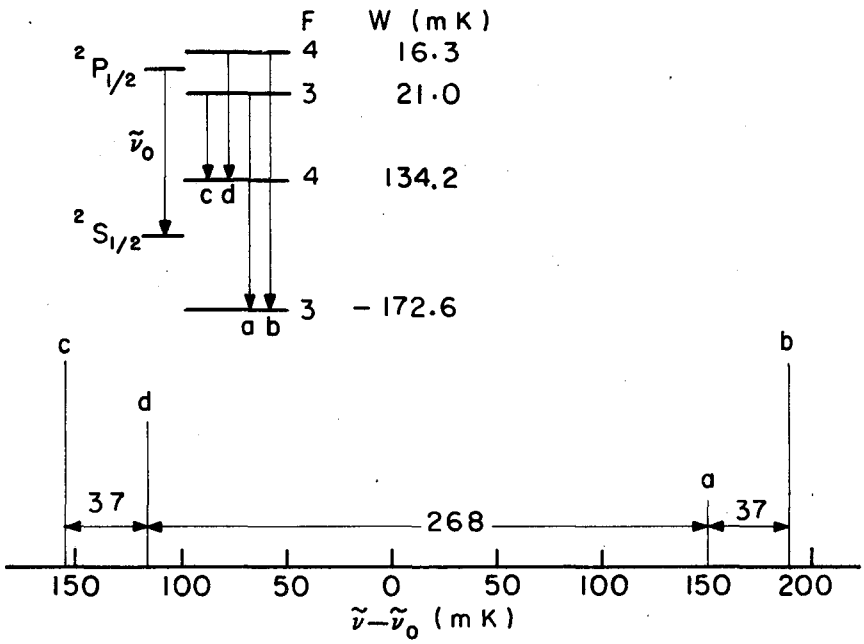

Fig. 56. Relative intensities and separations of hyperfine-structure components of the Cs^{133} (I=7/2) $6^2P_{1/2} \rightarrow 6^2S_{1/2}$ transition at 8944-Å. W is the energy relative to the fine-structure energy.[71]

Transition	$\tilde{\nu}-\tilde{\nu}_0$(mK)	I	f value
a	150.7	33.4	7/192
b	189.6	100.0	21/192
c	-156.1	100.0	21/192
d	-117.2	71.5	15/192

The relative intensities I are normalized so that the largest is 100. The f values are normalized so that their sum is 1/3 for the $^2P_{1/2} \rightarrow {}^2S_{1/2}$ transition.

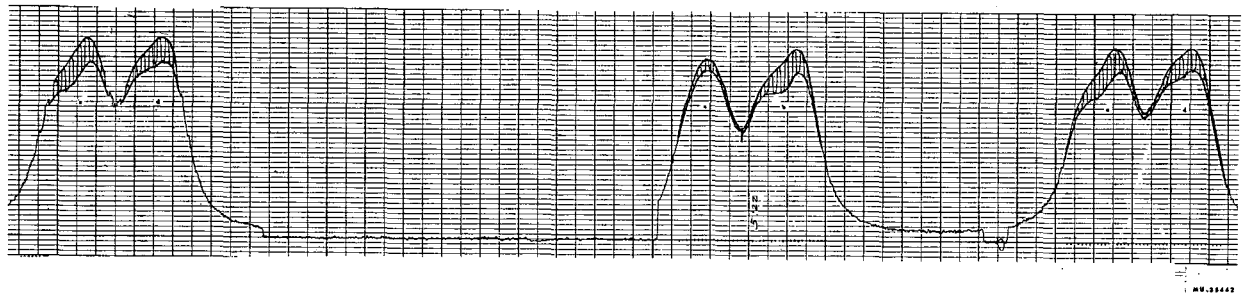

Fig. 57. Density measurement scan; absorption of 8944-Å line of Cs. Run 8, 2/13/65, 5:22 p.m., $T_{Cs} = 22°$ C.

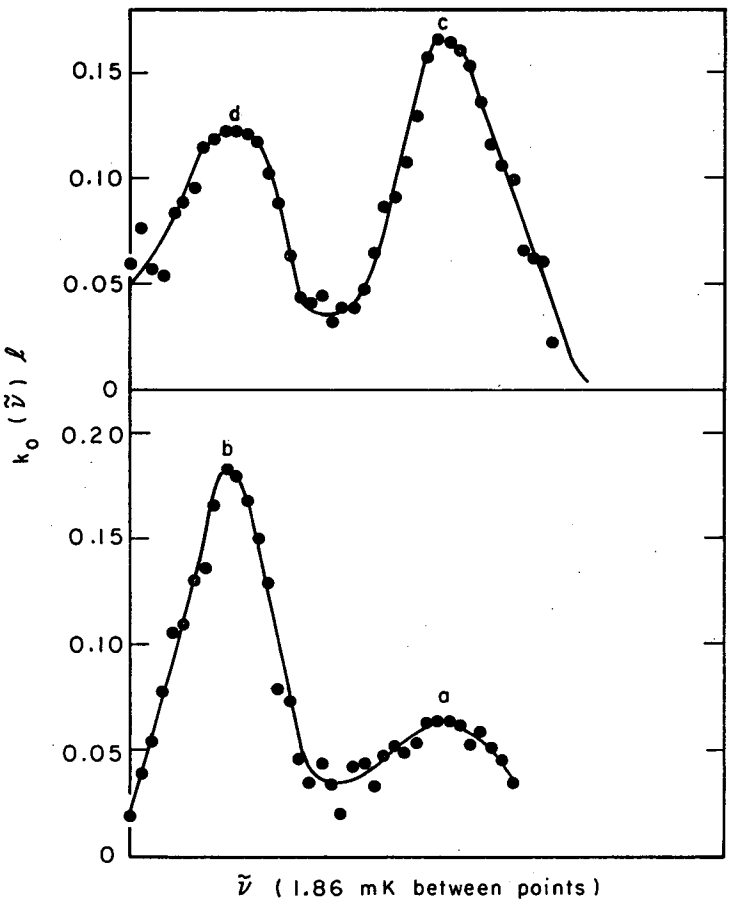

Fig. 58. Observed absorption coefficients for the 8944-Å line of Cs as read from the density scan shown in Fig. 57.

b. $\int k_0(\nu)\, d\nu$ method

Arguments have been given in IIIF.1 suggesting that $\int k_0(\nu)\, d\nu \approx \int k_T(\nu)\, d\nu$ for low absorption but not for high absorption. Figures 53 and 54 are the scan and resulting $k_0(\nu)$ of run 5. In computing the area, the frequency calibration for the abscissa is found by measuring the length of one order on the chart and using (153) to obtain the length-in mK from the spacer thickness. The density of Rb^{87} atoms is then found from the area by using (166). For Fig. 53, $F_\sigma \approx 18.7$ in., or by (153), $F_\sigma = 418$ mK, implying 22.4 mK/in. The $\int k_0(\tilde{\nu})\, \ell\, d\tilde{\nu}$ in (166) was found to be 0.417 in., yielding a density of 0.86×10^{10} cm^{-3}. A calculation by hand to check the above result agreed within 4%. Table VII displays the fact that the $k(\nu_0)$ and $\int k_0(\nu)\, d\nu$ methods agree within 5%, if the average values for the two methods are compared.

For Cs, multiply both sides of (171) by $\Delta(F, F')$ and sum over F':

$$n_{Cs^{133}} = 1.15 \times 10^{13} \left[\int k(\tilde{\nu})\, \ell\, d\tilde{\nu}\right] \Big|_{\substack{^2P_{1/2} \rightarrow F \\ 8944 \\ \ell = 1.96 \text{ in.}}} \Big/ (2F+1). \qquad (173)$$

The results for run 8 are given in Table VII for two different temperatures. At the higher temperature the $k(\nu_0)$ and $\int k_0(\nu)\, d\nu$ methods are in poor agreement as expected, but the agreement is good at the lower density. Good agreement between the two methods has been achieved at high densities by ignoring the between-order absorption in the integral; the area is taken only under the peak and Gaussian-shaped wings sketched in.

c. Relative density values

Once the density has been calibrated at one value of $k_T^1(\nu_0)\ell$, the density at any other $k_T^2(\nu_0)\ell$ is simply

$$n_2 = n_1 \left[k_T^2(\nu_0)\, \ell\right] / k_T^1(\nu_0)\ell. \qquad (174)$$

Table VII. Comparisons of densities estimated by the $k(\nu_0)$ and $\int k_0(\nu)d\nu$ methods. Densities are in units of 10^{10} cm^{-3}.

Run	5	8				8			
Date	1/24/65	2/13/65				2/13/65			
Time	12 50	17 22				20 07			
Sidearm temperature	24°	22°				26°			
Element	Rb^{87}	Cs^{133}				Cs^{133}			
Component	7800: e, f, g	8944: a	b	c	d	8944: a	b	c	d
n by $k(\nu_0)$	0.82	0.87	0.85	0.77	0.79	2.26	1.95	2.03	2.12
n by $\int k_0(\nu)d\nu$	0.86	0.84		0.88		3.0		2.5	

As has been discussed, the $\int k_0(\nu)\, d\nu$ method breaks down at the higher densities. The values of the density used in IIIG to determine the cross section were determined by using (174). The calibration density n_1 is taken from Table VII as a reasonable average of the densities determined by the two methods. For Rb^{87} a density of $n_1 = 0.84\times10^{10}$ atoms/cm^3 is taken to correspond to $k_T^1(\nu_0)\ell\big|_{a+b} = 0.42$ under the conditions of Table VI. The $[k_0(\nu_0)\ell]$'s are corrected by Fig. 55 to obtain the $[k_T(\nu_0)\ell]$'s, and then the densities are calculated from (174).

For Cs the $[k_T(\nu_0)\ell]$'s for each component are found by using Fig. 55 and are then normalized by dividing by $\Delta(F, F')$. The sum of the resulting quantities is then used to obtain absolute densities:

$$n_2 = n_1 \sum_{F\,F'} \{[k_T^2(\nu_0)\ell]_{F'F}/\Delta(F, F')\} \Big/ \sum_{F\,F'} \{[k_T^1(\nu_0)\ell]_{F'F}/\Delta(F, F')\}. \tag{175}$$

The calibration is $\sum_{F\,F'} [k_T^1(\nu_0)]_{F'F}/\Delta(F, F') = 0.069$ for $n_1 = 0.84\times10^{10}$ atoms/cm^3.

G. Summary of Results of Measurements of Spin-Exchange Cross Sections by Hyperfine Pumping

The details of the relaxation time and density measurements have been described. The results for runs 5 through 7 and 9 on Rb^{87} will now be given. In runs 5 and 6, at a given sidearm temperature, three or four relaxation-time measurements were made followed by three or four density scans or vice versa. The $1/\tau$ values and their standard deviations $\sigma(1/\tau)$ for each temperature were averaged. The corresponding densities were also averaged, and a fractional deviation was assigned to each value. Then $1/\tau$ was least-squares fitted to

$$1/\tau = 1/\tau' + B_{Sl}n, \tag{176}$$

where τ' is the non-spin-exchange relaxation time and B_{Sl} is given by (136). Figures 59 and 60 display the data points and the best-fit

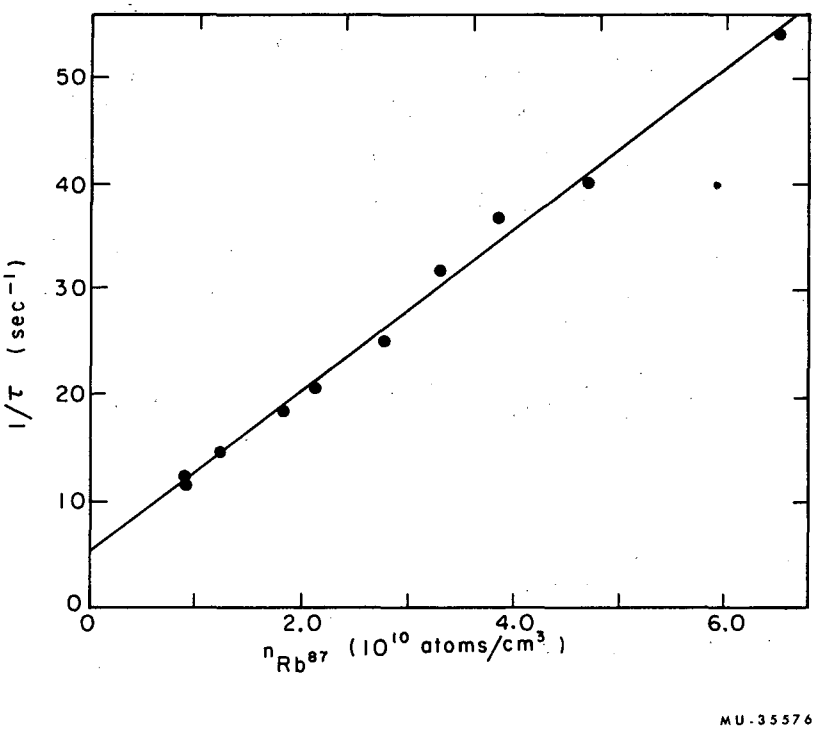

Fig. 59. Summary of run #5 (1/22-24/65) Rb^{87}-Rb^{87} spin-exchange cross-section measurement by hyperfine pumping. $1/\tau = A + Bn$; $A = 5.20 \pm 0.27$ sec^{-1}; $B = (7.63 \pm 0.19) \times 10^{-3}$ cm^3/sec.

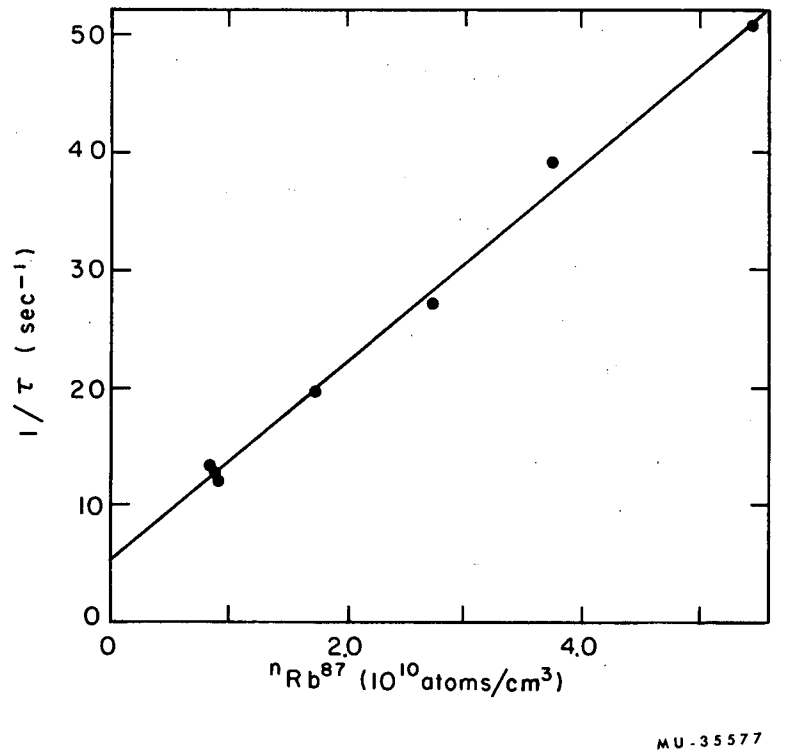

Fig. 60. Summary of run #6 (1/30-31/65) Rb^{87}-Rb^{87} spin-exchange cross-section measurement by hyperfine pumping. $1/\tau = A + Bn$; $A = 5.42 \pm 0.61$ sec^{-1}; $B = (8.41 \pm 0.48) \times 10^{-10}$ cm^3/sec.

straight lines. In runs 7 and 9 a density measurement was assigned to each $1/\tau$ by taking the relaxation data between orders; the results are presented in Figs. 61 and 62. Runs 5 through 7 were made in the same cubical cell with an edge of approximately 2 in. Run 9 was carried out in a $1\times2\times2$-in. cell with the density measurement made along the short path length. The Fabry-Perot plates were also recoated before run 9. Table VIII summarizes the Rb^{87} self-exchange cross-section measurements. Figure 63 shows the 1620 computer used in analyzing much of the data.

The Rb^{87}-Cs^{133} measurement, run 8, was performed in the same manner as runs 7 and 9; the data are displayed in Fig. 64 and Table IX. There is an advantage to the two-isotope experiment in that $1/\tau$ data can be obtained for one density known to perfect accuracy — zero density.

The errors on the parameters in the figures and tables are standard deviations of external consistency deduced from statistical considerations alone. The random errors are seen to be only a few per cent. The agreement between the Rb^{87} runs is not quite as good, giving rise to a 5% error.

In order to account for the possibility of systematic errors, the standard deviations are increased to 10% of the value. This choice is, of course, arbitrary, but is made on the basis of the estimated reliability of the density-measurement computations which are believed to be the primary source of systematic errors. The two methods used to estimate the densities agree within 5%. Computer calculations indicate that at low densities and high finesse the error in determining the density by the area method is no more than 10%. The accuracy of the density measurements is still under study.

It is believed that the systematic errors associated with the $1/\tau$ measurements are much smaller than those for the density measurement. The time base determined by the signal generators was measured by a Hewlett-Packard 5245L Electronic Counter and found to be stable, after warmup, to better than 1%. The linearity of the system has been checked repeatedly. The relaxation time is insensitive to the intensity of the pumping radiation, the particular oscilloscope scale,

Table VIII. Summary of Rb^{87}-Rb^{87} total spin-exchange cross-section measurements.

Experiment and reference	$B_{S1}=\int\int \lvert f_t-f_s \rvert^2_{S1} d\Omega\, v_{S1} f(v_{S1}) d^3 v_{S1}/4$ (10^{-10} cm^3 sec^{-1}) at 78±5° C	$\sigma=B/\bar{v}_{S1}$ (10^{-14} cm^2)
Carver - 72		4-7
Moos & Sands - 28		1.9 ± 0.4
Jarrett (Rb^{87}-Rb^{85}) - 73		1.85 ± 0.23
Davidovits & Kanble - 29		0.85 ± 0.10
Bouchiat & Brossel - 24		6
This experiment[a] (Gibbs and Hull):		
Run 5	8.0 ± 0.2	1.93 ± 0.05
Run 6	8.8 ± 0.5	2.13 ± 0.12
Run 7	8.6 ± 0.2	2.07 ± 0.05
Run 9	8.6 ± 0.2	2.08 ± 0.06
Average (weighted)	8.4 ± 0.5	2.03 ± 0.11
Average with increased error as an estimate of possible systematic errors	8.4 ± 0.8	2.03 ± 0.20

a. The values of B listed here for runs 5 through 7 are about 5% higher than those of Figs. 59 through 61 for two reasons: (a) The signal generator was found to be oscillating at 41 cps rather than 40 cps (the second signal generator was also 2.5% fast, because it is set to agree with the first); this implies a 2.5% increase in the values of $1/\tau$ in the figures, which were plotted using the uncorrected values. (b) An absolute density-measurement recalibration reduced the values of the density in the figures by 2.5%. As a result of (a), the values of A given in the figures should be increased by 2.5%. These corrections were made and the signal generator recalibrated before run 9.

The errors for each run are standard deviations of external consistency obtained from statistical considerations alone. The standard deviation for the average is $\sum_{i=1}^{m} (\sigma_i - \bar{\sigma})^2/n(n-1)$, where n is the number of cross sections to be averaged.

Table IX. Summary of Rb^{87}-Cs^{133} total spin-exchange cross-section measurements.

Experiment and reference	$B_{E1} = \int\int \lvert f_t - f_s \rvert^2_{E1} d\Omega\, v_{E1} f(v_{E1}) d^3 v_{E1}/4$ (10^{-10} cm^3 sec^{-1}) at 78±5°C	$\sigma = B/\bar{v}_{E1}$ (10^{-14} cm^2)
Grossetête - 25		2.1 ± 0.4
This experiment[a] (Gibbs and Hull):		
Run 8	8.21 ± 0.19	2.18 ± 0.05
Value including possible systematic errors	8.2 ± 1.2	2.18 ± 0.31

a. The value of B listed here is about 2.5% higher than that of Fig. 64, because the signal generators were found to be oscillating approximately 2.5% faster than recorded, and the times determined by them were used to determine the $1/\tau$'s of the figure.

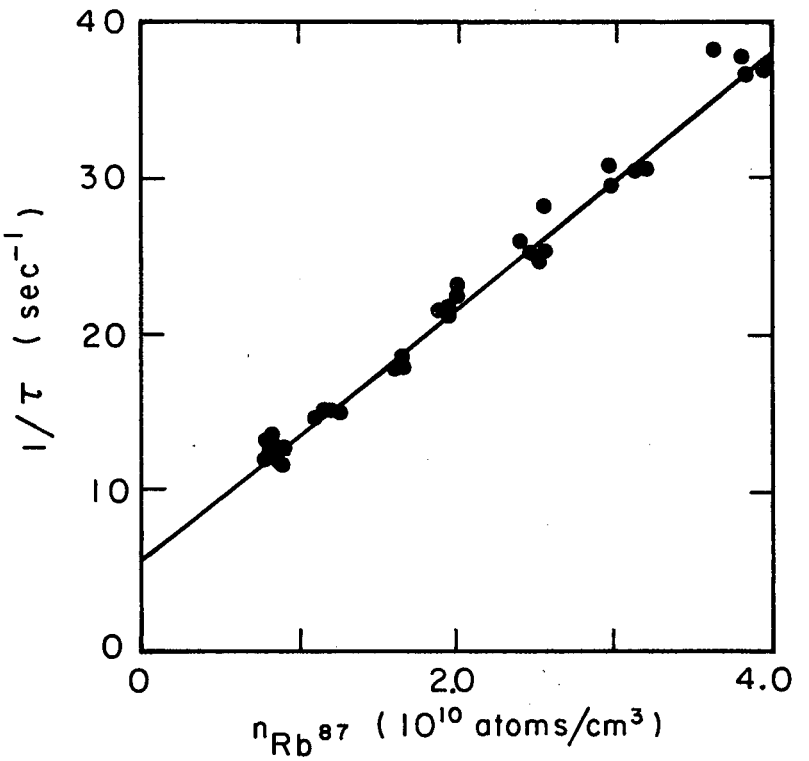

Fig. 61. Summary of run #7 (2/4/65) Rb^{87}-Rb^{87} spin-exchange cross-section measurement by hyperfine pumping. $1/\tau = A + Bn$; $A = 5.57 \pm 0.22$ sec^{-1}; $B = (8.17 \pm 0.18) \times 10^{-10}$ cm^3/sec.

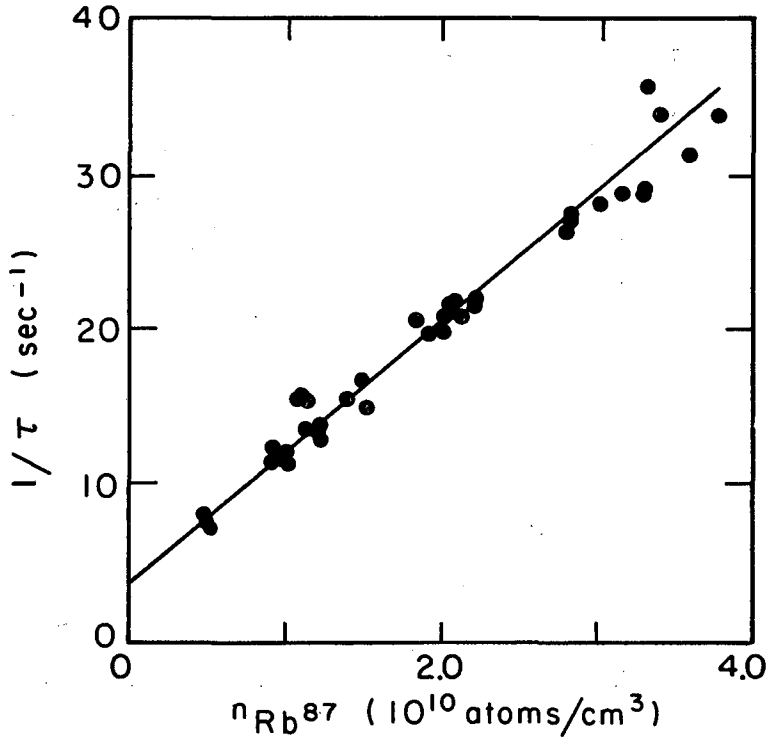

Fig. 62. Summary of run #9 (3/23/65) Rb^{87}-Rb^{87} spin-exchange cross-section measurement by hyperfine pumping. $1/\tau = A + Bn$; $A = 3.35 \pm 0.27$ sec^{-1}; $B = (8.60 \pm 0.23) \times 10^{-10}$ cm^3/sec.

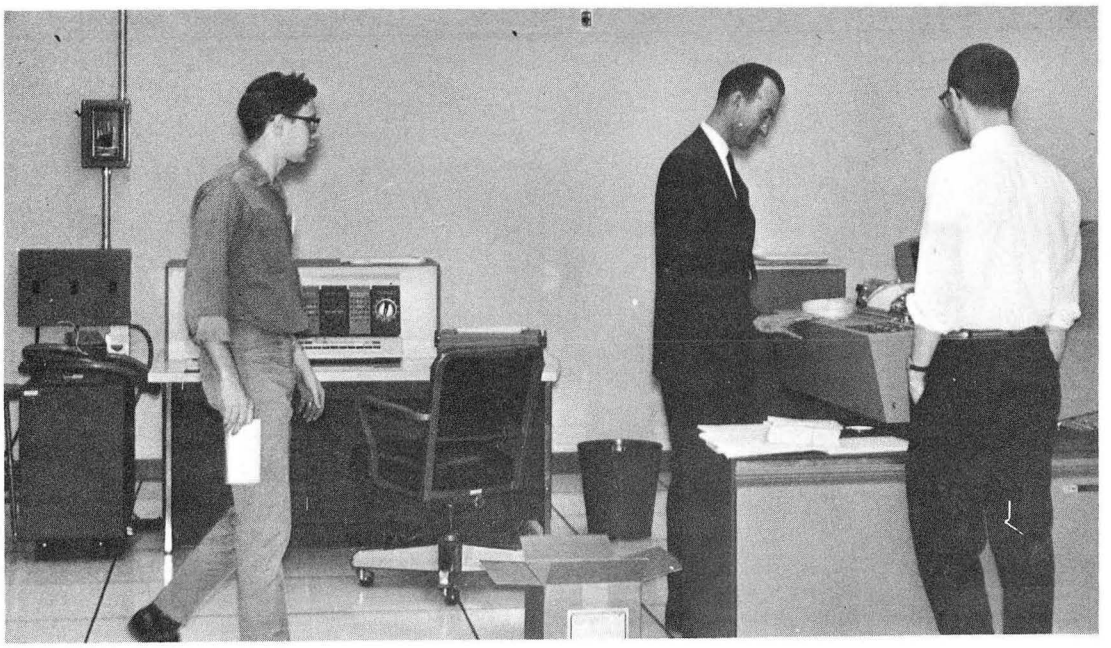

ZN-4893

Fig. 63. The physics department 1620 computer which was used to analyze much of the data. Professor Howard Shugart is in the center, Dr. Robert Hull on the right.

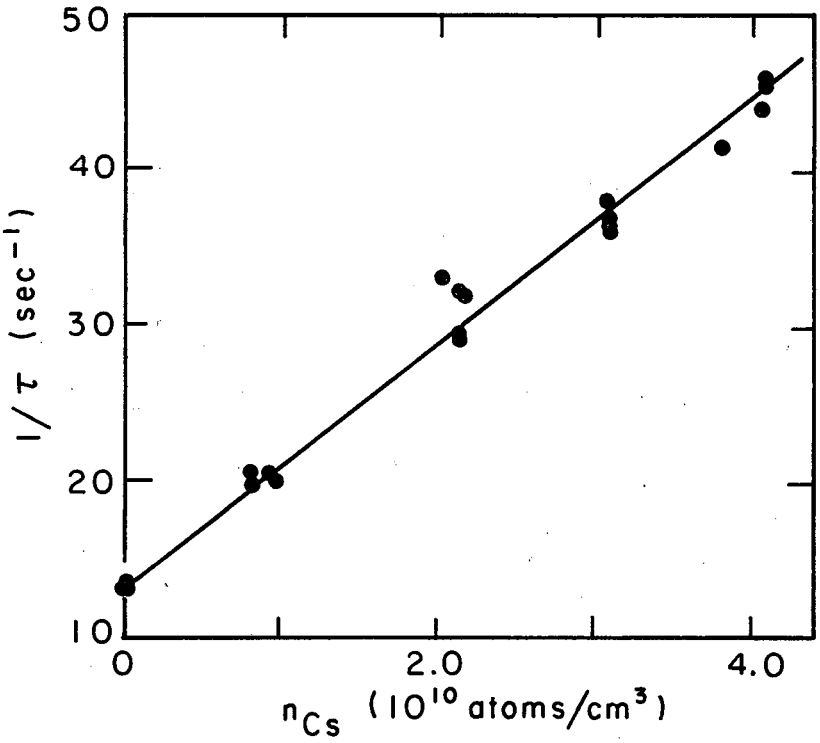

Fig. 64. Summary of run #8(2/13-14/65) Rb^{87}-Cs^{133} spin-exchange cross-section measurement by hyperfine pumping. $1/\tau = A + Bn$; $A = 13.13 \pm 0.09$ sec^{-1}; $B = (8.01 \pm 0.18) \times 10^{-10}$ cm^3/sec.

and the occurrence of the take-data pulse over a reasonable range of a few tenths of a millisecond. The more troublesome problems of the Kerr cell and detector have presumably been adequately solved. Consequently, the standard deviations by external consistency for $1/\tau$ as determined by the least-squares fit of the relaxation data are used, and generally range from 0.5 to 2% of $1/\tau$.

A subtle systematic error could be introduced by a wall relaxation process with a rate proportional to the alkali density as proposed recently be Berg for the atomic hydrogen maser.[74] It is believed that such is not the case here because: (a) the observed relaxation rate appears to be dominated by effusion from the cell into the sidearms (see IVB), (b) the results for the two cells of different size are consistent, and (c) the results are consistent from day to day.

The analysis of the data then indicates that

$$\sigma_{Rb^{87}\text{-}Rb^{87}} = (2.03 \pm 0.20) \times 10^{-14} \text{ cm}^2,$$

where the 10% standard deviation is assigned as a reasonable estimate of possible systematic errors. Similarly

$$\sigma_{Rb^{87}\text{-}Cs^{133}} = (2.18 \pm 0.31) \times 10^{-14} \text{ cm}^2,$$

where the 14% error includes an assigned 10% systematic error and a 10% uncertainty in the Cs lifetime.

IV. RELAXATION TRANSIENTS IN ZEEMAN OPTICAL PUMPING EXPERIMENTS

A. Introduction

The experimental apparatus for the Zeeman pumping experiments is essentially the same as that described in Part III for the hyperfine experiment. The hyperfine filter is removed and a filter to eliminate the D_2 line inserted. Care is taken to equalize the hyperfine components of the D_1 line. The transmitted light signal with the static field perpendicular to the optical axis (condition for no Zeeman polarization) is usually subtracted from the signal with the field parallel in order to eliminate the effects of slow drifts, detector imperfections, etc.

Section IVB contains a few results of non-spin-exchange relaxation data. Section IVC gives an illustrative example of the effect of spin exchange upon the transients, and demonstrates the importance of the nuclear spin in analyzing such an experiment.

B. Non-Spin-Exchange Relaxation of the Electronic Longitudinal Polarization

In subsection IIB.3 mechanisms for relaxation of the polarization were described and in IIC the signal was found to be the sum of two exponentials in general (see Eqs. (76)-(80)). In section IIIA the hyperfine polarization was found to relax as a single exponential (see Eqs. (134)-(135)). Figure 65 displays data for both Zeeman and hyperfine transient experiments with the same conditions in the resonance cell. The Zeeman signal is seen to be a single exponential, to an excellent approximation. This implies that the electron relaxation time T_1' is very long or that one of the coefficients in (76) vanishes. But the latter is unlikely since, for complete polarization, the coefficients are 4/7 and 3/7. Complete polarization should be approached, since

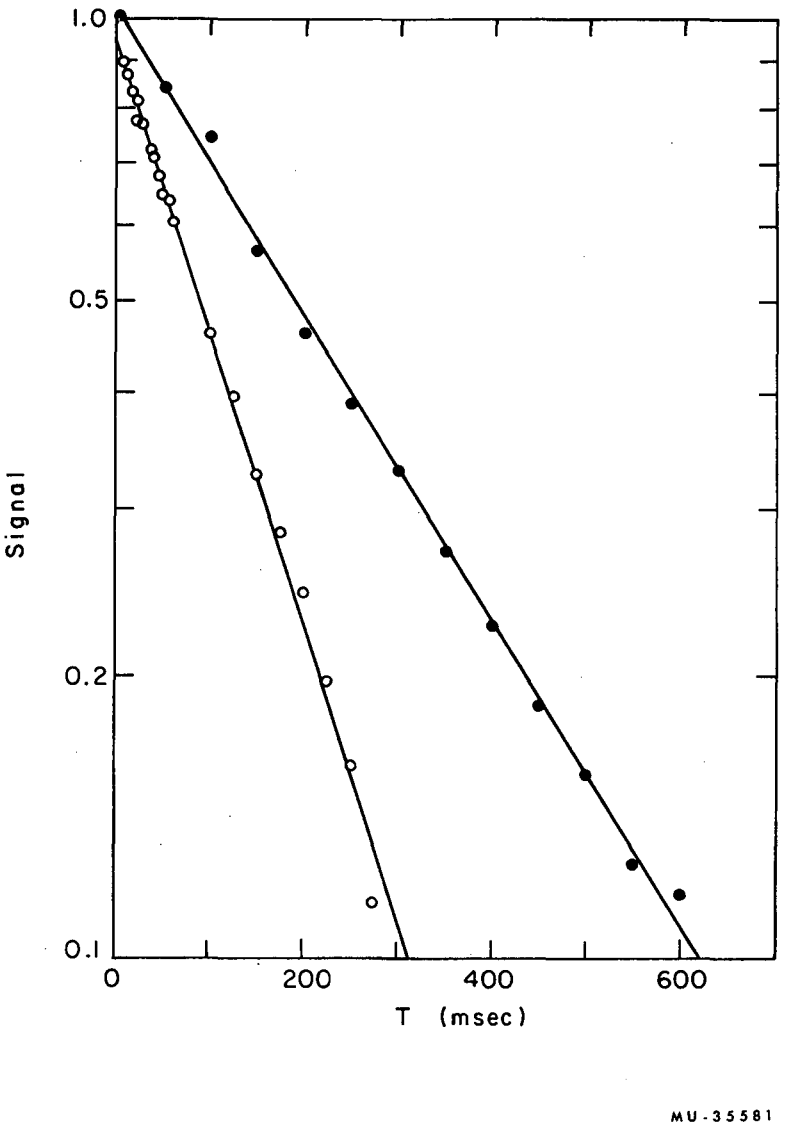

Fig. 65. Zeeman (solid circles) and hyperfine (open circles) pumping relaxation curves for the same conditions in the resonance cell. The hyperfine data (from tape 754, τ=139±9) do not extrapolate to 1.0 because the sag effect was not properly nulled. The sag effect is eliminated from the Zeeman data (tape 749, τ=267±18) by the manner in which they were taken. The data were taken 3/26/65 with the Rb^{87} sidearm at 28 °C and the resonance cell at 78 °C.

the pumping time is much shorter than the relaxation time. Assuming T_1' to be sufficiently long, the hyperfine relaxation time reduces to $1/\tau = 1/T_1'' + 1/T_{S1}$. A density measurement was made and $1/T_{S1}$ found to be 4.6 sec^{-1} by using the cross section from Part III. Then with $1/\tau = 7.17$, from Fig. 65, $T_1'' \approx 380$ msec. With $T_1' \approx \infty$ and for a single species, the Zeeman signal is a single exponential with characteristic time $T_1 T_1''/(T_1+T_1'')$; then $T_1 \approx 890$ msec.

These data were taken in a $1\times2\times2$-in. cell with two narrow seal-offs leading to sidearms. What diameter, d, must the seal-offs have to yield a uniform relaxation time of 380 msec? Atoms leave the cell at a rate $n\bar{v}A/4$, where A is the area of the openings. Then $T_1'' \approx 4V/A\bar{v}$, where V is the volume of the cell. For two sidearms the diameter of each must be about 1 mm; the seal-offs used appear to have a diameter approximately that large.

The relaxation time for the 2-in. cubical cell of runs 5-7 has been described in IIIC.5. In summary, after the cell had been baked for several hours at 110°C the Zeeman pumping relaxation time always returned to about 140 msec, and was represented well by a single exponential ($T_1' \approx \infty$). From Figs. 59 through 61, $T_1'' \approx 1/A \approx 180$ msec; then $T_1 \approx 625$ msec. The smaller value of T_1'' in the larger cell results from much larger seal-offs between the sidearms and cell. As discussed in IIIC.5, the relaxation time is shortened by exposing the cell to high densities for long periods of time. In one case $T_1'' \approx 45$ msec, with T_1 and T_1' too much longer than T_1'' to be deduced. In this case the relaxation is still apparently uniform even though effusion from the cell can no longer account for it. Perhaps the atoms are disoriented by sticking for a long time to small surface imperfections caused by interactions of the Rb atoms with, for example, impurities in the coating. It is believed that the relaxation is not the result of large deposits of Rb in the cell, since a reduction in sidearm temperature is immediately followed by a reproducible reduction in density. The 140-msec time achieved by melting and resolidifying

the coating and attributed to effusion is thought not to result from wall imperfections, because these would be expected to be different after each melting.

This discussion of the relaxation times occurring in the Zeeman experiment should reemphasize the advantage of the hyperfine experiment, in which a single time characterizes all the mechanisms under all conditions, for measuring spin-exchange cross sections. Of course, an atomic beam experiment should eliminate all relaxation problems.

C. Experimental Confirmation of the Importance of the Nuclear Spin in the Relaxation of the Electronic Longitudinal Polarization by Spin Exchange

Figure 66 demonstrates a relaxation curve of $Rb^{87}(I_1 = 3/2)$ polarization dominated by spin exchange with Cs^{133}. Before the Cs was introduced the relaxation was represented well by a single exponential of characteristic time of about 400 msec. As in IVB, contamination of the cell by the Cs atoms would be expected to reduce the relaxation time, but not to change the single-exponential character of the decay. The data points of Fig. 66 were least-squares-fitted to Eq. (76) with $T_1' = \infty$ (see IVB); the results are $1/T_1 + 1/T_1'' = 1/300$ msec^{-1} and $T_{E1} = 25.7$ msec. Unfortunately no density measurement was made, which prevents the deduction of a cross section. Several curves were taken as the density of Cs was increased; a gradual transition from a ratio of time constants almost equal to unity (i.e., very close to a single exponential) to a ratio of about 6 for the highest density reached was observed (theoretically a ratio of 8 should be obtainable for T_{E1} much shorter than the other times). If the nuclear spin were neglected in the analysis, a single exponential would have been predicted, in direct contradiction with the experimental data.

Grossetête has used the Zeeman pumping technique to estimate the Rb-Cs cross section and confirm Eq. (76), derived independently by her.[25,33]

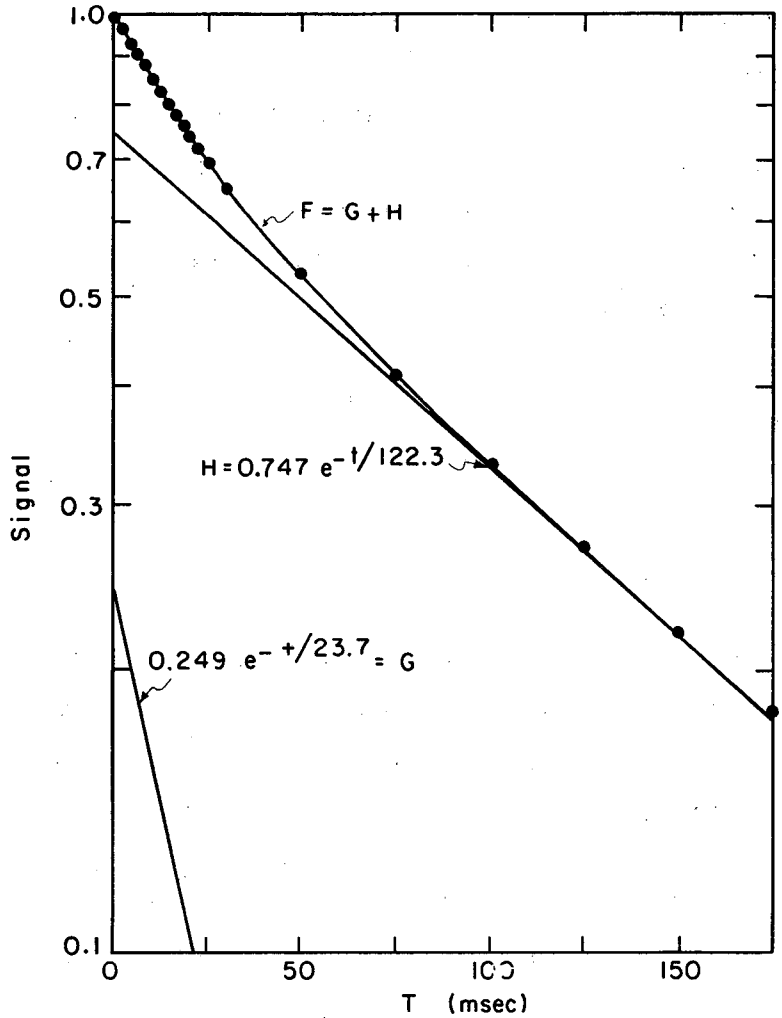

Fig. 66. The relaxation of the Rb^{87} electronic longitudinal polarization when dominated by spin exchange with Cs^{133}. The curve would be a single exponential if the nuclear spin were unimportant. The solid curves are the theoretical best-fit F to the data and the contributions G and H from each of the exponentials. The data were taken with the cell and Cs at 50° C and the Rb^{87} sidearm at 22° C; average of tapes 215 through 221, 6/11/64.

V. SUMMARY AND CONCLUSIONS

The theoretical calculations of Part II apply to Zeeman optical pumping experiments, with equal-intensity circularly polarized hyperfine components in the incident light, performed in weak magnetic fields. The solution for the Franzen-type transient experiment is given in Eq. (76). It is applied to the interpretation of non-spin-exchange relaxation data in IVB. In IVC experimental verification of the importance of the nuclear spin in the analysis is presented. Equation (93) is the theoretical expression for the Dehmelt-type steady-state experiment in the limit of low light intensity. It predicts that the nuclear spins are essential to the analysis if correct cross sections are to be deduced (except in the special case of relaxation by electron randomization only). Experimental confirmation of that equation has not been made.

Part III describes precise measurements of spin-exchange cross sections employing a transient hyperfine optical pumping experiment in which nuclear spin effects are unimportant. The alkali vapor density is determined by using a scanning Fabry-Perot interferometer. The techniques, problems, and results are discussed in detail.

The importance of the spin-exchange process is discussed in Part I. The primary motivation for accurate measurements of the cross sections is to aid in the study of interatomic potentials and to check the treatment of the dynamics of the scattering process. The cross sections reported here and elsewhere indicate that the Rb and Cs cross sections are close to 2×10^{-14} cm^2. This is many times the geometrical cross section, as expected, since the interaction distance is a molecular rather than an atomic radius (recall the crude estimate in IA). Glassgold and Lebedeff[8] have extended the semiclassical theory of Purcell and Field,[4] and predict that the spin-exchange cross section is proportional to

$$\sigma_0^2\ \epsilon_0^{1/3}, \tag{177}$$

where σ_0 and ϵ_0 are the parameters in the Lennard-Jones potential

$$V(r) = 4\epsilon_0 \left[(\sigma_0/r)^{12} - (\sigma_0/r)^6\right] \qquad (178)$$

for the singlet case. Here σ_0, the equilibrium separation, is about 1 A^0 for H_2 and about 4 A^0 for Rb_2 and Rb-Cs. The potential depths ϵ_0 are about 4.5 eV for H_2 and 0.5 eV for Rb_2 and Rb-Cs.[2] Glassgold and Lebedeff obtain reasonably good agreement between their estimate of the H-H cross section (obtained by adjusting the Purcell-Field result) and the experimental value $4(8.08\pi a_0^2) = 0.28\times10^{-14}$ cm^2, of Hildebrandt et al.[26] Assuming the cross section to vary as in (177), one would then expect for Rb-Rb collisions a cross section of $\approx 2\times10^{-14}$ cm^2, which is in excellent agreement with the value measured here. Also, in agreement with (177) and the approximate values of ϵ_0 and σ_0, the Rb^{87}-Rb^{87} and Rb^{87}-Cs^{133} cross sections are roughly equal.

Glassgold and Lebedeff emphasize that their extension of the Purcell-Field model ignores the triplet potential, which they found by exact calculations to play an important role in determining the character of the scattering. Perhaps a more detailed investigation would permit the extraction of triplet potential parameters from the existing singlet potential information and the cross sections reported here.

ACKNOWLEDGMENTS

It is a pleasure to thank in print the many persons who have contributed to this research. First and foremost I salute my wife, Lethia, for her hard work, good humor, and patience. She has been the chief sounding board for new ideas, she has made many helpful suggestions, and she has cushioned the blow of each defeat. In the same vein, I thank my parents, Maa and Pal, for their encouragement, confidence, and respect for education which have been paramount in my attending graduate school.

Dr. Robert Hull has been my close friend and an essential element in the experiment for the last two years. The construction of the Fabry-Perot system and the computer programs used in the density measurements are his work; without them an accurate cross-section measurement would have been impossible.

Professor Howard Shugart has often been a source of guidance throughout this research, particularly regarding electronics and computer problems. I am especially grateful for his assistance in modifying the pulse-height analyzer for use as a data accumulator. His dedication to physics, his enthusiasm and curiosity for the unknown and unexplored, and his frequent words of encouragement (and humor) have challenged and sustained me.

I would also like to acknowledge the following.

Professor Lee Bradley III, Dr. James Crichton, Professor Alfred Glassgold, Dr. Sergje Lebedeff, Professor Eyvind Wichmann, and Mr. Joseph Yellin for discussions about the calculations of Part II. Particular thanks are due Mr. Gerald Wick, who has checked many of the calculations.

Dr. Joseph Winocur for suggesting the use of the Franzen technique in cross section measurements and for guiding the early work.

Mr. Walt Wilson and Dr. Robert Pyle for the use of a high-voltage power supply during the design stage of the Kerr-cell switch. Mr. Vince Honey, Mr. Gerald Sims, and Mr. Al George for suggestions in the construction of the Kerr cell switch.

Mr. Morley Corbett and Mr. Robert Sedlack for the construction of many pieces of glass apparatus.

The Atomic Beam Group for the use of their many resources, particularly the 256-channel analyzer, and for their fellowship.

Professor John Reynolds for the use of his group's chart reader.

Mr. Dan O'Connell for his superb service in coating the Fabry-Perot plates.

Professor Alfred Glassgold, Professor Eugene Commins, Professor William Nierenberg, and Dr. Vernon Ehlers for handling the administrative and financial aspects of the research.

The National Science Foundation for a predoctoral fellowship for four years.

The Office of Naval Research and the U. S. Atomic Energy Commission for financial support.

APPENDICES

I. Justification for Neglecting One of the Self-Exchange Terms

Appendix I compares the quantities

$$I_1 = \int |f_t(\theta) - f_s(\theta)|^2 \, d\Omega \tag{A-1}$$

and

$$I_2 = \int 2 \, \mathrm{Re}\,(f_t^*(\theta) - f_s^*(\theta))(f_t(\pi - \theta) - f_s(\pi - \theta)) d\Omega, \tag{A-2}$$

which appear in (59). The author wishes to thank Dr. Sergje Lebedeff for outlining the following estimate.

Recall that[8]

$$f_n(\theta) = (1/2ik) \sum_{\ell=0}^{\infty} (2\ell+1)(\exp(2i\,\delta_{\ell,n}) - 1) P_\ell(\cos\theta), \tag{A-3}$$

where n refers to t for triplet or s for singlet. Using the orthogonality properties of the Legendre polynomials, one finds

$$I_1 = (4\pi/k^2) \sum_{\ell} (2\ell+1) \sin^2(\delta_{\ell,t} - \delta_{\ell,s}) \tag{A-4}$$

and

$$I_2 = (8\pi/k^2) \sum_{\ell} (-)^\ell (2\ell+1) \sin^2(\delta_{\ell,t} - \delta_{\ell,s}). \tag{A-5}$$

In order to proceed with the calculation, one needs a model for estimating the phase shifts. Glassgold and Lebedeff[8] have found that cross sections predicted by the Purcell-Field model[4] agree with the results of "exact" calculations to within a factor of 2. The Purcell-Field model divides all collisions into two classes: weak collisions ($\ell > \ell_0$) for which there is no exchange and $\left\langle \sin^2(\delta_{\ell,t} - \delta_{\ell,s}) \right\rangle = 0$, and strong collisions ($\ell < \ell_0$) for which $\delta_{\ell,t} - \delta_{\ell,s}$ is large and random, with the result that $\sin^2(\delta_{\ell,t} - \delta_{\ell,s})$ averages to 1/2. Then

$$I_1 \to (2\pi/k^2) \sum_{\ell=0}^{\ell_0} (2\ell+1) = (2\pi/k^2)(\ell_0+1)^2, \tag{A-6}$$

$$I_2 \to (4\pi/k^2) \sum_{\ell=0}^{\ell_0} (-)^{\ell}(2\ell+1) = (4\pi/k^2)\,(-)^{\ell_0}(\ell_0+1), \qquad (A-7)$$

and

$$I_2/I_1 \approx 2(-)^{\ell_0}/(\ell_0+1). \qquad (A-8)$$

For a Lennard-Jones potential of range σ and depth ϵ, the range of the strong collisions is approximately[8]

$$r_0 = \sigma\left\{\frac{1}{5}\left[1-(1-5K_0/4)^{1/2}\right]\right\}^{-1/6} \qquad (A-9)$$

and

$$\ell_0 + 1/2 = kr_0\left\{\frac{6}{5}\left[1+(2/5K_0)(1-\sqrt{1-5K_0/4})\right]\right\}^{1/2}, \qquad (A-10)$$

where $K_0 = E/\epsilon$, $E = \hbar^2k^2/2\mu$ is the kinetic energy in the center-of-mass system, and μ is the reduced mass. At room temperature, for Rb^{87} - Rb^{87} collisions, $E \approx 0.025$ eV, $\epsilon \approx 0.5$ eV, $\sigma \approx 4\text{A} \approx 7.6a_0$; then $K_0 \approx 0.05 << 1$. Therefore, $r_0 \approx \sigma(8/K_0)^{1/6}$ and $\ell_0 + 1/2 \approx \sqrt{3/2}\,k\sigma(8/K_0)^{1/6}$,

$$(ka_0)^2 = \frac{\mu}{m_e}\left(\frac{E}{\hbar^2/2m_e a_0^2}\right) = \frac{87}{2}(1836)\left(\frac{0.025}{13.6}\right),$$

$$ka_0 \approx 12,$$

$$\ell_0 \approx 260,$$

and $$I_2/I_1 \approx 0.8\%. \qquad (A-11)$$

Thus for Rb^{87} -Rb^{87} collisions the interference term in (59) should be small compared with the other terms, and can be neglected to a good approximation.

II. Simplification of the Rate Equations in the Limit of Low Light Intensity

The absorption, reemission, and exchange terms of (63) are found in the limit of low light intensity, i.e., for $\pi_{F_1M_1} << p/2(2I_1+1)$.

A. Absorption and Reemission

With

$$Lp_{F_1M_1} \approx Lp/2(2I_1+1), \tag{A-12}$$

then

$$(\dot{P}_\pm)_{Abs} \approx 2LC \sum_{M_1} M_1^2/(2I_1+1)^3. \tag{A-13}$$

Now consider the reemission term of (63). Equation (20) becomes, in the limit of low light intensity, i.e., for (A-12),

$$m_{J_1'F_1'M_1'} \approx \frac{p}{2(2I_1+1)} \sum_{F_1} P'(F_1M_1'-1, J_1'F_1'M_1') \delta_{J'_1, 1/2}. \tag{A-14}$$

Then (19) indicates that the excited-state populations $n_{J_1'F_1'M_1'}$ are independent of the deviations $\pi_{F_1M_1}$ of the ground-state populations from $p/2(2I_1+1)$, to first order in L. Therefore, in general, in order to include excited-state mixing of any amount and by any process,

$$(\dot{P}_\pm)_{Abs+Re} \approx \left[2C \sum_{M_1} M_1^2/(2I_1+1)^3\right] L_\pm. \tag{A-15}$$

The quantities

$$L_\pm = L\left[1 \pm \frac{(2I_1+1)^2}{Cp \sum_{M_1} M_1^2} \sum_{J_1'F_1'M_1'} \left(\frac{n_{J_1'F_1'M_1'}}{L}\right) \sum_{M_1} M_1 P''(J_1'F_1'M_1', F_1M_1)/\tau_{J_1'}\right] \tag{A-16}$$

are independent of the ground-state populations to first order in L. For complete mixing within each J_1' level,

$$n_{J_1'F_1'M_1'} = n_{J_1'}/(2J_1'+1)(2I_1+1); \; n_{J_1'} = \sum_{F_1'M_1'} n_{J_1'F_1'M_1'},$$

one has $L_{\pm}=L$, since $\sum_{M_1'} P''(J_1'F_1'M_1', F_1M_1)$ is independent of M_1 and $\sum_{M_1} M_1 = 0$.

Equations (A-15) become, if one uses Table X,

$$(\dot{P}_+)_{Abs+Re} = (2I_1+2)(2I_1+3)L_+C/6(2I_1+1)^2, \tag{A-17}$$

$$(\dot{P}_-)_{Abs+Re} = (2I_1-1)2I_1L_-C/6(2I_1+1)^2. \tag{A-18}$$

B. Cross Exchange

Equations (81) and (82) in (44) yield, to first order in L,

$$(\dot{P}_{F_1})_E = -3P_{F_1}/4T_{E1}+(1/4T_{E1})\sum_{F_1'} \Delta(F_1, F_1') \sum_{M_1'=-F_1'}^{F_1'} \frac{\pi_{F_1'M_1'M_1'}\Gamma(F_1, F_1')}{2(F_1-I_1)(I_1+1/2)p}$$

$$+ \frac{1}{2(F_1-I_1)(2I_1+1)^2T_{E1}d} \sum_{\substack{F_1'M_1' \\ F_2M_2 \\ F_2'M_2'M_1}} M_1(\delta_{F_2'M_2'}-\delta_{F_2M_2})W(I_1I_2F_1M_1F_2M_2F_1'M_1'F_2'M_2'), \tag{A-19}$$

where $\Delta(F_1, F_1')$ is defined by (5), $\Gamma(F_1, F_1')$ by (30), and

$$W(I_1I_2F_1M_1F_2M_2F_1'M_1'F_2'M_2') =$$

$$\frac{\Delta(F_1, F_1')\Delta(F_2, F_2')}{4} \sum_q \begin{pmatrix} F_1' & 1 & F_1 \\ -M_1' & q & M_1 \end{pmatrix}^2 \begin{pmatrix} F_2' & 1 & F_2 \\ -M_2' & -q & M_2 \end{pmatrix}^2 = W. \tag{A-20}$$

Table XI is useful in evaluating the second term in (A-19).

Table X. Values of $\sum_{M_1=-F_1}^{F_1} M_1^2$.

F_1	Values
$I_1 + 1/2$	$(2I_1 + 1)(2I_1 + 2)(2I_1 + 3)/12$
$I_1 - 1/2$	$(2I_1 - 1)2I_1(2I_1 + 1)/12$

Table XI. Values of $(2I_1+1)^2 \Gamma(F_1, F_1')\Delta(F_1, F_1')$.

F_1	F_1'	
	$I_1 + 1/2$	$I_1 - 1/2$
$I_1 + 1/2$	$4I_1^2 + 8I_1 - 1$	$2(2I_1 + 2)(2I_1 + 3)$
$I_1 - 1/2$	$4I_1(2I_1 - 1)$	$4I_1^2 - 5$

To evaluate the last term, interchange $F_2, -M_2$ and $F_2'M_2'$:

$$\sum_{\substack{F_1'M_1' \\ F_2M_2 \\ F_2'M_2' \\ M_1}} M_1 \delta_{F_2'M_2'} \; W = \sum_{\substack{F_1'M_1' \\ F_2M_2 \\ F_2'M_2' \\ M_1}} M_1 \delta_{F_2,-M_2} \; W, \qquad \text{(A-21)}$$

by Edmonds' (3.7.5). Table XII contains the values of a quantity $a(F_1, F_1', q)$ arising in the above sums; then,

$$\sum_{M_1}\delta_{F_2M_2}W = \sum_{F_2M_2}\delta_{F_2M_2}\sum_{\substack{F_1'F_2'\\M_1q}}\frac{a(F_1,F_1',q)a(F_2,F_2',-q)M_1}{4(2I_1+1)^2(2I_2+1)^2} \quad (A-22)$$

$$= \frac{16(F_1-I_1)\sum_{M_1}M_1^2}{(2I_1+1)(2I_2+1)}\sum_{F_2M_2}(F_2-I_2)M_2\delta_{F_2M_2}. \quad (A-23)$$

Table XII. Values of $a(F_1,F_1',q)=(2I_1+1)^2\Delta(F_1,F_1')\sum_{M_1'}\begin{pmatrix}F_1' & 1 & F_1\\ -M_1' & q & M_1\end{pmatrix}^2$

F_1	q	F_1': $I_1+1/2$	F_1': $I_1-1/2$
$I_1+1/2$	1	$2(I_1+3/2+M_1)(I_1+1/2-M_1)$	$2(I_1-1/2-M_1)(I_1+1/2-M_1)$
	0	$4M_1^2$	$4(I_1+1/2+M_1)(I_1+1/2-M_1)$
	-1	$2(I_1+3/2-M_1)(I_1+1/2+M_1)$	$2(I_1+1/2+M_1)(I_1-1/2+M_1)$
$I_1-1/2$	1	$2(I_1+1/2+M_1)(I_1+3/2+M_1)$	$2(I_1+1/2+M_1)(I_1-1/2-M_1)$
	0	$4(I_1+1/2+M_1)(I_1+1/2-M_1)$	$4M_1^2$
	-1	$2(I_1+1/2-M_1)(I_1+3/2-M_1)$	$2(I_1+1/2-M_1)(I_1-1/2+M_1)$

Substituting (81) into (13), one has

$$P_{F_1} = 2(F_1-I_1) \sum_{M_1=-F_1}^{F_1} M_1 \, \pi_{F_1 M_1} / (I_1+1/2)p, \qquad \text{(A-24)}$$

$$D_{F_2} = 2(F_2-I_2) \sum_{M_2=-F_2}^{F_2} M_2 \, \delta_{F_2 M_2} / (I_2+1/2)d. \qquad \text{(A-25)}$$

Equations (A-24) and (A-25) in(A-19) with (A-21) and (A-23) gives

$$(\dot{P}_+)_E \approx \frac{(2I_1+2)(2I_1+3)}{6(2I_1+1)^2 T_{E1}}(D_+ + D_- - 3P_-) - \frac{(2I_1^2+I_1+1)}{(2I_1+1)^2 T_{E1}} P_+ , \qquad \text{(A-26)}$$

$$(\dot{P}_-)_E \approx \frac{2I_1(2I_1-1)}{6(2I_1+1)^2 T_{E1}} (D_+ + D_- - 3P_+) - \frac{(2I_1^2+3I_1+2)P_-}{(2I_1+1)^2 T_{E1}}. \qquad \text{(A-27)}$$

C. Self Exchange

Examination of (63) reveals

$$(\dot{P}_\pm)_{S1} = (\dot{P}_\pm)_E \Big|_{\substack{D_\pm = P_\pm \\ T_{E1} = T_{S1}}} \approx \frac{-2I_1(2I_1-1)P_+}{3(2I_1+1)^2 T_{S1}} - \frac{(2I_1+2)(2I_1+3)P_-}{3(2I_1+1)^2 T_{S1}} , \qquad \text{(A-28)}$$

in the limit of low light intensity.

III. Expression of the Population Differences in Terms of the Polarizations in the Limit of Complete Mixing

In this appendix it is shown that $\pi_{F_1 M_1} = M_1 \pi_{F_1}$ in equilibrium if there is complete mixing in the excited state. Since this proof is of interest in connection with the experiment of Anderson and Ramsey,[22] in which a single species is present, set $T_{E1} = \infty$ in (1). Substituting (81) into (1), one finds, with the aid of the discussions of the various terms given in Section IIB,

$$\dot{\pi}_{F_1 M_1} = \alpha(F_1) M_1 + \beta(F_1 M_1) \pi_{F_1 M_1} + \sum_{F_1' M_1'} \gamma(F_1' M_1', F_1 M_1) \pi_{F_1' M_1'} = 0, \tag{A-29}$$

where $\beta(F_1, -M_1) = \beta(F_1, M_1)$ and $\gamma(F_1', -M_1'; F_1, -M_1) = \gamma(F_1' M_1', F_1 M_1)$. Then

$$\dot{\pi}_{F_1, -M_1} = -\Big[\alpha(F_1) M_1 + \beta(F_1 M_1)(-\pi_{F_1, -M_1}) + \sum_{F_1' M_1'} \gamma(F_1' M_1', F_1 M_1)(-\pi_{F_1', -M_1'})\Big] = 0. \tag{A-30}$$

Comparison of (A-30) with (A-29) reveals $\pi_{F_1, -M_1} = -\pi_{F_1 M_1}$; i.e., an expansion of $\pi_{F_1 M_1}$ in M_1 must be odd.

Set $T_{E1} = \infty$ and $L_+ = L_-$ (complete mixing) in (83) and (84) and find, at equilibrium,

$$P_- = \frac{-2I_1(2I_1 - 1)}{(2I_1 + 2)(2I_1 + 3)} \frac{\left(\frac{1}{T_1'} + \frac{1}{T_{S1}} - \frac{2I_1 + 1}{2T_1'''}\right)}{\left(\frac{1}{T_1'} + \frac{1}{T_{S1}} + \frac{2I_1 + 1}{2T_1'''}\right)} P_+, \tag{A-31}$$

i.e., $\sum_{M_1'} M_1' \pi_{F_1' M_1'} \propto \sum_{M_1} M_1 \pi_{F_1 M_1}$ for both values of F_1'. Equation (83) or (84) can then be written, for equilibrium,

$$\sum_{M_1} M_1 \pi_{F_1 M_1} = a(F_1) L \sum_{M_1} M_1^2, \tag{A-32}$$

where (A-15) has been used for the radiation term. Since $\pi_{F_1 M_1}$ must be an odd funtion of M_1, one has

$$\pi_{F_1 M_1} = M_1 \pi_{F_1}, \tag{A-33}$$

where π_{F_1} is independent of M_1. With (A-33) in (A-24),

$$\pi_{F_1} = \frac{(I_1+1/2)p\, P_{F_1}}{2(F_1-I_1) \sum_{M_1} M_1^2} \quad . \tag{A-34}$$

By (A-46), if more than a single line is included in determining $k(\nu)$, one merely sums over the included states. Examples are:

$$\int k(\nu)d\nu\Big|_{J'F'\to JF} = (\lambda_0^2/8\pi\tau_{J',J})\, n_F(2J'+1)(2F'+1)\begin{Bmatrix} J' & F' & I \\ F & J & 1 \end{Bmatrix}^2 ; \quad (A-51)$$

$$\int k(\nu)d\nu\Big|_{J'\to JF} = (\lambda_0^2/8\pi\tau_{J',J})\, n_F(2J'+1)/(2J+1); \quad (A-52)$$

$$\int k(\nu)d\nu\Big|_{J'\to J} = (\lambda_0^2/8\pi\tau_{J',J})\, n(2J'+1)/(2J+1); \quad (A-53)$$

$$\int k(\nu)d\nu\Big|_{1/2F'\to 1/2F} = (\lambda_0^2/8\pi\tau_{1/2,1/2})\, n_F\Delta(F,F')/3(2F+1), \quad (A-54)$$

where the $\Delta(F, F')$ are given in Table II. Eqs. (A-51), (A-52), and (A-54) are expressible in terms of the total ground-state density n if a Maxwell-Boltzmann distribution is approximated:

$$n_F \approx (2F+1)\, n/2(2I+1). \quad (A-55)$$

Since the relative intensities of spectral lines are proportional to $\int k(\nu)d\nu$, (A-50) through (A-54) can be used to obtain relative intensities.

FOOTNOTES AND REFERENCES

1. L. Pauling and E. B. Wilson, Introduction to Quantum Mechanics (McGraw-Hill Co., Inc., New York, 1935), p. 344.
2. G. Herzberg, Molecular Spectra and Molecular Structure (D. Van Nostrand Co., Inc., New York, 1950).
3. A. Messiah, Quantum Mechanics II (North-Holland Publishing Company, Amsterdam, 1962), p. 750. See reference 4 also.
4. E. M. Purcell and G. B. Field, Astrophys. J. 124, 542 (1956).
5. J. P. Wittke and R. H. Dicke, Phys. Rev. 103, 620 (1956).
6. A. Dalgarno, Proc. Roy. Soc. (London) A262, 132 (1961).
7. A. E. Glassgold, Phys. Rev. 132, 2144 (1963).
8. A. E. Glassgold and S. A. Lebedeff, Ann. Phys. 28, 181 (1964).
9. P. L. Bender, Phys. Rev. 134, A1174 (1964).
10. R. Mazo, J. Chem. Phys. 34, 169 (1961); R. R. Lewis, Phys. Rev. 130, 666 (1963).
11. J. E. Nafe and E. B. Nelson, Phys. Rev. 73, 718 (1948); A. G. Prodell and P. Kusch, Phys. Rev. 106, 87 (1957).
12. L. W. Anderson, F. M. Pipkin, and J. C. Baird, Jr., Phys. Rev. Letters 1, 229 (1958) and Phys. Rev. 120, 1279 (1958).
13. S. B. Crampton, D. Kleppner, and N. F. Ramsey, Phys. Rev. Letters 11, 338 (1963).
14. H. G. Dehmelt, Phys. Rev. 109, 381 (1958).
15. D. T. Wilkinson and H. R. Crane, Phys. Rev. 130, 852 (1963).
16. L. W. Anderson, F. M. Pipkin, and J. C. Baird, Jr., Phys. Rev. 116, 87 (1959); W. W. Holloway, Jr. and R. Novick, Phys. Rev. Letters 1, 367 (1958); R. H. Lambert and F. M. Pipkin, Phys. Rev. 128, 198 (1962).
17. R. E. Watson and A. J. Freeman, Phys. Rev. 123, 2027 (1961); A. J. Freeman and R. E. Watson, Phys. Rev. 127, 2058 (1962).
18. S. A. Lebedeff, J. Chem. Phys. 40, 2716 (1964).

19. R. Novick and H. E. Peters, Phys. Rev. Letters 1, 54 (1958).
20. P. Franken, R. Sands, and J. Hobart, Phys. Rev. Letters 1, 118 (1958).
21. S. M. Jarrett, Phys. Rev. 133, A111 (1964), from An Interferometric Technique of Density Measurement Applied to Alkali Metal Vapors Oriented by Optical Pumping (Ph. D. Thesis), University of Michigan, 1962 (unpublished).
22. L. W. Anderson and A. T. Ramsey, Phys. Rev. 124, 1862 (1961); 132, 712 (1963).
23. W. Franzen, Phys. Rev. 115, 850 (1959).
24. M. Bouchiat and J. Brossel, Compt. Rend. 257, 2825 (1963).
25. F. Grossetête, Compt. Rend. 259, 3211 (1964); 258, 3668 (1964).
26. A. F. Hildebrandt, F. B. Booth, and C. A. Barth, J. Chem. Phys. 31, 273 (1959).
27. M. Arditi and T. R. Carver, Phys. Rev. 136, A643 (1964).
28. H. W. Moos and R. H. Sands, Phys. Rev. 135, A591 (1964).
29. P. Davidovits and N. Knable, Bull. Am. Phys. Soc. 8, 352 (1963).
30. L. C. Balling, R. J. Hanson, and F. M. Pipkin, Phys. Rev. 133, A607 (1964); 135, AB1 (1964).
31. L. C. Balling and F. M. Pipkin, Phys. Rev. 136, A46 (1964).
32. K. Rubin, J. Perel, and B. Bederson, Phys. Rev. 117, 151 (1960).
33. F. Grossetête, J. Phys. Rad. 25, 383 (1964).
34. H. Gibbs, Bull. Am. Phys. Soc. 9, 741 (1964).
35. A. R. Edmonds, Angular Momentum in Quantum Mechanics (Princeton University Press, Princeton, New Jersey, 1957).
36. J. Yellin and R. Marrus, Bull. Am. Phys. Soc. 9, 720 (1964).
37. C. O. Alley, Investigations of the Effect of Gas Collisions and Optical Pumping on the Breadth of Spectral Lines (Princeton University, Princeton, New Jersey, 1960), p. II-10 and Table 13.
38. M. Bouchiat, J. Phys. Rad. 24, 379 (1963). This article contains a detailed analysis of relaxation in paraflint-coated bulbs.

39. A. Abragam, The Principles of Nuclear Magnetism (Oxford University Press, London, 1961), p. 272.

40. R. A. Bernheim, J. Chem. Phys. 36, 135 (1962).

41. M. Bouchiat and J. Brossel, Compt. Rend. 254, 3650 and 3828 (1962).

42. J. A. Jordan, Jr., and P. A. Franken, Bull. Am. Phys. Soc. 9, 90 (1964).

43. P. Davidovits and N. Knable, Rev. Sci. Instr. 35, 857 (1964).

44. M. Arditi, J. Phys. Rad. 19, 873 (1958).

45. E. C. Beatty, P. L. Bender, and A. R. Chi, Phys. Rev. 112, 450 (1958).

46. P. L. Bender, E. C. Beatty, and A. R. Chi, Phys. Rev. Letters 1, 311 (1958).

47. A. C. G. Mitchell and M. W. Zemansky, Resonance Radiation and Excited Atoms (Cambridge University Press, Cambridge, 1961), p. 96.

48. R. G. Brewer, Rev. Sci. Instr. 32, 1356 (1961).

49. The $^2S_{1/2}$ energies are given by B. Bederson and V. Jaccarino, Phys. Rev. 87, 228A (1952), and the ^2P energies by B. Senitzky and I. I. Rabi, Phys. Rev. 103, 315 (1956).

50. Page III-11 of reference 37.

51. A. M. Zarem, F. R. Marshall, and F. L. Poole, Elec. Eng. 68, 282 (1949).

52. The author is indebted to Moore and Munger, 33 Rector Street, New York 6, New York for a generous free sample.

53. R. G. Brewer, J. Opt. Soc. Am. 52, 832 (1962).

54. J. Sasuga, Solar Cell and Photocell Handbook (International Rectifier Corp., El Segundo, California, 1960).

55. U. S. Department of the Army, Basic Theory and Application of Transistors (Dover Publications, Inc., New York, 1963).

56. Reference 55, p. 85.

57. L. P. Hunter, Handbook of Semiconductor Electronics (McGraw-Hill Co., Inc., New York, 1962), p. 15-3.

58. Reference 57, p. 13-3.

59. J. F. Cleary, Transistor Manual (General Electric Co., Syracuse, New York, 1962), Sixth Ed., p. 237.

60. See references 21 and 67; H. G. Kuhn and H. J. Lucas-Tooth, J. Sci. Instr. 35, 413 (1958); R. C. Greenhow, Phys. Rev. 136, A660 (1964).

61. F. A. Jenkins and H. E. White, Fundamentals of Optics (McGraw-Hill Book Co., Inc., New York, 1957), p. 275.

62. D. H. Rank and J. N. Shearer, J. Opt. Soc. Am. 46, 463 (1956).

63. S. P. Davis, Appl. Opt. 2, 727 (1963).

64. This line has been tentatively identified as the 7943.9-Å line of the $8^2S_{1/2} \rightarrow 6^2P_{3/2}$ transition in Cs. If so, it has a total width ≈ 60 mK compared with the 110 mK width of the instrument as determined with a 0.15-mm spacer; see H. Kleiman, J. Opt. Soc. Am. 52, 441 (1962).

65. H. J. Kostkowski and A. M. Bass, J. Opt. Soc. Am. 46, 1060 (1956).

66. Reference 47, p. 99.

67. J. Winocur and R. V. Pyle, J. Appl. Phys. (to be published).

68. R. Minkowski and H. Bruck, Z. Physik 95, 299 (1935).

69. G. Stephenson, Proc. Phys. Soc. A64, 458 (1951). The theoretical value by O. S. Heavens, J. Opt. Soc. Am. 51, 1058 (1961), is 2.67×10^{-8} sec.

70. Reference 47, p. 146. The uncertainty of 10% is taken from the original f-value measurement by R. Minkowski and W. Mühlenbruch, Z. Physik 63, 198 (1930). The theoretical value by O. S. Heavens, J. Opt. Soc. Am. 51, 1058 (1961), is 3.5×10^{-8} sec.

71. The $^2S_{1/2}$ hyperfine structure separation is given by L. Essen and J. V. L. Parry, Nature 176, 280 (1955), and the $^2P_{1/2}$ by Landolt-Bornstein, Zahlenwerte and Funktionen, I Band, 5 Teil Atomkerne (Springer, Berlin, 1952), p. 37.

72. T. Carver, Ann Arbor Conference on Optical Pumping, Ann Arbor, Michigan, 1959, p. 29.

73. The value quoted by Jarrett (reference 21) assumes $\sigma = B/v_{RMS}$ whereas here $\sigma = B/\overline{v}$, therefore Jarrett's quoted value has been increased by $v_{RMS}/\overline{v}$ for easy comparison.

74. H. C. Berg, Phys. Rev. 137, A1621 (1965).

75. L. I. Schiff, Quantum Mechanics (McGraw-Hill Book Co., Inc., New York 1955), pp. 253 and 261.